1. Report No. NASA CR-135240	2. Government Accession No.	3. Recipient's Catalog No
4. Title and Subtitle EVALUATION OF A LOW ASPECT RATIO SMALL AXIAL COMPRESSOR STAGE, VOLUME I		5. Report Date November 1977 6. Performing Organization Code PWA FR-8499
7. Author(s) C. W. Sawyer, III		8. Performing Organization Report No 10. Work Unit No.
9. Performing Organization Name and Address United Technologies Corporation Pratt & Whitney Aircraft Group Government Products Division P. O. Box 2691 West Palm Beach, Florida 33402		11. Contract or Grant No. NAS3-19424 13. Type of Report and Period Covered Contractor Report
12. Sponsoring Agency Name and Address National Aeronautics and Space Administration Washington, D. C. 20546		14. Sponsoring Agency Code

15. Supplementary Notes

Project Manager, Dr. Wojciech Rostafinski, Fluid System Components Division
NASA-Lewis Research Center, Cleveland, Ohio 44135

16. Abstract

A program was conducted to evaluate the effects of scaling, tip clearance, and IGV reset on the performance of a low aspect ratio compressor stage.

The stage design was obtained by scaling an existing single-stage compressor by a linear factor of 0.304 (corrected flowrate was scaled from 16.595 kg/sec to 1.537 kg/sec). The design objective was to maintain the meanline velocity field of the base machine in the smaller size. However, adjustments were made to account for predicted blockage differences and to chord lengths and airfoil edge radii to obtain reasonable blade geometries.

The meanline velocity diagrams of the base stage were not maintained at the scaled size. At design speed and flowrate the scaled stage achieved a pressure ratio of 1.423, adiabatic efficiency of 0.822, and surge margin of 18.5%. The corresponding performance parameters for the base stage were 1.480, 0.872, and 25.2%, respectively. The base stage demonstrated a peak efficiency at design speed of 0.872; the scaled stage achieved a level of 0.838.

When the scaled stage rotor and stator tip clearances were doubled (from about 1% to 2% blade height), the stage achieved a pressure ratio of 1.413, efficiency of 0.799, and surge margin of 16.0% at the design flowrate. The peak stage efficiency at design speed was 0.825 with the increased clearance.

Increased prewhirl lowered the stage pressure ratio as expected. Stage efficiency was maintained with ten degrees of increased prewhirl and then decreased substantially with ten additional degrees of reset.

17. Key Words (Suggested by Author(s))	18. Distribution Statement
Compressor Low Aspect Ratio Scaling Clearance IGV Reset	Unclassified — Unlimited

19. Security Classif. (of this report)	20. Security Classif. (of this page)	21. No. of Pages	22. Price*
Unclassified	Unclassified	145	

* For sale by the National Technical Information Service, Springfield, Virginia 22161

FOREWORD

This report contains the tabulated performance data for NASA CR-135241 titled "Evaluation of a Low Aspect Ratio Small Axial Compressor Stage." The design, test equipment, data reduction procedures, and test result discussions are contained in CR-135240, Volume I. The tabulations presented herein are itemized in the table of contents.

CONTENTS

CONTENTS (Continued)

ILLUSTRATIONS

ILLUSTRATIONS (Continued)

ILLUSTRATIONS (Continued)

TABLES

SUMMARY

A program has been conducted under Contract NAS3-19424 to evaluate the effects of scaling, tip clearance, and increased prewhirl on a low aspect ratio, single-stage compressor.

The compressor design was obtained by scaling an existing single-stage compressor by a linear factor of 0.3043 (corrected flowrate was scaled from 16.595 kg/sec to 1.537 kg/sec). The design objective was to maintain the meanline velocity field in the scaled size. A major adjustment was made to an exact scale of the flowpath to account for predicted blockage differences, and slight adjustments were made to chord lengths and airfoil edge radii to obtain reasonable blade geometries.

The performance penalties of scaling were larger than expected. The scaled stage achieved lowered pressure ratio at all speeds, especially at design speed. This result has been attributed to increased losses at all speeds, and a substantial loss of work at the rotor hub at design speed. Moreover, surge margin decreased progressively toward design speed. The primary shortcoming of the design was a failure to account for the increase in critical Reynolds number at the rotor hub. Overestimation of the blockage at the rear of the stage was also a significant factor in not achieving the design vector diagrams. At design speed and flowrate the scaled stage achieved a pressure ratio of 1.423, adiabatic efficiency of 0.822, and surge margin of 18.5%. The corresponding performance parameters of the base stage were 1.480, 0.872, and 25.2%, respectively. The base stage demonstrated a peak efficiency at design speed of 0.872; the scaled stage achieved a level of 0.838.

When the scaled stage rotor and stator tip clearances were doubled (from 1 to 2% C/H), the stage achieved a pressure ratio of 1.413, efficiency of 0.799, and surge margin of 16.0% at the design flowrate. The peak stage efficiency at design speed was 0.825 with the increased clearances. In general, the test results showed that the scaled rotor experienced no discernible increase in loss with increased tip clearance. The stator losses, however, increased sufficiently to render the overall stage penalty comparable to that of some other previous experiments.

Increased prewhirl lowered the stage pressure ratio as expected. Stage efficiency was maintained with ten degrees of increased prewhirl and then decreased substantially with ten additional degrees of reset.

INTRODUCTION

Viable gas turbine engines for lightweight helicopters, trucks, and other similar applications require small, yet efficient, compressors. Direct scaling of large size compressors to smaller sizes generally results in some efficiency degradation. This degradation is attributed primarily to problems of boundary layer control, dimensional fidelity, and maintenance of small clearances. It would be economically expedient to be able to use the vast bulk of large scale compressor data to abbreviate the development of the small compressors without undue loss in performance.

It is reasoned this can be done by making the proper adjustments to a direct scaled flowpath to minimize the boundary layer effects and allow for changes in blockage and to adjust blade chords and thicknesses in a manner to improve dimensional fidelity with minimum effect on performance. Unfortunately, the methodology of making these adjustments and the scaling process has not been treated very extensively in the literature and the limited results show considerable dispersion.

The increasing attractiveness of small size axial-centrifugal compressors underlines the importance of off-design performance characteristics. Small axial flow compressor stages will be included as super-chargers for these designs. Matching considerations will demand that part speed performance be adequate and well understood.

The purpose of this program was to investigate the problems associated with development of small axial compressors, as noted above. Specifically, the test program was tailored to further define three important effects: scale, clearance, and inlet guide vane reset.

This two-volume Final Report presents the design and performance of a small, low aspect-ratio compressor stage. Volume I contains the aerodynamic and mechanical design of the stage, plus a description of test equipment, data reduction procedures, test results and conclusions. Volume II contains the complete tabulations of overall and blade element performance data for each test point in both S.I. and U.S. Customary units.

AERODYNAMIC DESIGN

The objective of the design was to reproduce the meanline velocity field of a large compressor stage ($W\sqrt{\theta}/\delta$ = 36.6 lbm/sec) in a small machine having a corrected inlet flowrate of 3-5 lbm/sec. Adjustments were allowed as required by predicted blockage differences and machining considerations.

Choosing a Base Stage

Recent studies have indicated that large size compressors can be fabricated at a lower cost, with no loss in efficiency, by using highly loaded, low aspect ratio blading. Such a machine was tested in 1973 as part of the Pratt & Whitney Aircraft Independent Research and Development Program. This 0.58 "D" factor, aspect ratio of one, single-stage compressor rig was chosen as the base stage for this program. A summary of the base stage scaling point performance has been included in table I. Detailed blade element data for selected points at 70, 85, and 100% corrected design rotor speed are included in Volume II of this report.

Sizing a Scaled Stage

A range of scale factors (SF) corresponding to the desired range of inlet corrected flowrates (i.e., 3-5 lbm/sec) was generated using the following formulation:

$$SF = \left[\frac{W\sqrt{\theta}/\delta \text{ (desired)}}{W\sqrt{\theta}/\delta \text{ (base stage)}} \right]^{1/2} = \left[\frac{W\sqrt{\theta}/\delta \text{ (desired)}}{36.586 \text{ lbm/sec}} \right]^{1/2}$$

This range was truncated at both ends by mechanical constraints: the test facility limited the lower end because the drive system could supply a maximum mechanical speed of only 36,000 rpm, and the proposed bearing compartment limited the upper end because an overly large rotating assembly could not be satisfactorily overhung from it. The scaled stage was sized at the best compromise between these limits as follows:

SF = 0.3043

$N/\sqrt{\theta}$ = 3603.26 rad/sec (34408.6 rpm)

$W\sqrt{\theta}/\delta$ = 1.5368 kg/sec (3.388 lbm/sec)

5% Overspeed Capability

Application of the Scale Factor

A recently developed meanline computer program was used to predict the effect of scaling the base stage by a factor of 0.3043. This program accounts for scaling effects by means of similarity principles which have been used extensively as correlation parameters for diffuser data, but only rarely for compressor data. The basis of this technique is that the performance of diffusers can be successfully predicted as a function of the amount of diffusion (area ratio), rate of diffusion (wall cone angle), inlet blockage, Reynolds number and turning angle (for curved diffuser passages). In an analogous manner, expressions can be derived for rectilinear cascade passages for amount of diffusion (e.g. Δ Ps/Pt-1's) and rate of diffusion ("equivalent" conical diffusion angle - θeq). A more detailed description of the meanline program is presented in Appendix A.

Inlet blockage was determined from a calculation of the boundary layer growth along both walls of the scaled rig inlet section. A computer program which provides a simultaneous solution

of the integral momentum equation, a skin friction equation, and a shape factor equation was used for the calculation. After the predicted inlet blockage had been calculated, the meanline computer program was used to predict the blockage increase behind the rotor and stator of the scaled rig.

The meanline program was first run for the best representation of the base configuration. The calculation was then performed in the off-design mode for the scaled stage using the blade geometry of the prototype. The flowpath envelope was altered as required to maintain the meanline vector diagrams of the base stage. A summary of results from the meanline study is presented below:

Parameter	*Meanline Calculation Base Stage*	*Meanline Calculation Scaled Stage*
Inlet $\bar{K}$	0.967	0.953
Rotor Exit $\bar{K}$	0.899	0.855
Stator Exit $\bar{K}$	0.908	0.873
θeq Rotor	9.013 degrees	9.013 degrees
θeq Stator	6.092 degrees	6.079 degrees

Where $\bar{K}$ = effective area/actual area

The summary shows that the scaled stage design maintains the base rate of diffusion in each blade row as indicated by the comparison of values of the equivalent conical diffusion angle. Hence, the scaled stage design would require no change to the base stage metal angle distributions on a percent of span basis.

Loss and Turning

The final two-dimensional aerodynamic design was completed using a computer program which provided a simple radial equilibrium solution for the axisymetric flow and interacted with cascade correlations to link airfoil geometry and aerodynamic performance. A single station was used to represent both the rotor trailing and stator leading edges. The design was accomplished station-by-station, axially rearward through the machine. The inlet section was designed directly. Base stage values of inlet guide vane geometry, loss, and turning were retained identically on a percent of span basis. The annulus area was enlarged as necessary to accommodate the blockage derived from the inlet boundary layer growth calculation. Additional annulus area was added equally to each wall to maintain the base mean diameter. In this way, the final design was fixed upstream of, and including, the rotor inlet station.

With the rotor inlet aerodynamics fixed and the rotor exit blockage determined from the meanline calculation, an iteration was performed to fix the rotor exit station. The iteration procedure is presented in schematic form in figure 1. The final value of rotor exit blockage from the meanline calculation ($\bar{K}$ = 0.855) was input at the rotor exit station. The rotor exit flowpath was then modified to match the base stage meanline vector diagram. The base loss profile was altered to account for reduced blade Reynolds number and rematching of blade elements removed from the meanline.

The increased loss due to reduced blade Reynolds number was estimated using an empirical correlation. The loss adder due to rematching of blade elements removed from the meanline was accomplished in a straightforward manner through use of the cascade correlations. The rematching occurred because of the changes to flowpath contour, i.e., opening the flowpath caused a slight decrease in wheel speed at the hub and a slight increase in wheel speed at the tip. This caused the relative inlet air angle to decrease slightly at the hub and increase slightly at the

tip, with accompanying shifts along the loss characteristics. The base loss profile was modified for each of the three loss adders. This distribution was input and rotor exit flowpath geometry was again changed to match the mean velocity diagrams of the base stage. At this point, turning was adjusted for three effects: reduced Reynolds number, rematching of blade elements removed from the meanline, and the altered density-velocity ratio across the blade row.

The correlation of Reynolds number effects showed that the Reynolds number of the scaled rig would not be sufficiently low to cause any change in turning. The two remaining effects were analyzed directly using the cascade turning correlations.

The turning adders were applied to the base distribution and the rotor exit flowpath geometry was again changed to maintain the base stage mean vector diagrams. The loss-turning iterations were repeated until a solution became stable. In this way, the rotor exit station was fixed.

The iteration was repeated for the stator row in the same manner. When the stator exit aerodynamics had converged to a stable solution, the design was completed.

Blading

Airfoils for the scaled stage were to be identical to those of the nominally scaled base stage on a percent of span basis with the following exceptions:

1. Chord length was changed to account for flowpath modifications while retaining the same number of airfoils per row and spanwise solidity distribution. The changes in chord length were of the order of ±1% of the nominally scaled value.

2. Leading and trailing edge radii for the rotor and stator blade rows were increased to 0.005 inch throughout. This represents an approximate doubling of the value which would be calculated using the formula for conventional blading.

3. A tangential tilt of 5 degrees was incorporated into the cantilevered inlet guide vane and stator design. Tight absolute tip clearances were planned for the scaled rig, and the tilt was included to provide additonal protection against a catastrophic stator rub.

Flowpath Modifications

Several small modifications were made to the scaled stage flowpath. These changes were necessary in order that straight-line machining cuts could be made on the flowpath faces of the rotor and all case segments. The aerodynamic design was reevaluated for the modified flowpath and no significant changes resulted.

The final scaled design differed from a rigid geometrical scale in the following ways:

1. Annulus area was added equally at each wall of the rotor and stator exit to account for the predicted blockage increase as calculated by a meanline computer program.

2. Airfoil metal angle distributions of the base stage were maintained exactly on a *percent of span* (not scaled diameter) basis.

3. Chord lengths were adjusted by about 1% to maintain the base solidity distributions.

4. Airfoil leading and trailing edge radii were about doubled to 0.005 inch everywhere.

5. A 5-deg tangential tilt was incorporated into the inlet guide vane and stator.

6. Predicted performance for the scaled stage was estimated on a spanwise basis from corrections for Reynolds number, rematching, and altered loading using currently available cascade data correlations. In general, these corrections were negligibly small.

A comparison of aerodynamic performance for the base stage scaling point and the scaled stage aerodynamic design point (ADP) is presented in table I.

Appendix B presents base and scaled stage flowpath dimensions, airfoil geometry tabulations, and airfoil section coordinates.

Figure 2 compares the flowpath of the rigidly scaled base stage and the final scaled stage configuration.

Figures 3 and 4 present a spanwise comparison of loss, loading, and turning distributions for the base and scaled stages.

MECHANICAL DESIGN

Base Stage Hardware

The base stage compressor rig configuration is shown in figure 5.

The rotor disk/drum assembly was overhung on the drive shaft ahead of the bearing support package. An overhung rotor design was selected because of lower fabrication costs and ease of changing rotor configurations. A roller bearing was used at the front of the shaft because of the support requirements of the overhung rotor. Critical speed problems with the large overhung mass of an early configuration dictated the use of an oil-damped bearing support at the forward bearing location. Critical speed problems were eliminated by using a free-floating outer race support which is surrounded by a 0.005-inch-thick oil film. Outer race skidding was prevented by a locating pin that allowed radial motion but prevented circumferential turning. The shaft thrust load was absorbed by a ball bearing at the rear end of the shaft. To prevent ball skidding with the single thrust bearing arrangement, it was necessary to preload the shaft during acceleration by pressurizing the cavity behind the rotor disk. During the data acquisition periods the axial load provided by the test stage allowed the pressurant flow to be shut off. Bearing lubrication was achieved with a test stand pressure supply-scavenge system.

The flowpath outer cases incorporated two movable traverse rings, one ahead of the rotor and one behind the stator. Each of these rings was capable of moving four radial traverse probes through 25 degrees of circumferential travel. Thus, complete blade element data could be taken by a combination of circumferential and radial transverse modes. The traverse ring assembly was held together by 12 tie-bolts and spacer tubes and had a compressible felt ring on each side to prevent leakage. The four center traverse ports were on a fixed ring located between the rotor and stator. The inlet assembly was supported by eight struts located upstream of the inlet guide vanes. Flowrate was varied by a sliding sleeve discharge valve which regulated stage discharge pressure.

Existing Scaled Rig Hardware

An existing centrifugal compressor rig was modified for testing the low aspect ratio small axial compressor stage. This rig employed a centrifugal impeller overhung from a self-contained bearing package. This design reduced the cost and complexity for multiple configuration testing by allowing changes to be made while at test.

The self-contained bearing package utilized a soft (oil damped) mounted roller bearing and a ball thrust bearing. A roller bearing was used at the front of the shaft because of the high radial load requirements of an over-hung rotor. The free-floating outer race support was surrounded by an 0.005-in. thick oil film to damp shaft critical speed excitation energy. The shaft thrust load was absorbed by the ball bearing at the rear of the shaft. This bearing was preloaded and rotor thrust load was sufficiently high to prevent ball skidding.

New Scaled Stage Hardware

A schematic of the scaled stage rig is presented in figure 6.

The scaled stage used an integrally bladed rotor. It was machined from a titanium alloy (AMS 4828) forging. The rear of the rotor was attached to the existing thrust balance piston by a toothed coupling. To minimize the possibility of a catastrophic stator rub, the rotor was sprayed with a bond coating of nickel-aluminide, then with an abrasive coating of aluminum-oxide (Al_2O_3). This coating scheme has successfully demonstrated the ability to wear away the tip of a steel stator in previous testing. Lastly, the rotor was made sufficiently thick under the area of the stator tip to provide adequate thermal capacity in the event of a rub.

A rotor critical speed analysis was performed with the following results:

Mode	*rpm*	*% Margin From Maximum Anticipated Speed (%)*
Compressor Bounce	10,730	− 70
Shaft Bounce	44,840	25
Rotor 1st Bending	75,040	108

A finite-element structural analysis was run to determine rotor and stator growth due to thermal and centrifugal forces. The rotor blade was machined oversize, then tipped to provide a running tip clearance of 1% of chord.

The cantilevered inlet guide vanes were 6% thick, NACA 63 series airfoils. Blade elements were stacked on the center of gravity. The vanes were inserted into the case from the inside surface. The vanes were secured such that they could be reset to obtain the desired stagger angle.

The stators were 65 series airfoils, stacked on the center of gravity of each element. A tangential tilt of 5 degrees, in the direction of rotor rotation, was provided to prevent the stator from digging into the rotor in event of a rub. The stators were secured like the inlet guide vanes.

The scaled stage employed traverse rings at the exit of the inlet guide vane and stator blade rows in an analogous manner to the base stage.

Airfoil Vibration Analysis

Mode shapes, and their corresponding frequencies, were determined for the IGV, rotor and stator using the "NASTRAN" finite element computer program. The results of the analysis have been presented in the Campbell diagrams included in figures 7, 8, and 9 for the scaled inlet guide vane (IGV), rotor and stator, respectively. The base stage rotor diagram is presented in figure 10.

The thickness distribution of the IGV was altered to eliminate the potential resonance (3E, first bending) at 74% of design speed. The IGV was designed with a constant maximum thickness to chord ratio (T/C) of 6%. The final IGV redesign employed a linear T/C distribution - 5% at the ID to 11% at the OD. The Campbell diagram for the revised IGV design is shown in figure 11.

Comparison of Blading

Figure 12 presents a comparison of the base and scaled stage rotor and stator blading.

INSTRUMENTATION

The instrumentation of the base and scaled stages was similar in overall layout.

The plenum total pressure was used for the rig inlet value in the scaled stage, but since the base stage employed an inlet screen, it was necessary to measure total pressure behind it. Behind the IGV, total pressure was measured over at least one vane gap at several spanwise locations. Air angle was sensed radially at the midgap position. Circumferential traverses of total pressure and temperature were also taken over at least one gap at the stator exit. Air angle was also sensed radially at the midgap position at the stator exit. Both stages employed numerous wall static pressure taps.

The instrumentation station designation for the base stage is shown in table II; that for the scaled stage is shown in table III.

Airflow

Compressor airflow was measured by a thin-plate, sharp-edged orifice in accordance with ASME standard procedures. The orifice was located approximately 11.58 meters upstream of the rig inlet bellmouth. The orifice diameter was 44.450 cm for the base stage; 13.386 cm for the scaled stage.

Rotor Speed

Multiple speed signals were recorded for each stage. Both stages employed speed pickups on both the gearbox and clutch shafts. In addition, the base stage utilized a magnetic speed pickup on the rotor shroud. The base stage was fitted with two electromagnetic sensors which operated as proximity probes to monitor passing frequencies of six gear teeth on the bearing compartment spacer sleeve.

Special Instrumentation

1. Vibrations

The rig rear mount flange and facility gearbox, clutch, and drive motor were instrumented with velocity pickups. Horizontal and vertical accelerometers were provided on the bearing supports. All vibration measurements were monitored continuously in the control room during testing.

2. *Airfoil Stress Measurements*

Four base stage blades and four vanes were instrumented with strain gages to provide vibratory stress data. Gage locations were determined from bench vibrator tests with the aid of stress-coat, and selected locations were verified by fatigue tests. The gage outputs were displayed on oscilloscopes and usually monitored during tests.

No strain gages were used on the scaled stage.

Base-Stage Performance Instrumentation

Inlet total temperature and total pressure were measured in the plenum by a precision platinum resistance temperature probe and four fixed, single Kiel-head total pressure probes, respectively. Four equally spaced static pressure orifices were located on the inner wall upstream of the inlet guide vane. Radial distribution of total pressure at Station ½ was measured by two fixed, four-sensor Kiel-head total pressure rakes.

Radial distributions of total pressure and air angle were measured downstream of the IGV (Station 2) with two, five-sensor Kiel-head total pressure circumferential traverse rakes (at centers of equal areas) and two 30-deg radial traverse wedge probes, respectively. Four equally spaced outer wall and two equally spaced inner wall static pressure orifices were located at Station 2; two of the outer and inner wall orifices were at mid-channel with the other two outer wall orifices downstream of the IGV trailing edge.

Radial distributions of total pressure/temperature and static pressure/air angle were measured at the rotor exit (Station 3) by means of two Kiel-head and 30-deg wedge traverse probes, respectively.

Radial distributions of total pressure/temperature and air angle were measured downstream of the stator (Station 4) by four, five-sensor Kiel-head circumferential traverse rakes and two 30-deg wedge traverse probes, respectively.

Figure 13 shows the base-stage traverse instrumentation.

Scaled-Stage Performance Instrumentation

Inlet total pressure was measured in the plenum, just upstream of the rig bellmouth, by three Kiel-head probes. Inlet total temperature was measured in the same plenum plane by five platinum resistance temperature bulbs.

At the IGV inlet, instrumentation Station 1, four static pressure taps were provided at the OD wall.

IGV exit/rotor inlet (Station 2) total pressure was measured by two five-sensor rakes. The sensors of each rake were located at 10, 30, 50, 70 and 90 percents of span. Two 30-deg wedge probes were provided to obtain radial distributions of static pressure and air angle. Four static pressure taps were used to provide OD wall static pressure measurements. A four-sensor total pressure rake was provided at the OD wall to measure the boundary layer total pressure gradient. All Station 2 instrumentation were affixed to a ring which could be circumferentially traversed over a range of 2.3 IGV gaps.

Rotor exit/stator inlet (Station 3) instrumentation consisted of four OD wall static pressure taps, two low response and two high response. Radial distributions of pressure, temperature, and

air angle were not measured at the rotor exit due to the limited space available. A four-sensor total pressure rake was provided at the OD wall to measure the boundary layer total pressure.

Stator exit (Station 4) total pressure was measured by two five-sensor rakes. Two five-sensor rakes were also provided to measure total temperature. The sensor locations of each rake were 10, 30, 50, 70 and 90 percents of span. Two 30-deg wedge probes were used to measure the radial distributions of static pressure and air angle. Four static pressure taps were provided at the OD wall. A three-sensor total pressure rake was provided at the OD wall to measure the boundary layer pressure gradient. The entire Station 4 instrumentation assembly was attached to a ring which could be circumferentially traversed through 2 stator gaps.

The scaled-stage stator exit traverse ring is shown in figure 14.

An instrumentation schedule for the base stage is presented in table IV; one for the scaled stage is shown in table V. Conical instrumentation unwraps are presented in figures 15 and 16 for the base and scaled stages, respectively.

TEST FACILITY

Drive System

Both the base and scaled stages were tested in the B-33 compressor test stand at the Pratt & Whitney Aircraft, Government Products Division facility. A schematic of the test facility is presented as figure 17. Figure 18 shows the base stage rig mounted in the test stand. The scaled stage is shown in figure 19. The compressor was driven by a constant speed electric motor which was coupled to the rig shaft through a clutch and a fixed-ratio speed-increasing gearbox. At a constant speed of 1800 rpm, the motor is rated at 1500 hp; maximum available horsepower was a function of the torque capability of the clutch at a constant gearbox input speed. The base stage required a set of gears which provided a ratio of 7.1:1; the scaled stage gear ratio was 20.626:1.

Ductwork

Air was drawn through a 15.54m (51 ft) long, 0.762m (30 in.) diameter inlet duct designed to ASME standards for flow measurement with thin plate orifices. Low velocity uniform airflow was provided at the rig inlet bellmouth by a 1.27m (50 in.) diameter plenum. Transition from the 0.762m diameter duct to the plenum was accomplished with a 4.5 deg half-angle transition duct. At maximum flowrate for the base stage rig, the Mach number at the bellmouth inlet was 0.03.

Discharge airflow was routed radially outward for both stages. In the base stage the air passed through a sliding sleeve discharge valve and was then dumped to ambient. The scaled-stage discharge air was directed through a diffuser section and into a collection chamber. Four flexible lines connected the collector to an overhead exhaust line. Two throttle valves were provided in the discharge line to provide back pressure capability: a large valve for coarse settings and a smaller vernier valve for finer settings.

DATA ACQUISITION AND REDUCTION

Acquisition

Both the base and scaled stages were tested on the same test stand using identical data acquisition equipment.

Data were recorded on magnetic tape at rates specified by the test engineer. A typical data point was recorded as follows:

1. Stationary pressure data were recorded via a pneumatic scanner system. Each of the 48 port readings were sampled twice at a rate of approximately 2 scans per second.

2. Each 30 deg wedge probe was run to the Cal "O" position (fully inboard). The probes were then drawn outward, and pressure and angle measurements were recorded at a rate of 10 scans per second.

3. Each traverse ring (inst sta 2 and 4) was run to the Cal "O" position. The rings were then traversed simultaneously over at least one stator gap while pressure and temperature data were recorded at a rate of 10 scans per second.

Thermocouple temperature measurement devices utilized continuous lengths of chromel-alumel (C/A) wire. Temperature measurements were referenced to an ice point reference via a Universal Temperature Reference (UTR) junction box.

Data Reduction

A schematic of the general data reduction procedure is presented in figure 20. Test data for both stages were recorded on magnetic tape in electrical (millivolt) units. A computer program was used to convert the data into U. S. Customary engineering units: pressure in psia, temperature in °R, radial and circumferential travel in inches, etc. The data were presented in tabular form as a function of microsadic time for ease in isolating recording modes: i. e., transient, traverse, etc.

A second computer program was used to perform four operations on the above results as noted below:

1. Correct all data to standard day inlet conditions.

2. Apply Mach number corrections: i. e., reduce wedge probe static pressure data by its sensed component of total head and increase total temperature measurements by the required temperature recovery.

3. Calculate gapwise mass-average values of stator exit pressure and temperature for each radial probe location.

4. Provide machine plots of all radial and circumferential traverse data.

A third computer progam was used to finalize the test data for analysis. This streamline analysis program uses a mesh point matrix technique to solve for the static pressure distribution which is consistent with the equations of continuity, energy and radial equilibrium. All flow variables were translated to blade edges assuming constant angular momentum. The individual velocity diagram components were calculated using compressible flow functions and standard trigonometric techniques.

Mass-average values of total pressure at the IGV and stator exit stations and total temperature at the stator exit station were plotted versus spanwise location. A curve fit was applied to these data and appropriate extrapolation was used to choose wall values. A similar technique was applied to the rotor exit total pressure data which were not measured directly but were inferred from the circumferential traverse data at the stator exit station.

IGV and stator exit air angle values were determined from the machine plots of the 30 deg wedge probe data. With the addition of inlet corrected rotor speed, flowrate, total pressure and temperature, and geometrical information, the input was complete.

Since the streamline analysis program uses an iterative technique to solve for a static pressure distribution, static pressure data were not directly involved in the calculation of the velocity field.

Iterations were made within the streamline analysis program to establish values of $\bar{R}$ (a blockage factor equal to the ratio of effective to actual flow areas) required to match the calculated value of OD static pressure to the measured data.

After the $\bar{R}$ balance process was completed, the streamline analysis computation was considered finalized. The program used an output sub-routine to summarize the results of the calculation. This summary presents various blade element performance parameters presented at 100, 90, 70, 50, 30 10, and 0% spans in both S.I. and U.S. Customary units. The summary pages for each data point, in both systems of units, are presented in Volume II of this report.

Clearance Measurements

Clearance values for the base stage were calculated from assembly measurements and predicted behavior at speed; scaled stage rotor clearance values were measured using three rub probes which consisted of aluminum wire which was cut by the closest blade tip at a given speed. Scaled stage cantilevered stator clearance was calculated by geometric techniques from the measured rotor data.

Measurement Uncertainty

Total uncertainty estimates for the scaled stage data are presented in table VI. Similar calculations for the base stage were not available.

RESULTS

Description of Data

One-hundred four (104) data points were analyzed in conjunction with Contract NAS3-19424. The points were numbered after completion of the data reduction effort in order to make analysis more convenient. Data were grouped so as to be able to better isolate the effects of scale, clearance, and IGV reset.

A detailed tabulation of rotor and stage performance and clearance data for all data points is presented in table VII.

The variations of clearance within a given speedline should be noted. A stator rub during shakedown testing, and two independent bearing failures necessitated three separate rig builds, each having a slightly different orientation of the rotor relative to its casing. The problems were corrected as they occurred, and the clearance data in table VII reflect the actual orientation for any given data point.

Overall Performance — The Effects of Scale

The effects of scale on rotor performance are shown in figure 21. The scaled stage demonstrated reduced rotor pressure ratio at all values of equivalent rotor speed. Figure 21 shows that the reduced rotor pressure ratio was attributable to increased loss at part speeds; at design speed, the scaled stage also achieved significantly lower work.

Lastly, the surge margin decreased substantially at design speed, decreased slightly at 85% $N/\sqrt{\theta}$, and remained virtually unchanged at 70% $N/\sqrt{\theta}$. The data listed below detail the effects of scale on rotor performance.

Stage	*Point*	PR_R	TR_R		$\%\eta ad_R$
Base	100% $W\sqrt{\theta}/\delta$	1.515	1.136		92.5
Scaled	100% $W\sqrt{\theta}/\delta$	1.456	1.128		88.7
				$\Delta\eta$ =	−3.8
Base	100%, Peak ηad_R	1.554	1.143		94.1
Scaled	100%, Peak ηad_R	1.496	1.135		90.5
				$\Delta\eta$ =	−3.6
Base	85%, Peak ηad_R	1.356	1.097		93.8
Scaled	85%, Peak ηad_R	1.321	1.090		91.5
				$\Delta\eta$ =	−2.3
Base	70%, Peak ηad_R	1.244	1.069		94.1
Scaled	70%, Peak ηad_R	1.220	1.067		90.5
				$\Delta\eta$ =	−3.6

Figure 22 shows the effects of scale on stage performance. The following data quantify these results:

Stage	*Point*	PR_{stg}	$\%\eta ad_{stg}$		*% SM*
Base	100% $W\sqrt{\theta}/\delta$	1.480	87.2		25.2
Scaled	100% $W\sqrt{\theta}/\delta$	1.423	82.2		18.5
			Δ= −5.0	Δ=	−6.7
Base	100% Peak ηad_{stg}	1.490	87.2		21.9
Scaled	100% Peak ηad_{stg}	1.450	83.8		11.6
			Δ= −3.4	Δ=	−10.3

Stage	Point	PR_{stg}		$\%\eta ad_{stg}$		% SM
Base	85% Peak ηad_{stg}	1.329		87.5		23.1
Scaled	85% Peak ηad_{stg}	1.300		83.3		24.8
			Δ=	−4.2	Δ=	1.7
Base	70% Peak ηad_{stg}	1.212		87.9		19.1
Scaled	70% Peak ηad_{stg}	1.200		83.3		30.8
			Δ=	−4.6	Δ=	11.7

Overall Performance — The Effects of Clearance

The effects of clearance on rotor performance are shown in figure 23. In general, the rotor pressure rise characteristic remained unchanged at the two part speeds, but increased at design speed. The four data points at part speed which were run at less than nominal clearance showed a slight improvement in performance, as expected. The improvement in rotor efficiency at 85% $N/\sqrt{\theta}$ and the increased work with increased clearance at design speed was unexpected. It is still not clear whether these trends were real or due to data scatter. The surge line was basically unaffected by clearance. A detailed listing of the effects of clearance on rotor performance follows:

	Rotor % C/H	Point	PR_R	TR_R		$\%\eta ad_R$
	1.3%	100% $W\sqrt{\theta}/\delta$	1.456	1.128		88.7
	1.8%	100% $W\sqrt{\theta}/\delta$	1.452	1.130		88.2
Δ=	+0.5%				Δ=	−0.5
	1.3%	100%, Peak ηad_R	1.496	1.135		90.5
	1.8%	100%, Peak ηad_R	1.512	1.139		90.5
Δ=	+0.5%				Δ=	0.0
	0.6	85%, Peak ηad_R	1.364	1.101		92.1
	0.9	85%, Peak ηad_R	1.321	1.090		91.5
	1.9	85%, Peak ηad_R	1.361	1.100		92.2
Δ=	0.3/1.0				Δ=	−0.6/0.7
	0.8	70%, Peak ηad_R	1.243	1.069		93.6
	1.1	70%, Peak ηad_R	1.220	1.067		90.5
	2.1	70%, Peak ηad_R	1.234	1.068		91.9
Δ=	0.3/1.0				Δ=	−3.1/1.4

The effects of clearance on stage performance are shown in figure 24. It should be noted that the stage efficiency characteristic at design speed shows a decrease with increased clearance, indicating that stator loss rose appreciably as clearance was opened; the 85% $N/\sqrt{\theta}$ efficiency characteristic, however, shows an unexplainable increase in performance with increased clearance. The following data summarize the results:

	Avg % C/H	*Point*	PR_{stg}		$\%\eta ad_{stg}$		*% SM*
	1.05	100% $W\sqrt{\theta}/\delta$	1.423		82.2		18.5
	1.95	100% $W\sqrt{\theta}/\delta$	1.413		79.9		16.0
Δ=	0.90			Δ=	−2.3	Δ=	−2.5
	1.05	100%, Peak ηad_{stg}	1.450		83.8		11.6
	1.95	100%, Peak ηad_{stg}	1.461		82.5		6.3
Δ=	0.90			Δ=	−1.3	Δ=	−5.3
	0.65	85%, Peak ηad_{stg}	1.332		84.8		10.4
	1.20	85%, Peak ηad_{stg}	1.300		83.3		24.8
	2.10	85%, Peak ηad_{stg}	1.309		83.4		22.9
Δ=	0.55/0.90			Δ=	−1.5/0.1	Δ=	14.4/−1.9
	0.85	70%, Peak ηad_{stg}	1.219		85.0		5.8
	1.15	70%, Peak ηad_{stg}	1.200		83.3		30.8
	2.30	70%, Peak ηad_{stg}	1.205		82.5		23.2
Δ=	0.3/1.15			Δ=	−1.7/−0.8	Δ=	25.0/−7.6

Overall Performance — The Effects of Prewhirl

The effects of prewhirl on rotor performance are shown in figures 25 and 26, for 10 and 20 degrees more prewhirl, respectively. As expected, increased prewhirl tended to decrease pressure ratio and flowrate at all values of equivalent rotor speed. Unexpectedly, the rotor efficiency increased at design speed with increased prewhirl; efficiency decreased at part speed. The surge line was not changed at design speed with the IGV reset, but receeded slightly at part speed. The following data note the effects of prewhirl on rotor performance.

IGV Setting	*Point*	PR_R	TR_R	$\%\eta ad_R$
− 0	100%, Peak ηad_R	1.496	1.135	90.5
−10	100%, Peak ηad_R	1.455	1.123	92.5
−20	100%, Peak ηad_R	1.395	1.107	92.5

IGV Setting	*Point*	PR_R	TR_R	$\%\eta ad_R$
− 0	85%, Peak ηad_R	1.321	1.090	91.5
−10	85%, Peak ηad_R	1.320	1.088	93.0
−20	85%, Peak ηad_R	1.281	1.081	90.4
− 0	70%, Peak ηad_R	1.220	1.067	90.5
−10	70%, Peak ηad_R	1.189	1.054	91.5
−20	70%, Peak ηad_R	1.168	1.050	89.8

Figures 27 and 28 show the effects of prewhirl on stage performance for 10 and 20 degrees more prewhirl, respectively. Stage efficiency showed no significant change at 10° more prewhirl, but decreased appreciably at 20° more prewhirl. The following data detail the stage performance:

IGV Setting	*Point*	PR_{stg}	ηad_{stg}	*%SM*
− 0	100%, Peak ηad_{stg}	1.450	83.8	11.6
−10	100%, Peak ηad_{stg}	1.405	83.7	16.8
−20	100%, Peak ηad_{stg}	1.336	80.1	18.0
− 0	85%, Peak ηad_{stg}	1.300	83.3	24.8
−10	85%, Peak ηad_{stg}	1.284	84.0	21.4
−20	85%, Peak ηad_{stg}	1.238	77.8	12.0
− 0	70%, Peak ηad_{stg}	1.200	83.3	30.8
−10	70%, Peak ηad_{stg}	1.178	82.5	27.3
−20	70%, Peak ηad_{stg}	1.151	78.3	27.0

Blockage

As discussed in a previous section of this report (see page 12), a blockage factor was calculated for each instrumentation station, for each data point as required to match the static pressure measurements at the OD wall. A tabulation of the final selected values of lockage factor ($\bar{K}$), and the corresponding ratio of calculated to measured wall static pressure, is presented in table VIII.

Meanline Velocity Diagrams

Velocity diagrams were constructed at the meanline (root-mean-square) diameter for the base stage scaling point (point 1), the nominal scaled stage at nearest to design flowrate and speed (point 15), and the scaled stage with increased clearance at nearest to design flowrate and speed (point 38). The triangles were corrected to the design equivalent flowrate and speed at the IGV inlet assuming rotor work, IGV, rotor, and stage total pressure rise characteristics, and IGV and stator exit air angles would remain unchanged. A tabulation of the velocity triangle calculation results is shown in table IX; some of these triangles are shown graphically in figures 52, 67, and 68.

Average Bladerow Performance

Bladerow performance parameters for all data points were calculated based on average calculations for each station. Figures 29-33 present loss data for all data points at design speed. Figure 29 shows IGV loss coefficient and turning angle versus inlet Mach number. Figures 30 and 31 show rotor inlet Mach number, turning angle, loss coefficient and diffusion factor versus meanline incidence angle. Figures 32 and 33 present stator inlet Mach number, turning angle, loss coefficient and diffusion factor versus equivalent circular arc meanline incidence.

Reynolds Number

Average blade chord Reynolds numbers were calculated for each airfoil. These values are plotted versus percent design equivalent flowrate for all data points in figures 34-36 for the IGV, rotor, and stator, respectively.

Flowrate

Figure 37 presents a plot of plenum total pressure (gage) versus actual orifice flowrate for all scaled stage data points, including surge points. The dashed lines indicate the calculated limits of uncertainty on both measurements. All data fall within the calculated error band.

Spanwise Blade Element Performance

Spanwise plots of diffusion factor, deviation angle, and loss coefficient versus incidence were constructed for all data at design speed. The data are presented at five radial positions: 90, 70, 50, 30 and 10 percents of span from the OD. Figures 38-42 describe the rotor; stator performance is presented in figures 43-47.

Actual Traverse Data

Stator exit traverse data are presented in figures 48 and 49. Figure 48 shows total pressure over one stator gap for data point 15. Figure 49 shows the corresponding total temperature.

Circumferential travel is shown positive in the direction of rotor rotation. The pileup of total temperature on the pressure side of the stator is evident from figure 49. The centers of the total pressure wakes clearly show evidence of the 5-deg stator tilt. For all data points, the peak total pressure was used for the rotor exit value and is denoted by a solid line on figure 48.

A dashed line indicates the mass-average values of P_t and T_t both figures 48 and 49. Final profiles were faired through the average of the two rakes and extrapolated to both walls.

DISCUSSION

The Effects of Scale

The test results show that the base stage meanline velocity diagrams were not maintained in the scaled size.

IGV Performance

In order to isolate the scaling effect, it is necessary to consider each blade row. Since the IGV influences everything downstream, it will be considered first.

Figure 29 shows that nominal scaled IGV consistently turned the air to within 1 to 2 degrees of the design value and exhibited losses that were slightly lower than predicted. Table VIII shows that the blockage values necessary to match the static pressure data were in excellent agreement with the design prediction. This verifies the inlet blockage calculation procedure and underlines the basic validity of the inlet total and static pressure measurements.

In summary, the test data show that the IGV behaved almost exactly as predicted on an average basis.

Rotor and Stator Overall Performance

It was previously noted (page 13) that the effect of scaling was a decrease in rotor and stator pressure ratio at all values of equivalent rotor speed. This was attributed to a general loss of efficiency at part speed and a combination of inefficiency and lowered work at design speed. In addition, it was noted that the scaled stage exhibited a progressively depressed surge line as rotor speed was increased to the design value.

Quantitatively, the scaled stage at design corrected speed and flowrate achieved a rotor pressure ratio of 1.456 and a rotor adiabatic efficiency of 0.887, as compared to the design values of 1.508 and 0.914, respectively. The corresponding stage parameters were a demonstrated pressure ratio of 1.423 and efficiency of 0.822, as compared to predicted values of 1.471 and 0.857, respectively. The base stage achieved 25.2% surge margin at design flow; the scaled stage achieved 18.5%.

Figure 50 presents rotor and stage efficiency values versus inlet flowrate for both the base and nominal scaled stages at design speed. Both rotors were matched for peak efficiency at about the same incidence (corresponding to roughly 94% design flowrate). At this point the effect of scaling is a decrease in rotor efficiency of 3.6 points. Movement along the characteristics toward more negative incidence causes negligible change to the scaling effect.

The stage efficiency characteristics indicate that the base and scaled stators were not matched similarly, as were the rotors. Specifically, if the base stage had been matched for its minimum loss to occur at the base rotor minimum loss (around 94% $W\sqrt{\theta}/\delta$), the base stage had the potential to achieve a stage efficiency of about 88.8%. The scaled stage, on the other hand, achieved its peak stage efficiency at about the same flowrate as its rotor and showed a potential stage efficiency of about 84.6%. The effect of scale, then, was realistically more like a decrease of 4.2 points of stage efficiency. Since the effect of scale on rotor efficiency has been shown to be about 3.6 points, and the effect on stage efficiency to be about 4.2 points, then about 0.6 points can be attributed to the stator.

A similar calculation was performed for the other speedlines. The results of the calculation are presented in figure 51. The circular symbols show the peak rotor efficiency values for each speedline. The square symbols indicate the minimum additional decrease in efficiency due to the stator alone. The diamond-shaped symbols show the peak stage efficiency at whatever flowrate it occurred for each speedline. Thus, a comparison of the square symbols eliminates the inefficiency due to matching differences.

The effects of scaling on efficiency, as shown in figure 51, are summarized below:

$\%N/\sqrt{\theta}$	$\%\Delta\eta$ Stage	=	$\%\Delta\eta$ Rotor	+	$\%\Delta\eta$ Stator	+	$\%\Delta\eta$ Matching
100	−3.4		−3.6		−0.6		+0.8
85	−4.2		−2.3		−1.7		−0.2
70	−4.6		−3.6		−0.9		−0.1

It has been shown that the performance penalties due to scaling were greater than anticipated. The scaled stage was characterized by reduced total pressure ratio at all speeds but especially at design speed. The reduction in total pressure ratio for the scaled configuration was caused by increased rotor and stator losses at all values of equivalent rotor speed. A loss of about four points of peak stage efficiency was typical of the scale effect. About ¾ of this loss was contributed by the rotor. The reduction in pressure ratio was exaggerated at design speed by a reduction in rotor work. Relative to the base stage, the scaled stage experienced a negligibly small loss of efficiency due to rotor and stator mismatching at part speed; at the design speed the scaled rotor experienced a small efficiency increase due to a rotor/stator matching improvement.

Rotor Meanline Velocity Triangles

Figure 52 shows a comparison of the meanline (root-mean-square diameter) velocity triangles for the base and scaled stage rotor at design flowrate. The individual vector magnitudes and angles are tabulated in table IX. Figure 52 shows that the scaled rotor produced less work: its lowered ΔV_θ and turning is evident. Note also that the exit velocity of the scaled rotor is noticeably shortened, thus verifying that the scaled rotor is more highly loaded than the base rotor.

Spanwise Rotor Performance

Figure 53 shows rotor total pressure ratio, total temperature ratio, and adiabatic efficiency versus percent of span for the base and nominal scaled rotors at design speed and flowrate. It can be seen that the decrease in scaled stage work is concentrated in the rotor hub region. In the tip region the scaled stage equaled or surpassed the base stage level of work. The efficiency characteristics reverse. In the hub region where work is drastically decreased, the rotor loss was much lower than in the tip where work reached the base stage level. The net result was a lowered total pressure ratio across the span. A similar set of plots for the peak rotor efficiency points at design speed and for midpoints on the 85 and 70% $N/\sqrt{\theta}$ speedlines is shown in figures 54-56 respectively. These figures show that the trends noticed for the design flowrate points are qualitatively no different at the other values of equivalent rotor speed.

Spanwise plots of loss coefficient, diffusion factor, and exit total temperature versus V_{z_1}/U_1 are presented for all data points at design speed. Figures 57, 58 and 59 show these data for 90, 50 and 10 percents of span from the OD, respectively.

The figures show that the trends identified previously hold true for all the design speed data points; namely, that the scaled stage was characterized by reduced work in the hub region and increased loss in the tip region.

In an effort to find the cause of the reduced work, a generalized work characteristic was constructed for the base stage scale point using the following formulation:

$$\Delta T_t = \frac{U^2}{gJc_p}\left[1 - \frac{V_{z_1}}{U_1}\left\{\left(\frac{V_{z_2}}{V_{z_1}}\right)\tan\beta'_2 + \tan\beta_1\right\}\right]$$

These characteristics are overlaid on figures 57, 58 and 59 and show that the scaled stage work loss is attributable to a reduction in turning, an effect that is lessened toward the outboard airfoil sections. The next section will present a model which might account, at least qualitatively, for this effect.

The Relationship of Reynolds Number and Camber

Reference 1 presents a systematic evaluation of cascade data over a wide range of Reynolds number and incidence by H. G. Rhoden. Although these data have been available for decades, they show a trend which was not fully utilized in the design technique used for the scaled stage of this contract; namely, that airfoil deviation at a given Reynolds number is a strong function of camber.

The scaled stage design presumed that no loss in turning would occur over the projected range of Reynolds number. That correlation is presented in figure 60; the scaled stage design point has been noted. The data from reference 1, however, suggest a completely different result. Appropriate cross-plotting shows that the Reynolds number at which deviation rises markedly (i.e. turning falls off dramatically) increases rapidly as camber increases. This effect is shown in figure 61.

Implications of Reduced Hub Turning

The Reynolds number/camber relationship implies that the scaled rotor hub experienced a marked fall-off in turning (work) even though it operated within its design Reynolds number range. The data show that the turning decrease was predominant at design speed and much less significant at part speeds. This is an interesting result because the Reynolds number at the part speeds were lower yet. Examination of the loss characteristics of the scaled rotor show that it tended to operate more on the stall side of its characteristic at part speed; hence, the critical Reynolds number would be lower for the part speed points at higher values of incidence (see figure 61).

The scaled rotor loading characteristics are also interesting. Figure 62 presents these data for all speeds for the hub, mean, and tip blade elements. The blockage values of table VIII show that the additional rotor exit annulus area adjustment which was incorporated in the scale stage design to account for an expected blockage increase was not needed. This result should have had the effect of increasing the blade loading across the span. The loss in turning at the hub, however, tended to nullify the effect of the additional exit area locally and produced the loading distribution shown in figure 62, i.e., unloaded at the hub, more loaded at the mean and tip. Figure 62 also suggests that the reduced hub turning was responsible for the lowered surge line at design speed, as evidenced by the flatness of the hub diffusion factor characteristic.

The loss characteristics also followed this model. The base stage profile loss was lowered at the hub due to the reduction in aerodynamic loading; the mean tip loss increased alternatively. The additional loss due to the Reynolds number/camber effect restored the base hub loss level. The overall result, then, was decreased hub work, increased tip loss, and a uniformly lowered rotor pressure ratio across the span.

Stator Performance

Spanwise stator loss coefficient and diffusion factor distributions are shown in figures 63-66 for the same data points which were discussed in the rotor performance section (see figures 53-56). Figures 65-66 show that the scaled stator was more lightly loaded than the base stator for all values of equivalent rotor speed and flowrate. This result is not surprising because of the overestimation of rotor exit blockage in the scaled stage design.

Figures 43-47 show that the scaled stator operated at slightly more positive incidence and produced higher losses across the span, a result that became more severe at the part speeds. It was already noted that the scaled stator produced a decrease of about one point in peak stage efficiency relative to the base stator. These notions are evident from the comparison of base and scaled stator meanline velocity triangles which are shown in figure 67.

It would be expected that the scaled stator losses would be no worse than those of the base stator since the scaled vane was more lightly loaded. This, however, was not the case. Furthermore, the shift to slightly more positive incidence angle does not account for the additional loss. Since the stator operated at lower values of Reynolds number than did the rotor (see figures 35 and 36) and had camber angles of the order of those at the rotor hub (see appendix B), it is not unreasonable to suspect that the stator was operating just on the verge of incipient separation.

Summary of the Effects of Scale

The scaled stage did not meet its design objective: the base stage meanline velocity diagrams were not maintained in the smaller size. Specifically, at design speed and flowrate, the scaled stage achieved a stage pressure ratio of 1.423, adiabatic efficiency of 0.822, and surge margin of 18.5%, as compared to base stage values of 1.480, 0.872, and 25.2%, respectively. Furthermore, the scaled stage achieved peak stage efficiency levels of 0.840 at design speed, and 0.833 at 85% and 70% $N/\sqrt{\theta}$. Base stage peak efficiency levels were 0.87?, 0.875, and 0.899 at 100, 85, and 70% $N/\sqrt{\theta}$ respectively.

The scaled stage performance was characterized by a reduction in total pressure ratio, especially at design speed. As the values in the previous paragraph attest, the typical effect of scaling was a loss of about four points of peak stage efficiency. Prior analysis showed that about ¾ of the efficiency differential (i.e., 3 points) was contributed by the rotor. A reduction in rotor work at design speed, coupled with the increased loss, resulted in the exaggerated reduction of pressure ratio at high speed. The scaled stage surge line intersected that of the base stage at 70% $N/\sqrt{\theta}$, but its more shallow slope progressively degraded stability at higher speeds.

Spanwise analysis of the design speed data indicated that the scaled rotor was characterized by lowered work at the hub and increased loss at the tip. At part speeds the hub work deficit lessened while the tip losses became more severe. Cascade data reported by Rhoden in 1953 suggest an explanation for this behavior: The Reynolds number at which incipient separation occurs (i.e., lowered work) decreases rapidly as camber angle increases (i.e., hub). Even though the stage operated at even lower values of Reynolds number at the part speeds, a shift to slightly more positive incidence angles evaded the onset of wholesale separation.

Additional annulus area was incorporated into the scaled stage design to account for the expected blockage increase in the smaller size. The data indicate, however, that the blockage increase never materialized. This would have had the effect of loading the rotor uniformly across the span, but the hub separation lowered the loading locally to the base level. The data also suggest that the loss in high speed surge margin can be attributed to the premature breakup of flow at the rotor hub. The scaled stator was characterized by higher losses than the base stator but operated at lighter levels of loading and at slightly more positive incidence angles. The decreased loading can be explained by the overestimation of rotor exit annulus area. The increased losses at light loading suggest that the stator, like the rotor hub at high speed, was operating on the verge of incipient separation.

DISCUSSION

The Effects of Clearance

Overall Performance — The Effects of Clearance

As shown in figure 23, the rotor work increased at design speed and remained relatively unchanged at the two part speeds, when the clearance of the nominal scaled stage was increased. Losses were unchanged at design speed but decreased progressively toward the lower speeds. The result was a negligible change to rotor pressure ratio at the part speeds and an improvement at design speed. Figure 24 shows that there was no significant difference in the pressure rise characteristics of the scaled stage with the clearance differences evaluated for this contract. The stage demonstrated about the same efficiency with increased clearance at 85% $N/\sqrt{\theta}$. Increased clearance had negligible effect on the stage surge line location.

The overall efficiency results have been distributed between rotor, stator, and matching losses using a technique described previously (see figure 51). The results of this calculation follow:

$\%N/\sqrt{\theta}$	$\%\Delta\eta$ *Stage*	=	$\%\Delta\eta$ *Rotor*	+	$\%\Delta\eta$ *Stator*	+	$\%\Delta\eta$ *Matching*
100	−1.3		+0.0		−2.1		+0.8
85	+0.1		+0.7		+0.3		−0.9
70	−0.8		+1.4		−2.1		−0.1

The data suggest that the scaled rotor suffered no increase in loss when its clearance was increased. The stator loss, however, increased noticeably. Matching effects were mixed. If the 85% $N/\sqrt{\theta}$ data is weighted less heavily in the analysis, one could say that the effect of increased clearance was a general decrease of about one point of stage efficiency. This decrease consists of an increase of about ½ point due to decreased rotor losses, a decrease of about 2 points due to increased stator losses, and an increase of about ½ point due to improved matching.

Rotor Meanline Velocity Triangles

At design speed, the rotor achieved higher work levels, on the average, with increased clearance (C/H = 1.8%) than with nominal clearance (C/H = 1.3%). The meanline velocity diagrams at design flowrate bear this out as shown in figure 68. The inlet triangles were not included because they are virtually congruent.

Spanwise Rotor Performance

Spanwise plots of rotor pressure ratio, temperature ratio, and adiabatic efficiency are presented in figures 53-56 for selected data points. These data show that the increase in work for the larger clearances was distributed uniformly across the span. It is unlikely that this effect is real because the Reynolds number/camber relationship should not be different for the increased clearance configuration. The improved work characteristic, then, will be attributed to data scatter. This result seems justifiable when the nominal and increased clearance scaled rotor data are compared to those of the base stage.

Spanwise loss and loading characteristics, however, cannot be accounted for quite as easily. These data (at design speed) are shown versus incidence in figures 38-42 and versus V_{z_1}/U_1 in figures 57-59. It is not clear why the tip rotor losses did not increase as clearance was increased; furthermore, the improvement in efficiency for all data points at 85% $N/\sqrt{\theta}$ is unexpected and difficult to explain.

The detailed clearance data shown in figures 53-56 do not agree favorably with similar data reported in recent literature (see References 3 and 4). Unlike the scale effect, the clearance effect seems much too complicated to model from the data taken. Specifically, the loss in flowrate and tip total pressure ratio so evident in the Reference 3 data do not appear as clearly defined in these data.

The following should be noted at this time. The data of Reference 3 compare a substantially larger difference in rotor clearances at design speed (% C/H of about 0.8 to 2.1) than do the data of this report (% C/H of about 1.3 to 1.8). In addition, the boundary layer total pressure instrumentation of this report was found to be of negligible aid in constructing the profiles from 10% of span to the OD wall. The rotor exit boundary layer rake was constructed from .508mm (.020 in.) OD hypo tubing which was brazed together to sample an annulus area which extended out from the OD wall to about 10% of span. Either because of poor response or improper design orientation, the boundary layer data were found to be unbelievably low for all data taken at a nominal tip clearance; to further confuse the test results, the instrumentation was irretrievably broken during assembly of the last rig build. Hence, no boundary layer survey was available for any of the increased clearance data points.

Spanwise Stator Performance

Figures 63-66 show the spanwise stator loss and diffusion factor characteristics for selected data points at each value of equivalent rotor speed. The figures show that stator loss did increase at the ID of the stage, as expected, when the stator tip clearance was increased. In general, the stator loss increased for all increased clearance configuration data points.

Summary of the Effects of Clearance

It was noted that the effect of increased clearance was smaller than expected or totally unexpected. The rotor data evidenced reduced hub work (presumably the Reynolds number/camber effect mentioned in the previous section) relative to the base stage but increased work across the span relative to the nominal scaled stage, especially at design speed. This result has been attributed to data scatter. The rotor loss, blockage, and loading characteristics remain unexplained. The stator showed increased losses everywhere as expected.

Although some aspects of the increased clearance data remain unexplained, the data do exhibit reasonable trends when considered on an overall stage basis. Figure 69 summarizes these trends. For each configuration, for each speedline, a stage efficiency value was calculated using the technique explained and shown in figure 50. The clearance value for each point is the average of the best estimate of rotor and stator clearance for that particular speedline. The dashed lines represent the best fit of data correlations by Williams, and Jefferson and Turner as reported in Reference 2. All of the data, with the exception of the 85% $N/\sqrt{\theta}$ increased clearance configuration, agree reasonably well with the results from Reference 2.

DISCUSSION

The Effect of IGV Reset

Overall Performance - The Effect of IGV Reset

Figures 25-28 show the effect of IGV reset on rotor and stage performance for 10 and 20 degrees more prewhirl, respectively. As expected, the work and pressure rise characteristics decreased everywhere as prewhirl was increased. Surge line remained basically unchanged relative to the nominal scaled stage. Unexpectedly, the stage efficiency showed no significant change with 10 degrees more prewhirl. It did, however, decrease noticeably as prewhirl was further increased to 20 degrees.

The technique described on page 18 was applied to the reset data. These results are shown in figure 51 and tabulated below:

$\%N/\sqrt{\theta}$	$\Delta\eta$ Stage	= $\Delta\eta$ Rotor	+ $\Delta\eta$ Stator	+ $\Delta\eta$ Matching
IGV − 10				
100	−0.1	+2.0	−2.9	+0.8
85	+0.7	+1.5	−1.0	+0.2
70	−0.8	+1.0	−2.0	+0.2
IGV − 20				
100	−3.7	+2.0	−6.5	+0.8
85	−5.5	−1.1	−4.6	+0.2
70	−5.0	−0.7	−4.4	+0.1

The data show that the predominant effect of increased prewhirl was a significant increase in stator loss. Rotor loss was virtually unaffected except at a reset value of 20 degrees. Matching differences were negligible.

Spanwise Performance

Spanwise rotor loss, deviation, and diffusion factor distributions versus incidence are presented in figures 38-42. Corresponding stator characteristics are shown in figures 43-47. The rotor data are replotted versus V_{z_1}/U_1 in figures 57-59.

Summary of the Effects of IGV Reset

Increased prewhirl tended to decrease rotor work and stage pressure ratio as expected. It had negligible effect on surge line. The interesting result of the experiment was that the stage maintained good efficiency at 10 degrees more prewhirl, but demonstrated a marked fall-off as the IGV was reset still further positive. The implication of the efficiency trend is that a similar supercharging stage in an axial-centrifugal compressor could be reset to properly match the impeller airflow requirements without suffering a large aerodynamic performance penalty.

REMARKS

Figure 70 presents a miscellaneous collection of compressor data. For each machine, the peak stage efficiency point at design speed was selected to represent the compressor. The plot notes the relationship of overall polytropic efficiency versus the square root of inlet corrected flowrate. An experience curve has been constructed through the data; this curve reflects the suspicion that compressor efficiency is inversely proportional to absolute size. Appropriate test results from the scaling experiments of References 3 and 4, as well as those from this contract,

have been noted on the figure. It should be noted that the results from previous scaling experiments have shown considerable dispersion. The experiment of Reference 3 employed a rigorous linear scale, but chord length was added to maintain reasonable rates of diffusion, and blades were removed to restore base stage solidities. As a result, the average aspect ratio of the stage was reduced by about thirty-six percent. The test results showed that this stage underflowed but suffered only a slight decrease in efficiency.

The scaled eight-stage compressor experiment (Reference 4) was based on an exact linear scaling. The test results showed that the smaller machine experienced no efficiency degradation whatsoever. The experiment of this report basically employed an exact linear scale but allowed the annulus area at the rotor and stator exits to be opened (approximately 8%) to accommodate the expected blockage increase. Figure 70 shows that the stage of this contract experienced a much greater efficiency penalty due to scaling than did the compressors of References 3 and 4.

CONCLUSIONS

The scaling technique used in this experiment did not maintain the meanline vector diagrams of the base stage at the smaller size. Consequently, the scaled stage aerodynamic performance differed from its predicted values at all speeds.

The test data suggest three important results:

1. The performance penalties of scaling were larger than expected. The scaled stage achieved lowered pressure ratio at all speeds, especially at design speed. This result has been attributed to increased losses at all speeds, and a substantial loss of work at the rotor hub at design speed. Moreover, surge margin decreased progressively toward design speed. The primary shortcoming of the design was a failure to account for the increase in critical Reynolds number at the rotor hub. Overestimation of the blockage at the rear of the stage was also a significant factor in not achieving the design vector diagrams.

2. The scaled rotor experienced no discernible increase in loss with increased tip clearance. The stator losses, however, increased sufficiently to render the overall stage penalty comparable to that of some other previous experiments.

3. The data showed that the scaled stage could operate at moderate values of increased prewhirl with no significant loss of efficiency. Still more prewhirl, however, affected the stage performance adversely.

It is apparent that more scaling work is needed. Only by diligent investigation of the entire three-dimensional flow field will designers be able to successfully exercise boundary layer control — the likely key to the development of good small compressors.

For Rotor and Stator Bladerows:

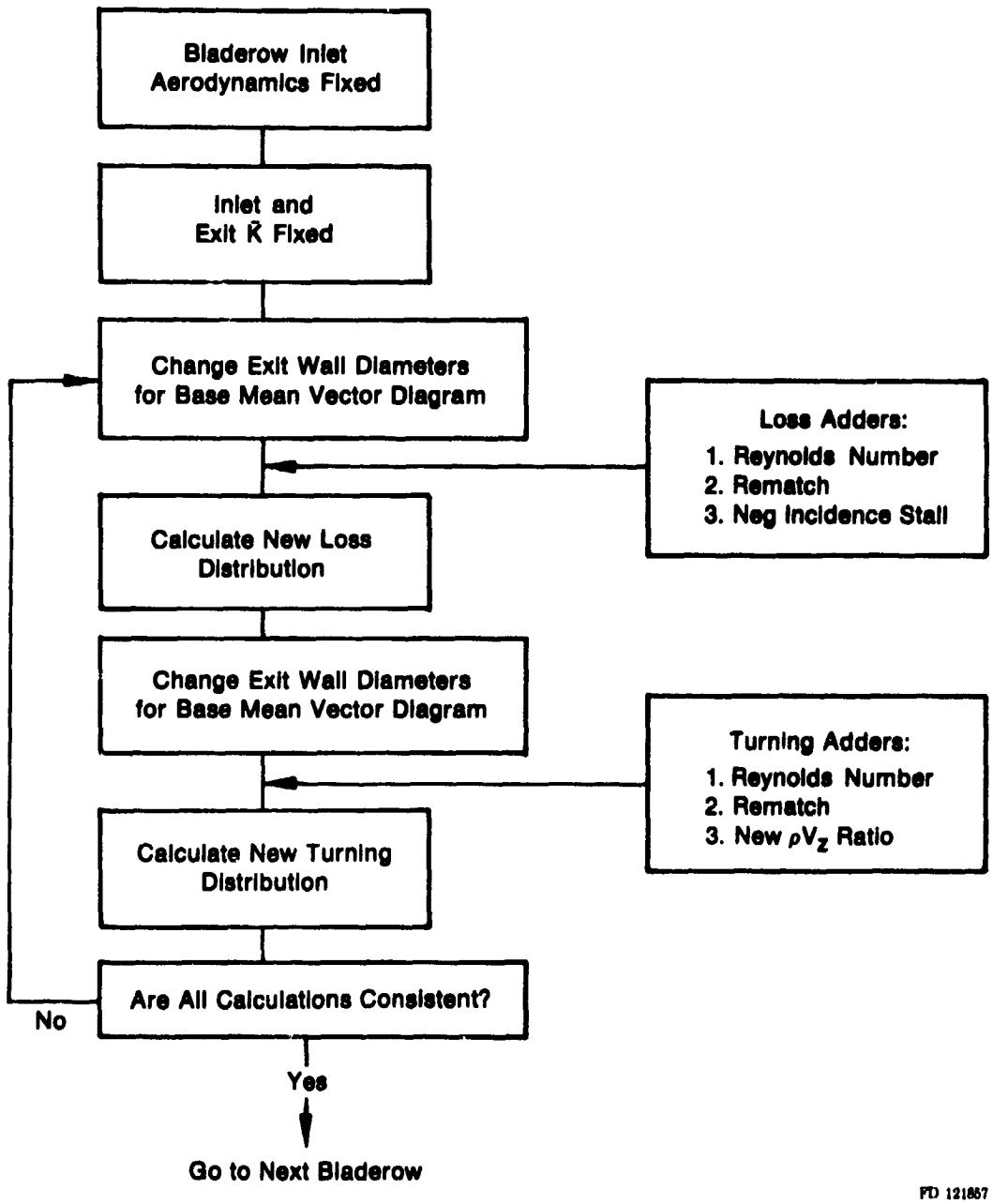

Figure 1. Loss and Turning Iteration

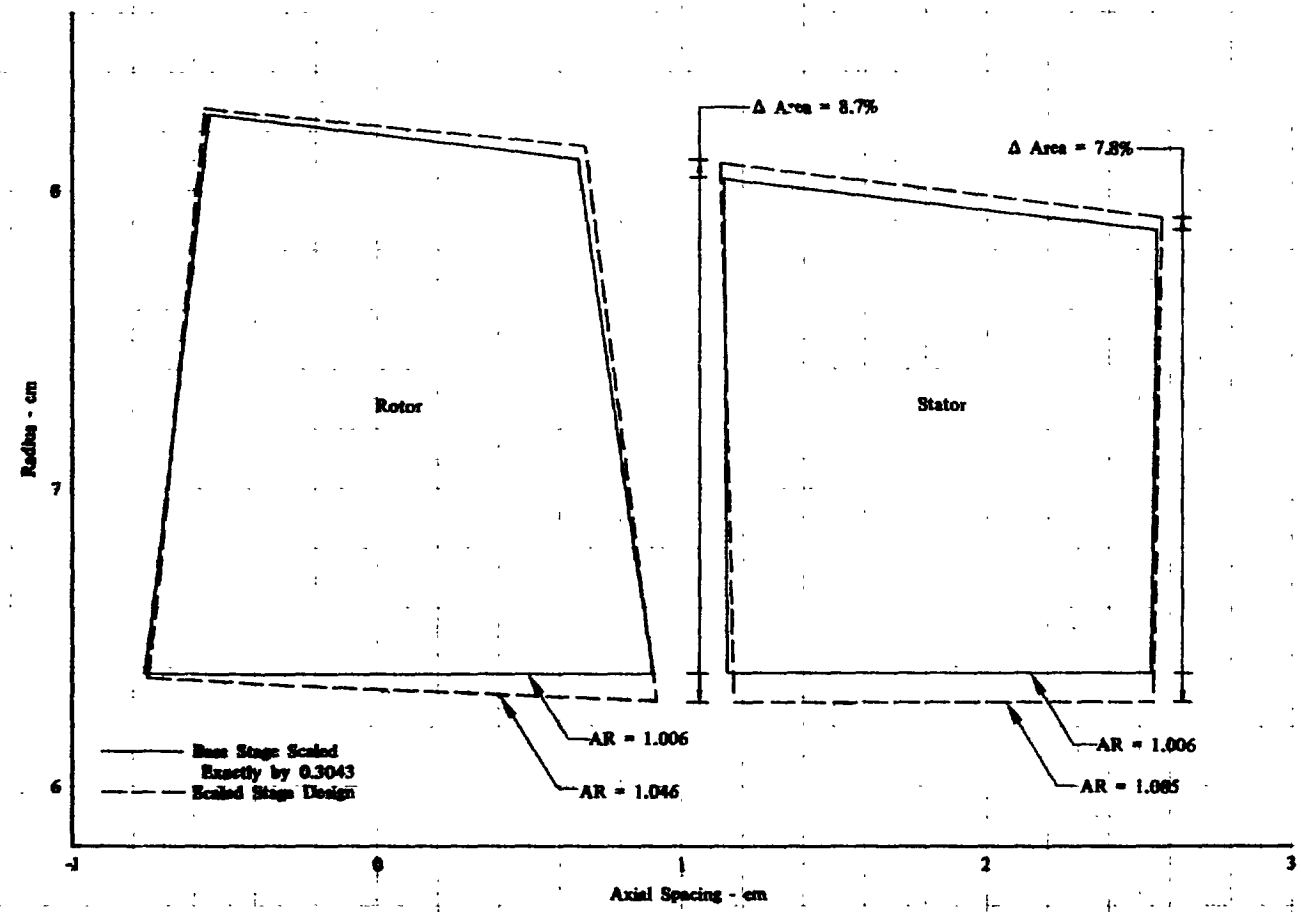

FD 121858

Figure 2. Comparison of Base and Scaled Flowpaths

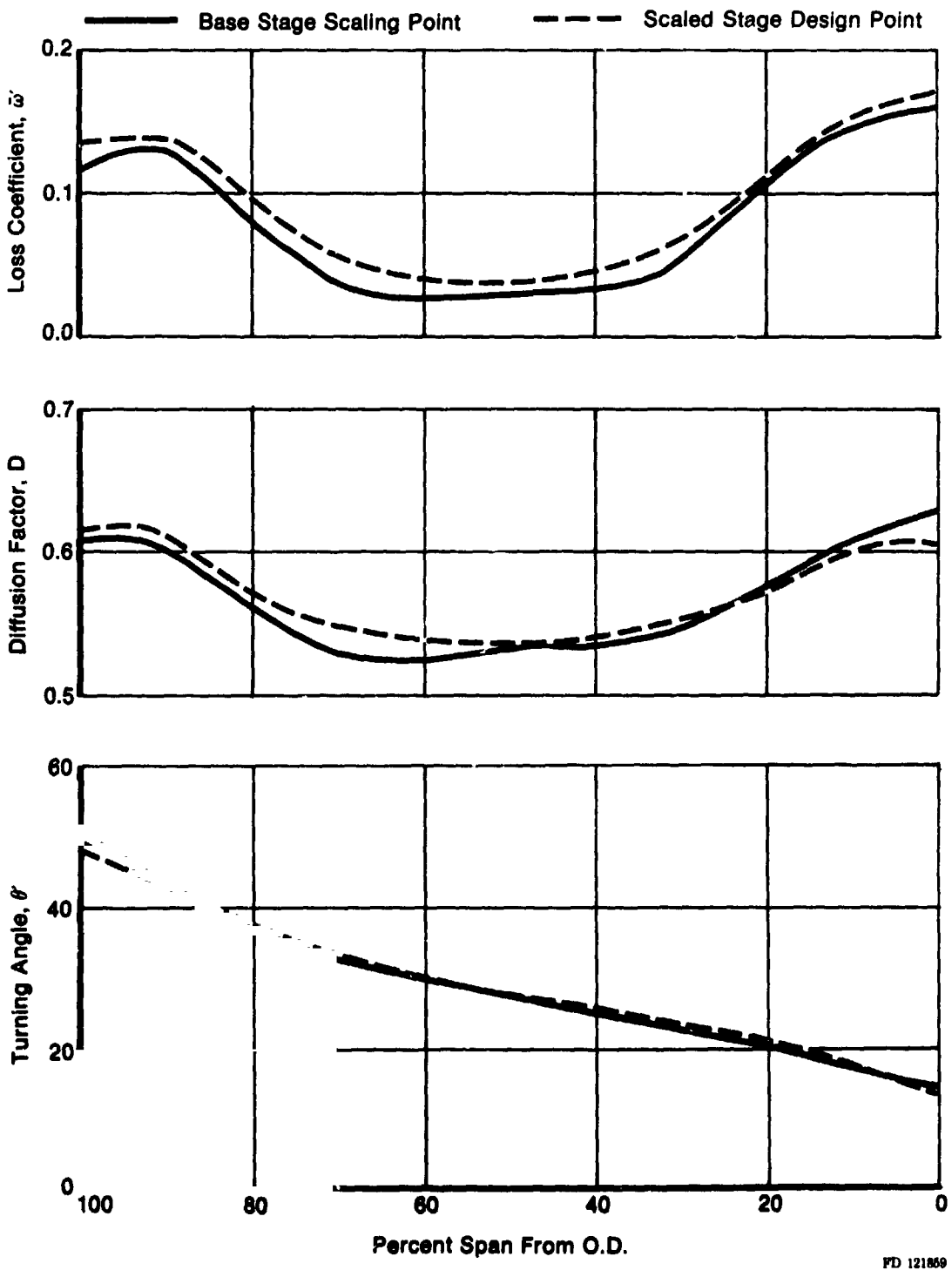

Figure 3. Design Point Rotor Performance

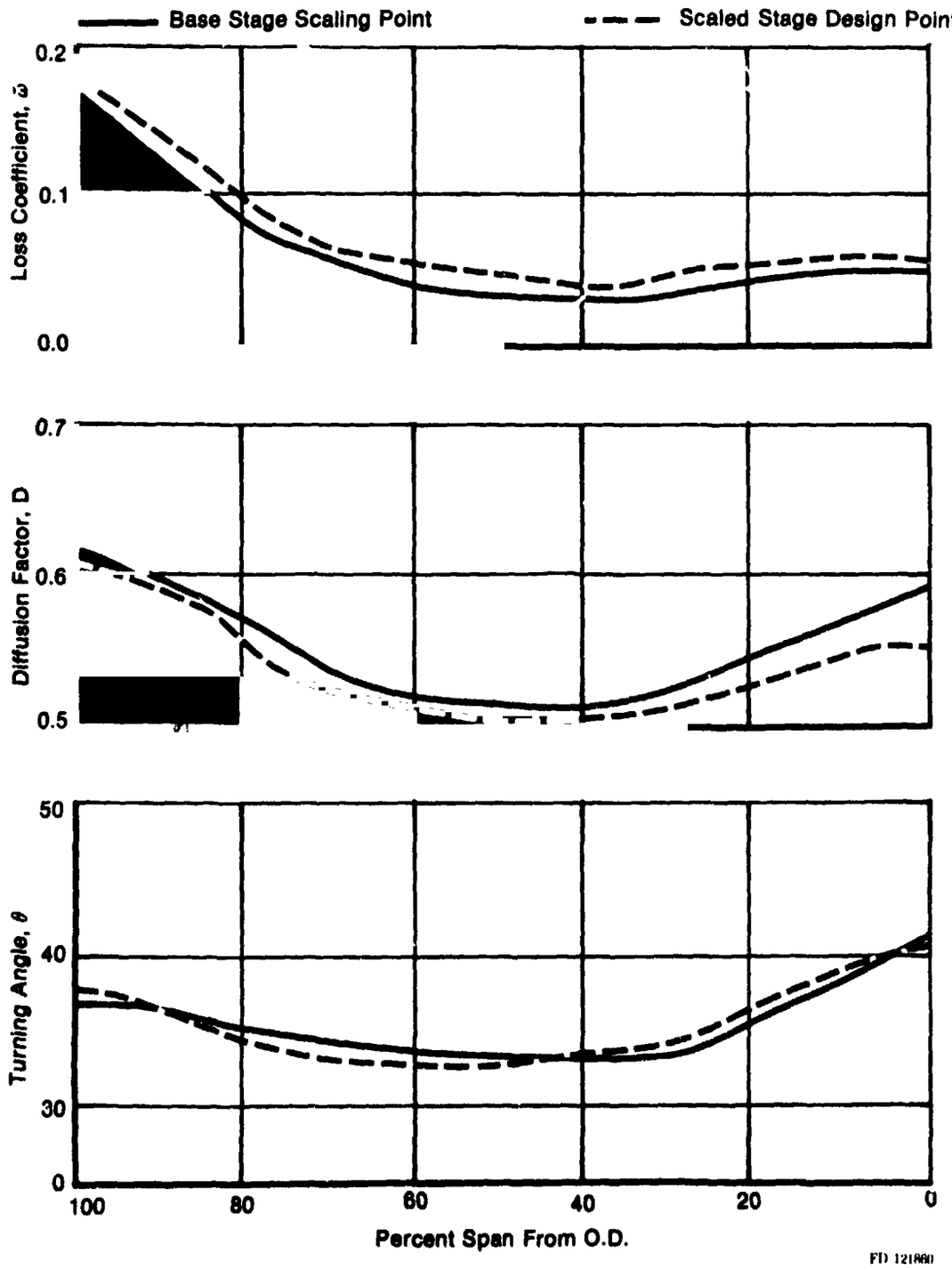

Figure 4. Design Point Stator Performance

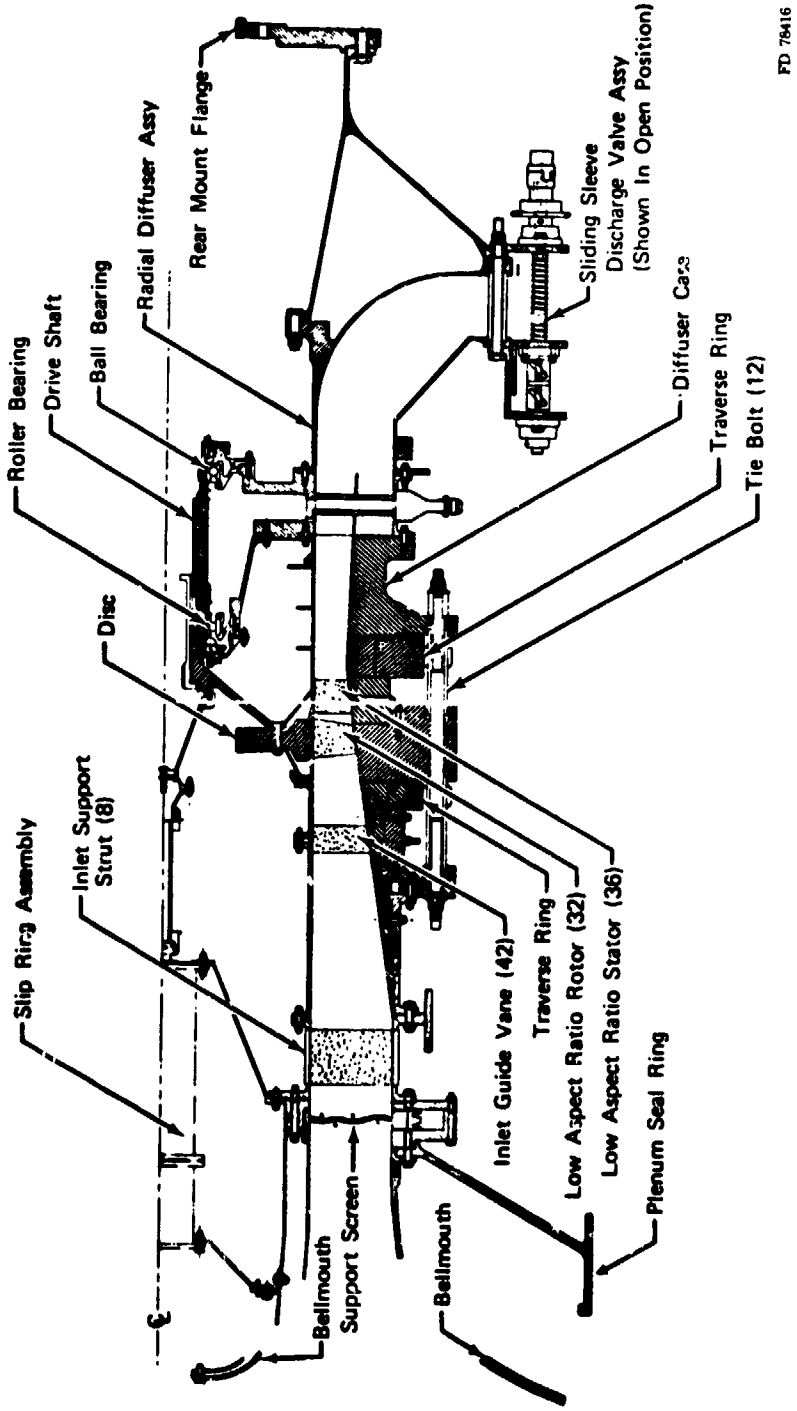

Figure 5. Base Stage Compressor Rig

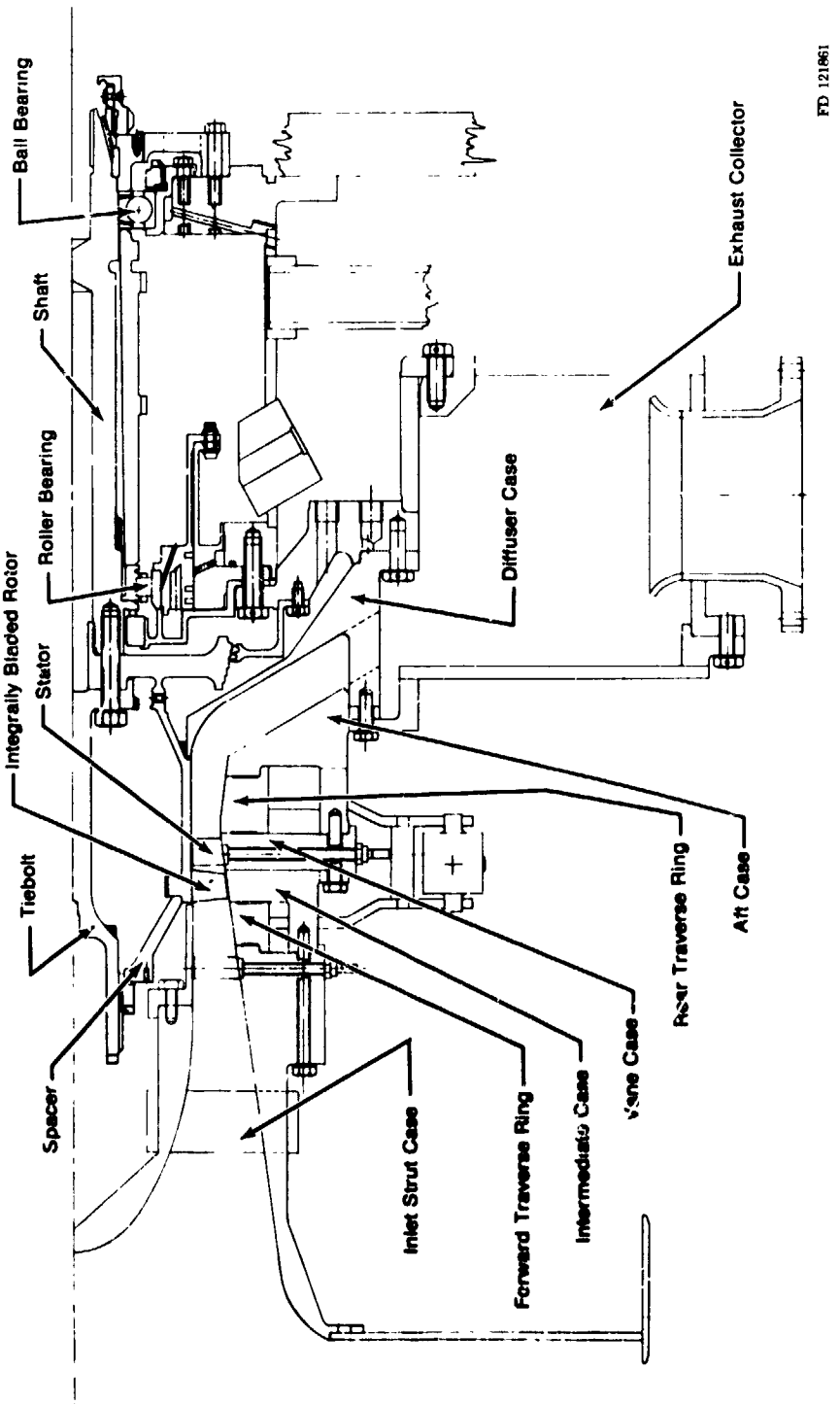

Figure 6. Scaled Stage Compressor Rig

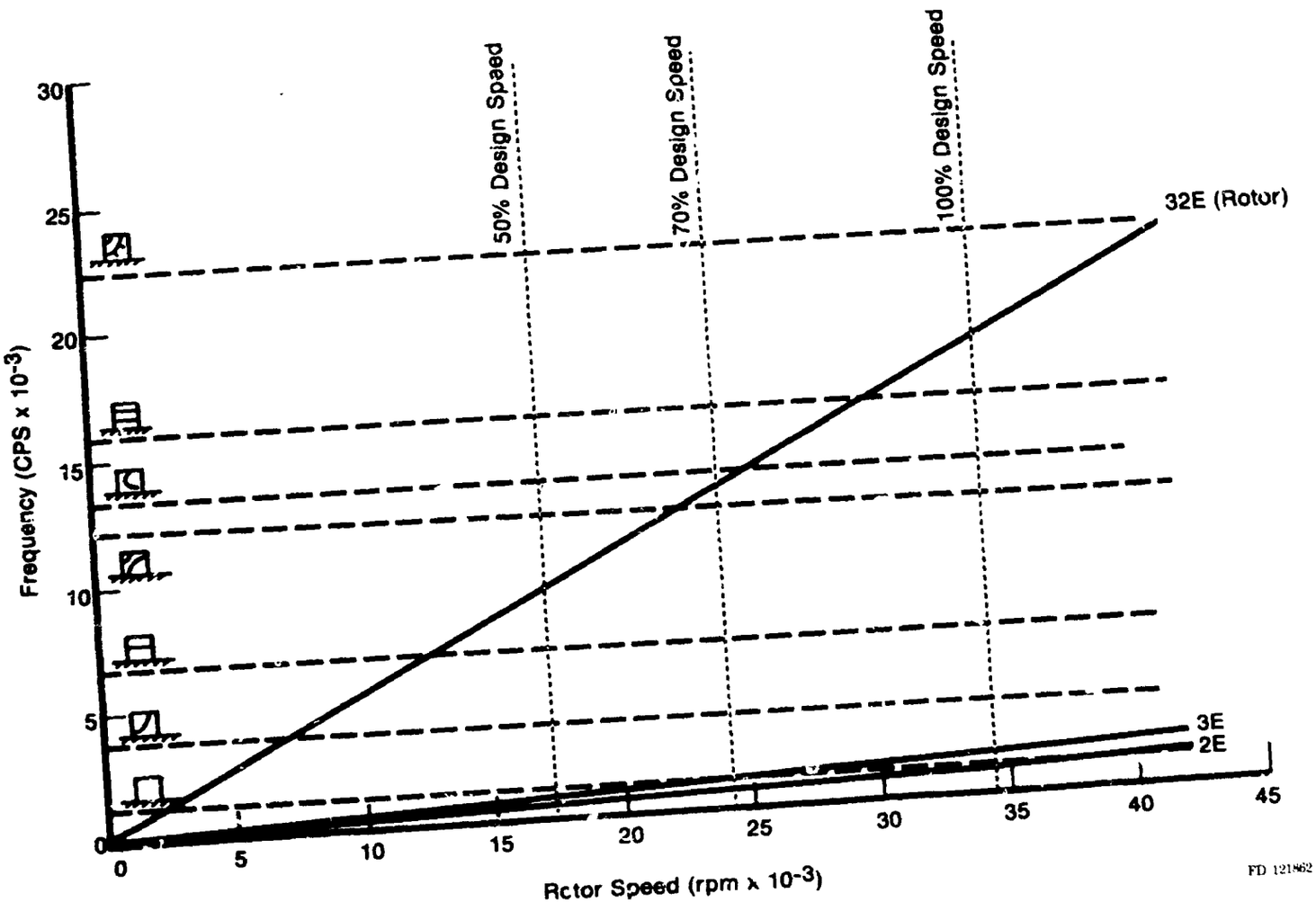

Figure 7. Scaled Stage IGV Campbell Diagram

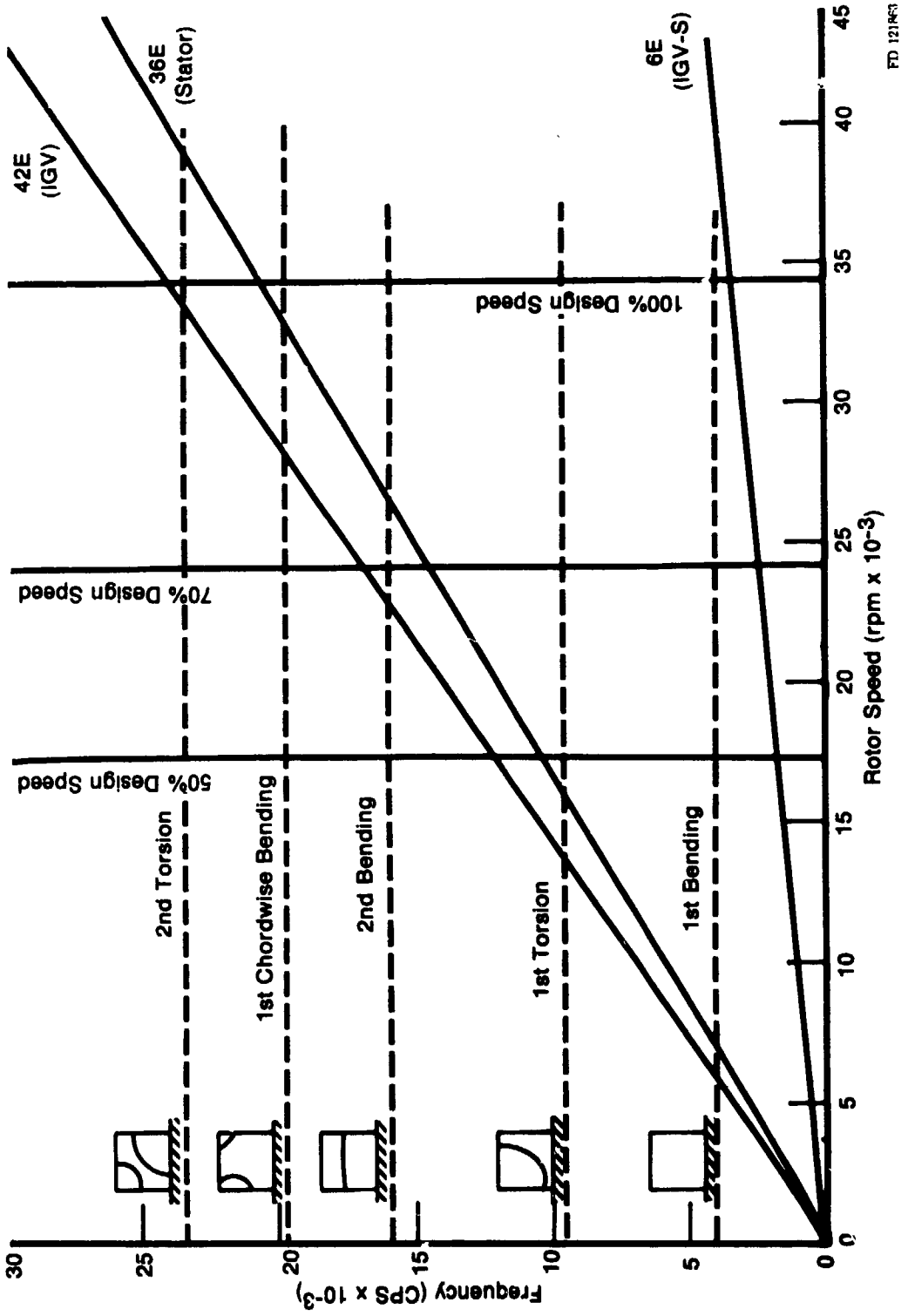

Figure 3. Scaled Stage Rotor Campbell Diagram

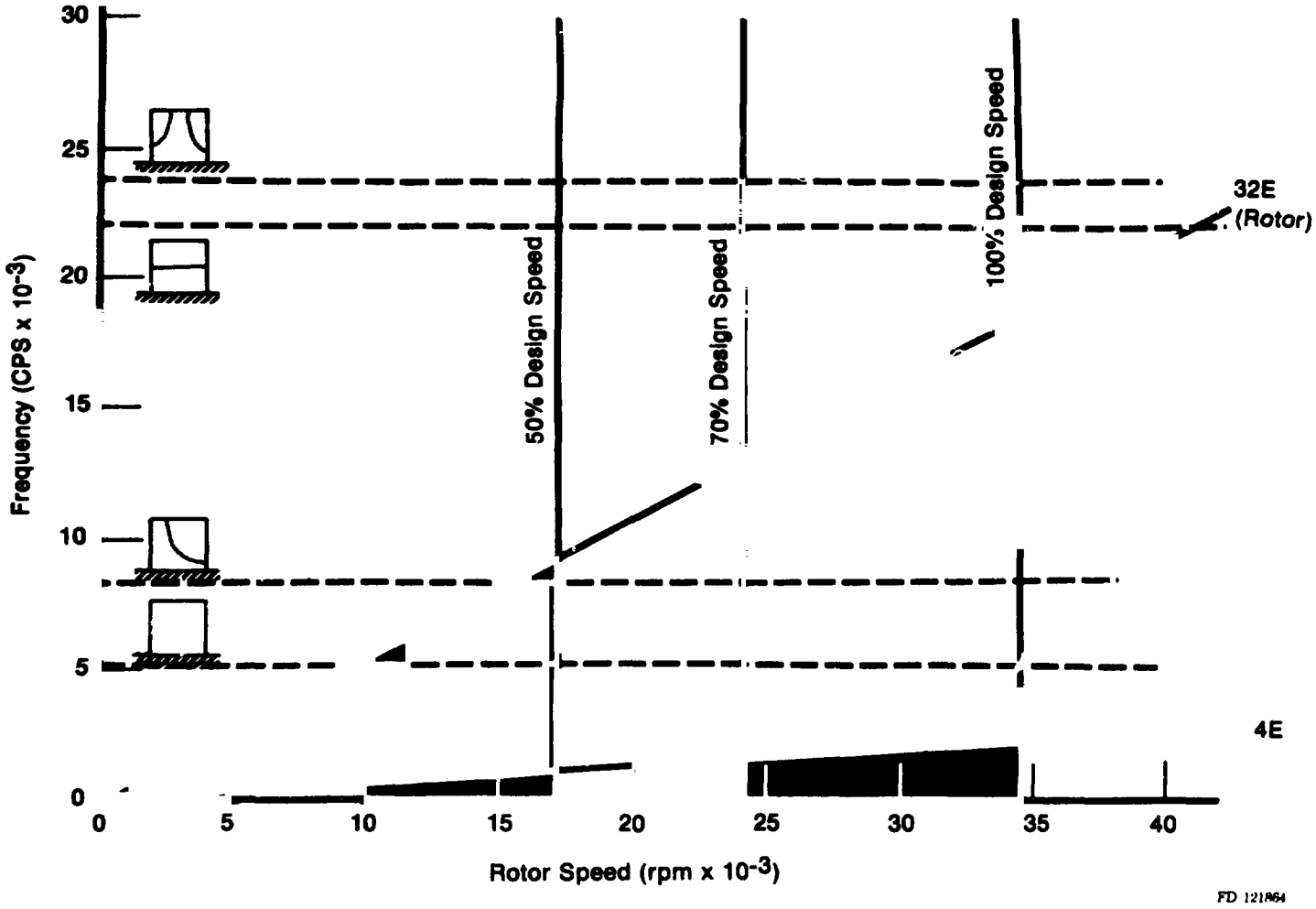

Figure 9. Scaled Stage Stator Campbell Diagram

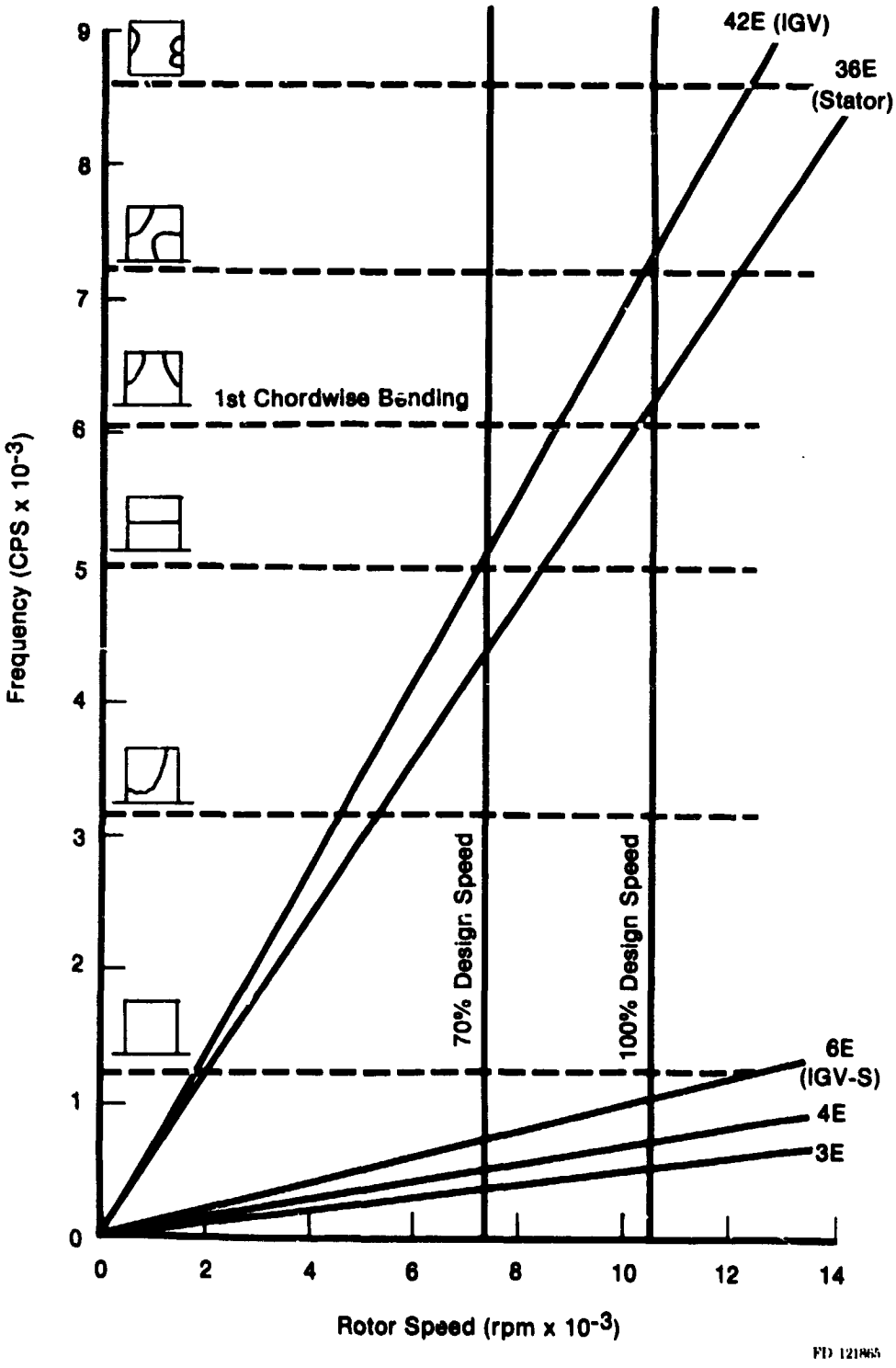

Figure 10. Base Stage Rotor Campbell Diagram

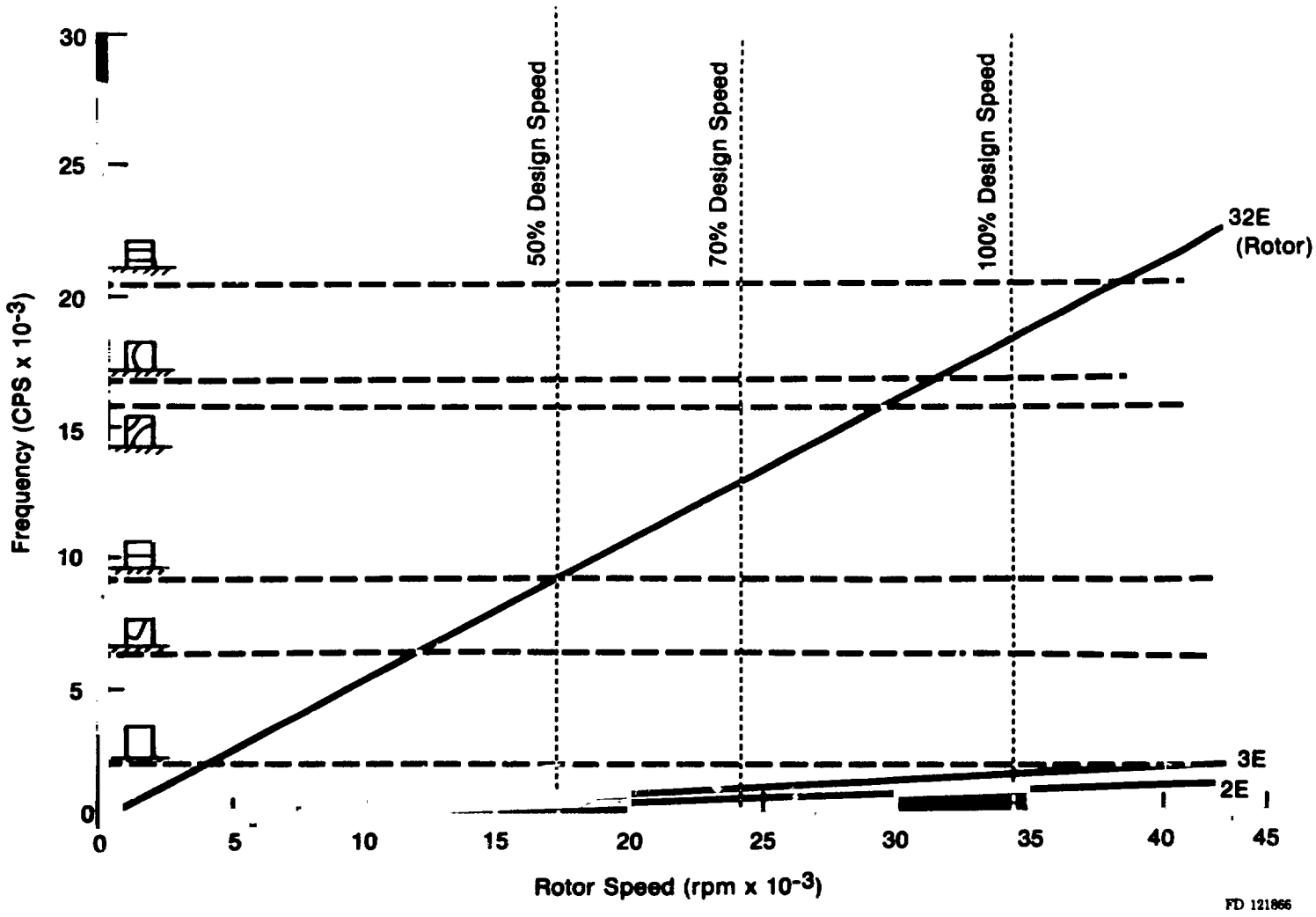

Figure 11. Scaled Stage Revised IGV Campbell Diagram

FE 147564

Figure 12. Comparison of Base and Scaled Stage Blading

a. IGV INLET TOTAL AND STATIC PRESSURE, ROTOR INLET, STATOR EXIT AIR ANGLE AND STATIC PRESSURE 30-deg PROBE, RADIAL TRAVERSE

b. IGV EXIT TOTAL PRESSURE, 5 SENSOR RADIAL RAKES, CIRCUMFERENTIAL TRAVERSE

c. STATOR EXIT TOTAL PRESSURE, TOTAL TEMPERATURE, 5 SENSOR RADIAL RAKES, CIRCUMFERENTIAL TRAVERSE

FD 87786

Figure 13. Fuse Stage Traverse Instrumentation

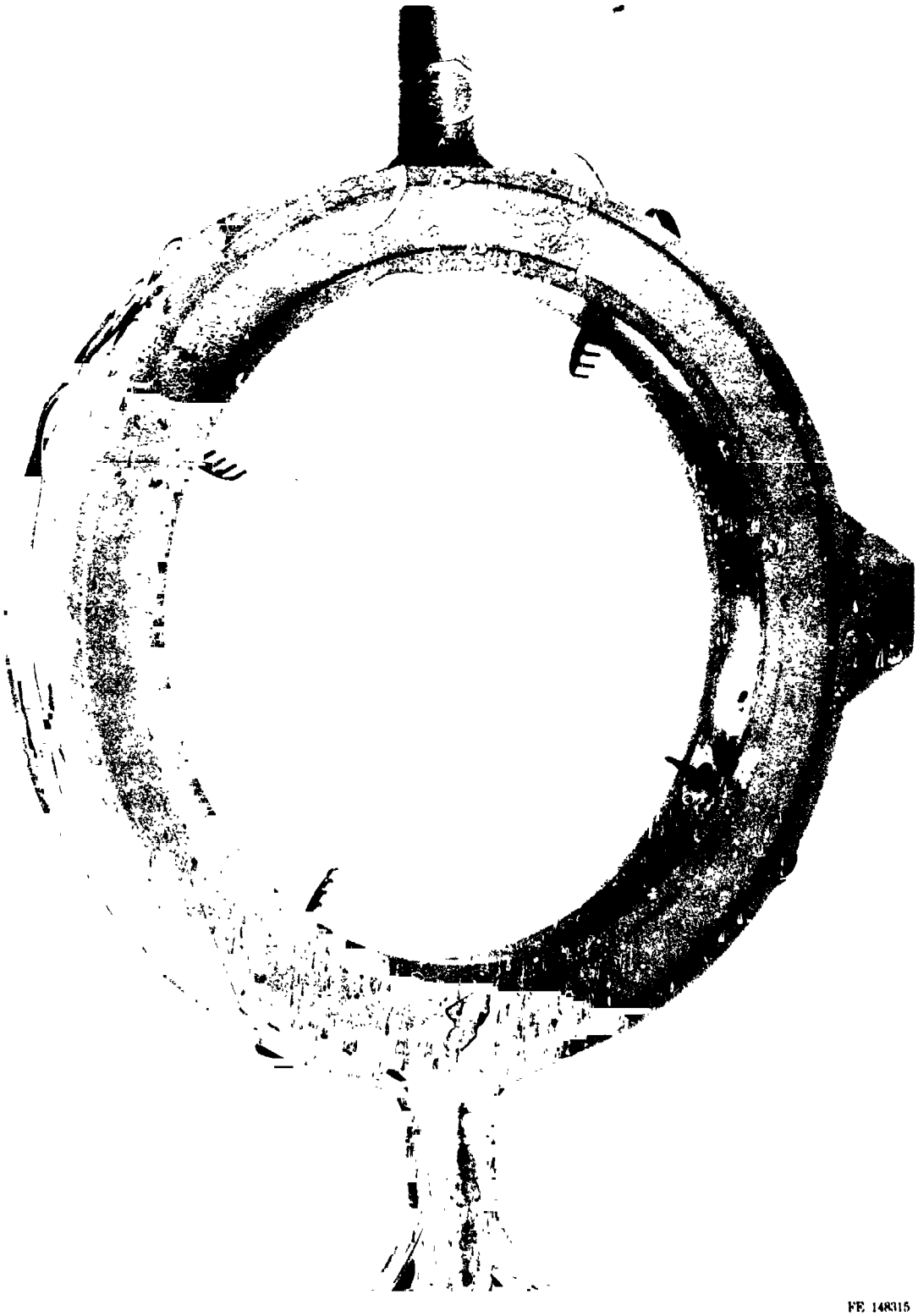

FE 148315

Figure 14. Scaled Stage Station 4 Traverse Ring Assembly

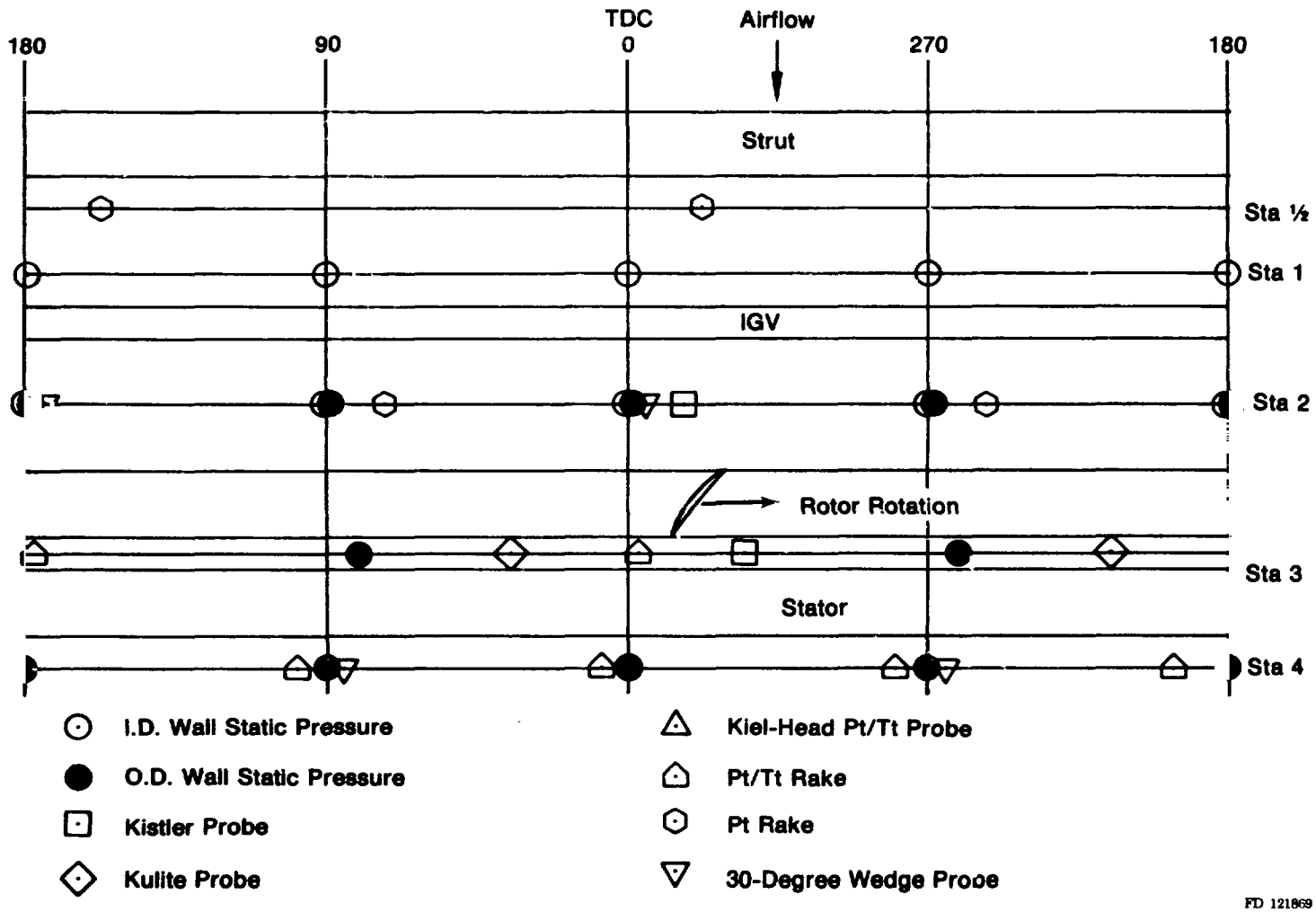

Figure 15. Base Stage Instrumentation Unwrap

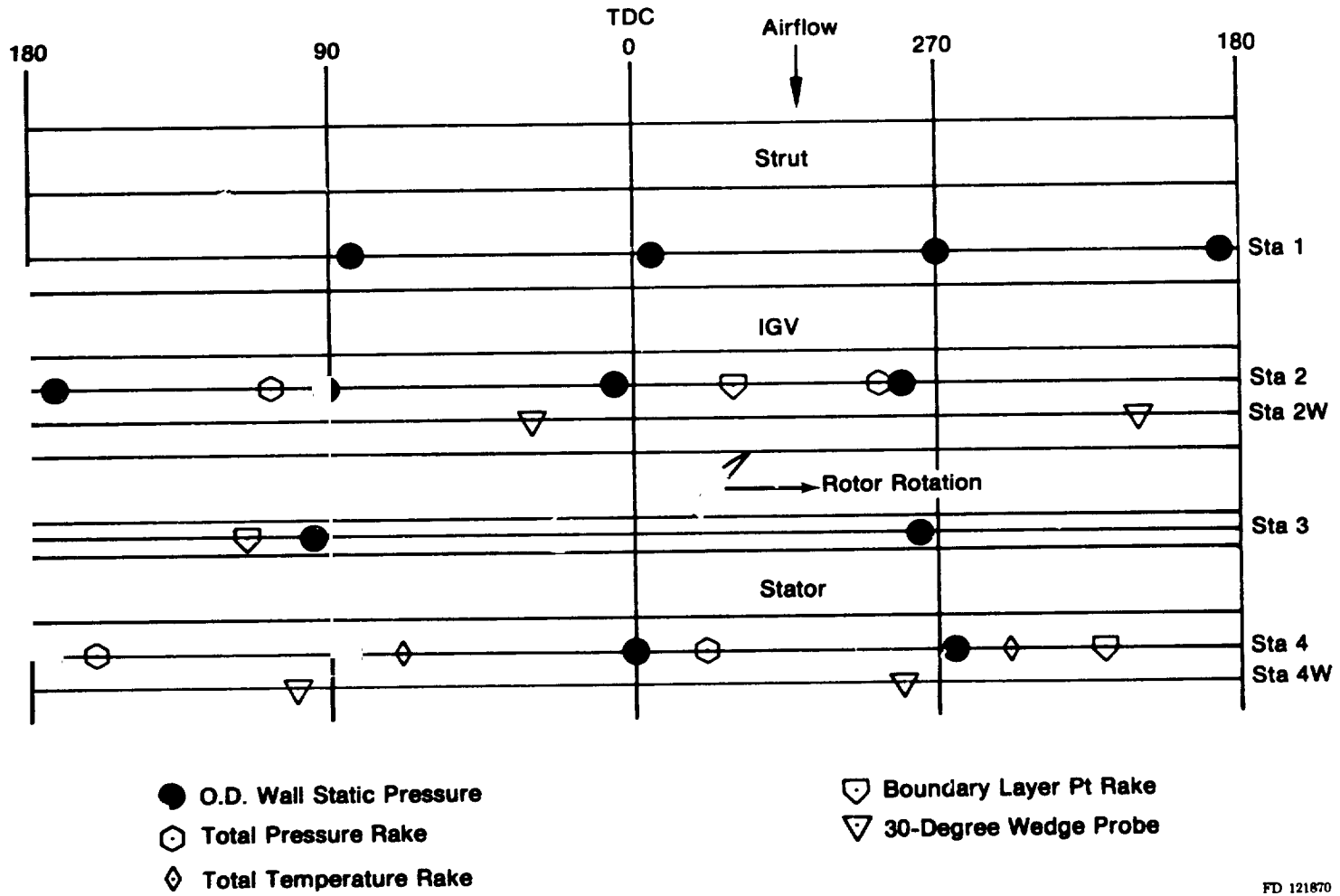

Figure 16. Scaled Stage Instrumentation Unwrap

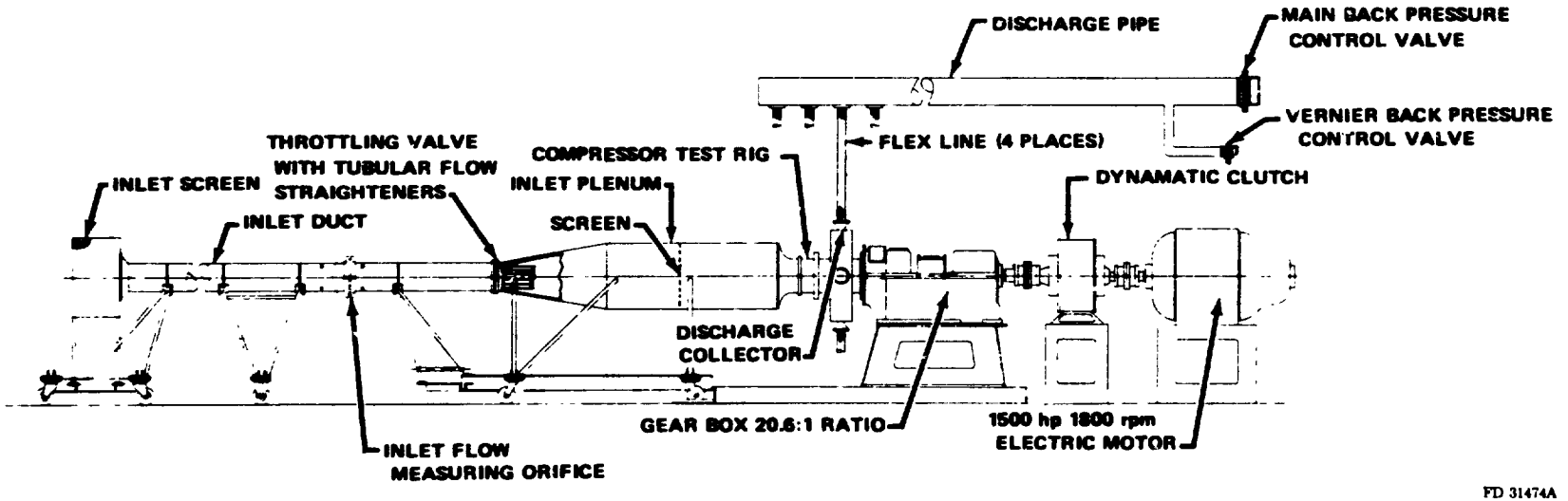

Figure 17. Elevation View of B-33 Compressor Test Stand

FE 96198

Figure 18. Base Stage Mounted in B-33 Compressor Test Stand

FE 339280

Figure 19. Scaled Stage Mounted in B-33 Compressor Test Stand

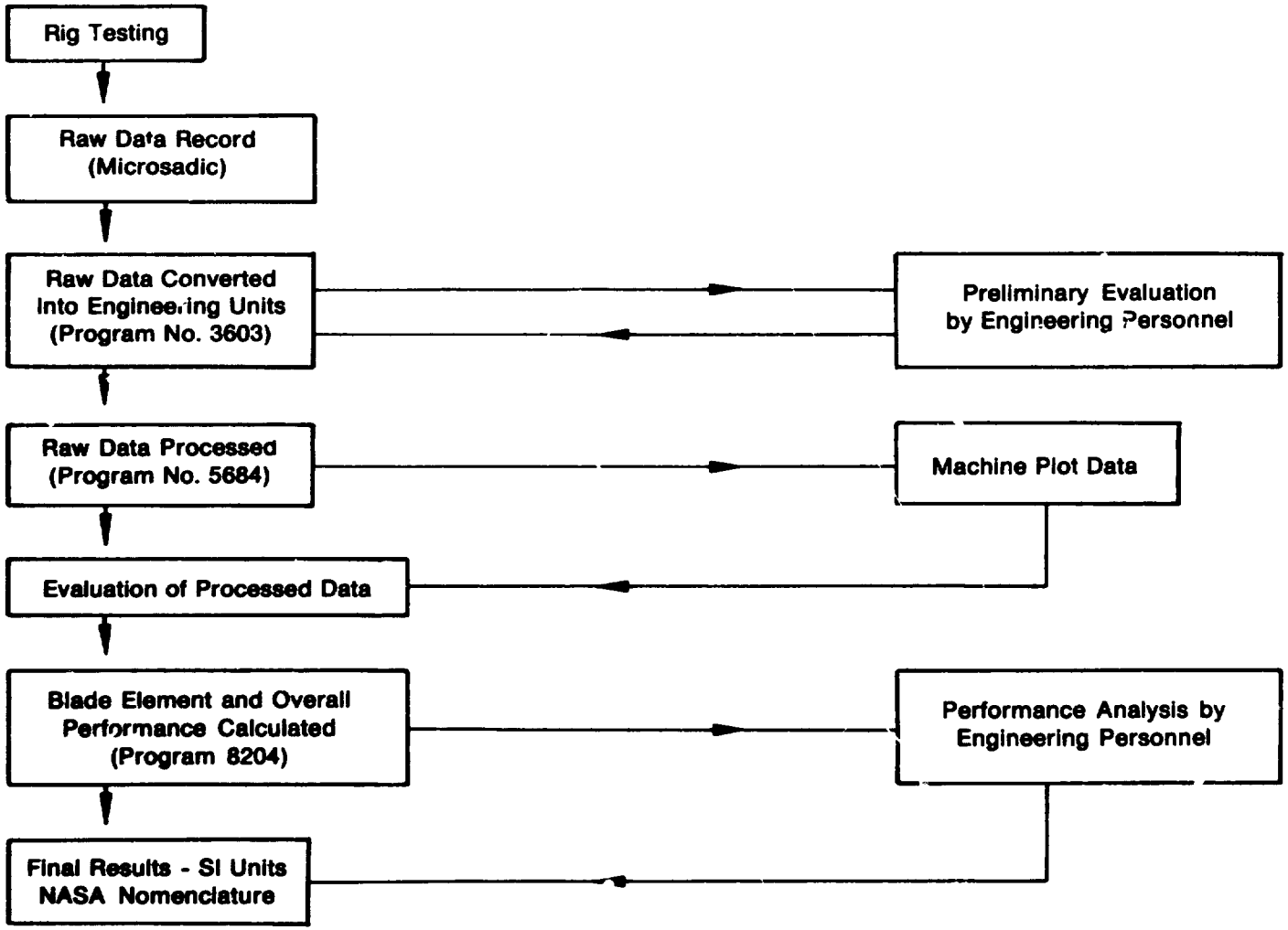

Figure 20. Data Reduction Procedure for Low Aspect Ratio Small Axial Compressor Stage

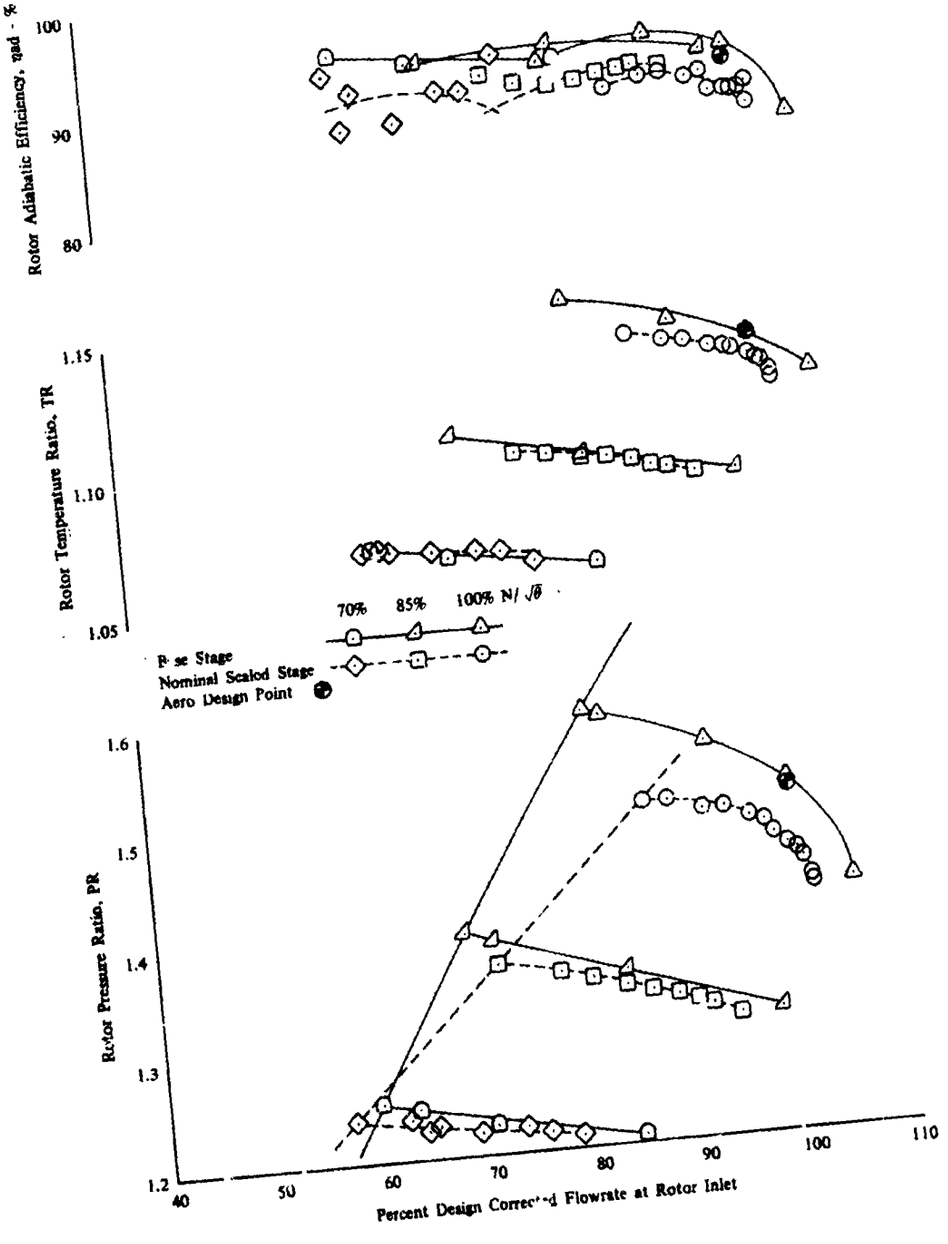

Figure 21. Effect of Scale on Rotor Performance

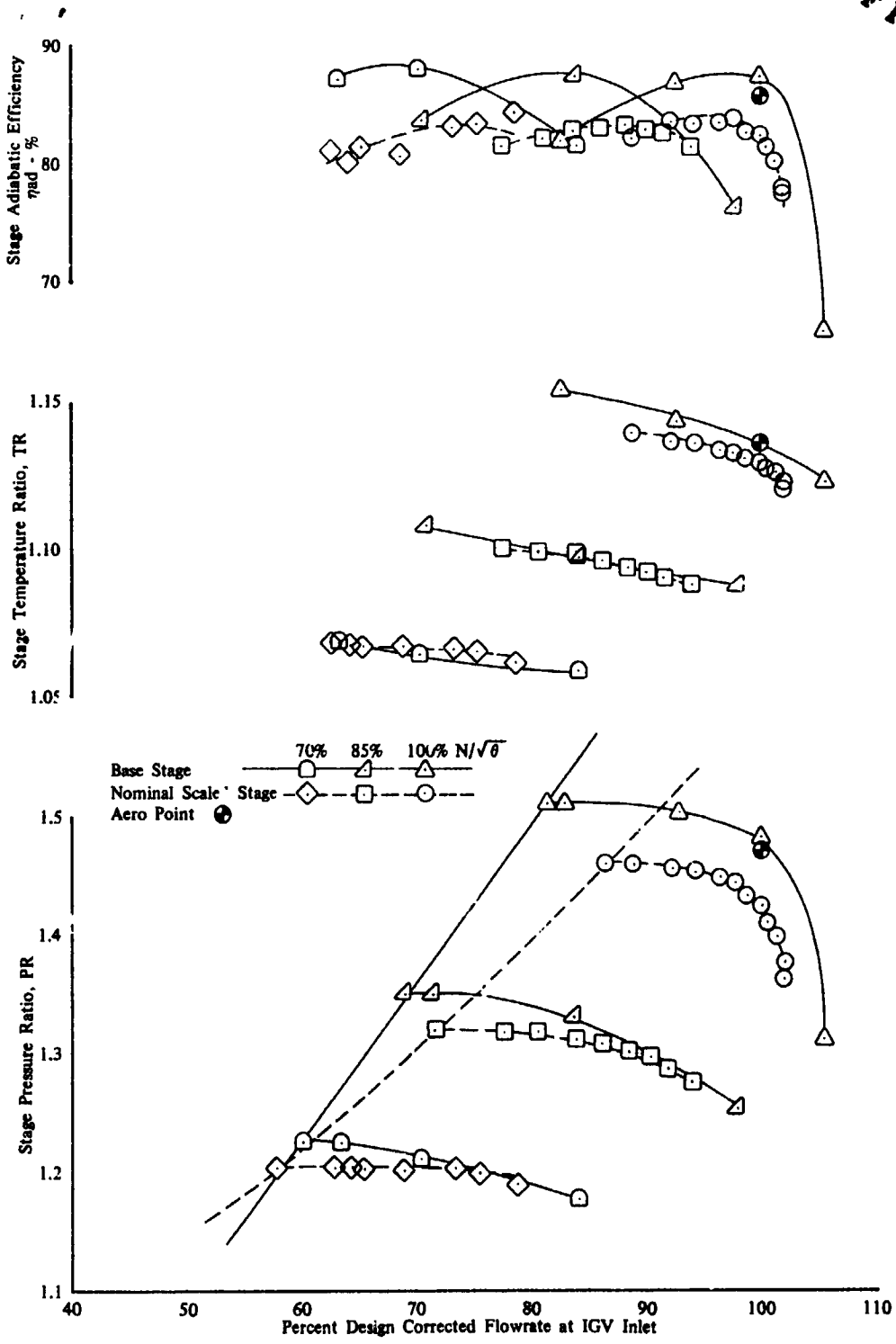

DF 103868

Figure 22. Effect of Scale on Stage Performance

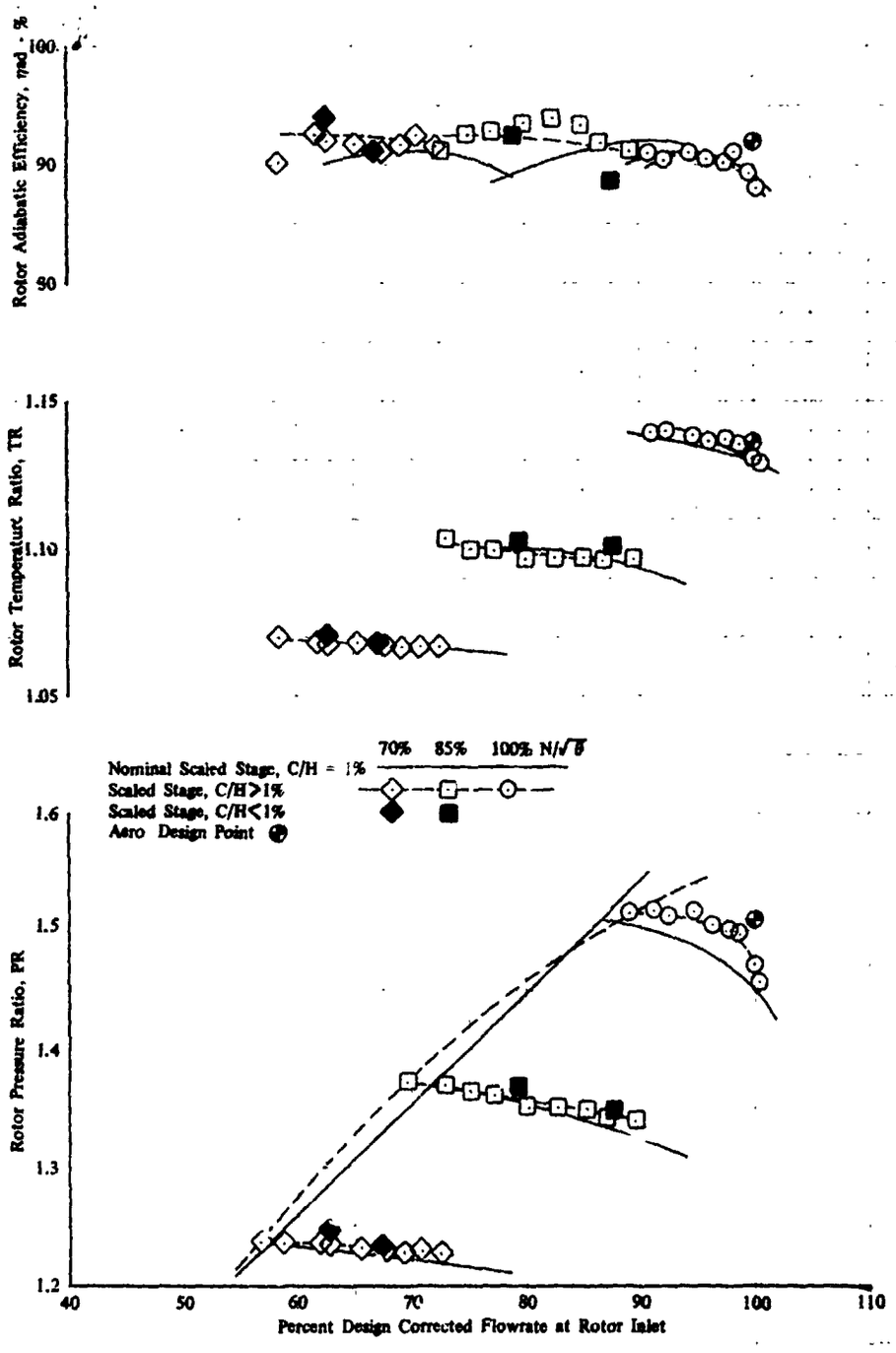

Figure 23. Effect of Clearance on Rotor Performance

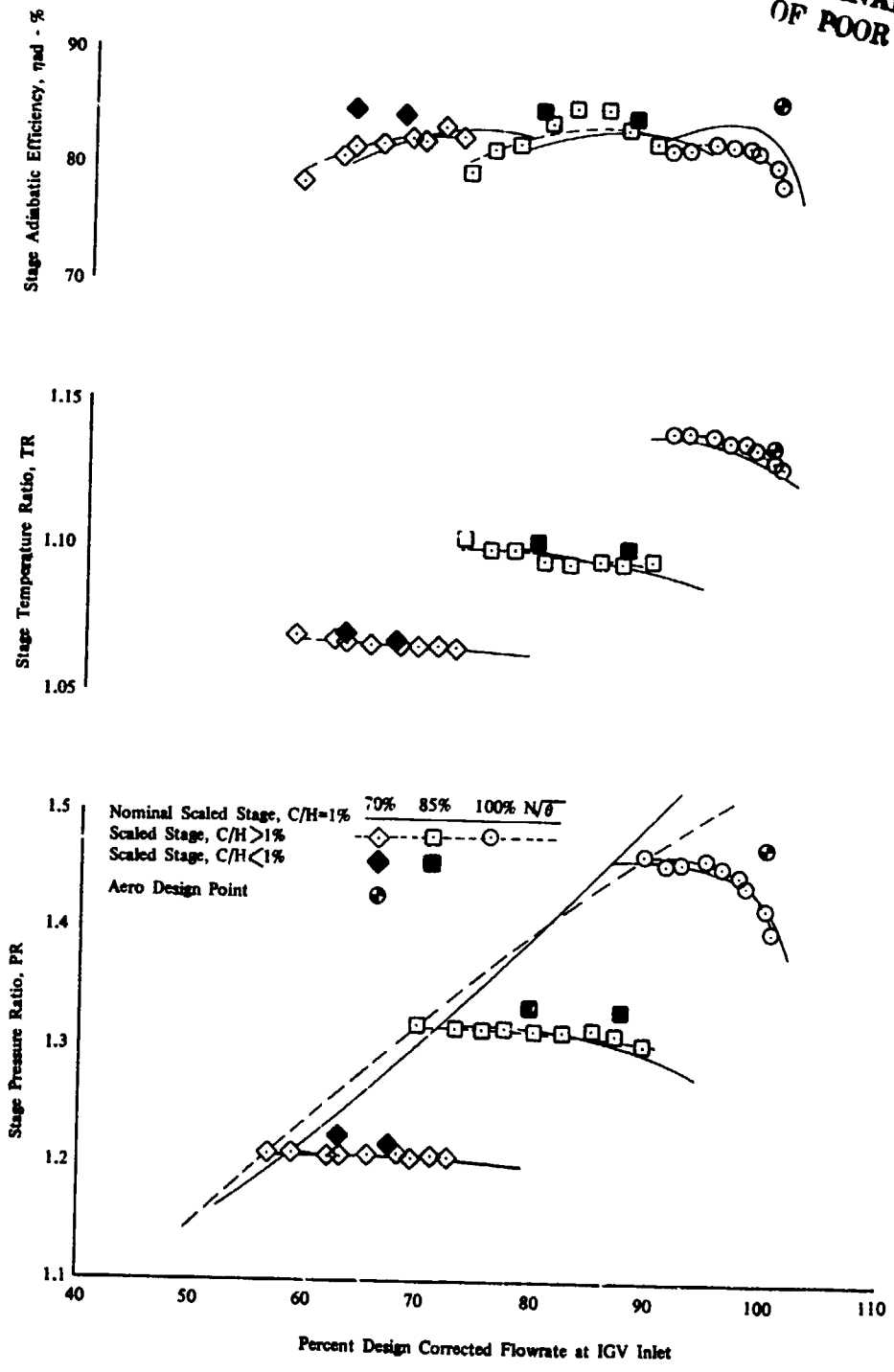

DF 103870

Figure 24. Effect of Clearance on Stage Performance

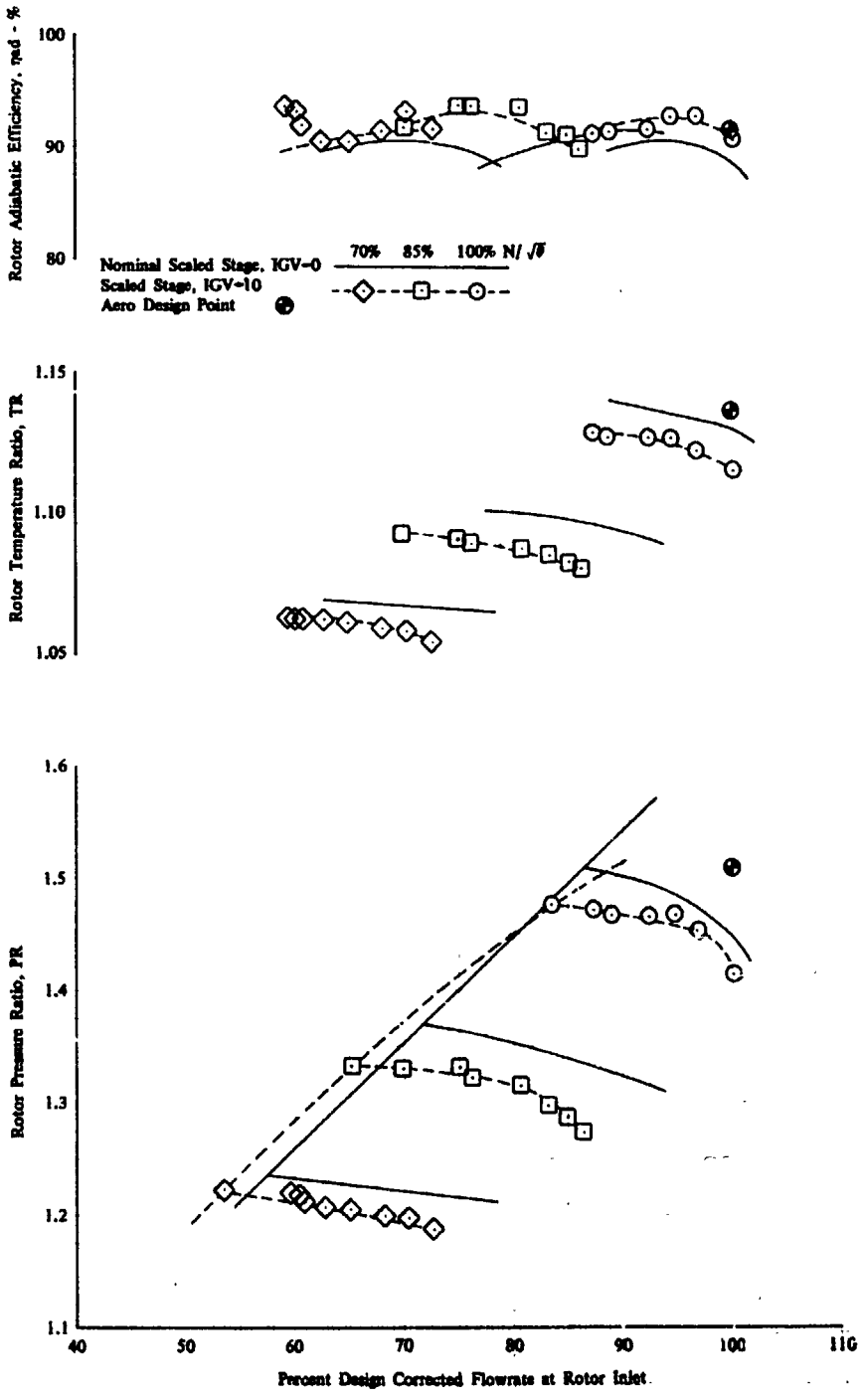

Figure 25. Effect of 10 deg More Prewhirl on Rotor Performance

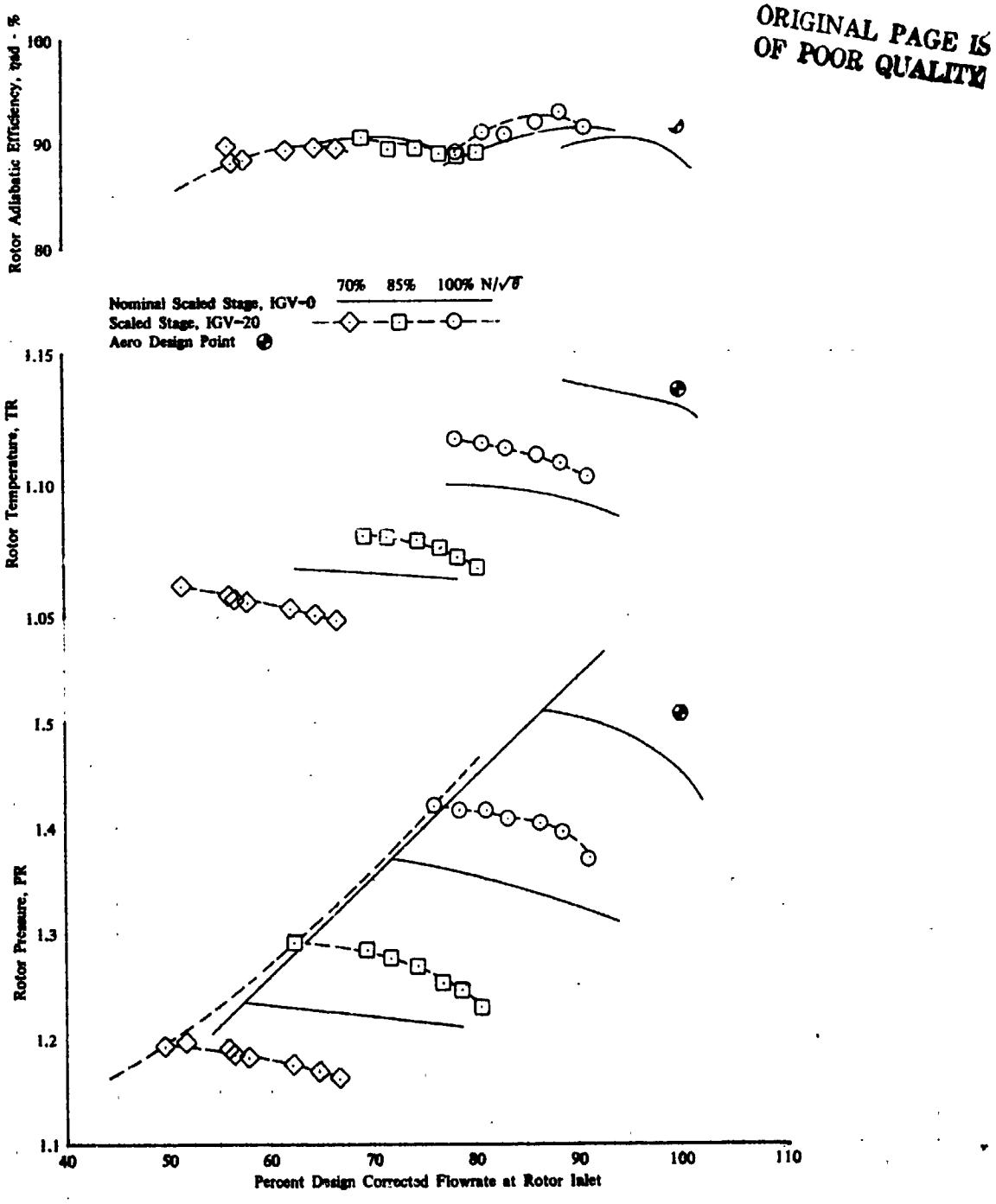

DF 103872

Figure 26. Effect of 20 deg More Prewhirl on Rotor Performance

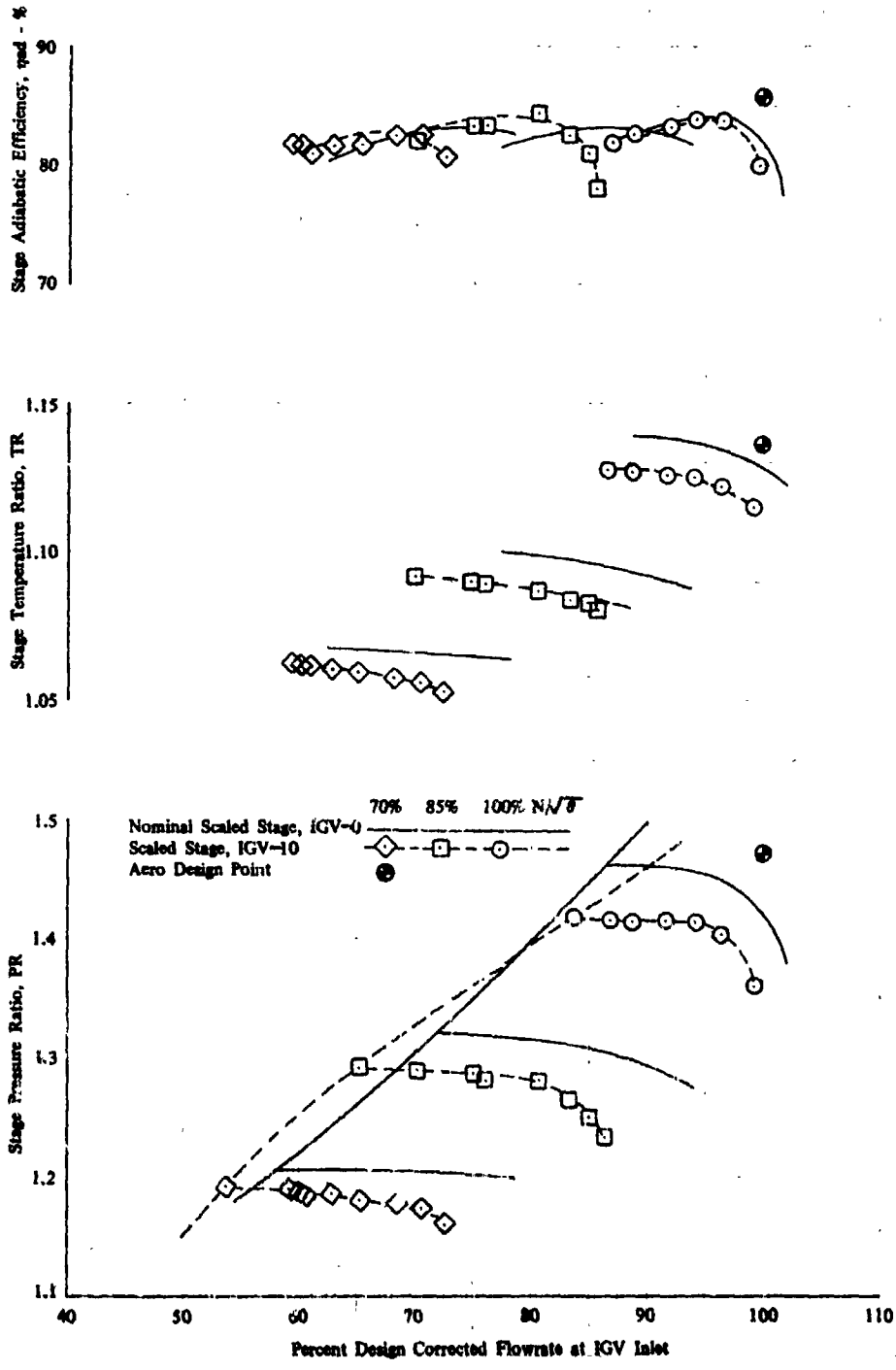

DF 103873

Figure 27. Effect of 10 deg More Prewhirl on Stage Performance

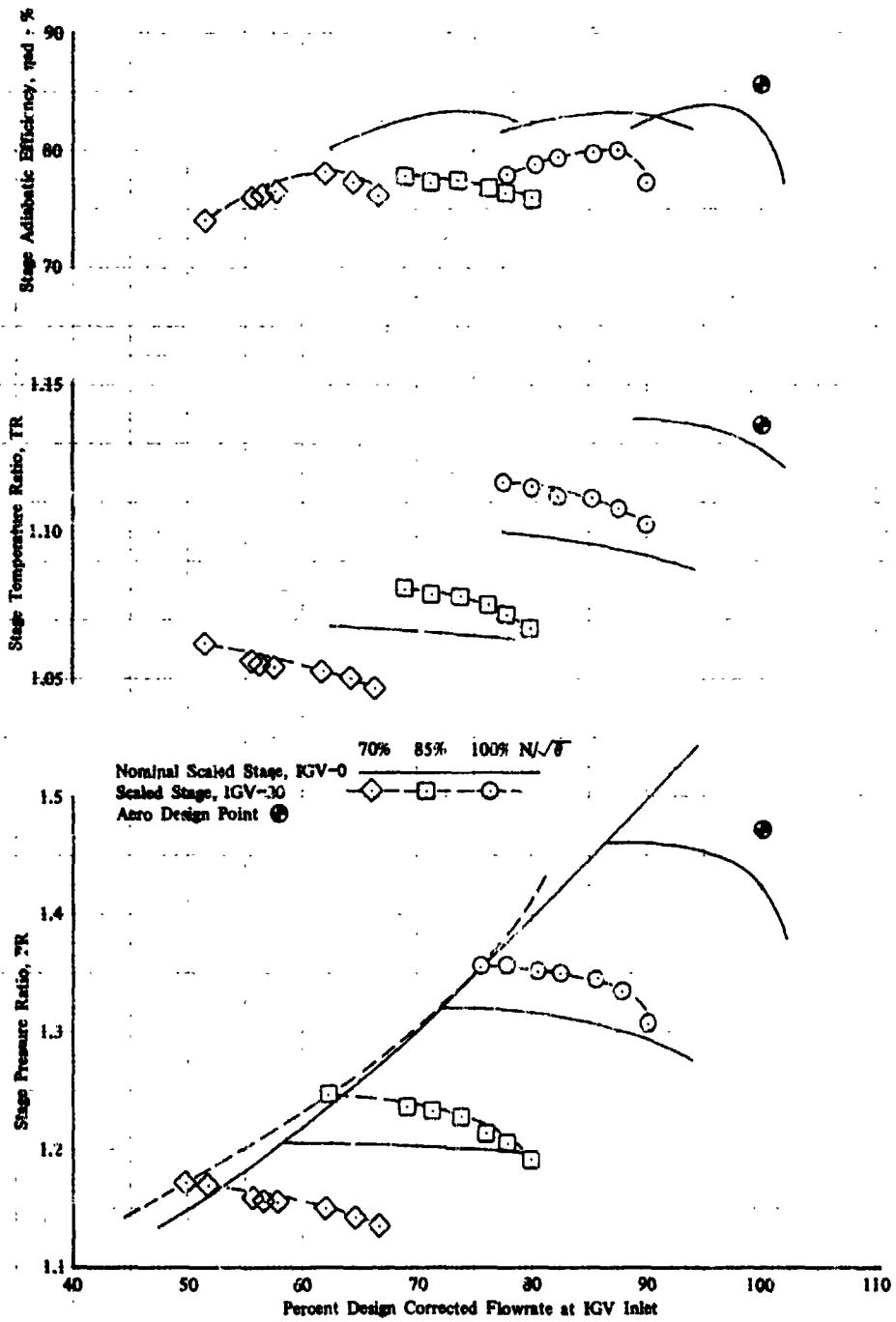

DF 103874

Figure 28. Effect of 20 deg More Prewhirl on Stage Performance

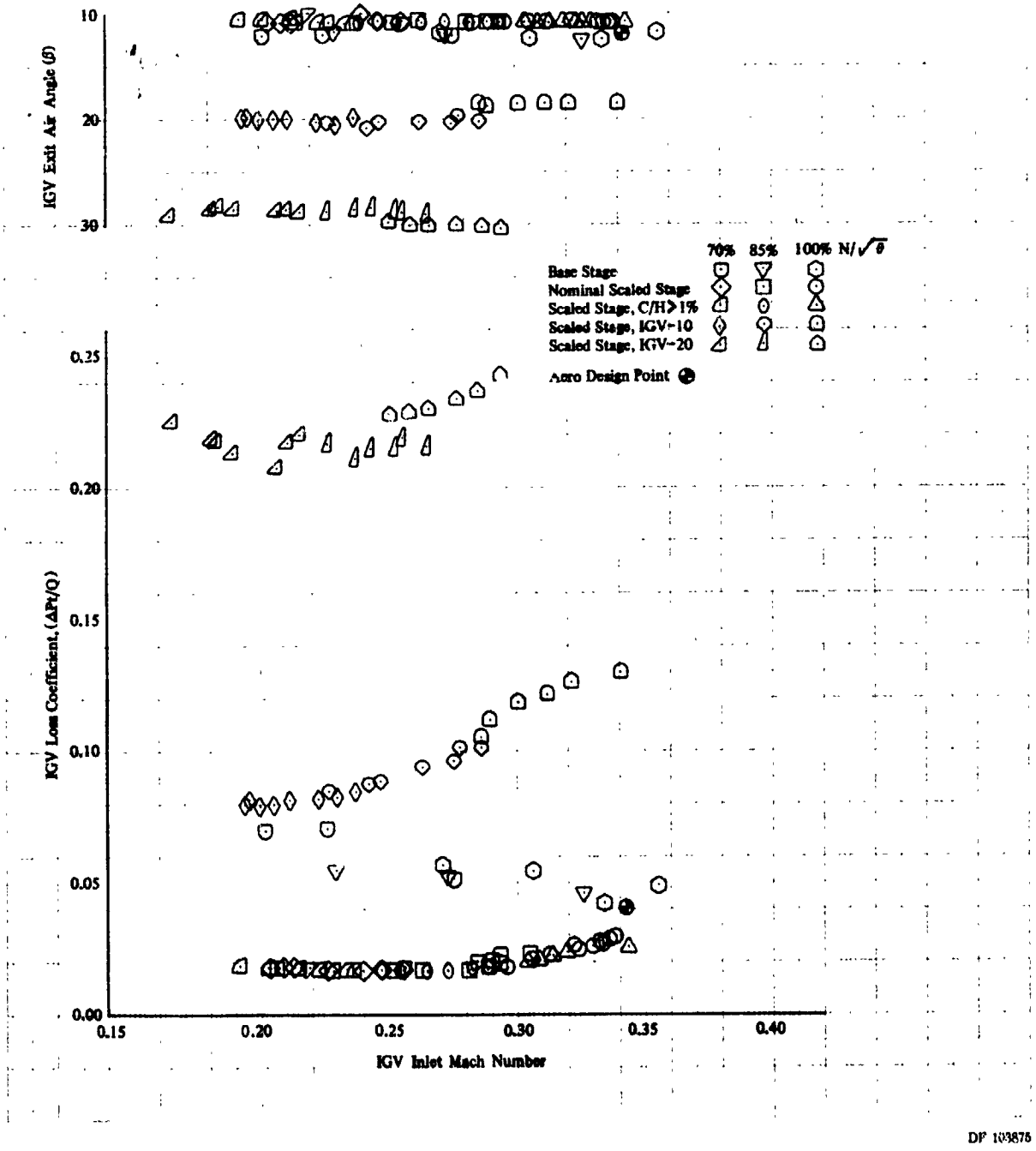

Figure 29. Average IGV Exit Air Angle and Loss vs Inlet Mach Number

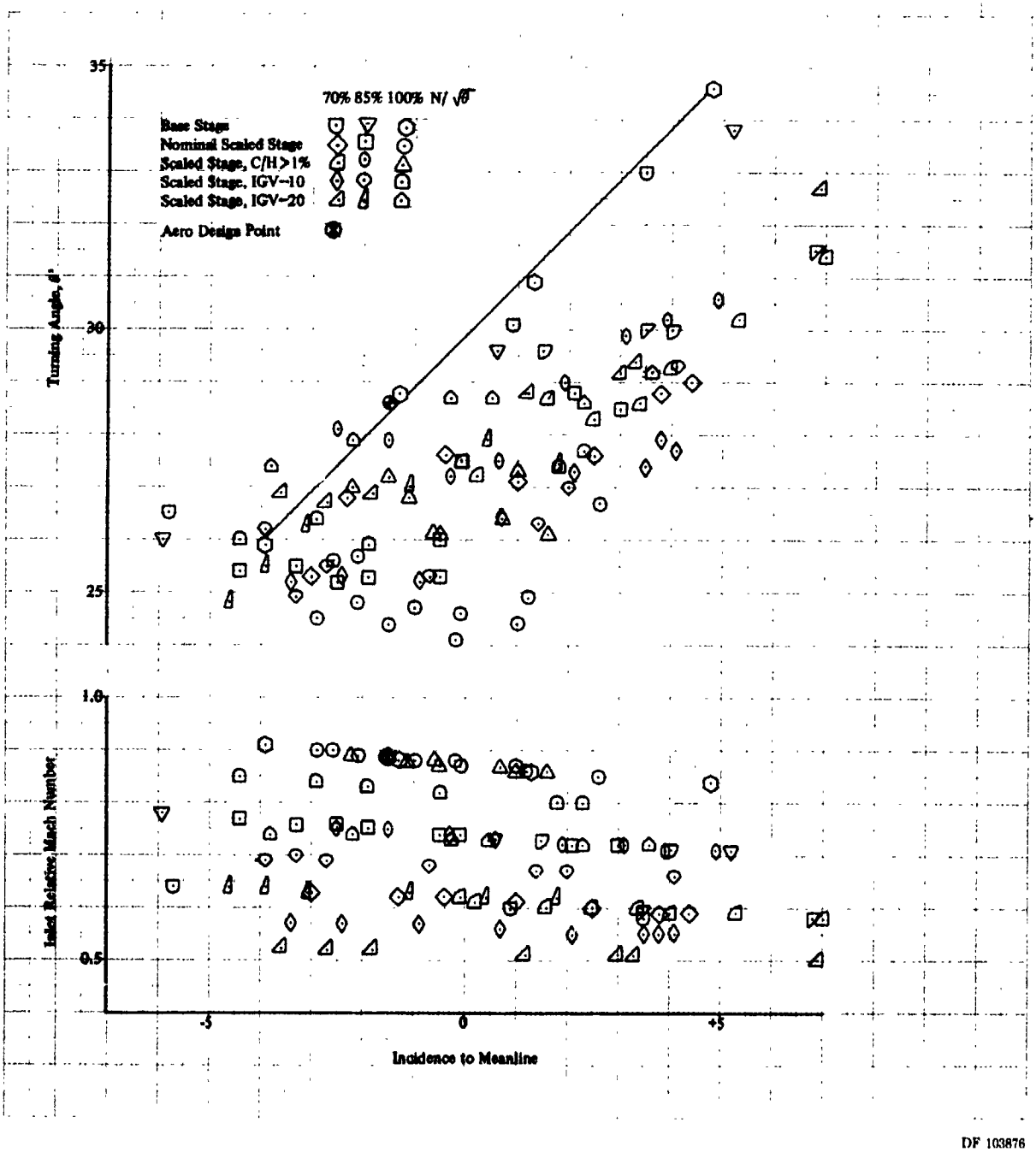

Figure 30. Average Rotor Turning and Inlet Relative Mach Number vs Incidence

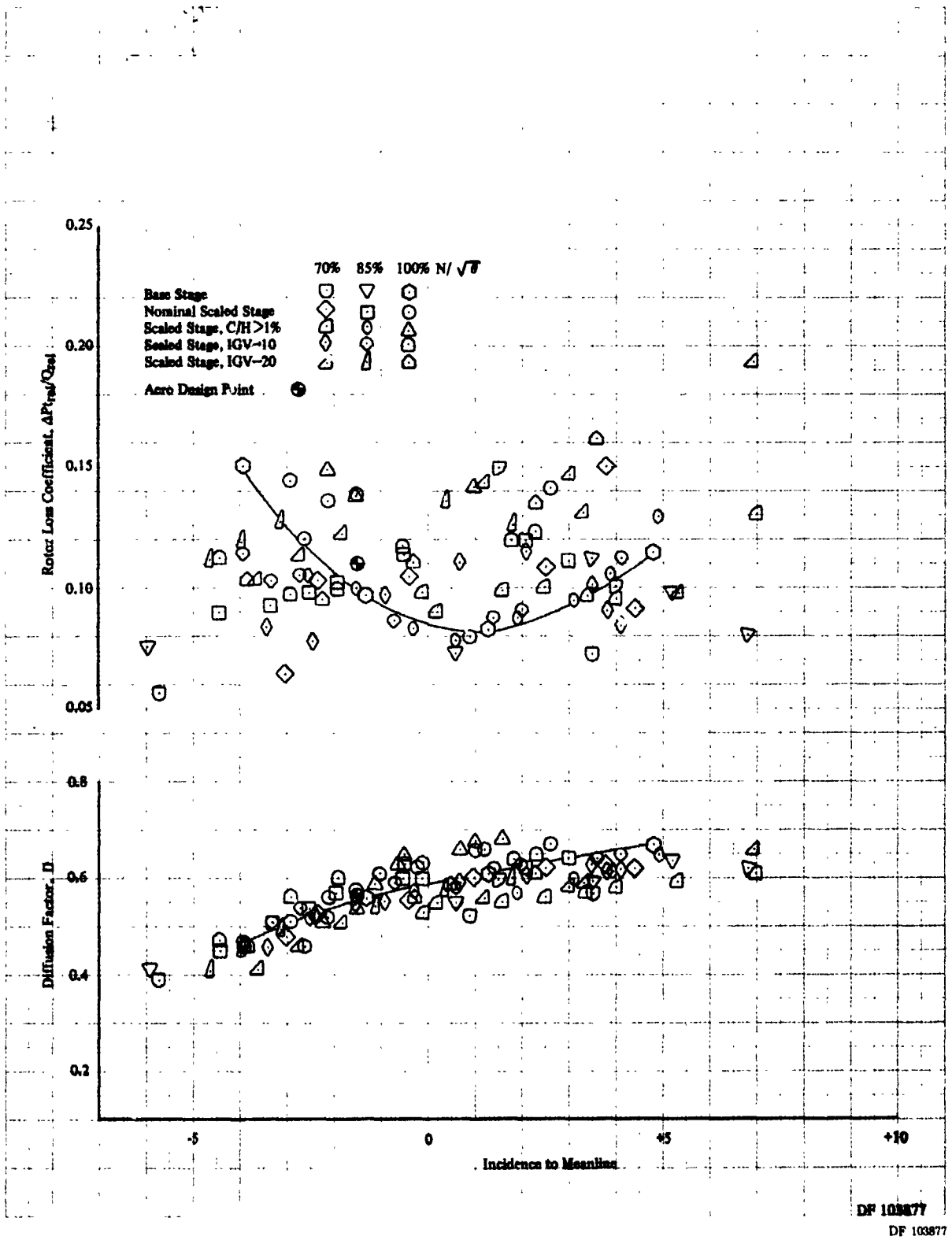

Figure 31. Average Rotor Diffusion Factor and Loss vs Incidence

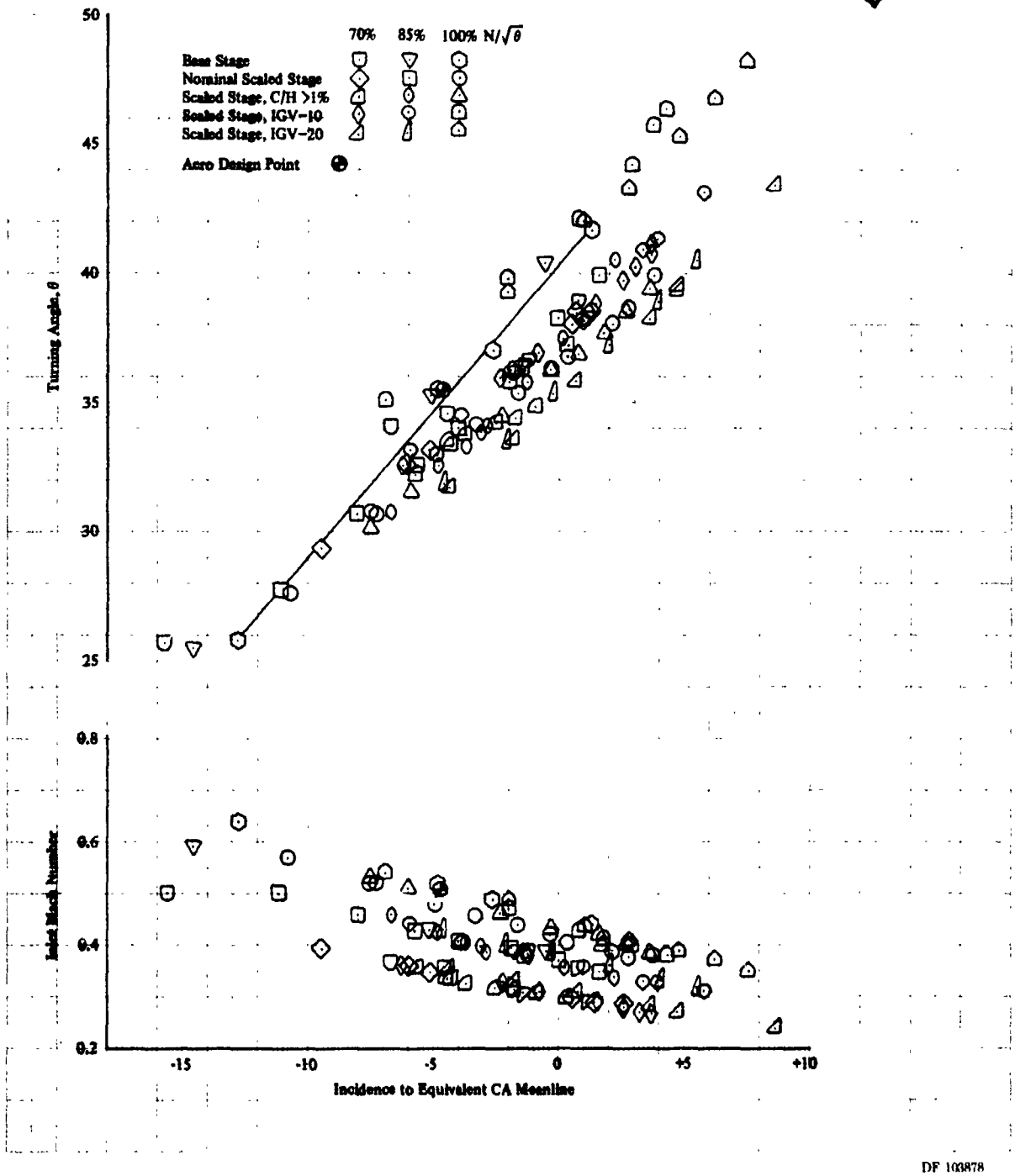

Figure 32. Average Stator Turning and Inlet Mach Number vs Incidence

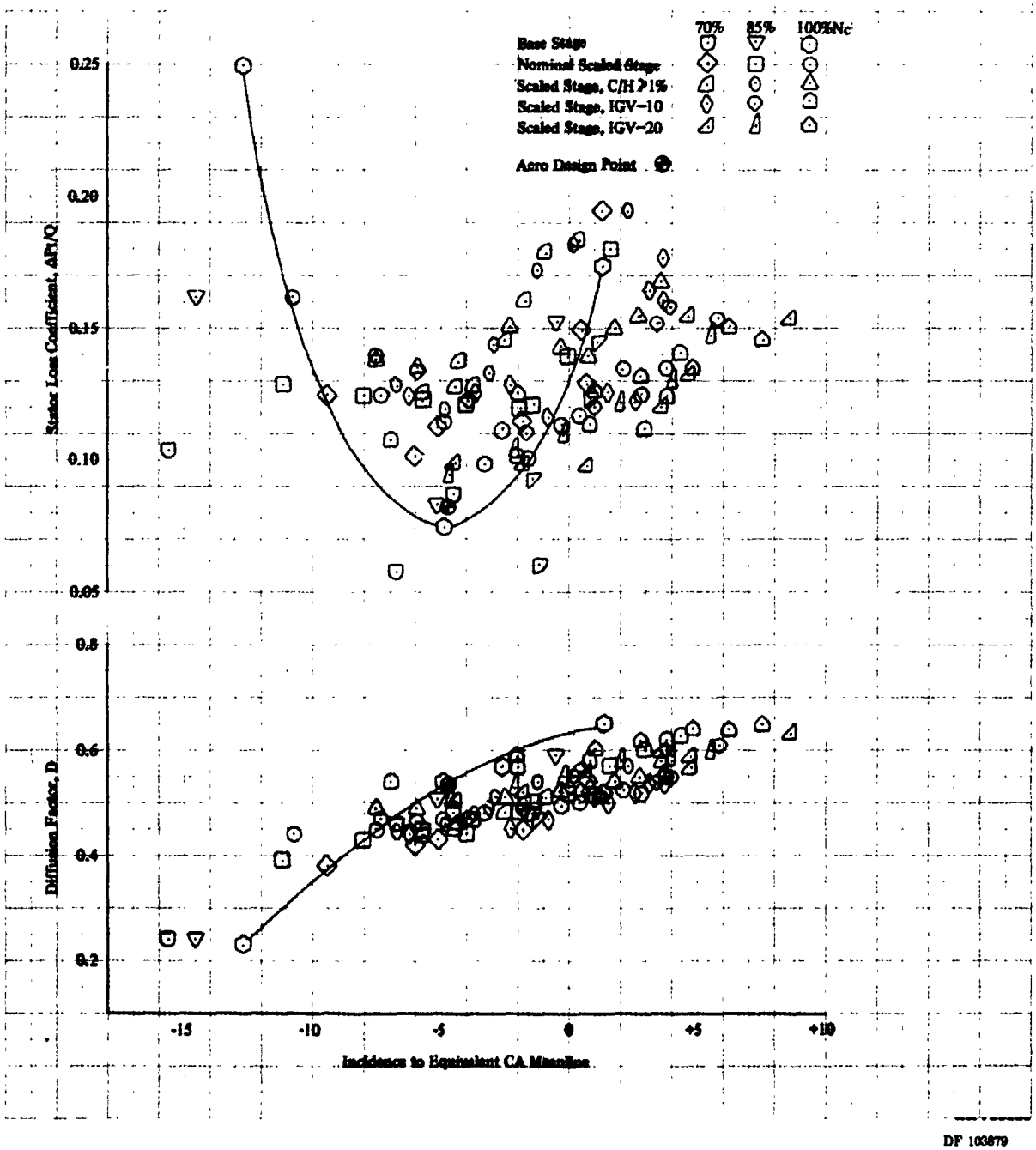

Figure 33. Average Stator Diffusion Factor and Loss vs Incidence

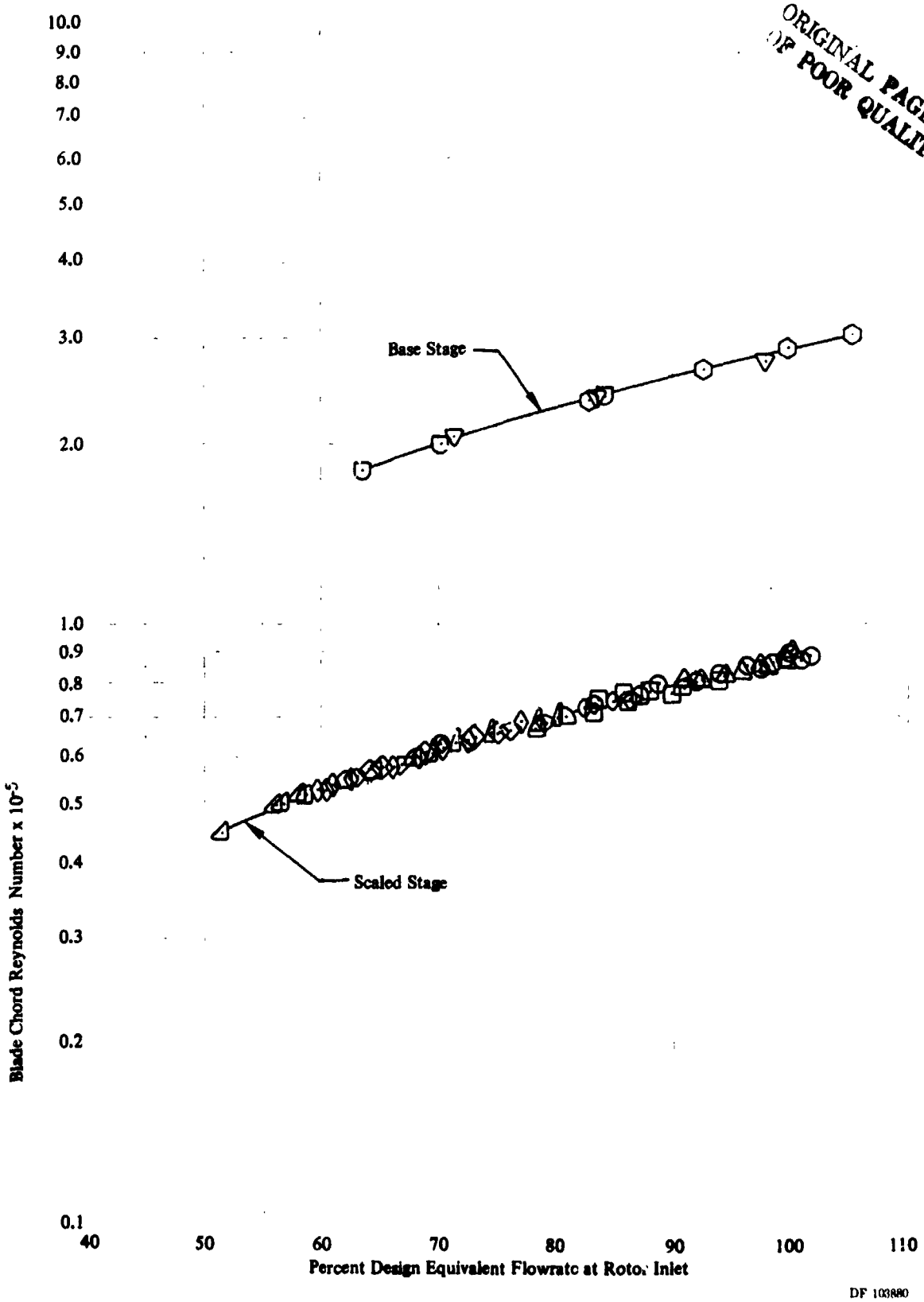

Figure 34. IGV Blade Chord Reynolds Number

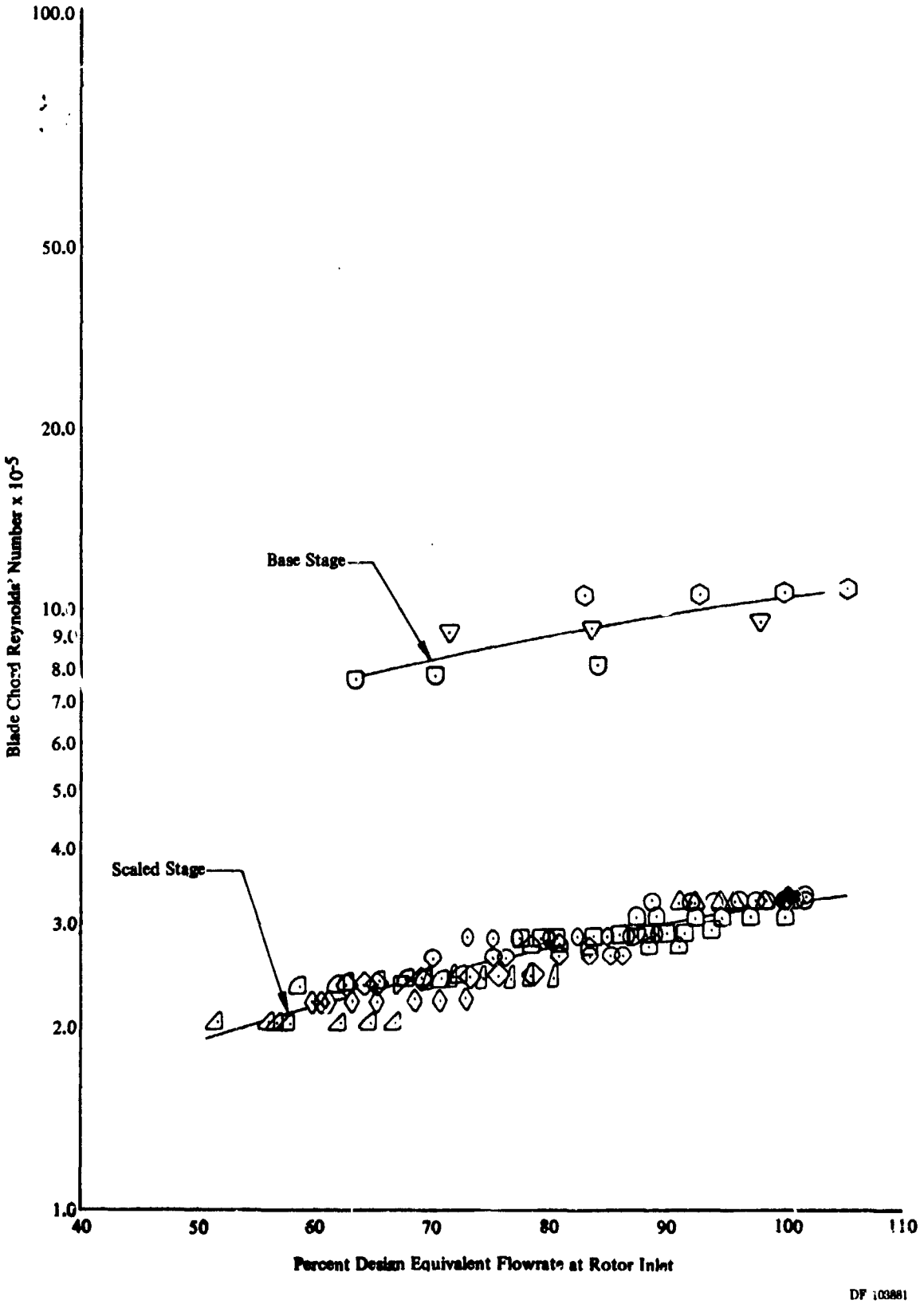

Figure 35. Rotor Blade Chord Reynolds Number

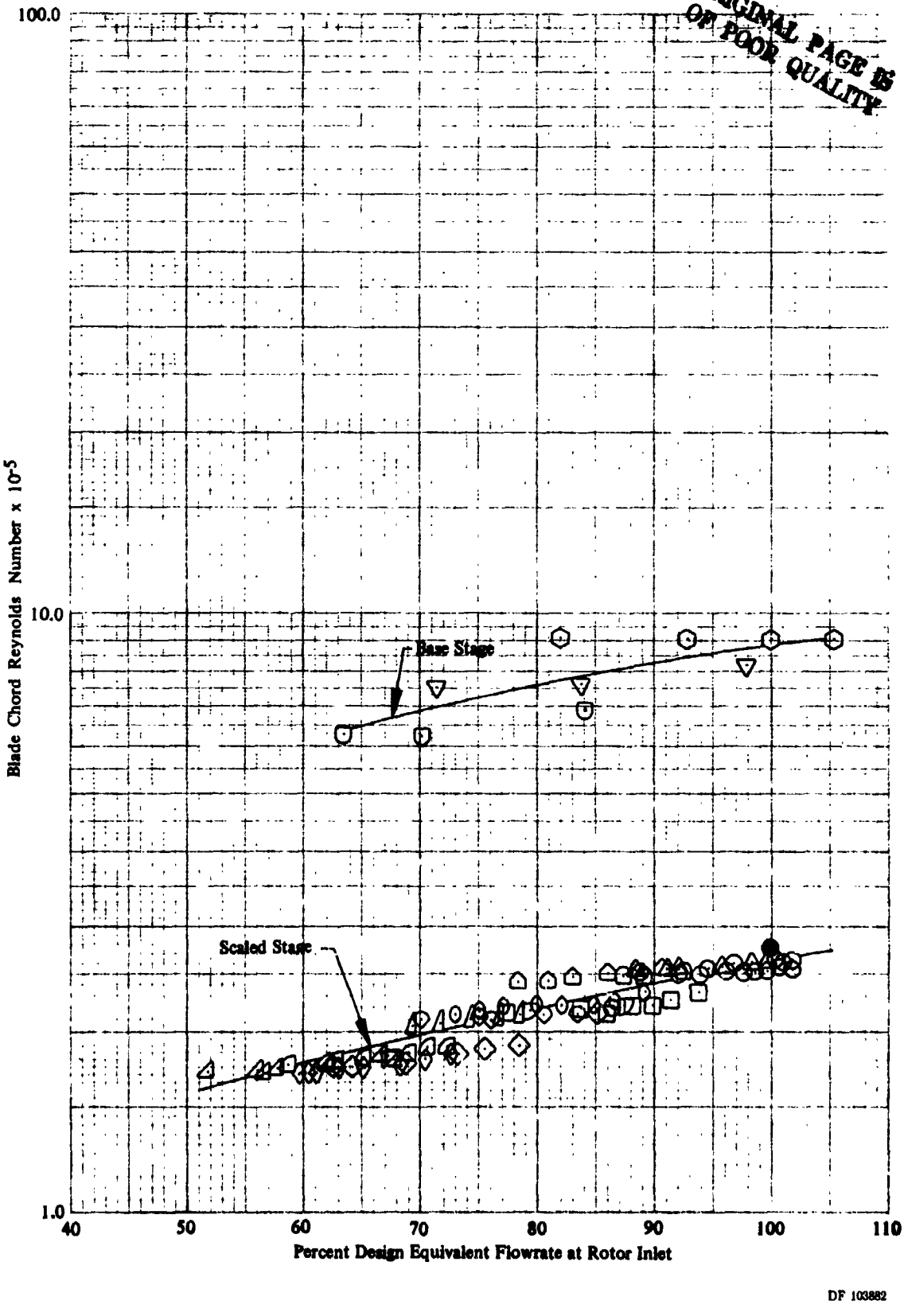

Figure 36. Stator Blade Chord Reynolds Number

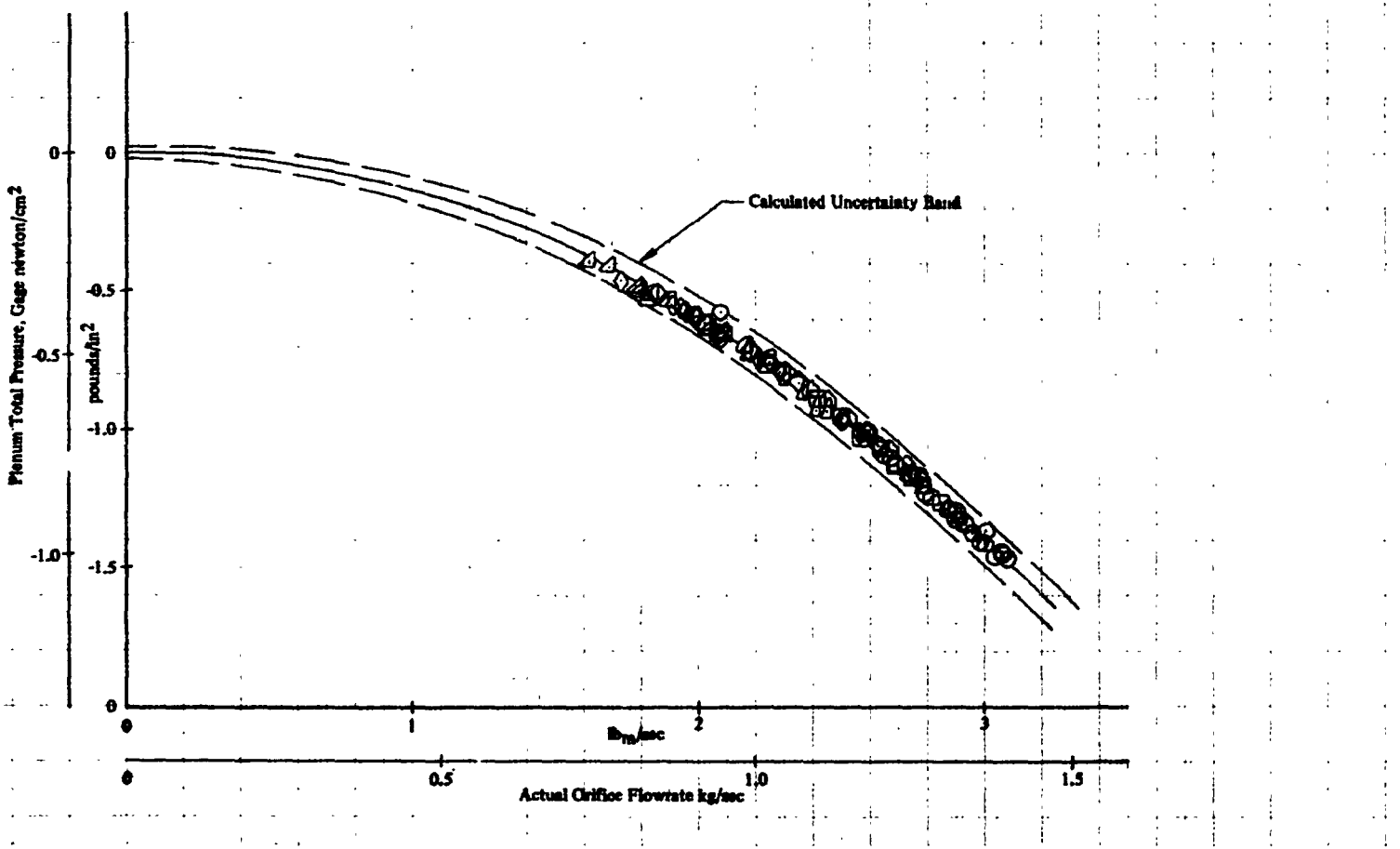

Figure 37. Plenum Total Pressure vs Actual Flowrate

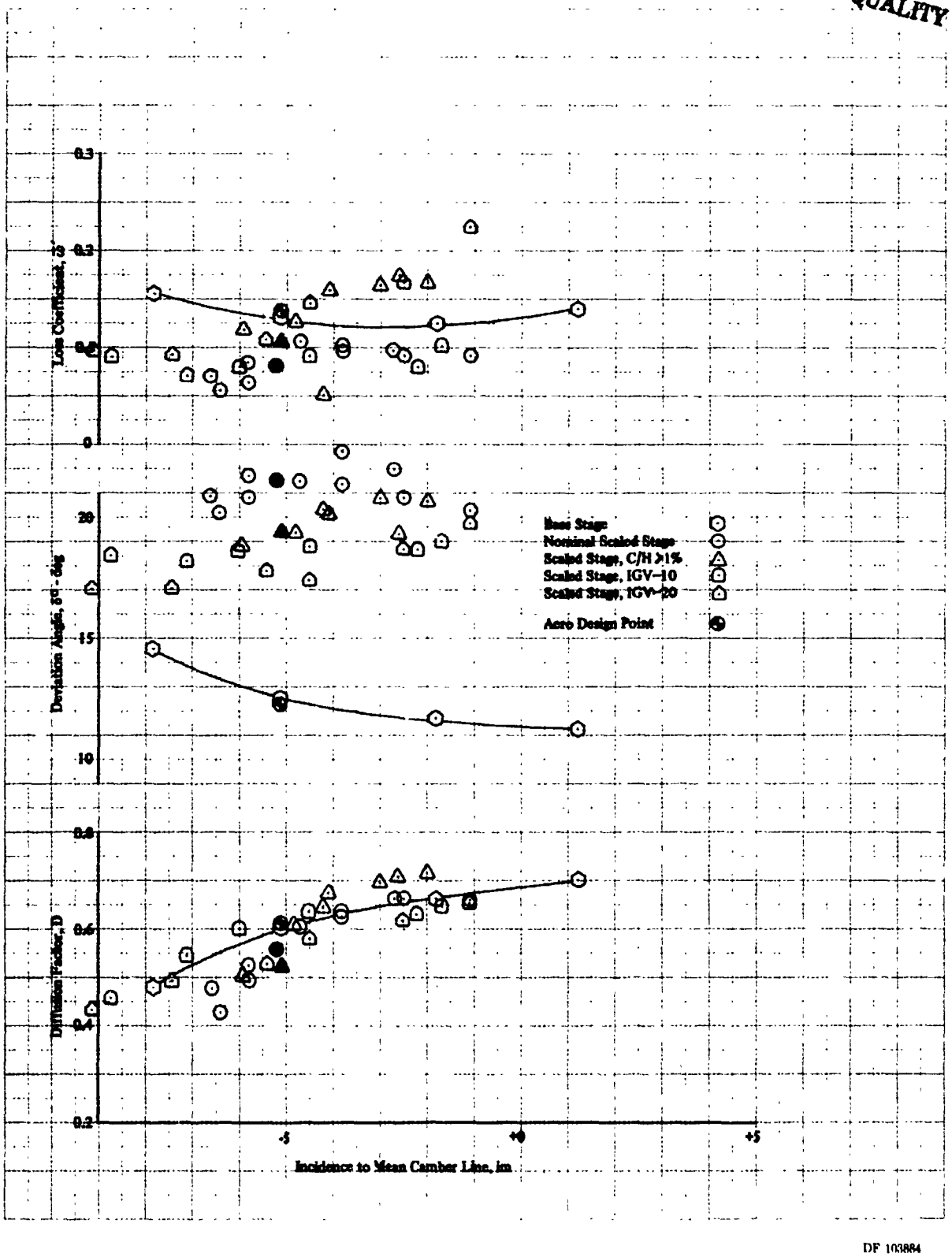

Figure 38. Spanwise Rotor Performance at Design Speed, 90% Span

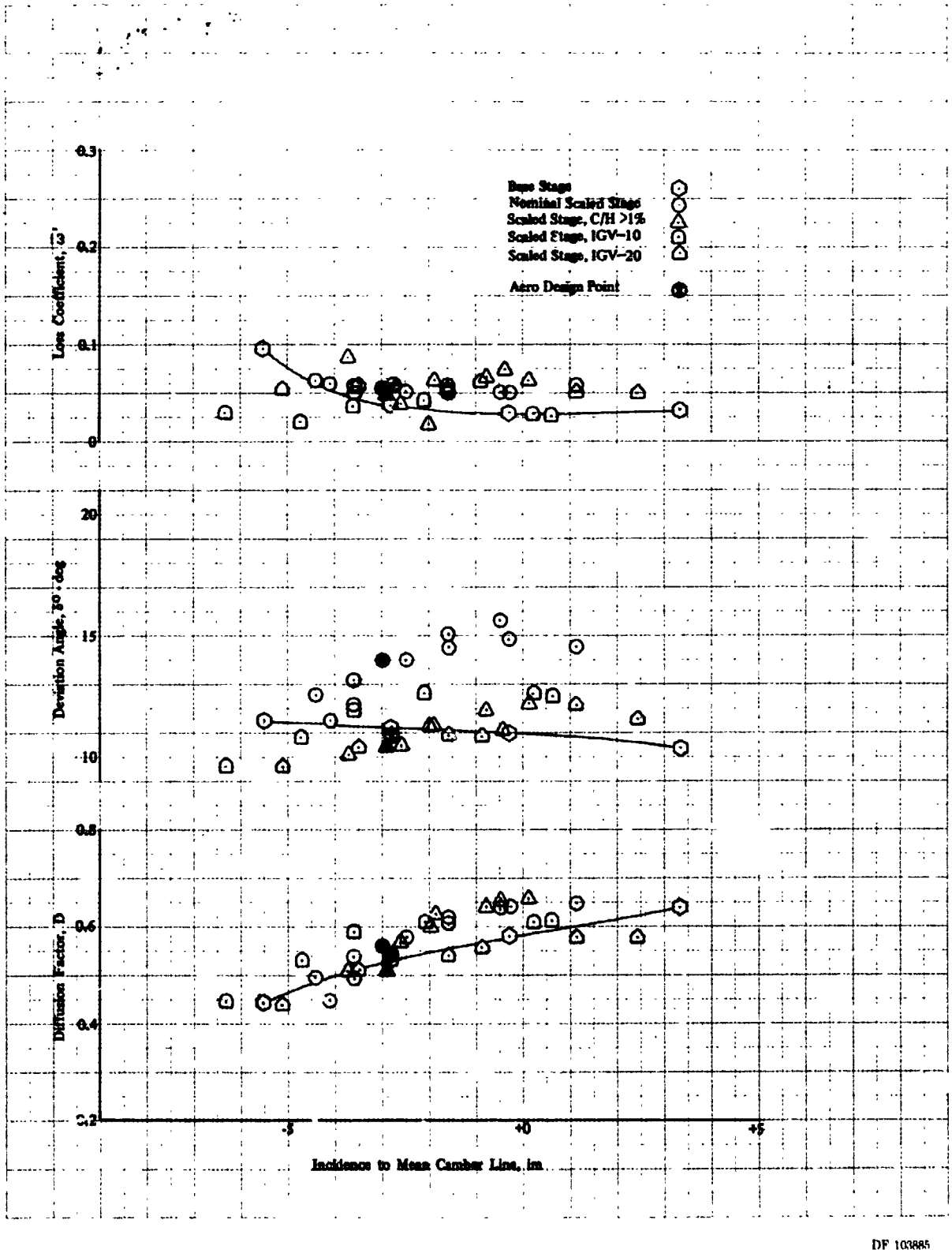

Figure 39. Spanwise Rotor Performance at Design Speed, 70% Span

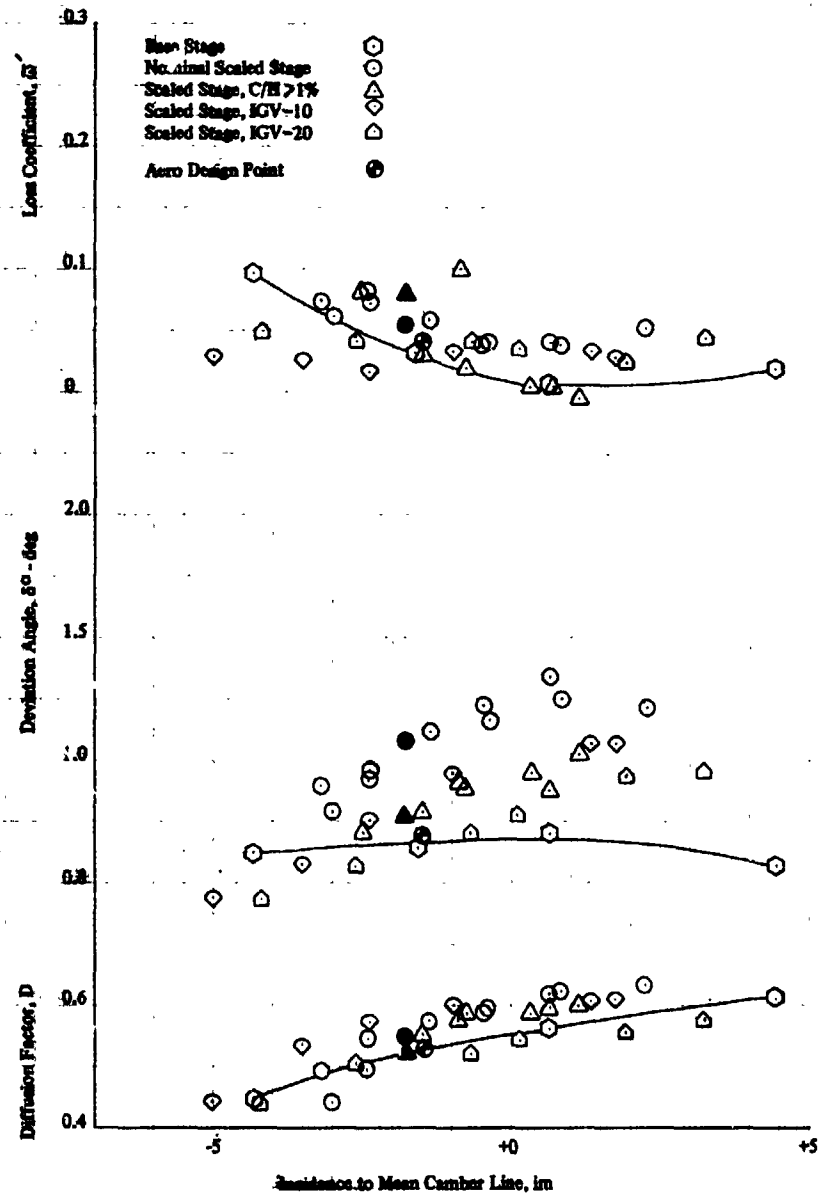

DF 103886

Figure 40. Spanwise Rotor Performance at Design Speed, 50% Span

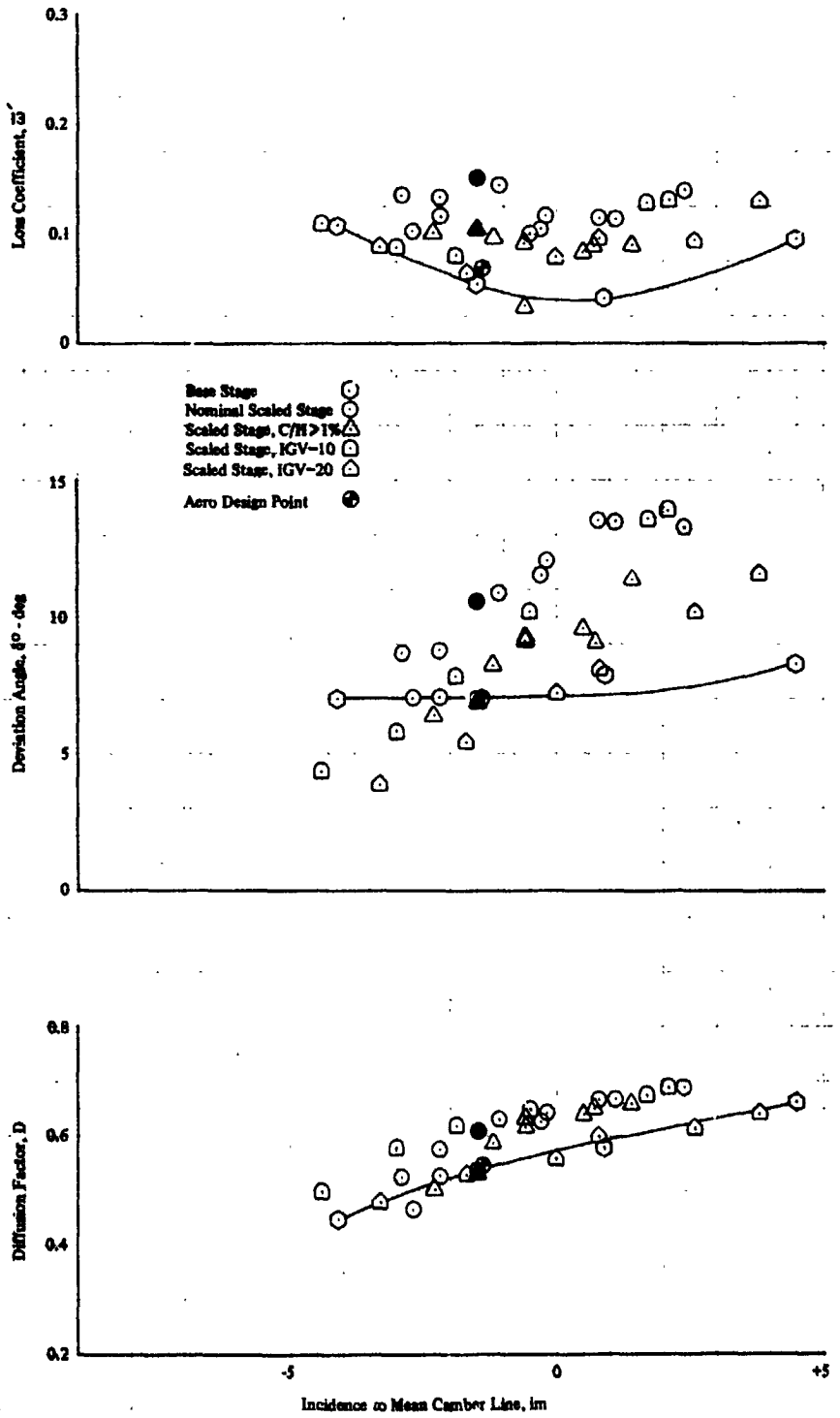

Figure 41. Spanwise Rotor Performance at Design Speed, 30% Span

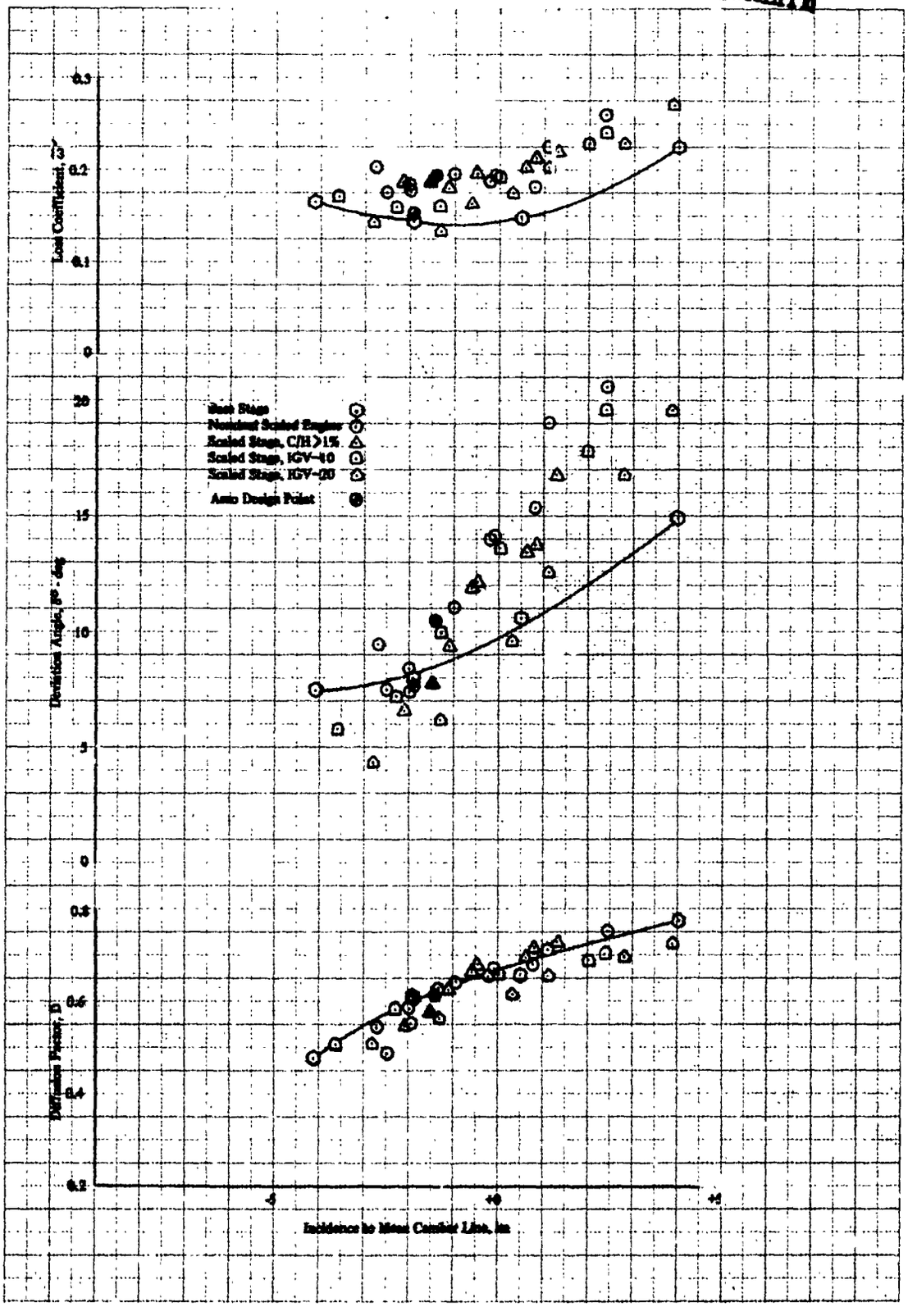

Figure 42. Spanwise Rotor Performance at Design Speed, 10% Span

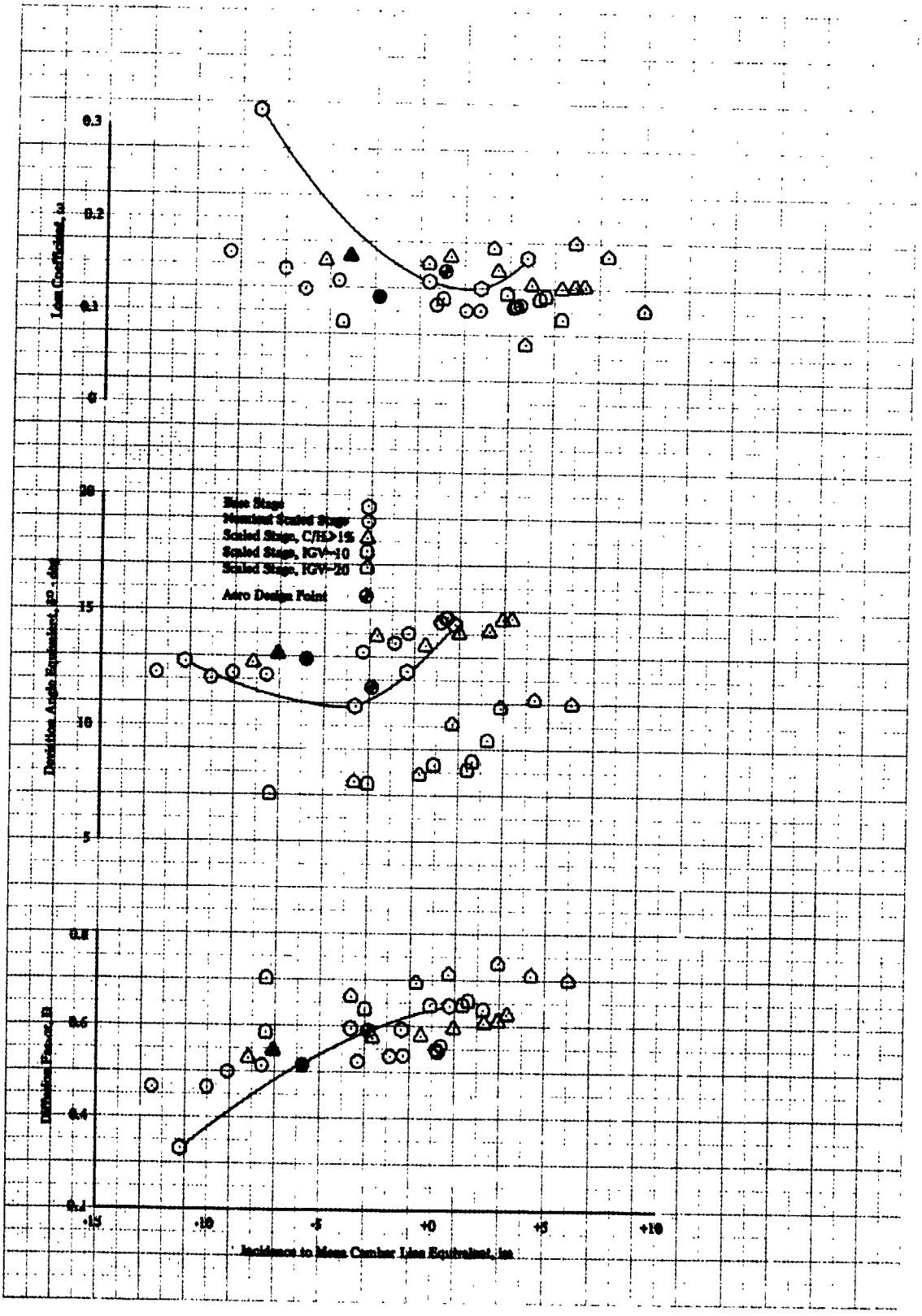

DF 103869

Figure 43. Spanwise Stator Performance at Design Speed, 90% Span

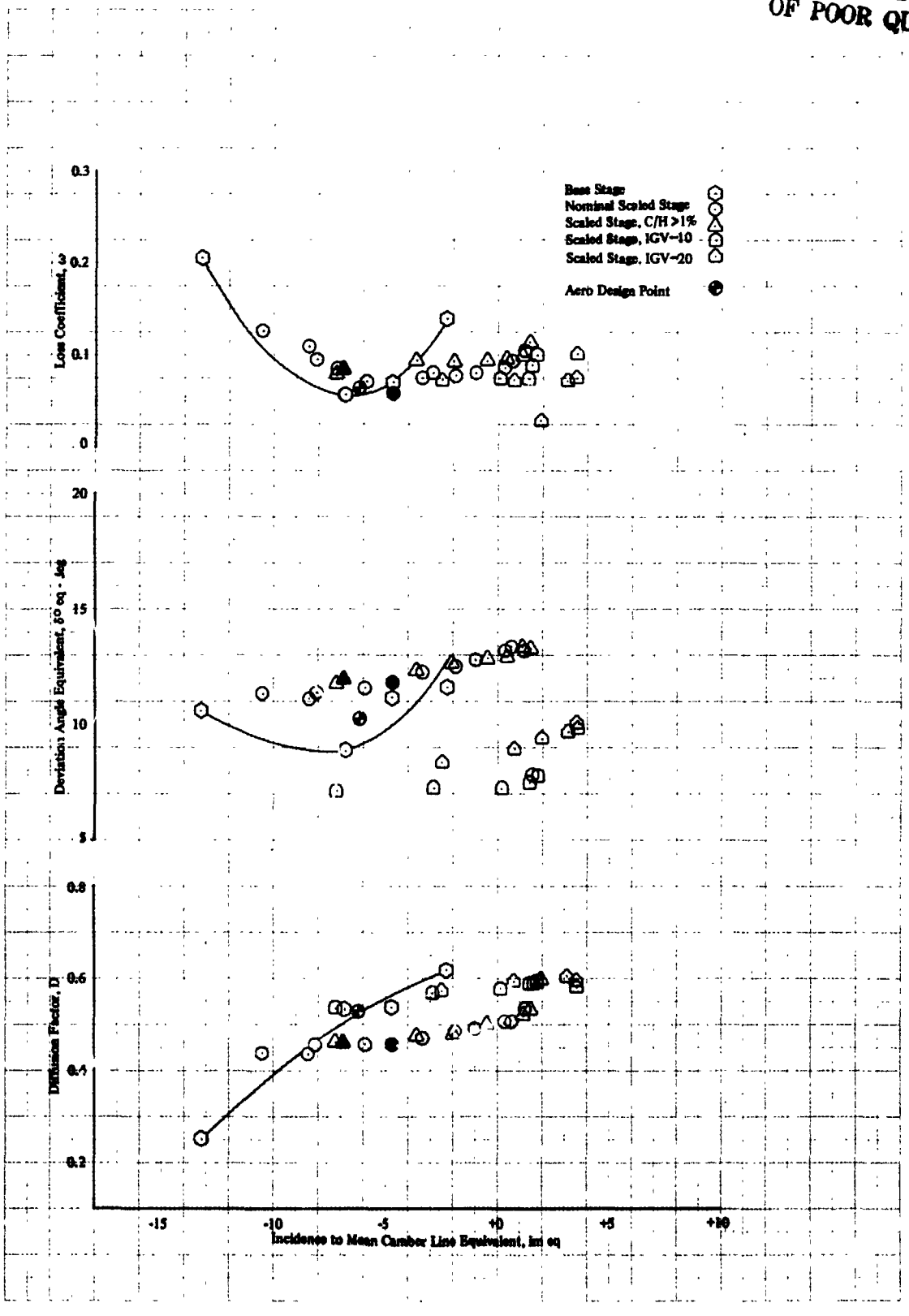

Figure 44. Spanwise Stator Performance at Design Speed, 70% Span

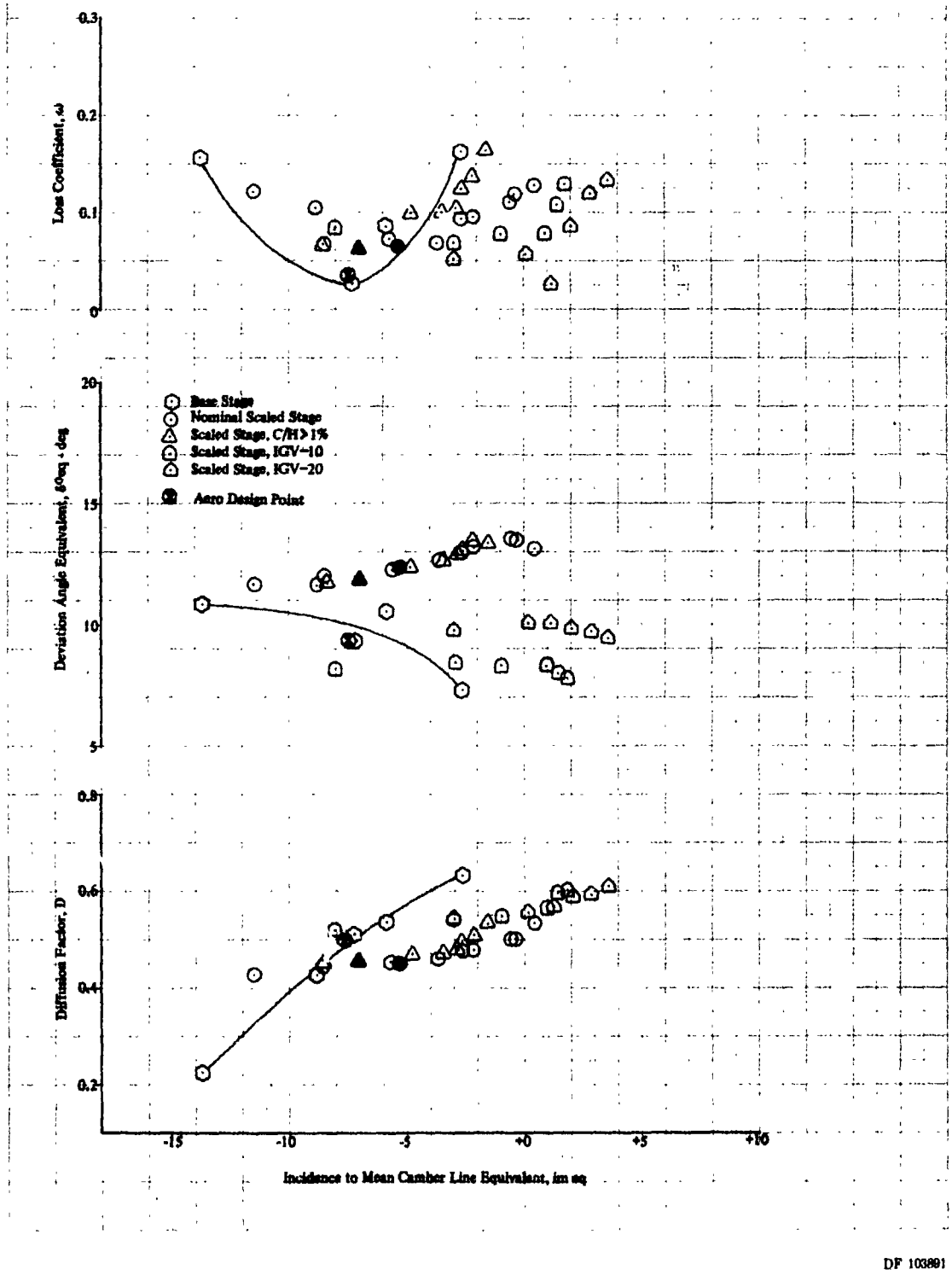

Figure 45. Spanwise Stator Performance at Design Speed, 50% Span

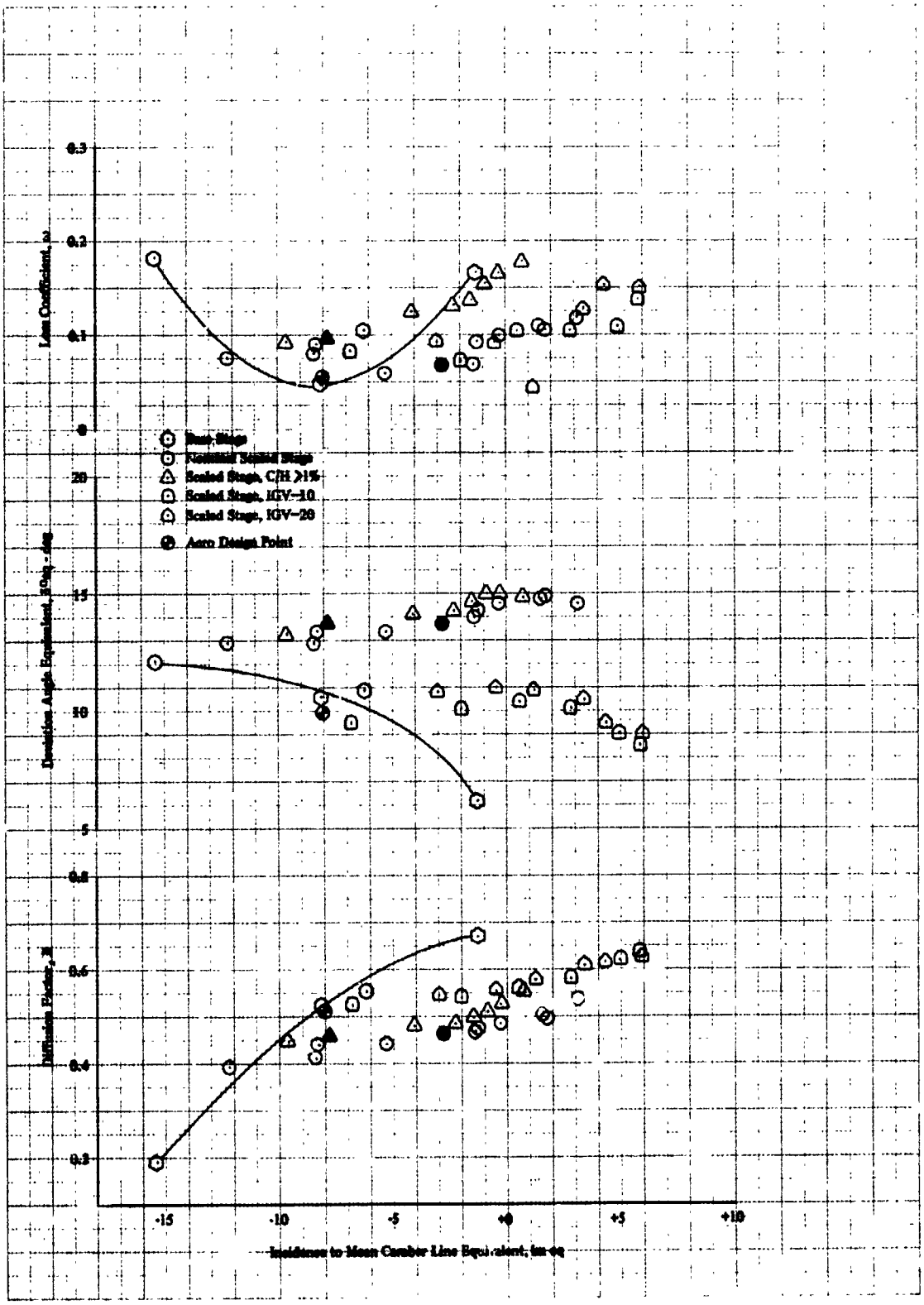

Figure 46. Spanwise Stator Performance at Design Speed, 30% Span

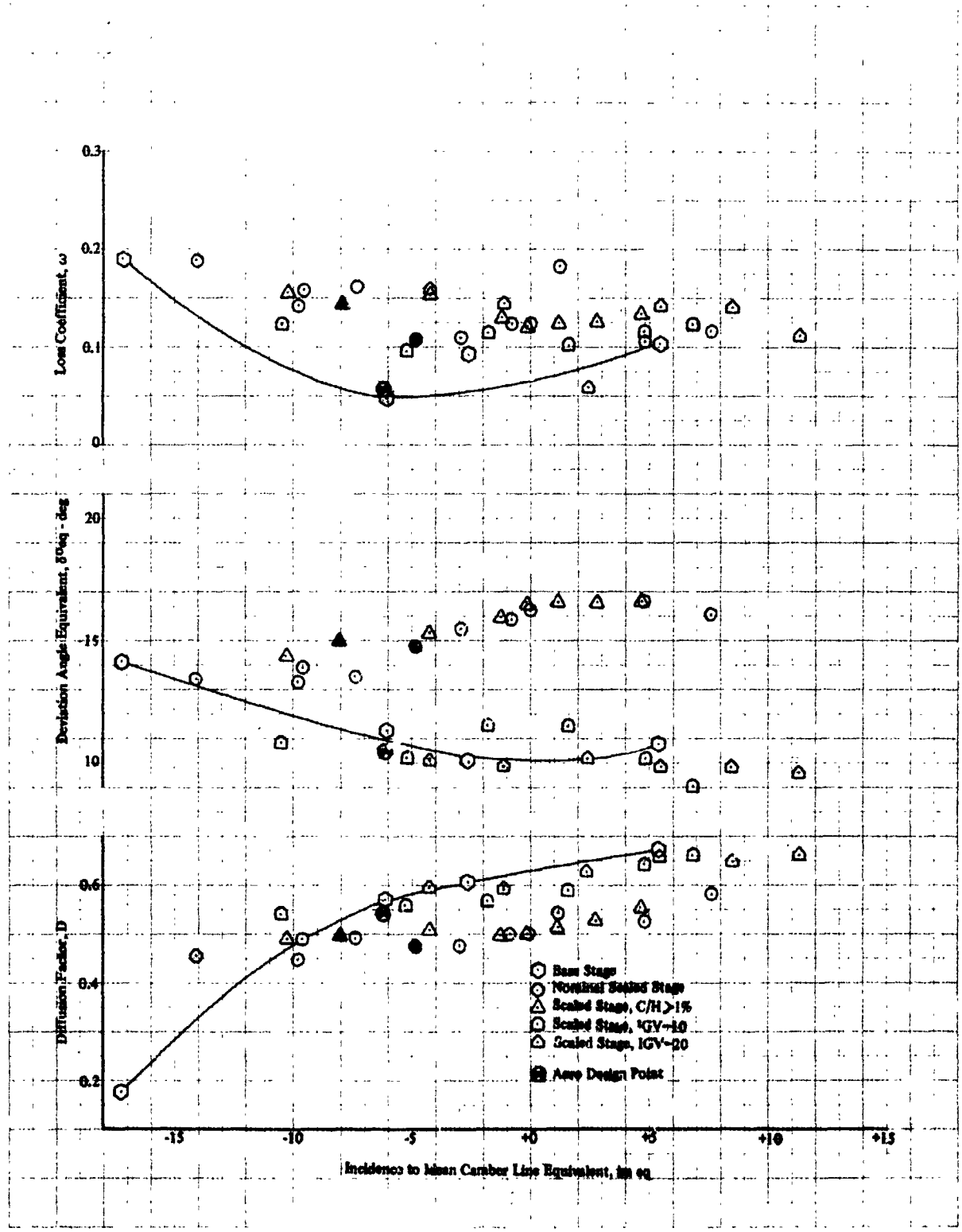

Figure 47. Spanwise Stator Performance at Design Speed, 10% Span

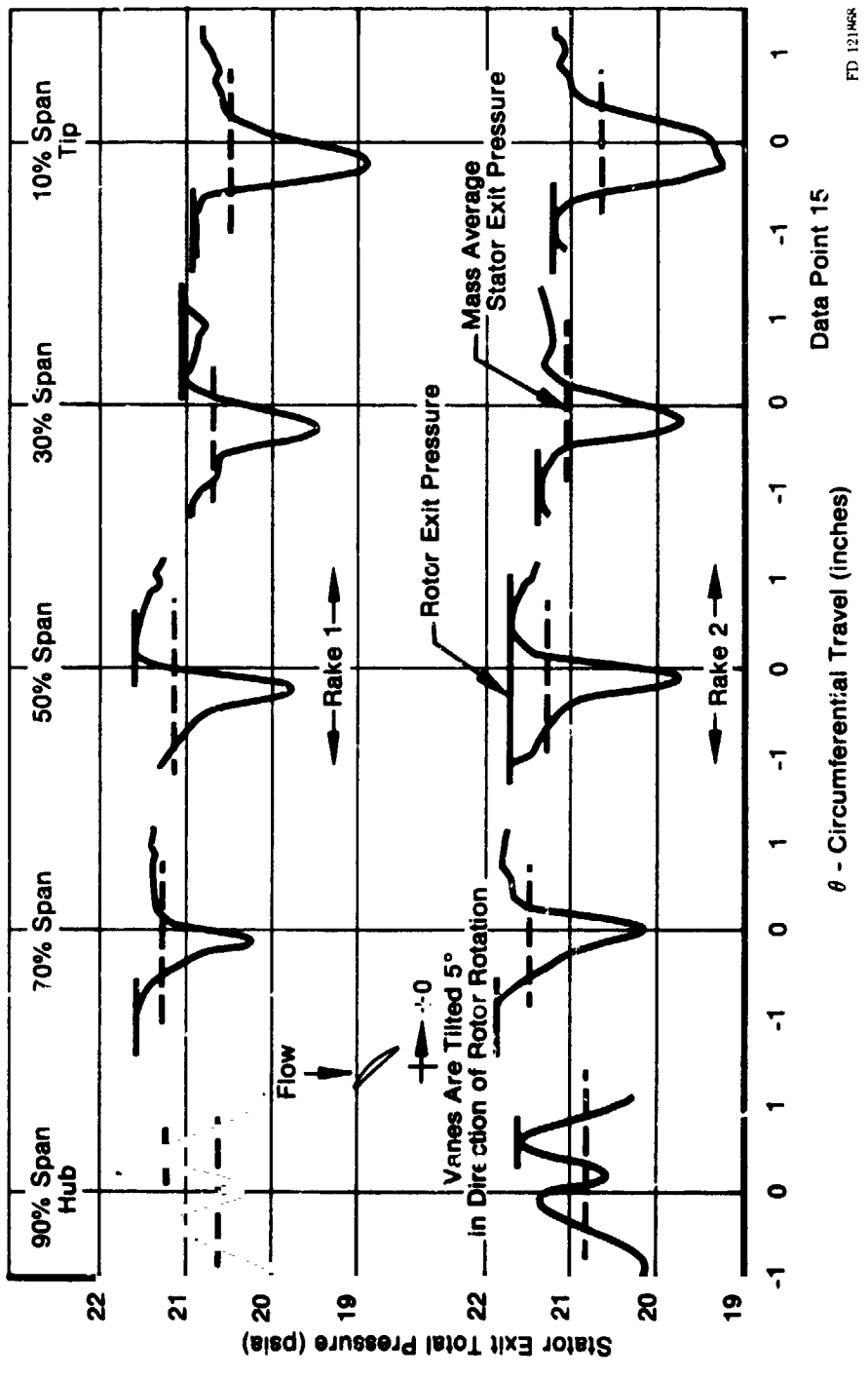

Figure 48. Stator Exit PT Traverse Data for Point 15

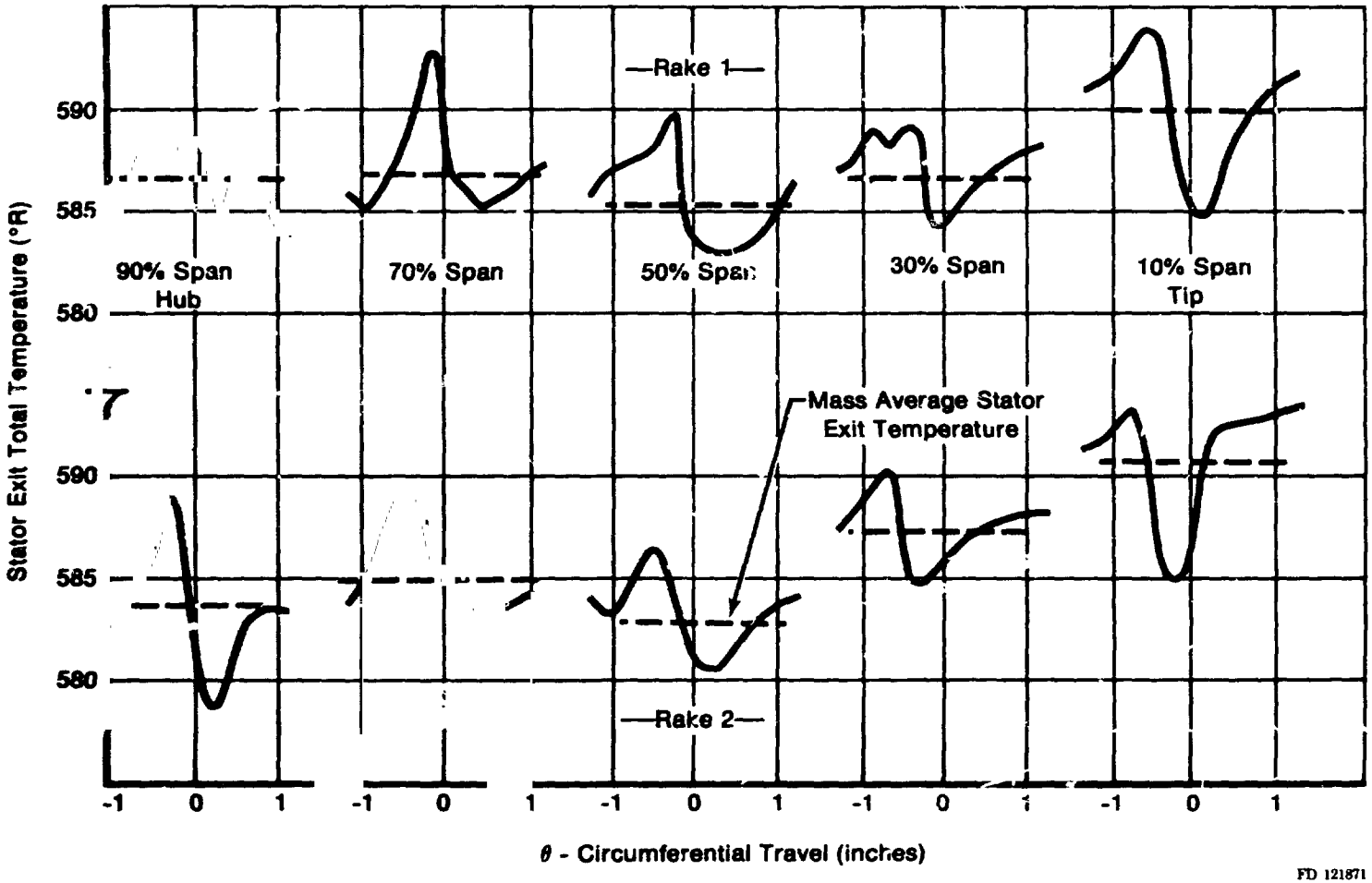

Figure 49. Stator Exit TT Traverse Data for Point 15

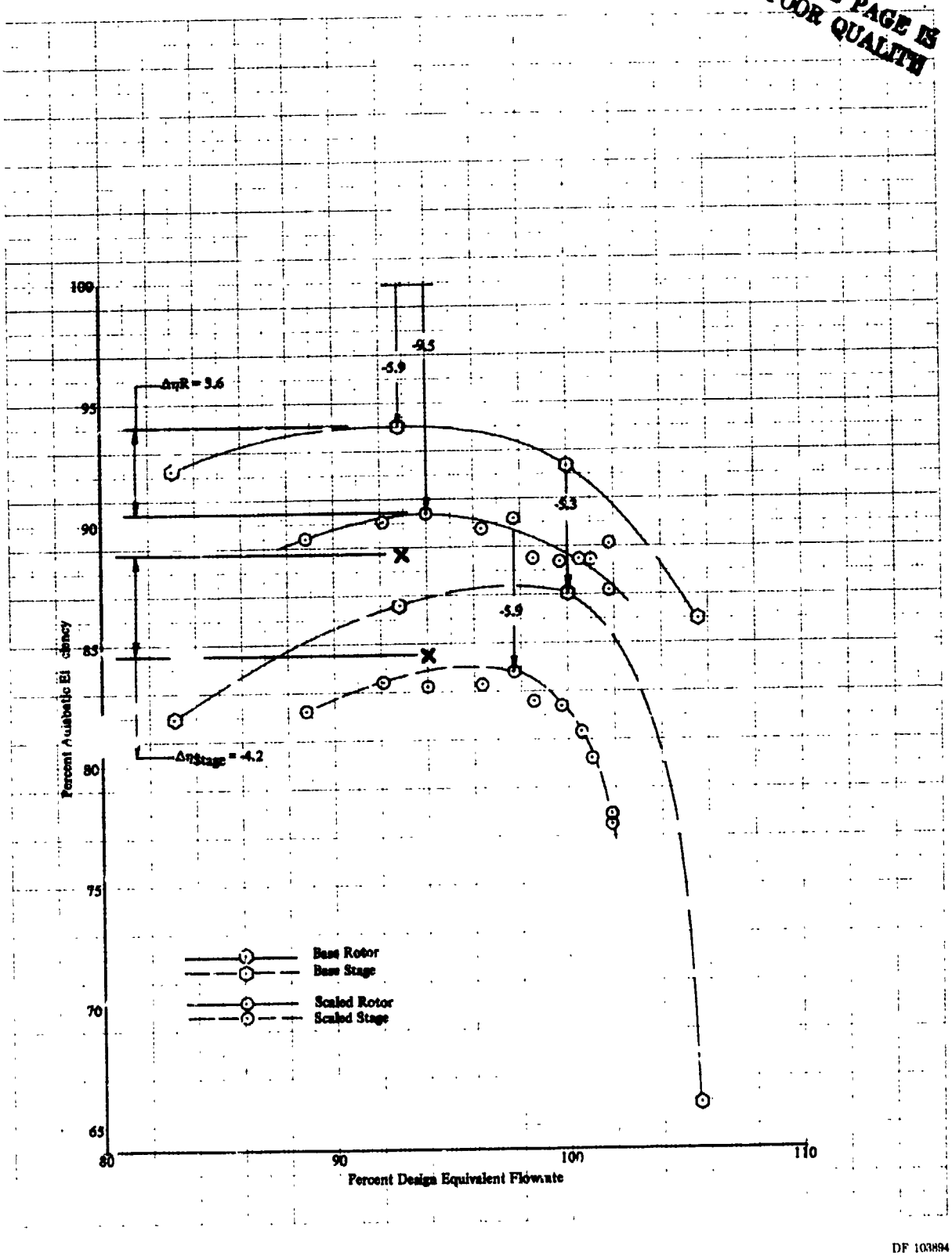

Figure 50. 100% Equivalent Rotor Speed Efficiency Map

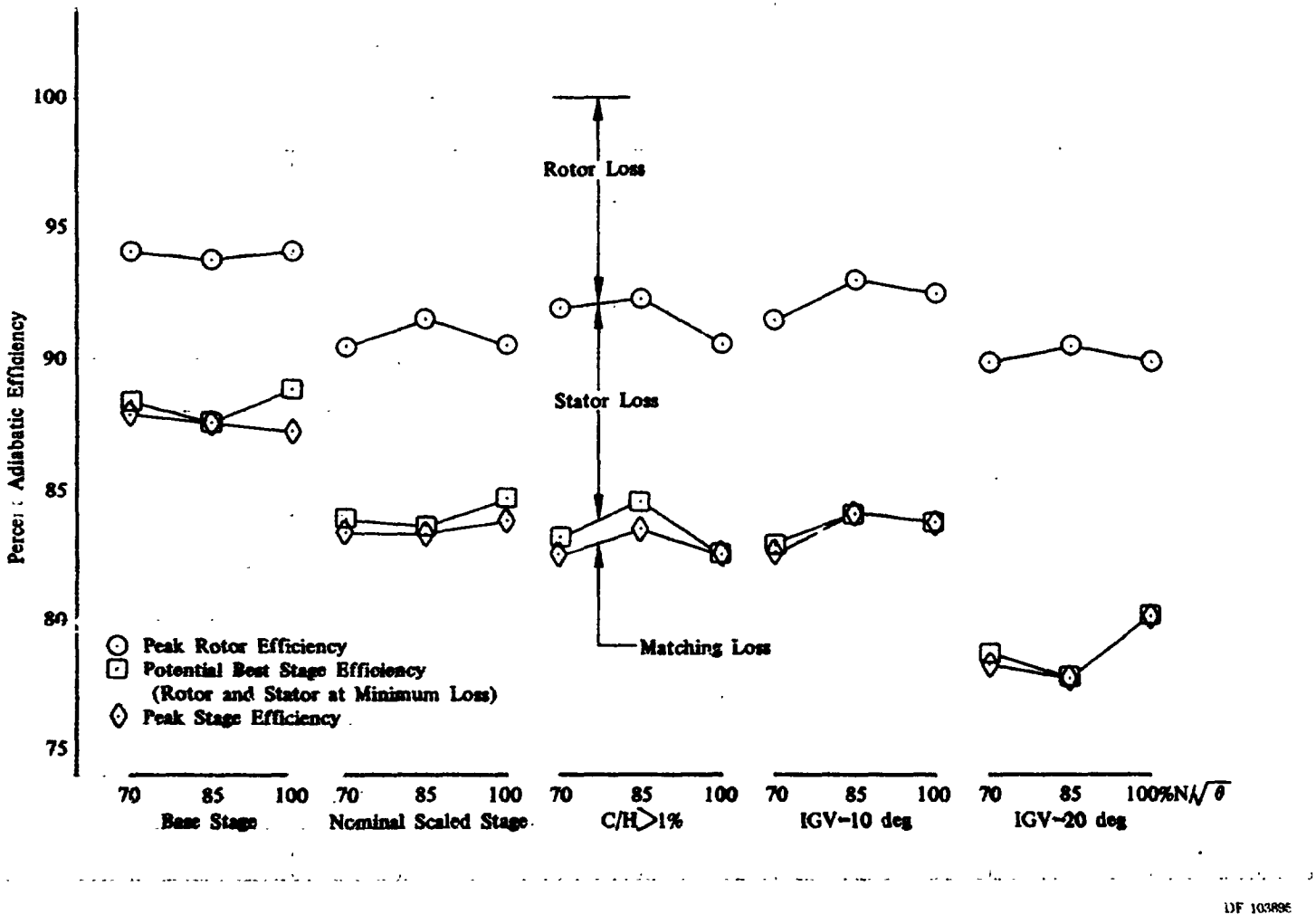

Figure 51. Performance at Minimum Rotor and Stator Loss

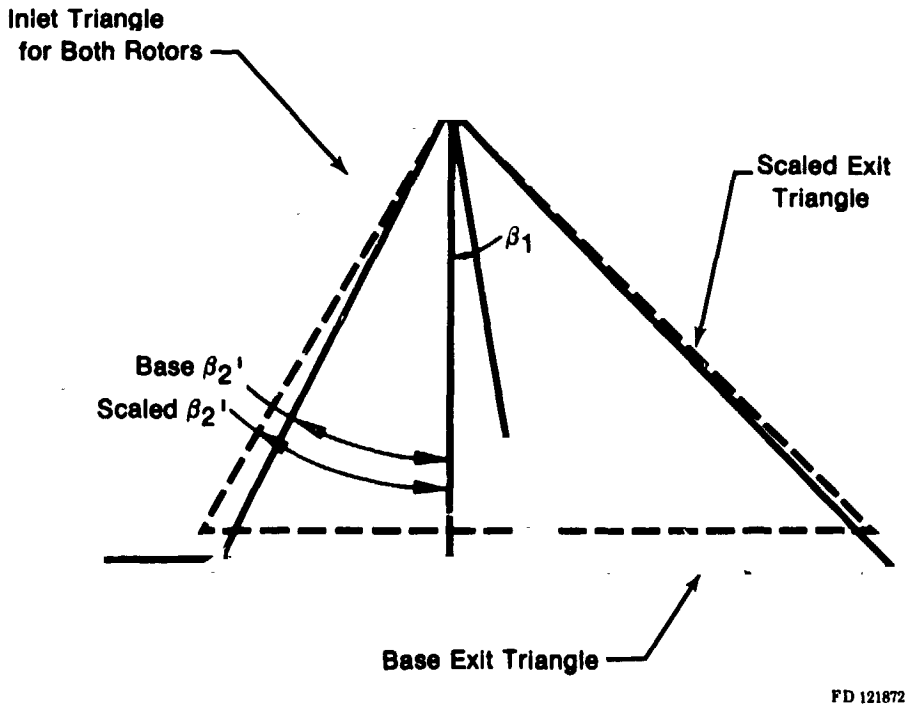

Figure 52. Comparison of Base and Scaled Rotor Velocity Triangles

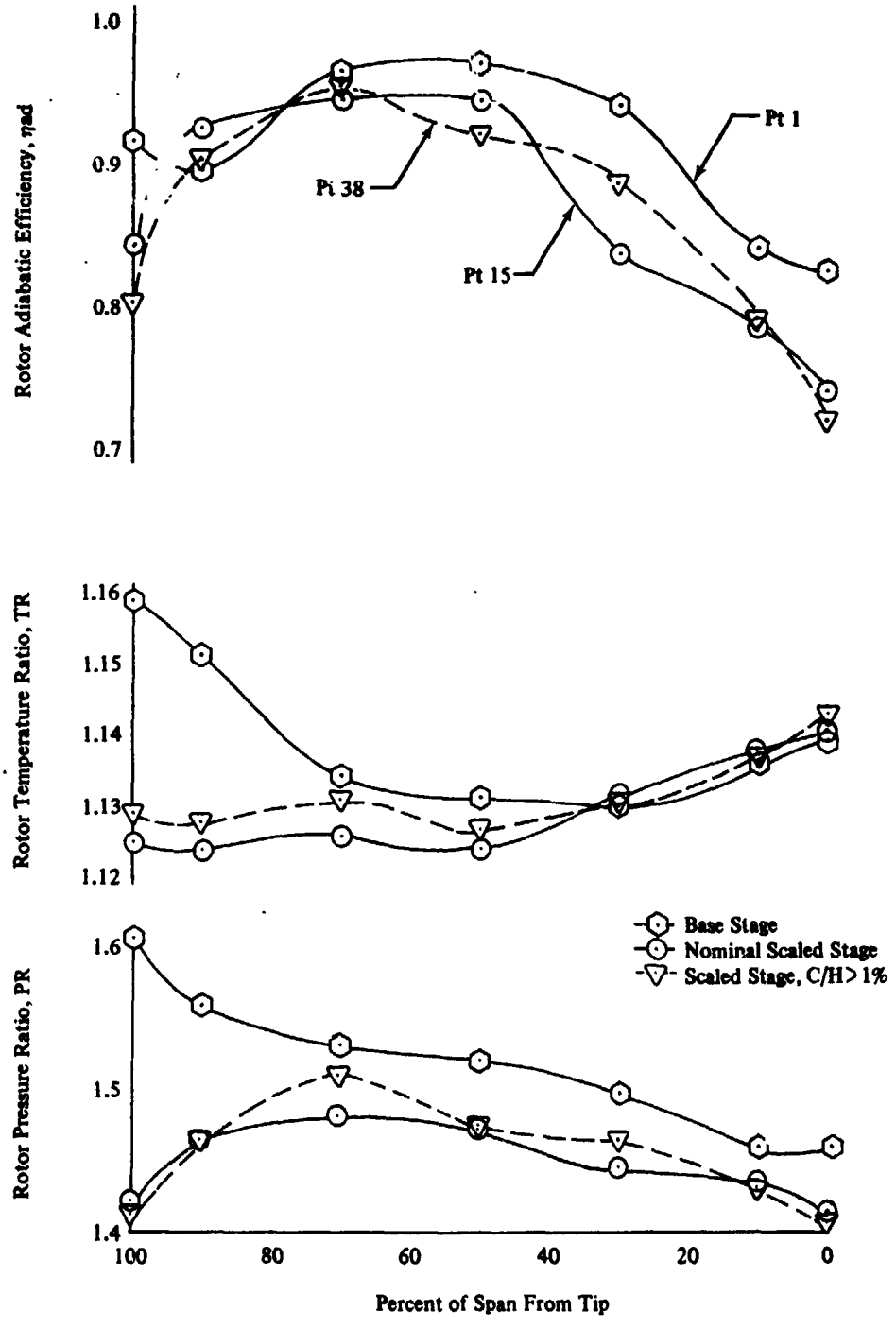

Figure 53. Spanwise Rotor Performance, 100% $N/\sqrt{\theta}$ and $W\sqrt{\theta}/\delta$

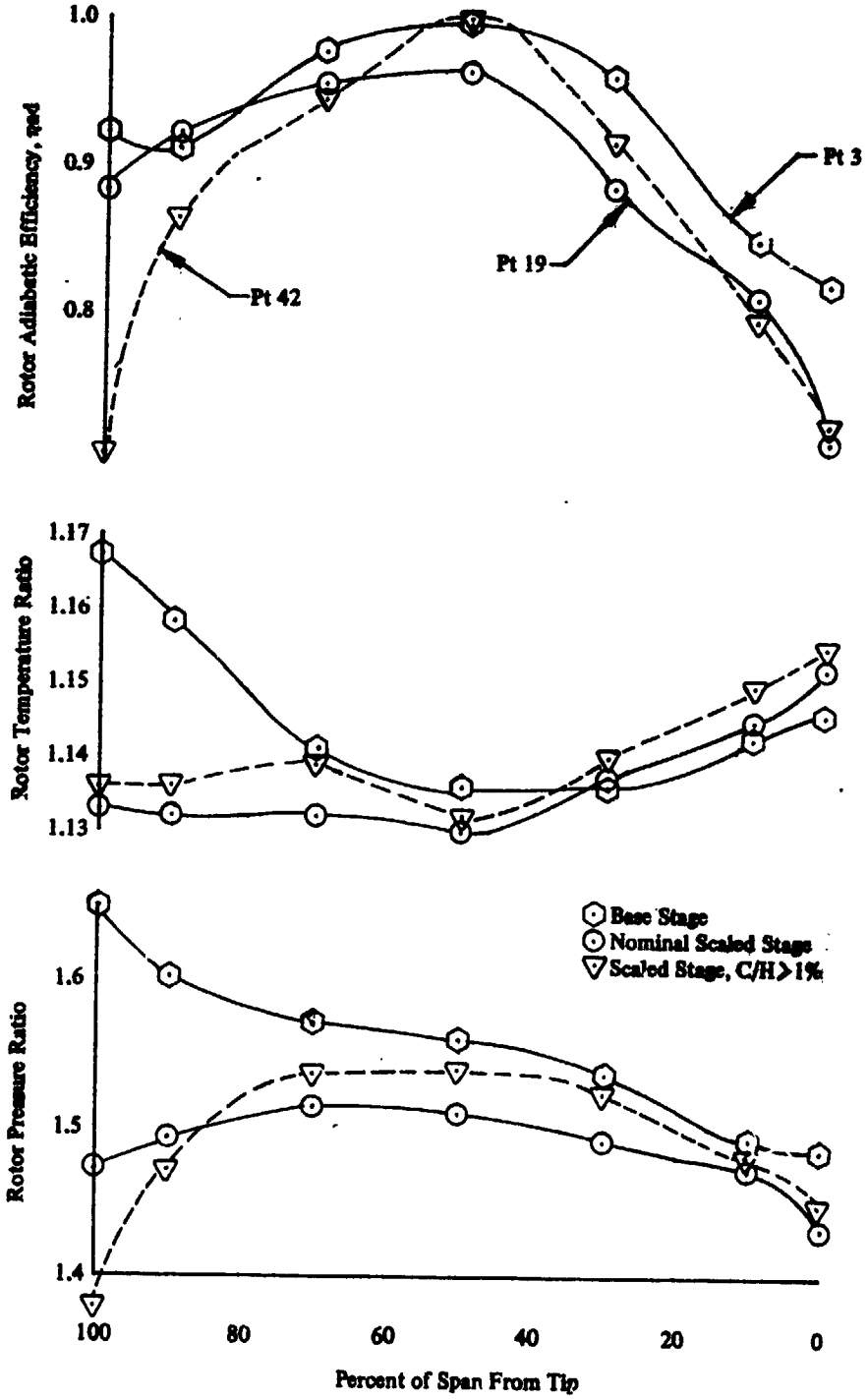

Figure 54. Spanwise Rotor Performance, 100% $N/\sqrt{\theta}$ Peak ηR

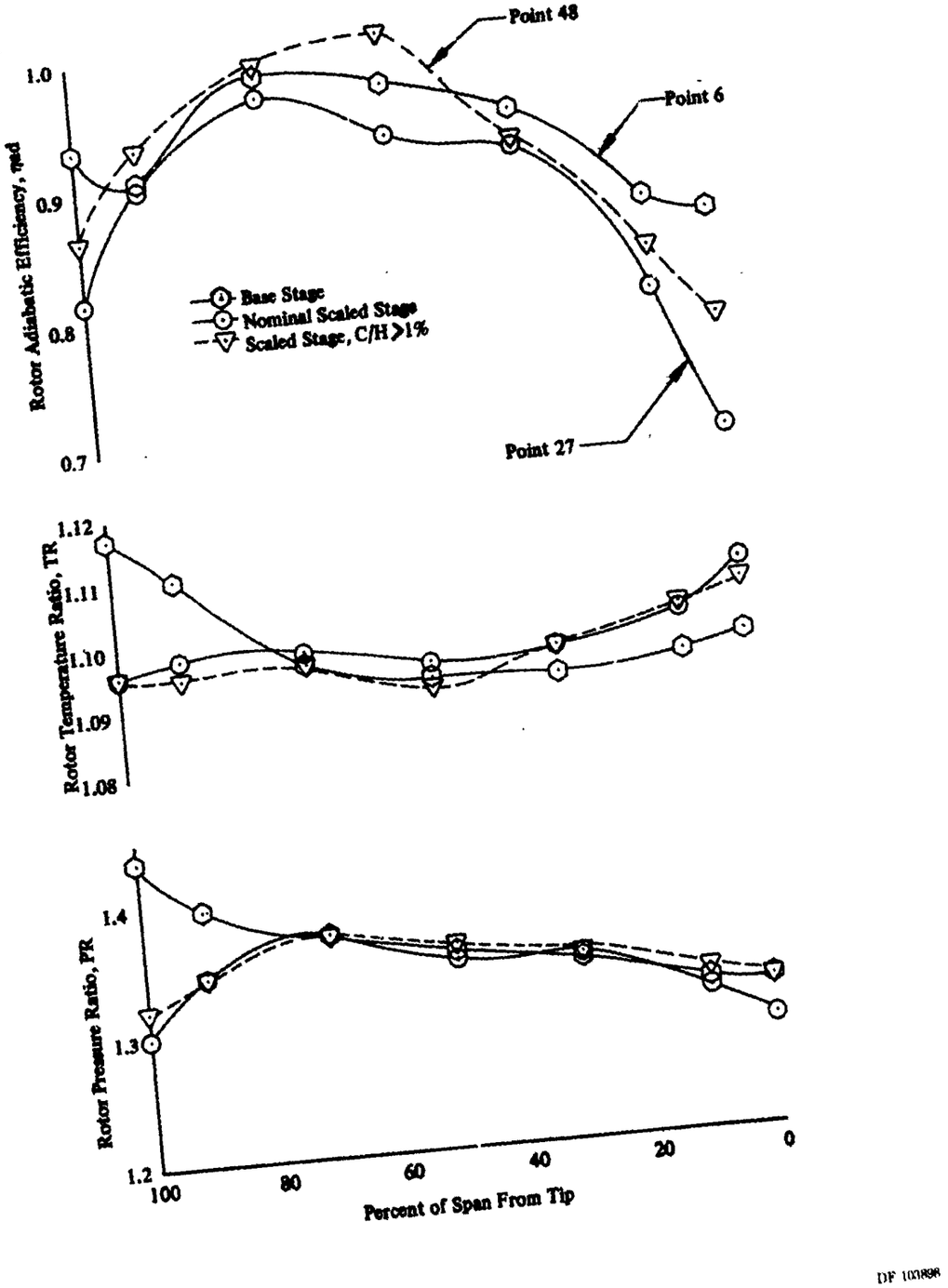

Figure 55. Spanwise Rotor Performance, 85% $N/\sqrt{\theta}$ Midpoint

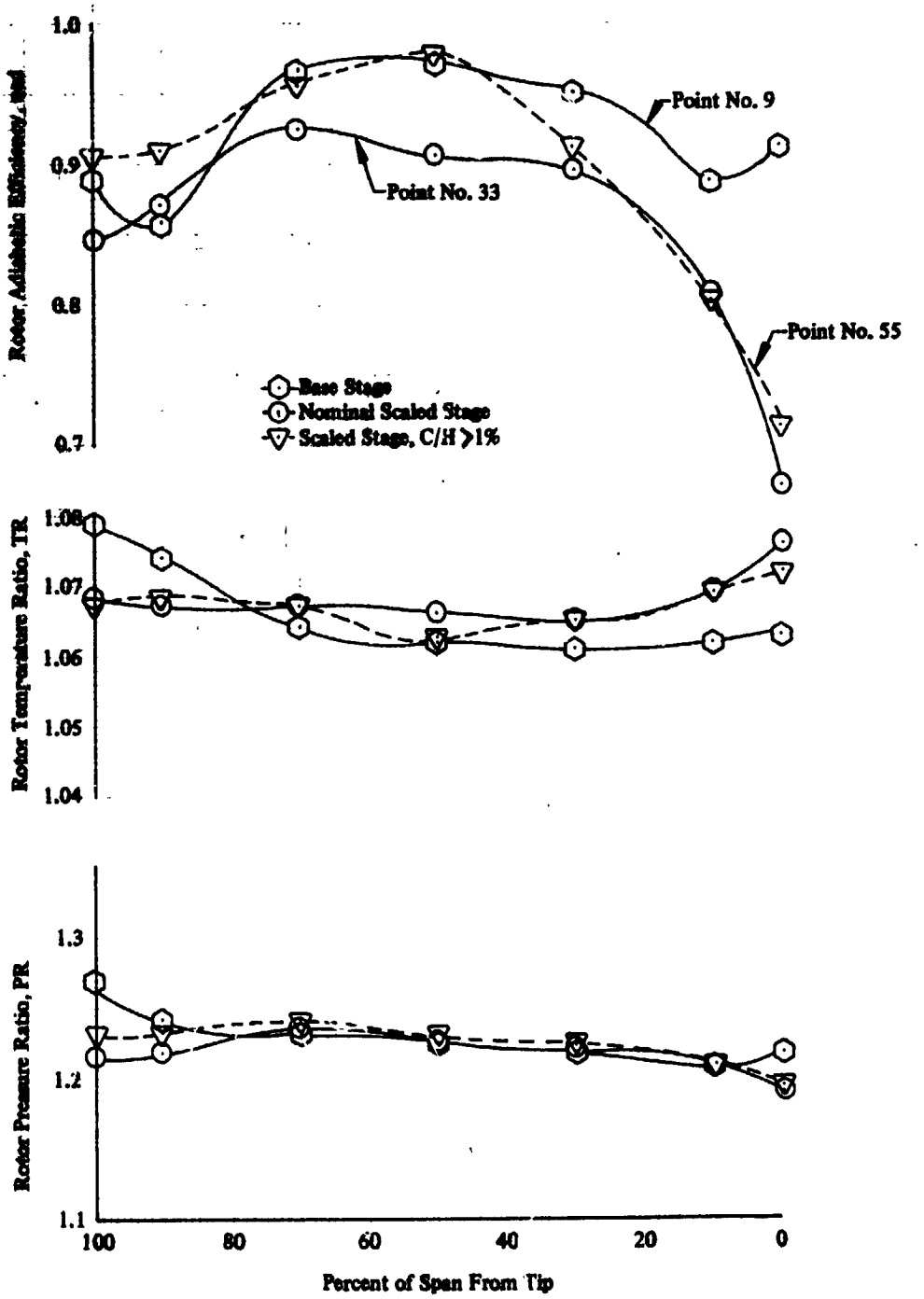

Figure 56. Spanwise Rotor Performance, 70% $N/\sqrt{\theta}$ Midpoint

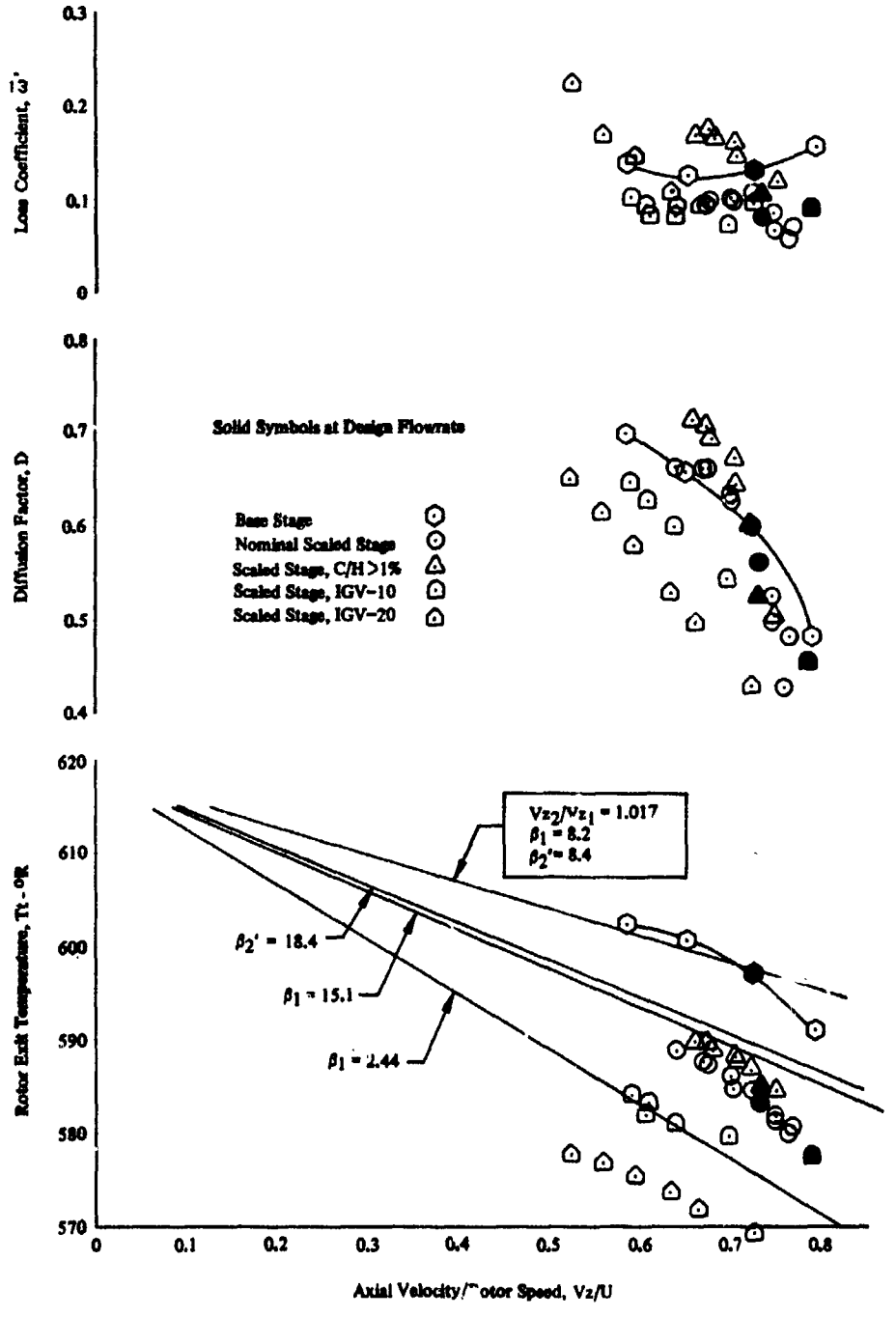

DF 103900

Figure 57. Rotor Performance at Design Speed, 90% Span

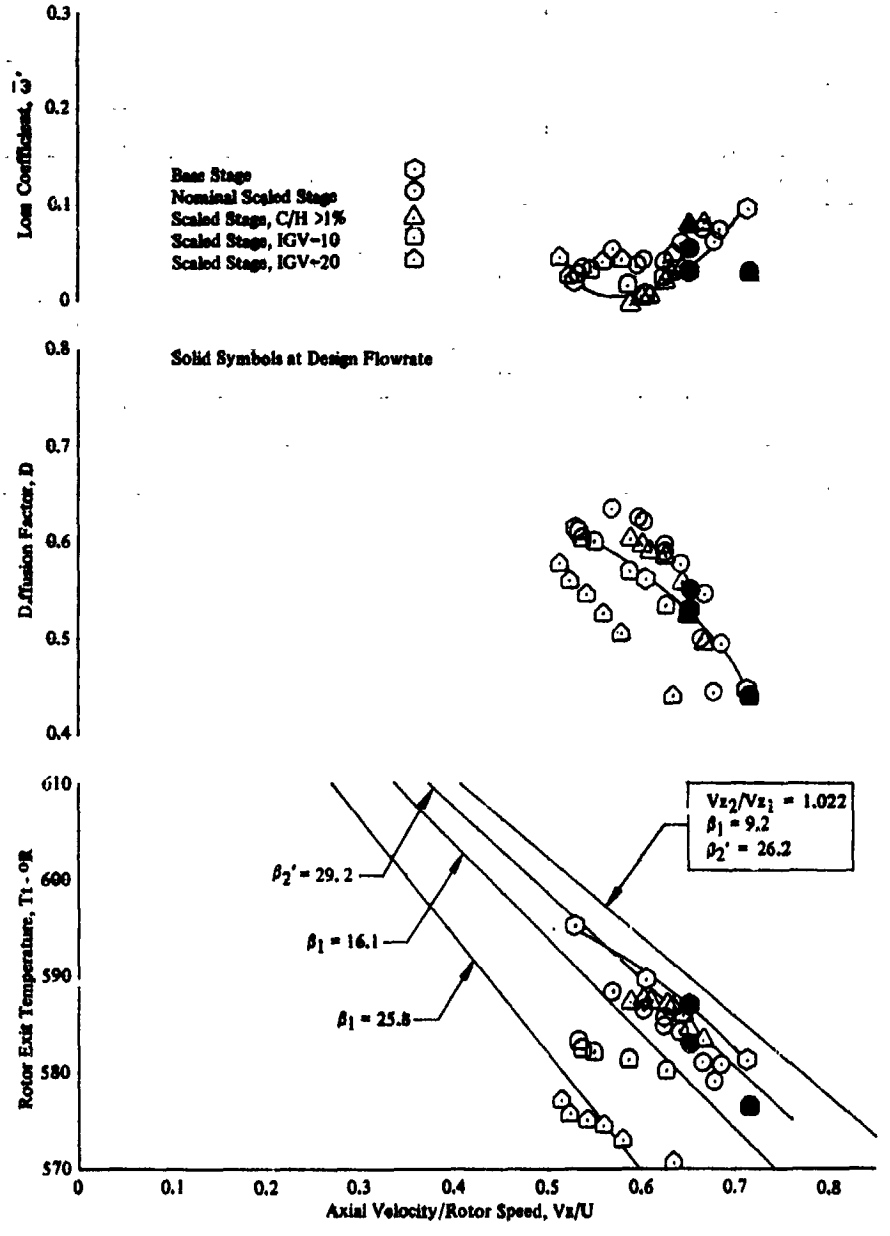

DF 103901

Figure 58. Rotor Performance at Design Speed, 50% Span

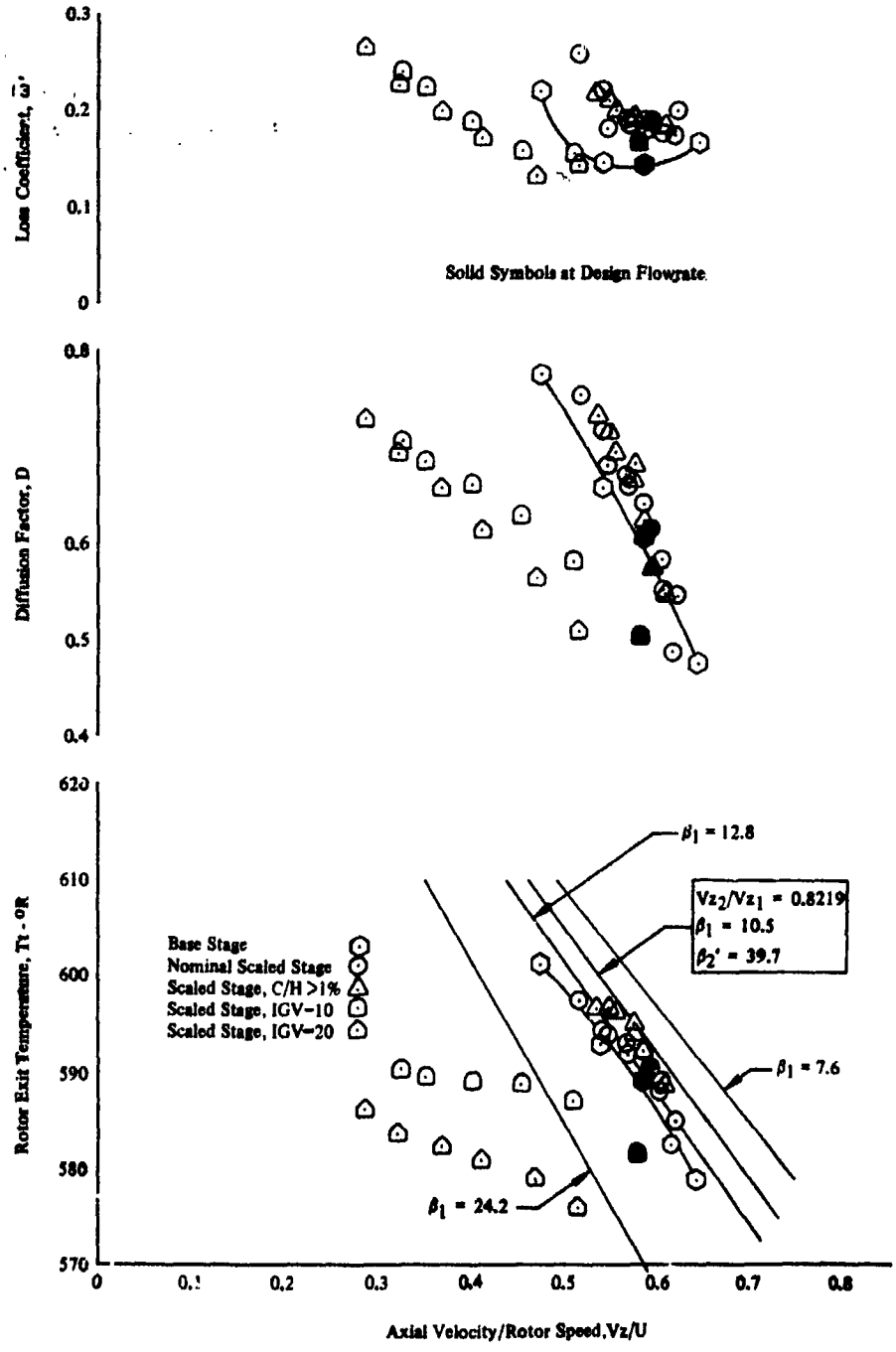

DF 103902

Figure 59. Rotor Performance at Design Speed, 10% Span

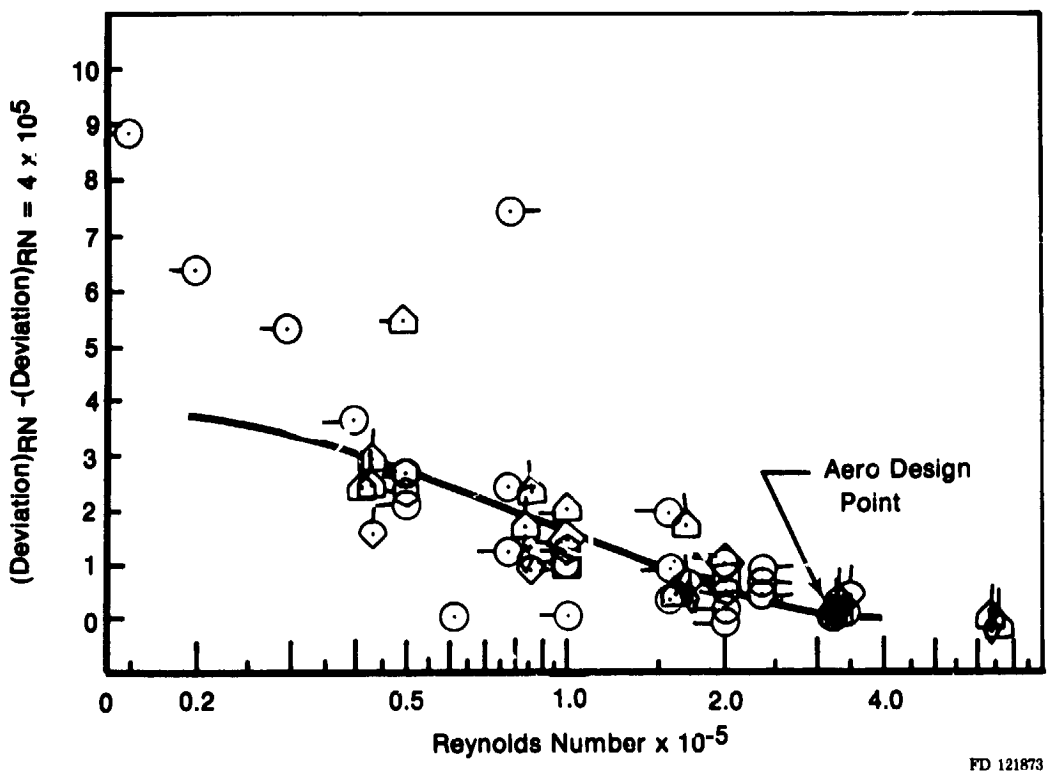

Figure 60. Scaled Stage Design Reynolds Number/Deviation Correlation

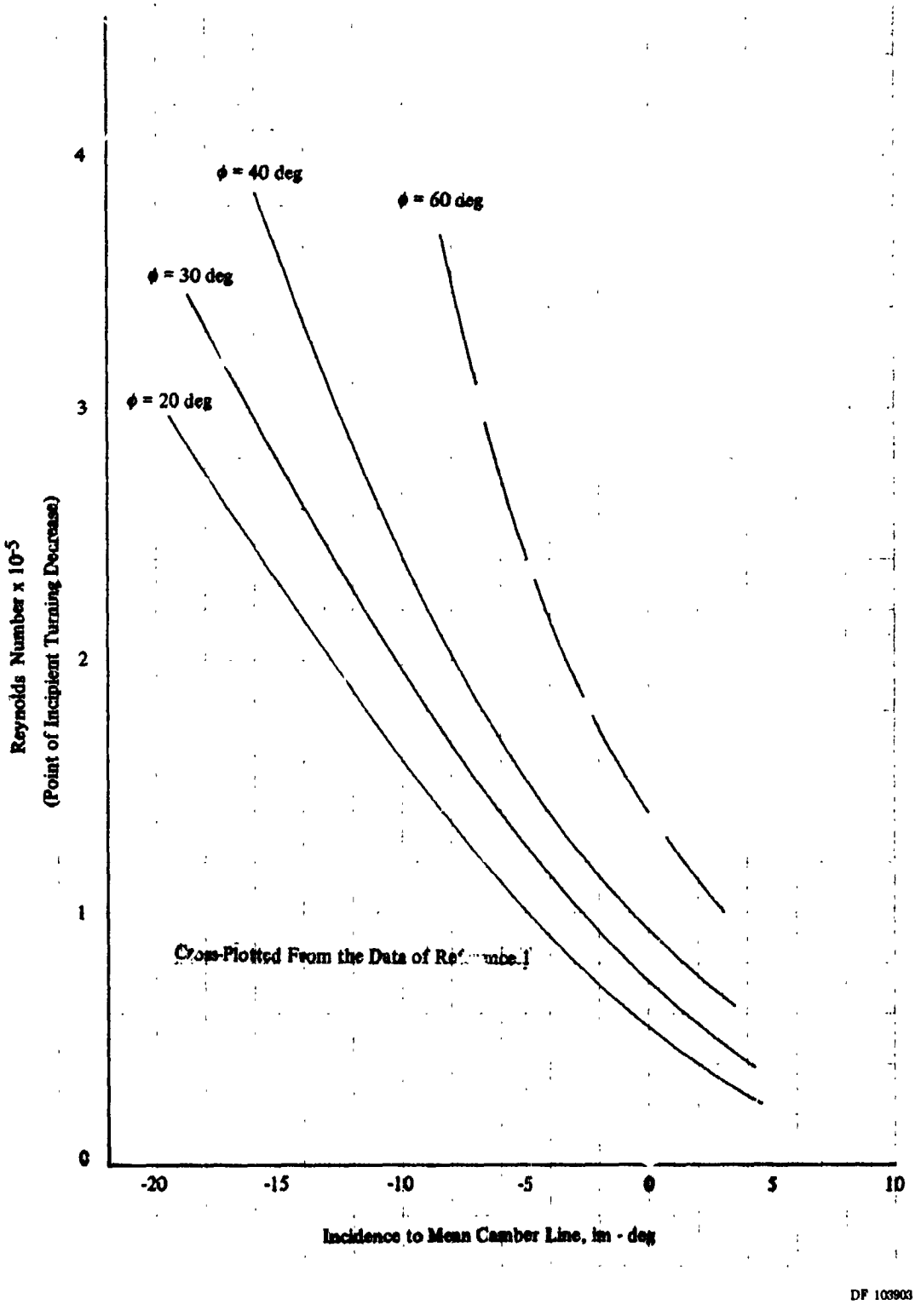

Figure 61. Effect of Camber on Critical RN per Rhoden (1956)

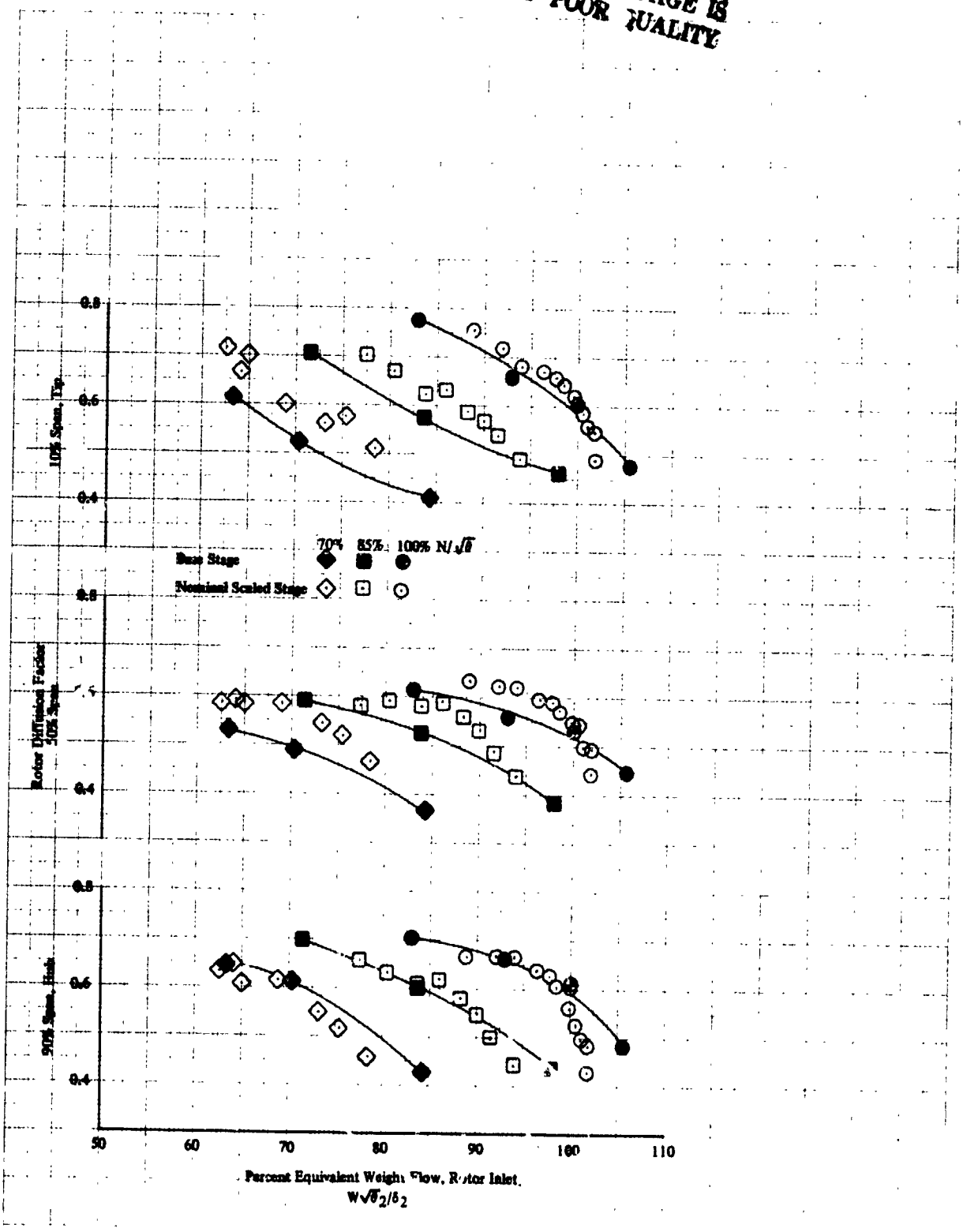

DF 103904

Figure 62. Spanwise Rotor Diffusion Factor

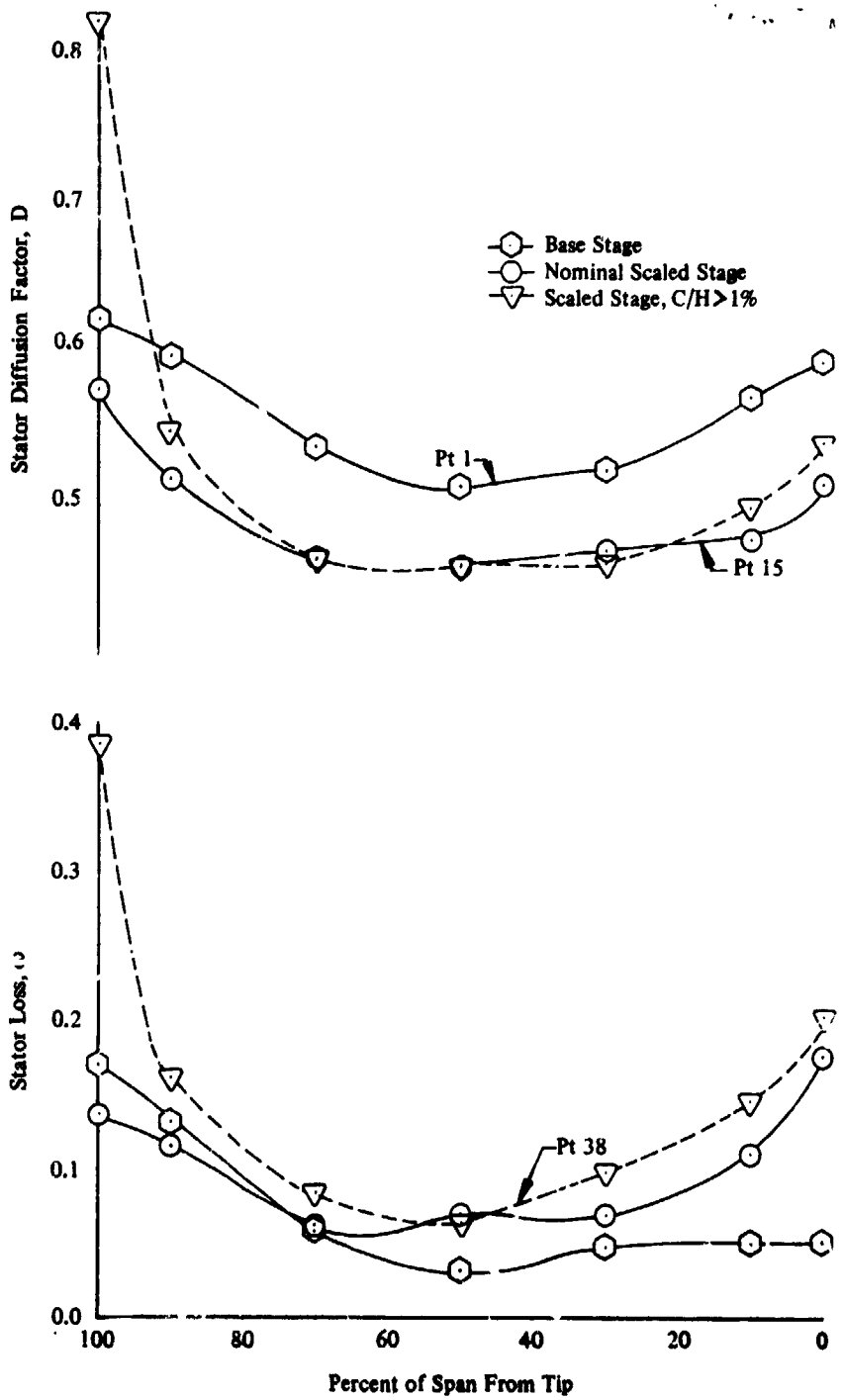

DF 103906

Figure 63. Spanwise Stator Performance, 100% $N/\sqrt{\theta}$, 100% $W/\sqrt{\theta}/\delta$

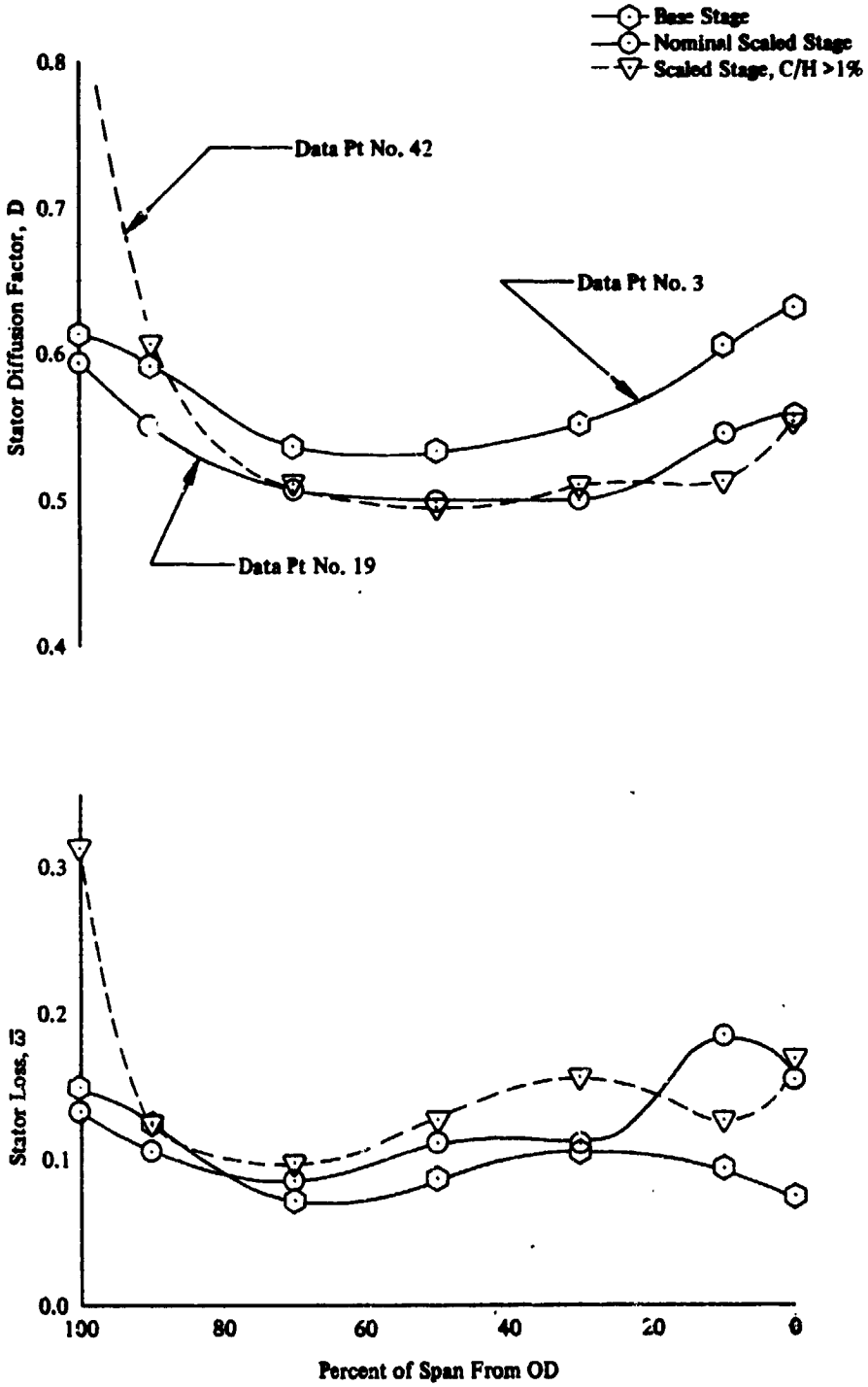

Figure 64. Spanwise Stator Performance, 100% $N/\sqrt{\theta}$, Peak η_{ad} Rotor

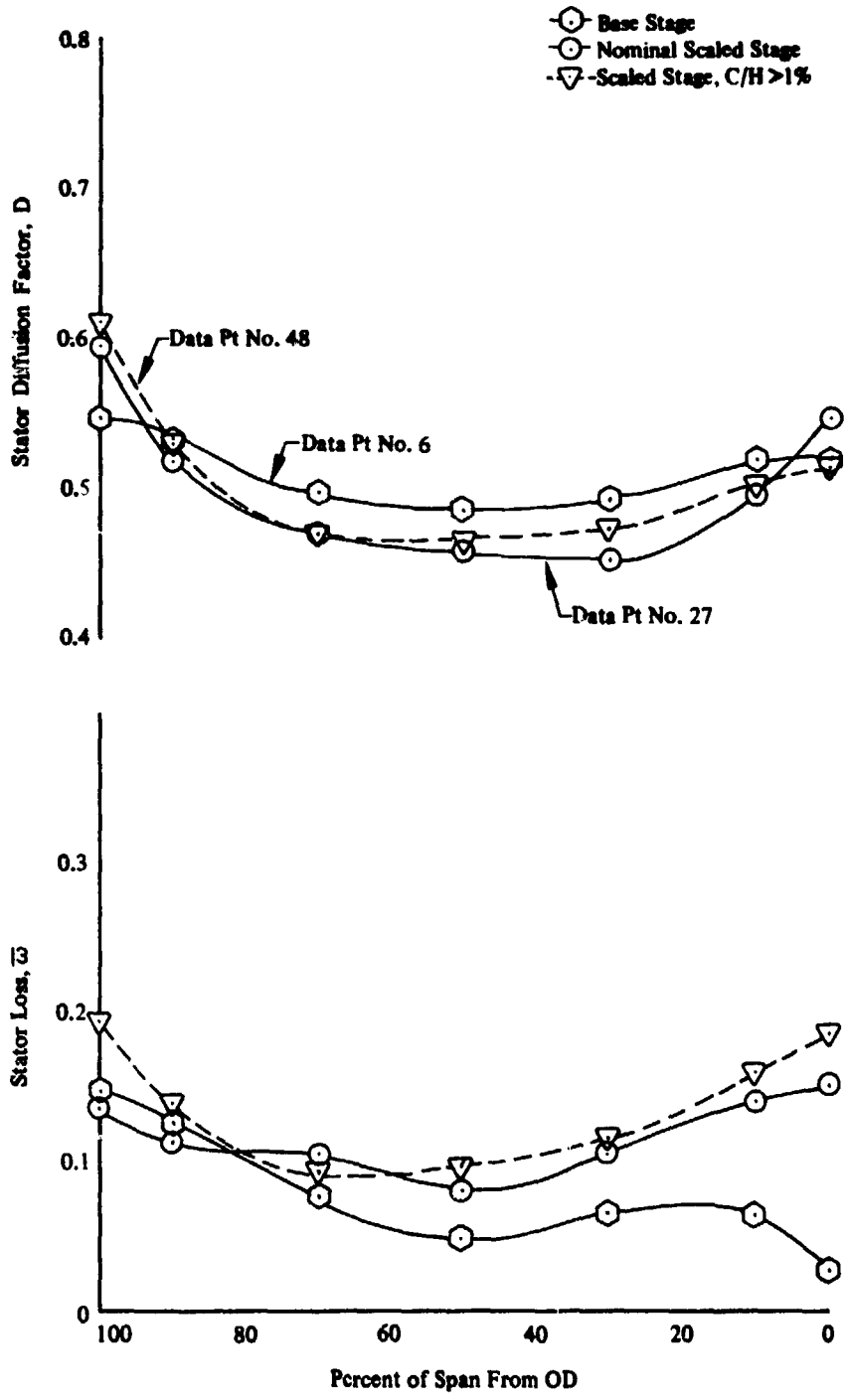

Figure 65. Spanwise Stator Performance, 85% $N/\sqrt{\theta}$, Midpoint

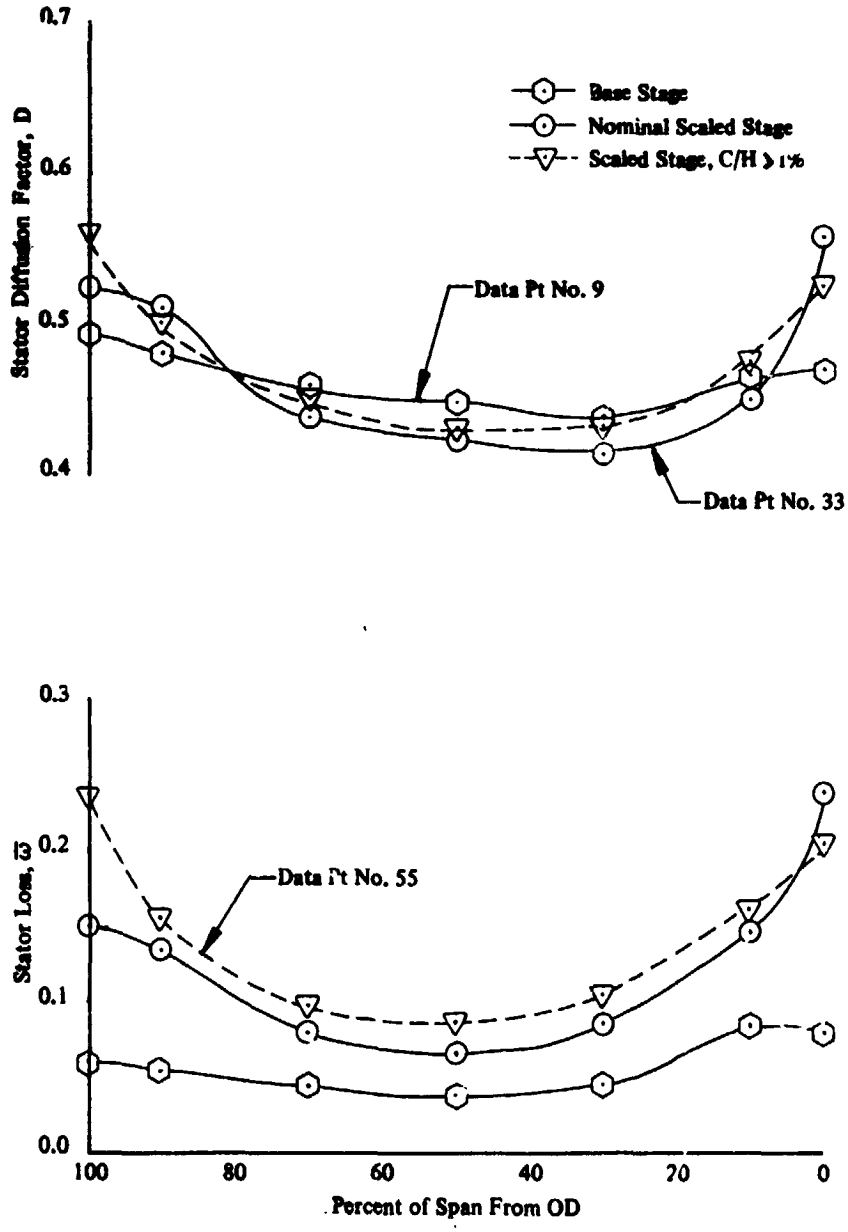

Figure 66. Spanwise Stator Performance, 70% $N/\sqrt{\theta}$, Midpoint

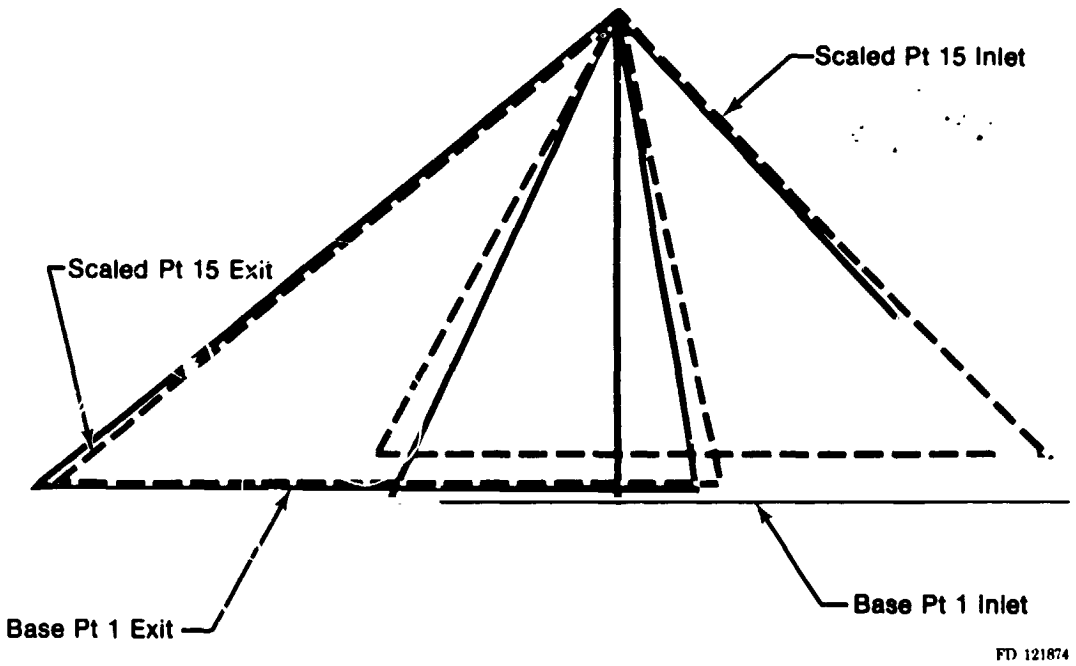

Figure 67. Stator Meanline Velocity Triangles

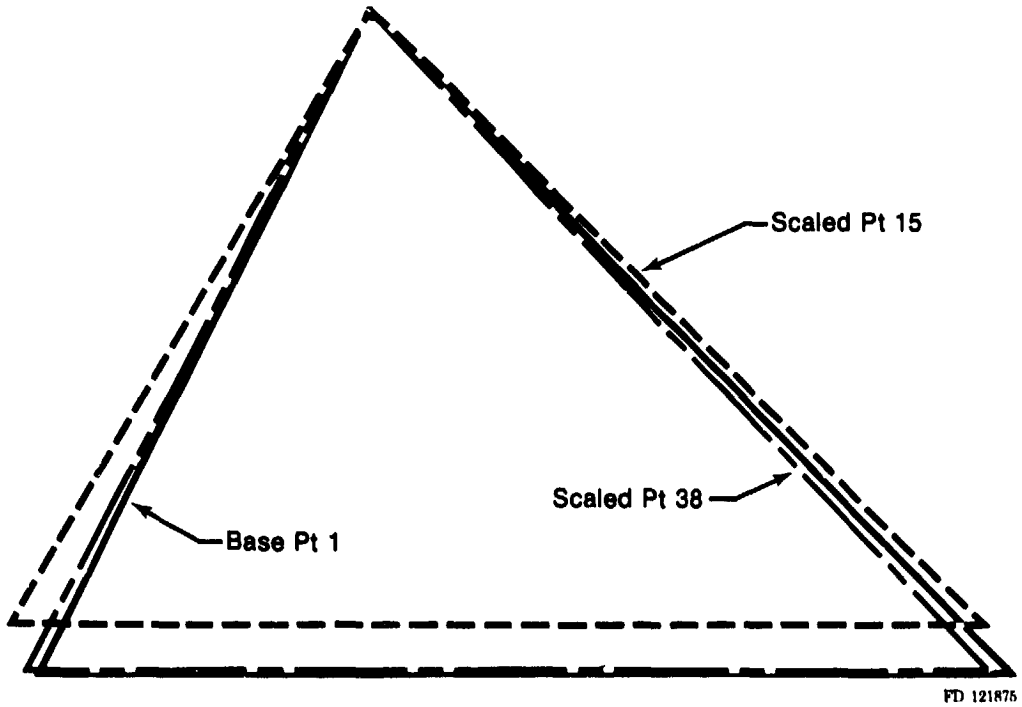

Figure 68. Rotor Exit Meanline Velocity Triangles

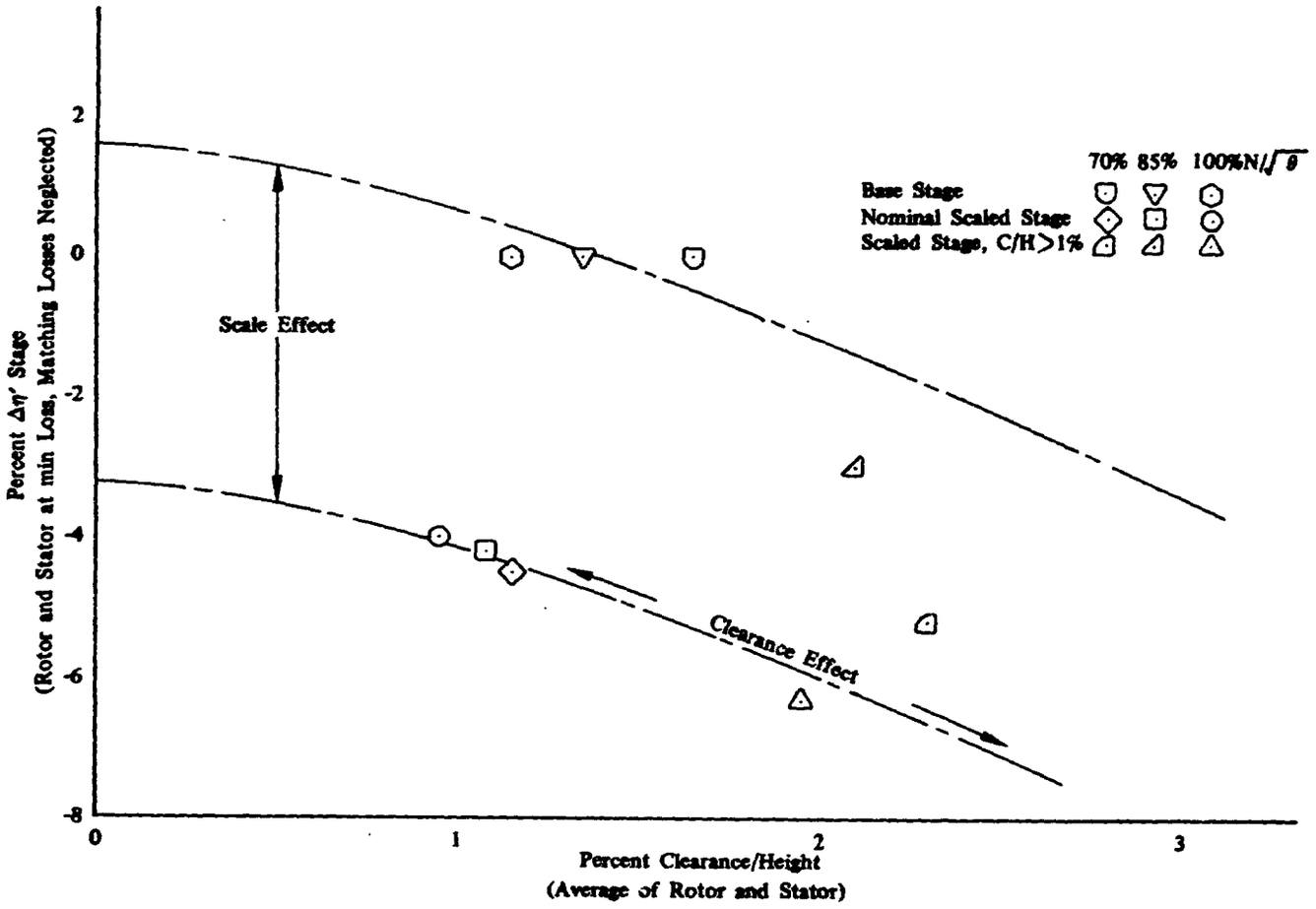

DF 103909

Figure 69. Effect of Scale and Clearance on Efficiency

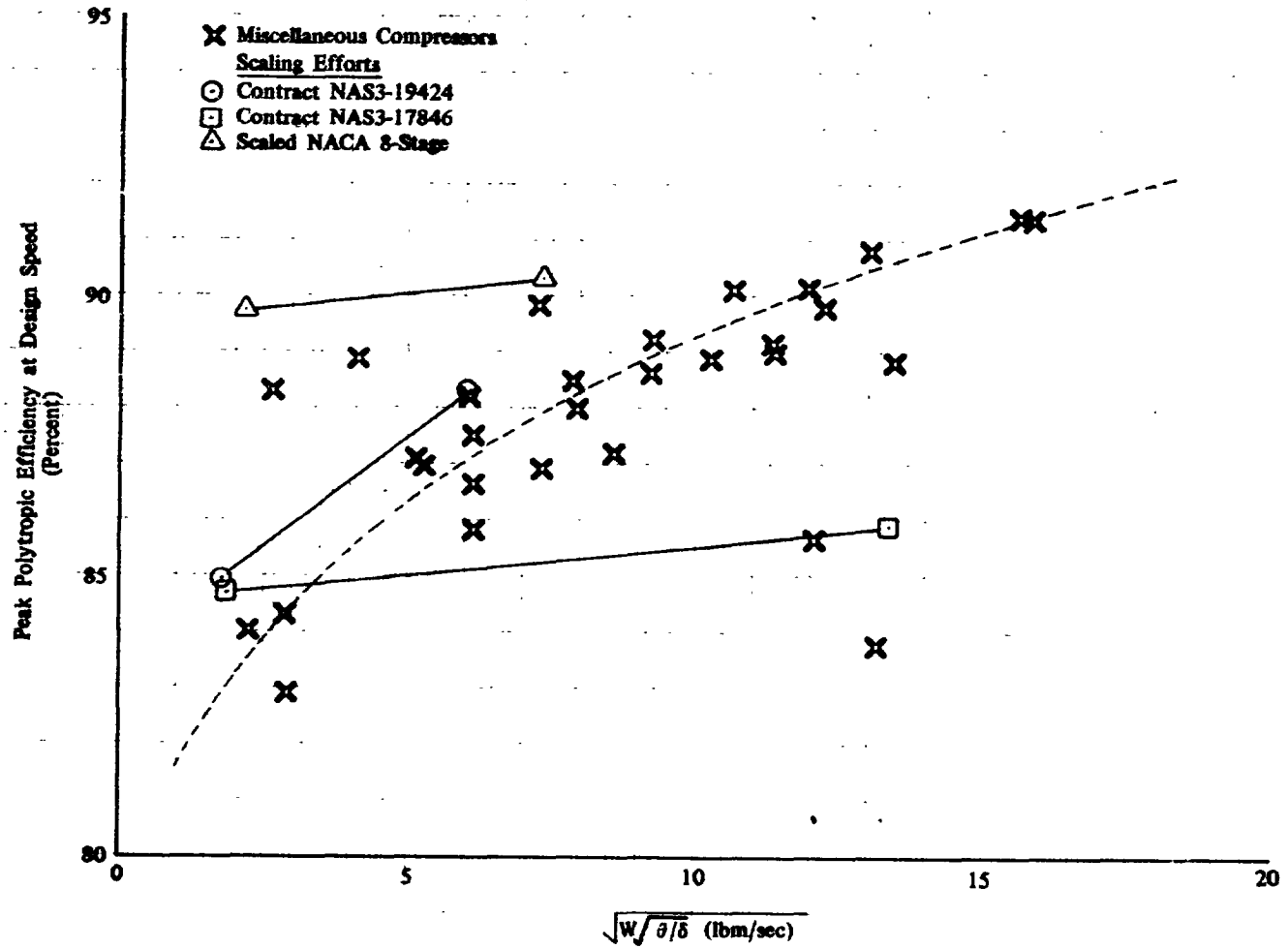

Figure 70. Historical Effect of Scaling

Table I. Design Point Performance Comparison

Parameter	*Base Stage Scaling Point*	*Scaled Stage Final Design*
SF, Scale factor	1.0	0.3043
$W\sqrt{\theta_1}/\delta_1$, IGV inlet	16.544kg/sec (36.473 lbm/sec)	1.532 kg/sec (3.378 lbm/sec)
$W\sqrt{\theta_2}/\delta_2$, Rotor inlet	16.595 kg/sec (36.586 lbm/sec)	1.537 kg/sec (3.388 lbm/sec)
$N/\sqrt{\theta_2}$	1,096.50 rad/sec (10,470.8 rpm)	3,603.26 rad/sec (34,408.6 rpm)
Utip	297.45 m/sec (975.88 ft/sec)	298.23 m/sec (978.43 ft/sec)
Hub/Tip Ratio	0.772	0.771
AR, Rotor	1.006	1.046
AR, Stator	1.006	1.085
σ, Rotor	1.244	1.244
σ, Stator	1.248	1.248
$\bar{K}$, Rotor inlet	0.967	0.953
$\bar{K}$, Rotor exit	0.900	0.855
$\bar{K}$, Stator exit	0.940	0.873
RN $\times 10^6$, IGV	2.89	0.89
RN $\times 10^6$, Rotor	10.73	3.24
RN $\times 10^6$, Stator	9.07	2.71
DF, Rotor	0.562	0.566
DF, Stator	0.547	0.534
PR, Rotor	1.515	1.508
ηad, Rotor	92.5	91.4
PR, Stage	1.480	1.471
ηad, Stage	87.2	85.7

Where: AR = Aspect Ratio
σ = Solidity
$\bar{K}$ = Effective area/actual area
RN = Reynolds Number
DF = Diffusion factor
PR = Total pressure ratio
ηad = Adiabatic efficiency

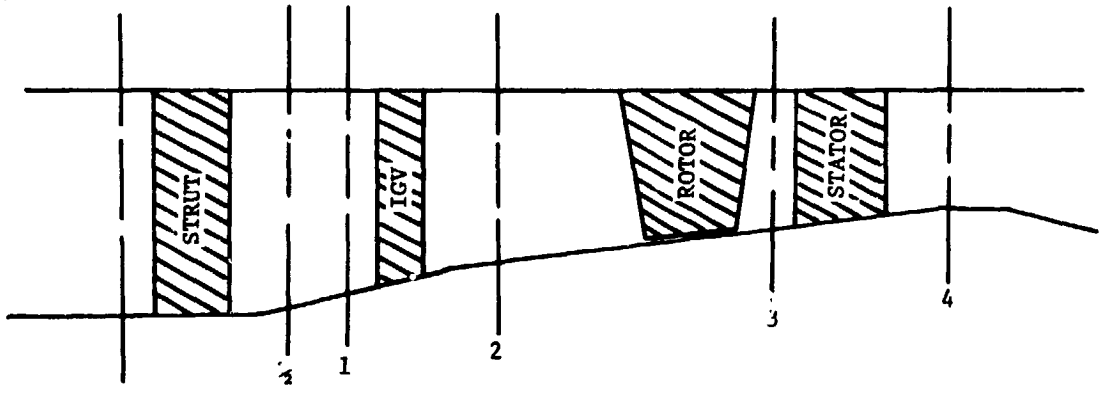

Table II. Base Stage Instrumentation Station Designation

Location	ID		OD		Axial Dist	
	cm	in.	cm	in.	cm	in.
Base Grate Screen	41.910	16.500	64.922	25.560	−53.574	−21.092
Strut Lead Edge	41.910	16.500	64.922	25.560	−47.752	−18.800
Strut Trail Edge	41.910	16.500	64.922	25.560	−40.132	−15.800
Station ½	41.910	16.500	61.341	24.150	−26.421	−10.402
Station 1	41.910	16.500	59.324	23.356	−19.743	−7.773
IGV Stacking Line	41.910	16.500	57.556	22.660	−13.924	−5.482
Station 2	41.910	16.500	55.753	21.950	−7.577	−2.983
Rotor Stacking Line	41.910	16.500	53.802	21.182	0.000	0.000
Station 3	41.910	16.500	52.941	20.843	3.340	1.315
Stator Stacking Line	41.910	16.500	52.400	20.630	6.566	2.585
Station 4	41.910	16.500	51.247	20.176	10.709	4.216

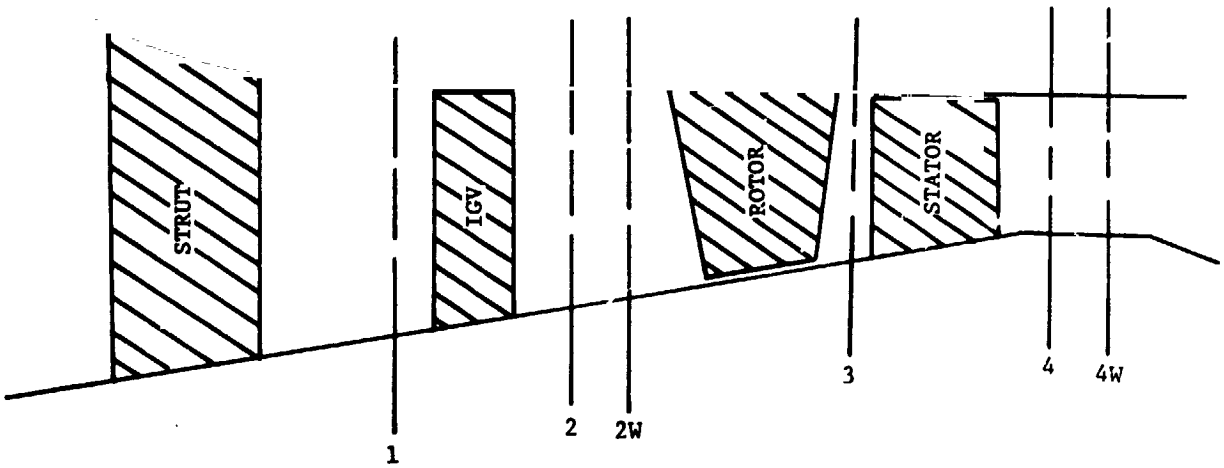

Table III. Scaled Stage Instrumentation Station Designation

Location	ID		OD		Axial Dist	
	cm	in.	cm	in.	cm	in.
Strut Lead Edge	10.236	4.030	20.251	7.973	−13.719	−5.401
Strut Trail Edge	11.976	4.715	19.360	7.622	−10.544	−4.151
Station 1	12.746	5.018	18.214	7.171	−6.507	−2.562
IGV Stacking Line	12.746	5.018	17.579	6.921	−4.249	−1.673
Station 2	12.746	5.018	17.028	6.704	−2.327	−0.916
Station 2 (Wedge probes)	12.746	5.018	16.836	6.656	−1.895	−0.746
Rotor Stacking Line	12.667	4.987	16.441	6.473	0.000	0.000
Station 3	12.591	4.957	16.210	6.382	1.057	0.416
Stator Stacking Line	12.573	4.950	16.040	6.315	1.704	0.671
Station 4	12.621	4.969	15.723	6.190	3.305	1.301
Station 4 (Wedge probes)	12.634	4.974	15.723	6.190	4.221	1.662

Table IV. Base Stage Instrumentation Schedule

Sta	Param	Fix	Radial Trav	Circ Trav	No. Rakes	No. Sensors Per Rake	Total Sensors	Circumferential Position	Radial Position
0	PS	X					2		
	ΔPS	X					2		
P	PT	X					4	30, 270, 90, 80	30, 50, 50, 70
	TT	X					1	75	50
½	PT	X			2	4	8	337.5, 157.5	18.9, 42.1, 65.2, 88.4
1	PS	X					4	270, 180, 90, 0	ID Wall
2	PT			X	2	5	10	253, 73	8.8, 27.2, 46.4, 66.8, 88.5
	PS	X					4	270, 180, 90, 0	ID Wall
	PS	X					4	270, 180, 90, 0	OD Wall
	PS	X					1	343	OD Kistler
	Angle		X				2	354.5, 174.5	30° Wedge Probes
3	PT		X				2	356.5, 176.5	Kiel-Head Sensor
	PT	X					2	215, 35	Kulite Probe
	TT		X				2	356.5, 176.5	Kiel-Head Sensor
	PS	X					2	261, 81	OD Wall
	PS	X					1	325	OD Kistler
3½	PS	X					4		90, Stator Surfaces
	PS	X					4		50, Stator Surfaces
	PS	X					4		10, Stator Surfaces
4	PT			X	4	5	20	279.5, 196.5, 98.5, 7.5	9.1, 28, 47.5, 67.8, 89
	TT			X	4	5	20	279.5, 196.5, 98.5, 7.5	9.1, 28, 47.5, 67.8, 89
	PS	X					4	270, 180, 90, 0	OD Wall
	Angle		X				2	264.5,84.5	30° Wedge Probes

Note: (1) Circumferential position is clockwise looking in direction of airflow
(2) Radial location is percent of span from OD

Table V. Scaled Stage Instrumentation Schedule

Sta	Param	Fix	Radial Trav	Circ Trav	No. Rakes	No. Sensors Per Rake	Total Sensors	Circumferential Position	Radial Position
0	PS	X					4		
	ΔPS	X					4		
P	PT	X					3	315, 67.5, 0	33, 67, 100
	TT	X					5	0, 330, 270, 45, 90	9, 13, 20, 36, 81
	PS	X					1	337.5	OD Wall
1	PS	X					4	354.5, 270, 185.5, 81.5	OD Wall
2	PT			X	2	5	10	287, 107.5	10, 30, 50, 70, 90
	PT	X			1	4	4	330	3, 5, 8, 10
	PS	X					4	279.5, 170.5, 91, 6	OD Wall
	PS		X				2	210, 30	30° Wedge Probes
	Angle		X				2	210, 30	30° Wedge Probes
3	PT	X			1	3	3	115	4, 7, 10
	PS	X					2	275, 95	OD Wall
4	PT			X	2	5	10	339, 160	10, 30, 50, 70, 90
	PT	X			1	3	3	220	3, 7, 10
	TT			X	2	5	10	248.5, 68.5	10, 30, 50, 70, 90
	PS	X					4	265, 175, 85, 0	OD Wall
	PS		X				2	280, 100	30° Wedge Probes
	Angle		X				2	280, 100	30° Wedge Probes

Note: (1) Circumferential position is clockwise looking in direction of airflow
(2) Radial location is percent of span from OD

Table VI. Scaled Stage Measurement Estimates

Station	*Flow Variable*	*Instrumentation Type*	*Qty*	*Range*	*± Uncertainty*
Measurements:					
Orifice	P	Flange tap	4	5 psid	0.042 psia
	P	Differential static pressure	4	5 psid	0.007 psid
Plenum	P	+ Kiel-head probe	3	25 psia	0.061 psia
	T	Rosemount	5	Ambient	0.52°F
1	P	+ Outer wall tap	4	25 psia	0.061 psia
2	P	+ 5-sensor rake	2	10 psid	0.041 psid
	P	30° wedge probe	2	15 psia	0.062 psia
	P	+ Outer wall tap	4	25 psia	0.061 psia
		30° wedge probe	2	0 - 180°	1.0°
3	P	+ Outer wall tap	2	25 psia	0.102 psia
4	P	+ 5-sensor rake	2	10 psid	0.041 psid
	T	5-sensor rake	2	75-200°F	1.05°F
	P	30° wedge probe	2	25 psia	0.102 psia
	P	+ Outer wall tap	4	25 psia	0.061 psia
		30° wedge probe	2	0 - 180°	1.0°
—	C	Clearance probe	3	—	0.001 inch

Calculations:

Parameter	*Total Uncertainty (% of Design Value)*
$W\sqrt{\theta_2}/\delta_2$	1.92
$N/\sqrt{\theta_2}$	0.26
PR_{STAGE}	0.15
ηad_{STAGE}	2.07

Table VII. Overall Performance Summary

POINT	STAGE	WC1	IGV	TEST DATE	ROTOR % C/H	STATOR % C/H	AVG % C/H	WC2	PR_R	TR_R	η_{ADR}	% WC1	PR_{STG}	η_{ADSTG}
ADP	SCALED	100.0	-					100.0	1.508	1.136	.914	100.0	1.471	.857
1	BASE	100.0	+0	10/73	1.3	1.0	1.15	100.0	1.515	1.136	.925	100.0	1.480	.872
2		99.8						105.5	1.423	1.123	.861	105.4	1.311	.659
3		100.3						92.8	1.554	1.143	.941	92.8	1.503	.867
4		100.1						83.1	1.585	1.153	.923	83.1	1.510	.820
SURGE								81.5	1 589			81.5	1.510	
5		85.0		10/73		2	1.35	98.1	1.313	1.088	.923	98.1	1.253	.762
6		85.0						83.7	1.356	1.097	.938	83.7	1.329	.875
7		85.1						71.5	1.391	1.107	.929	71.6	1.348	.837
SURGE								68.9	1.399			69.0	1.349	
8		70.0		10/73	1.8	1.5	1.65	84.2	1.206	1.059	.925	84.2	1.177	.816
9		70.0						70.4	1.225	1.064	.930	70.4	1.212	.879
10		69.9						63.4	1.244	1.069	.941	63.5	1.224	.872
SURGE								59.9	1.250			60.0	1.230	
11	SCALED	99.2	+0	10/22/76	0.8	0.9	0.85	101.8	1.425	1.120	.892	101.9	1.363	.776
12		99.3		11/29/76	1.3	0.8	1.05	101.8	1.426	1.122	.873	101.9	1.375	.780
13		99.2		10/22/76	0.8	0.9	0.85	101.0	1.445	1.126	886	101.2	1.398	.803
14		99.1		10/22/76	0.8	0.9	0.85	100.5	1.452	1.127	.886	100.6	1.410	.814
15		99.4		11/29/76	1.3	0.8	1.05	99.7	1.458	1.129	.885	99.9	1.423	.825
16		99.3						98.5	1.469	1.131	.886	98.7	1.433	.827
17		99.5						97.7	1.481	1.132	.903	97.8	1.442	.839
18		99.4						96.3	1.485	1.135	.899	96.5	1.445	.834
19		99.7						94.0	1.496	1.135	.905	94.2	1.452	.833
20		99.3						92.1	1.496	1.136	.902	92.3	1.454	.835
21		99.4						88.8	1.504	1.139	.895	88.9	1.458	.823
SURGE								86.5	1.508			86.6	1.460	
22		84.7		10/19/76	0.9	1.0	0.95	93.9	1.310	1.088	.913	94.1	1.274	.816
23		84.5						91.6	1.321	1.091	.915	91.8	1.287	.826
24		84.8						90.0	1.326	1.092	.912	90.2	1.294	.829
25		84.7		11/29/76	1.4	1.0	1.20	88.2	1.332	1.094	.910	88.4	1.300	.833
26		84.9		10/19/76	0.9	1.0	0.95	86.0	1.337	1.096	.903	86.2	1.307	.829
27		84.6		11/29/76	1.4	1.0	1.20	83.8	1.342	1.098	.901	84.0	1.311	.827
28		84.5		10/19/76	0.9	1.0	0.95	80.6	1.351	1.099	.905	80.8	1.316	.822
29		84.7						77.5	1.359	1.100	.916	77.7	1.315	.814
SURGE								71.7	1.370			71.9	1.320	
30		70.3		10/19/76	1.1	1.2	1.15	78.6	1.212	1.061	934	78.8	1.190	.842
31		70.2						75.4	1.218	1.065	.902	75.5	1.200	.833
32		70.4						73.3	1.224	1.066	.903	73.5	1.205	.831
33		70.6		11/12/76				69.0	1.221	1.067	.879	69.1	1.202	.808
34		70.3		10/19/76				65.3	1.230	1.067	.907	65.5	1.204	.814
35		70.4						64.2	1.224	1.068	.874	64.4	1.205	.803
36		70.3						62.7	1.237	1.068	.926	62.9	1.205	.810
SURGE								57.5	1.235			58.1	1.208	

Table VII. Overall Performance Summary (Continued)

POINT	STAGE	%NC1	IGV	TEST DATE	ROTOR %C/H	STATOR %C/H	AVG %C/H	%WC2	PR_R	TR_R	ηAD_R	$%WC_1$	PR_{STG}	ηAD_{STG}
37	SCALED	99.5	+0	12/14/76	1.8	2.1	1.9	100.3	1 452	1.129	.876	100.4	1.401	.788
38		99.5						99.7	1.468	1.131	.888	99.8	1.419	.805
39		99.4						98.2	1.494	1.135	.904	98.3	1.440	.817
40		99.5						97.4	1.498	1.137	.898	97.6	1.448	.819
41		99.1						95.9	1.502	1.137	899	96.1	1.454	.823
42		99.4						94.5	1.512	1.139	.905	94.7	1.461	.825
43		98.6						92.3	1.511	1.140	.906	92.4	1.458	.817
44		99.0						91.1	1.514	1.139	.906	91.3	1.456	.817
SURGE								89.1	1.515			89.3	1.464	
45		84.4		12/14/76	1.9	2.3	2.10	89.2	1.337	1.096	.907	89.4	1 302	.821
46		84.2						86.8	1.341	1.096	.913	87.0	1.309	.835
47		84.8						85.1	1.347	1.096	.929	85.3	1.315	.852
48		84.5						82.4	1.349	1.096	.934	82.6	1.314	.852
49		84.4						80.0	1.348	1.096	.929	80.1	1.311	.839
50		84.7						77.3	1.358	1.099	.926	77.5	1.314	.821
51		84.6						75.3	1.361	1.100	.922	75.5	1.315	.814
52		84.7						73.1	1.365	1.103	.907	73.2	1.315	.794
SURGE								69.5	1.372			69.6	1.317	
53		71.3		12/14/76	2.1	2.5	2.30	72.4	1.226	1.066	.909	72.6	1.203	.826
54		71.1						70.8	1.227	1.066	.918	71.0	1.205	.834
55		70.7						69.2	1.226	1.066	.911	69.3	1.203	.822
56		71.3						67.8	1.227	1.067	.907	68.0	1.205	.826
57		71.1						65.4	1.229	1.067	.913	65.6	1.204	.821
58		70.9						62.9	1.232	1.067	.917	63.1	1.205	.815
59		70.7						62.0	1.234	1.068	.919	62.1	1.204	.807
60		71 0						58.7	1.235	1.070	.897	58.8	1.204	.787
SURGE								56.7	1.237			56.8	1.205	
61		99.4	-10	11/29/76	1.3	0.8	1.05	100.2	1.413	1.115	.904	99.6	1.359	.799
62		99.4						97.1	1.453	1.122	.924	96.5	1.405	.837
63		99.4						94.7	1.464	1.125	.924	94.3	1.415	.837
64		99.4						92.4	1.462	1.126	.912	92.1	1.416	.831
65		99.4						89.1	1.466	1 127	.911	88.9	1.416	.826
66		99.4						87.4	1.470	1.128	.910	87.1	1.417	.819
SURGE								83.7	1.474			83.4	1.418	
67		83.7		10/19/76	0.9	1.0	0.95	86.4	1.272	1.080	.895	86.2	1.234	.780
68		84.5						85.2	1.285	1.082	.909	85.0	1.251	.810
69		84.6						83.6	1.296	1.084	.911	83.4	1.265	.824
70		84.9						80.9	1.312	1.087	.933	80.8	1.280	.843
71		84.5						76.3	1.321	1.089	.935	76.3	1.283	.833
72		84.8						75.2	1.327	1.090	.935	75.2	1.287	.830
73		84.4		11/29/76	1.4	1.0	1.30	70.3	1.328	1.092	.918	70.3	1.290	.819
SURGE								65.0	1.330			65.0	1.291	

Table VII. Overall Performance Summary (Continued)

POINT	STAGE	%WC1	IGV	TEST DATE	ROTOR %C/H	STATOR %C/H	AVG %C/H	%WC2	PR_R	TR_R	η_{AD_R}	%WC1	PR_{STG}	$\eta_{AD_{STG}}$
74	SCALED	70.2	-10	10/19/76	1.1	1.2	1.15	72.8	1.185	1.054	.915	72.8	1.162	.808
75		70.2		" "	"	"	"	70.6	1.196	1.057	.928	70.7	1.172	.824
76		70.8		11/29/76	1.7	1.2	1.45	68.5	1.198	1.058	.913	68.5	1.178	.825
77		70.2		10/19/76	1.1	1.2	1.15	65.3	1.203	1.060	.905	65.4	1.181	.814
78		70.5		11/29/76	1.7	1.2	1.45	63.1	1.207	1.061	.903	63.1	1.185	.815
79		70.3		10/19/76	1.1	1.2	1.15	61.1	1.213	1.062	.919	61.1	1.186	.811
80		70.3						60.6	1.215	1.062	.930	60.6	1.188	.818
81		70.4						59.8	1.218	1.062	.935	59.9	1.188	.817
SURGE								53.4	1.223			53.5	1.189	
82		99.4	-20	11/29/76	1.3	0.8	1.05	91.1	1.369	1.103	.915	90.1	1.308	.776
83		99.3						88.6	1.395	1.108	.927	87.7	1.336	.801
84		99.6						86.2	1.403	1.111	.919	85.5	1.345	.798
85		99.3						83.2	1.407	1.113	.909	82.5	1.349	.792
86		99.5						81.0	1.414	1.115	.909	80.4	1.352	.787
87		99.5						78.5	1.416	1.117	.893	78.0	1.357	.779
SURGE								76.3	1.418			75.8	1.357	
88		84.5		10/20/76	0.6	0.7	0.65	80.4	1.228	1.068	.891	79.9	1.193	.761
89		84.6						78.6	1.244	1.072	.890	78.0	1.207	.765
90		84.1						76.8	1.251	1.075	.891	76.3	1.215	.768
91		84.5						74.4	1.267	1.078	.897	74.0	1.228	.776
92		84.5						71.8	1.274	1.080	.894	71.4	1.234	.773
93		84.7						69.5	1.281	1.081	.904	69.2	1.238	.778
SURGE								62.4	1.288			62.1	1.244	
94		69.8		10/20/76	1.1	1.2	1.15	66.7	1.159	1.048	.898	66.4	1.134	.762
95		70.0						64.8	1.167	1.051	.895	64.5	1.143	.774
96		70.3						62.2	1.174	1.053	.893	62.0	1.151	.783
97		69.9						57.9	1.182	1.055	.884	57.8	1.156	.767
98		69.9						56.7	1.185	1.056	.883	56.5	1.158	.762
99		70.0						56.2	1.188	1.057	.897	56.1	1.158	.760
100		70.3		11/29/76	1.7	1.2	1.45	51.7	1.197	1.062	.857	51.7	1.169	.741
SURGE								49.6	1.195			49.6	1.169	
101		70.1	+0	9/21/76	0.6	0.7	0.65	67.3	1.229	1.067	.903	67.5	1.213	.845
102		70.5			0.6	0.7	0.65	62.8	1.243	1.069	.936	62.9	1.219	.850
SURGE								59.5	1.252			59.6	1.222	
103		85.0			0.8	0.9	0.85	87.4	1.346	1.101	.880	87.6	1.329	.841
104		85.0			0.8	0.9	0.85	79.3	1.364	1.101	.921	79.5	1.332	.848
SURGE								72.0	1.376			72.2	1.335	

Table VIII. Blockage Factors

Data Point	Station 1 IGV Inlet		Station 2 Rotor Inlet		Station 3 Rotor Exit		Station 4 Stator Exit	
	K	PSR	K	PSR	K	PSR	K	PSR
ADP	0.97	—	0.96	—	0.86	—	0.87	—
1	1.00	—	0.97	—	0.90	—	0.94	—
2	1.00	—	0.96	—	0.88	—	0.89	—
3	1.00	—	0.96	—	0.86	—	0.88	—
4	1.00	—	0.95	—	0.84	—	0.86	—
5	1.00	—	0.96	—	0.88	—	0.89	—
6	1.00	—	0.97	—	0.90	—	0.94	—
7	1.00	—	0.95	—	0.84	—	0.86	—
8	1.00	—	0.96	—	0.88	—	0.89	—
9	1.00	—	0.97	—	0.90	—	0.94	—
10	1.00	—	0.95	—	0.84	—	0.86	—
11	1.00	1.00	0.94	1.00	0.83	1.00	0.91	1.00
12	1.00	1.00	0.94	1.00	0.89	1.00	0.92	1.00
13	1.00	1.00	0.95	1.00	0.87	1.00	0.91	1.00
14	1.00	1.00	0.94	1.00	0.91	1.00	0.91	1.00
15	0.99	1.00	0.95	1.00	0.94	1.00	0.91	1.00
16	0.99	1.00	0.95	1.00	0.96	1.00	0.91	1.00
17	1.00	1.00	0.96	1.00	0.98	1.00	0.92	1.00
18	0.98	1.00	0.95	1.00	0.98	1.00	0.91	1.00
19	0.99	1.00	0.95	1.00	0.99	1.00	0.91	1.00
20	0.99	1.00	0.94	1.00	1.00	1.00	0.89	1.00
21	0.98	1.00	0.94	1.00	0.99	0.99	0.88	1.00
22	1.01	1.00	0.94	1.00	0.86	1.00	0.92	1.00
23	1.02	1.00	0.94	1.00	0.90	1.00	0.93	1.00
24	1.01	1.00	0.94	1.00	0.93	1.00	0.95	1.00
25	0.98	1.00	0.94	1.00	0.95	1.00	0.93	1.00
26	0.97	1.00	0.95	1.00	0.99	1.00	0.97	1.00
27	0.97	1.00	0.94	1.00	0.94	1.00	0.91	1.00
28	0.99	1.00	0.96	1.00	0.95	1.00	0.91	1.00
29	0.99	1.00	0.95	1.00	0.95	1.00	0.92	1.00
30	0.99	1.00	0.95	1.00	0.91	1.00	0.94	1.00
31	0.98	1.00	0.93	1.00	0.93	1.00	0.93	1.00
32	0.98	1.00	0.95	1.00	0.93	1.00	0.93	1.00
33	0.97	1.00	0.93	1.00	0.96	1.00	0.91	1.00
34	0.98	1.00	0.93	1.00	0.98	1.00	0.94	1.00
35	0.98	1.00	0.95	1.00	0.96	1.00	0.94	1.00
36	0.98	1.00	0.95	1.00	0.96	1.00	0.91	1.00
37	0.97	1.00	0.94	1.00	0.85	1.00	0.90	1.00
38	1.00	1.00	0.95	1.00	0.86	1.00	0.90	1.00
39	1.00	1.00	0.94	1.00	0.91	1.00	0.91	1.00
40	0.99	1.00	0.95	1.00	0.95	1.00	0.91	1.00
41	0.99	1.00	0.94	1.00	0.96	1.00	0.91	1.00
42	0.99	1.00	0.95	1.00	0.96	1.00	0.91	1.00
43	0.98	1.00	0.94	1.00	0.96	1.00	0.90	1.00
44	0.98	1.00	0.94	1.00	0.98	1.00	0.92	1.00
45	0.99	1.00	0.94	1.00	0.88	1.00	0.91	1.00
46	0.98	1.00	0.94	1.00	0.90	1.00	0.91	1.00
47	0.98	1.00	0.95	1.00	0.91	1.00	0.92	1.00
48	0.98	1.00	0.94	1.00	0.90	1.00	0.91	1.00
49	0.98	1.00	0.95	1.00	0.88	1.00	0.91	1.00
50	0.98	1.00	0.95	1.00	0.88	1.00	0.90	1.00
51	0.98	1.00	0.95	1.00	0.89	1.00	0.89	1.00
52	0.98	1.00	0.95	1.00	0.91	1.00	0.87	1.00

Table VIII. Blockage Factors (Continued)

Data Point	Station 1 IGV Inlet $\bar{K}$	Station 1 IGV Inlet PSR	Station 2 Rotor Inlet $\bar{K}$	Station 2 Rotor Inlet PSR	Station 3 Rotor Exit $\bar{K}$	Station 3 Rotor Exit PSR	Station 4 Stator Exit $\bar{K}$	Station 4 Stator Exit PSR
53	0.98	1.00	0.94	1.00	0.90	1.00	0.92	1.00
54	0.97	1.00	0.93	1.00	0.91	1.00	0.92	1.00
55	0.97	1.00	0.95	1.00	0.89	1.00	0.91	1.00
56	0.97	1.00	0.95	1.00	0.90	1.00	0.91	1.00
57	0.97	1.00	0.95	1.00	0.90	1.00	0.91	1.00
58	0.97	1.00	0.93	1.00	0.88	1.00	0.90	1.00
59	0.97	1.00	0.96	1.00	0.89	1.00	0.90	1.00
60	0.97	1.00	0.96	1.00	0.87	1.00	0.89	1.00
61	0.97	0.98	0.95	0.98	0.87	0.95	0.92	1.00
62	0.99	0.99	0.95	0.98	0.92	0.96	0.91	1.00
63	0.99	0.99	0.95	0.98	0.96	0.97	0.91	1.00
64	1.00	0.99	0.96	0.98	1.00	0.97	0.91	1.00
65	1.00	0.99	0.98	0.99	1.00	0.98	0.91	1.00
66	0.99	0.99	0.97	0.99	1.00	0.98	0.90	1.00
67	0.98	1.00	0.96	1.00	0.91	1.00	0.93	1.00
68	0.99	1.00	0.95	1.00	0.94	1.00	0.93	1.00
69	0.98	1.00	0.95	1.00	0.96	1.00	0.92	1.00
70	0.99	1.00	0.96	1.00	0.99	1.00	0.93	1.00
71	0.99	1.00	0.96	1.00	1.00	1.00	0.91	1.00
72	0.99	1.00	0.96	1.00	0.99	1.00	0.90	1.00
73	0.99	0.99	0.96	0.99	1.00	0.98	0.90	1.00
74	0.98	1.00	0.95	1.00	0.92	1.00	0.94	1.00
75	0.98	1.00	0.95	1.00	0.97	1.00	0.93	1.00
76	0.98	0.99	0.95	0.99	0.99	0.98	0.93	0.98
77	0.98	1.00	0.95	1.00	1.00	1.00	0.94	1.00
78	0.97	0.99	0.95	0.99	1.00	0.98	0.92	0.99
79	0.97	1.00	0.96	1.00	1.00	1.00	0.92	1.00
80	0.98	1.00	0.96	1.00	0.97	1.00	0.91	1.00
81	0.97	1.00	0.92	1.00	0.98	1.03	0.92	1.00
82	1.00	1.00	0.97	1.00	0.89	0.96	0.90	1.00
83	1.00	1.00	0.98	1.00	0.92	0.96	0.88	1.00
84	1.00	1.00	0.99	1.00	0.94	0.96	0.89	1.00
85	1.00	1.00	0.97	1.00	0.96	0.96	0.88	1.00
86	1.00	1.00	0.99	1.00	0.98	0.96	0.86	1.00
87	1.00	1.00	0.99	1.00	1.00	0.97	0.85	1.00
88	0.97	1.00	0.95	1.00	0.90	0.97	0.95	1.00
89	0.93	1.00	0.94	1.00	0.92	0.97	0.95	1.00
90	0.97	1.00	0.94	1.00	0.94	0.97	0.95	1.00
91	0.97	1.00	0.95	1.00	0.96	0.97	0.95	1.00
92	0.96	1.00	0.95	1.00	0.98	0.97	0.93	1.00
93	0.97	1.00	0.95	1.00	1.00	0.97	0.92	1.00
94	0.98	1.00	0.95	1.00	0.88	0.97	0.94	1.00
95	0.97	1.00	0.94	1.00	0.91	0.98	0.95	1.00
96	0.95	1.00	0.92	1.00	0.93	0.97	0.95	1.00
97	0.96	1.00	0.92	1.00	0.95	0.97	0.94	1.00
98	0.97	1.00	0.95	1.00	0.97	0.98	0.90	1.04
99	0.97	1.00	0.9[illegible]	1.00	0.98	0.98	0.91	1.00
100	0.98	1.00	0.98	1.00	1.00	0.98	0.87	
101	0.98	1.00	0.99	1.00	0.95	1.00	0.91	1.00
102	0.98	1.00	1.03	1.00	0.95	1.00	0.89	1.00
103	1.00	1.00	1.02	1.00	0.99	0.99	0.92	1.00
104	1.00	1.00	1.00	1.00	0.95	1.00	0.08	1.00

where $\bar{K}$ = Blockage Factor = Effective Area/Actual Area

PSR = $\frac{\text{Calculated OD Ps}}{\text{Measured OD Ps}}$

Table IX. Meanline Velocity Triangle Comparison

Parameter	*Point 1*		*Point 15*		*Point 38*	
$W\sqrt{\theta_1}/\delta_1$	16.5971	(36.5902)	1.5369	(3.3882)	..5369	(3.3882)
$N/\sqrt{\theta_1}$	1,096.5	(10,470.5)	3,603.3	(34,408.6)	3,603.3	(34,408.6)
V_1	113.5	(372.4)	112.7	(369.9)	115.9	(380.2)
V_{x1}	113.5	(372.4)	112.7	(369.9)	115.9	(380.2)
V_1'	300.1	(984.5)	300.3	(985.3)	301.5	(989.3)
$V_{\theta 1}$	0.0	(0.0)	0.0	(0.0)	0.0	(0.0)
$V_{\theta 1}'$	277.8	(911.4)	278.4	(913.3)	278.4	(913.3)
U_1	277.8	(911.4)	278.4	(913.3)	278.4	(913.3)
β_1	0.0		0.0		0.0	
β_1'	67.8		67.4		67.4	
D_1	50.63	(19.932)	15.44	(6.078)	15.44	(6.078)
R_1	1.000		0.990		1.000	
V_2	127.9	(419.5)	133.2	(436.9)	133.2	(437.0)
V_{x2}	125.0	(410.0)	130.2	(427.1)	130.2	(427.2)
V_2'	277.1	(909.2)	279.0	(915.3)	279.1	(915.7)
$V_{\theta 2}$	27.1	(88.8)	28.2	(92.4)	28.1	(92.1)
$V_{\theta 2}'$	247.3	(811.5)	246.8	(809.6)	246.9	(809.9)
U_2	274.4	(900.4)	274.9	(902.0)	274.9	902.0)
β_2	12.2		12.2		12.2	
β_2'	63.2		62.2		62.2	
D_2	50.02	(19.692)	15.2	(6.003)	15.25	(6.003)
R_2	1.000		0.950		0.950	
V_3	172.9	(567.4)	174.2	(571.4)	174.3	(571.9)
V_{x3}	170.7	(560.0)	171.8	(563.6)	171.9	(563.9)
V_3'	293.0	(961.2)	293.0	(961.4)	293.2	(961.9)
$V_{\theta 3}$	27.9	(91.4)	29.0	(95.3)	29.0	(95.0)
$V_{\theta 3}'$	238.1	(781.2)	237.4	(778.9)	237.5	(779.2)
U_3	266.0	(872.6)	266.5	(874.2)	266.5	(874.2)
β_3	9.3		9.6		9.6	
β_3'	54.4		54.1		54.1	
D_3	48.48	(19.085)	14.78	(5.818)	14.78	(5.818)
R_3	0.967		0.950		0.950	
V_4	245.2	(804.3)	231.2	(758.6)	242.5	(795.6)
V_{x4}	174.0	(570.9)	160.1	(525.3)	173.7	(569.8)
V_4'	196.0	(643.1)	186.6	(612.3)	197.3	(647.2)
$V_{\theta 4}$	172 7	(566.5)	166.8	(547.3)	169.2	(555.2)
$V_{\theta 4}'$	90.3	(296.1)	95.9	(314.7)	93.5	(306.8)
U_4	262.9	(862.6)	262.7	(862.0)	262.7	(862.0)
β_4	44.8		46.2		44.2	
β_4'	27.4		30.9		28.3	
D_4	47.92	(18.865)	14.57	(5.737)	14.57	(5.737)
R_4	0.933		0.940		0.865	
V_5	253.0	(829.9)	235.2	(771.5)	248.1	(813.9)
V_{x5}	183.8	(603.1)	165.3	(542.3)	180.4	(591.9)
V_5'	203.7	(668.4)	190.3	(624.2)	202.2	(663.3)
$V_{\theta 5}$	173.8	(570.1)	167.2	(548.7)	170.3	(558.6)
$V_{\theta 5}'$	87.9	(288.3)	94.2	(309.1)	91.2	(299.2)
U_5	261.6	(858.4)	261.5	(857.8)	261.5	(857.8)
β_5	43.4		45.3		43.3	
β_5'	25.5		29.7		26.8	
D_5	47.69	(18.774)	14.50	(5.709)	14.50	(5.709)
R_5	0.920		0.940		0.865	
V_6	181.8	(596.3)	181.6	(595.8)	189.1	(620.5)
V_{x6}	179.1	(587.5)	177.1	(580.9)	184.8	(606.2)
V_6'	289.3	(949.2)	280.4	(920.1)	285.4	(936.4)
$V_{\theta 6}$	31.0	(101.8)	40.4	(132.4)	40.3	(132.3)
$V_{\theta 6}'$	227.2	(745.5)	217.5	(713.5)	217.5	(713 6)
U_6	258.3	(847.3)	257.8	(845.9)	257.8	(845.9)
β_6	9.8		12.8		12.3	
β_6'	51.8		50.8		49.7	
D_6	47.07	(18.531)	14.30	(5.630)	14.30	(5.630)
R_6	0.940		0.915		0 905	

Table IX. Meanline Velocity Triangle Comparison (Continued)

Parameter	*Point 1*	*Point 15*	*Point 38*
PR, rotor	1.519	1.467	1.470
η_{ad}, rotor	0.967	0.928	0.916
PR, stage	1.501	1.439	1.440
η_{ad}, stage	0.937	0.883	0.866
DF, rotor	0.537	0.561	0.529
DF, stator	0.510	0.446	0.450

Velocity	=	m/sec (ft/sec)	1	=	IGV Leading Edge
Flowrate	=	kg/sec (lbm/sec)	2	=	IGV Trailing Edge
Rotor speed	=	rad/sec (rpm)	3	=	Rotor Leading Edge
Diameter	=	cm (in.)	4	=	Rotor Trailing Edge
			5	=	Stator Leading Edge
			6	=	Stator Trailing Edge

APPENDIX A

MEANLINE COMPUTER PROGRAM FORMULATION

Diffuser performance can be successfully described by five parameters: amount of diffusion (area ratio), rate of diffusion (cone angle), inlet blockage, Reynolds number, and turning angle. A similar analysis technique has been applied to compressors using a meanline approach.

For a conical diffuser,

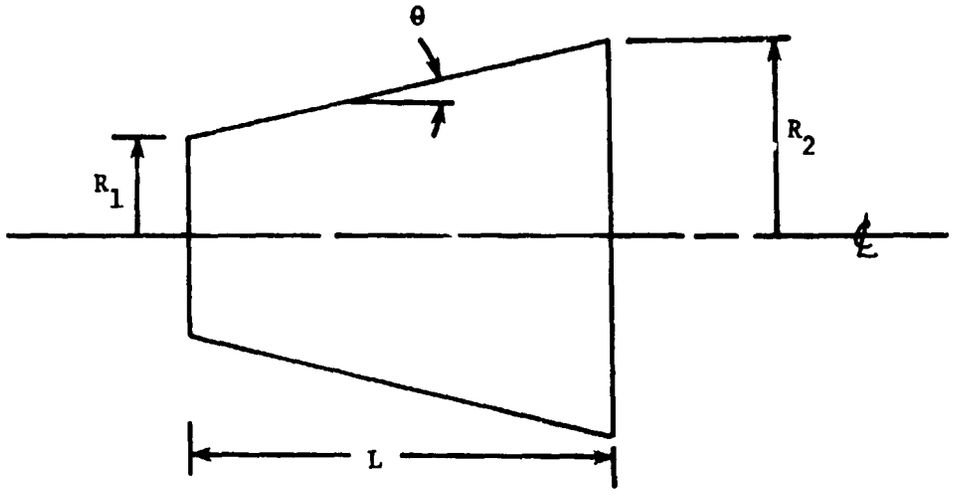

θ = rate of diffusion

$$= \tan^{-1}\left[\frac{R_2 - R_1}{L}\right]$$

η_D = diffusion efficiency

$$= \frac{(\Delta P_s/P_{T1} - P_{s1})_{TEST}}{(\Delta P_s/P_{T1} - P_{s1})_{IDEAL}} = \frac{(\Delta P_s/P_{T1} - P_{s1})_{TEST}}{1-(1/\text{AREA RATIO})^2}$$

Some typical 2-D diffuser performance results (from NACA TN 2888) are shown in an adjacent figure.

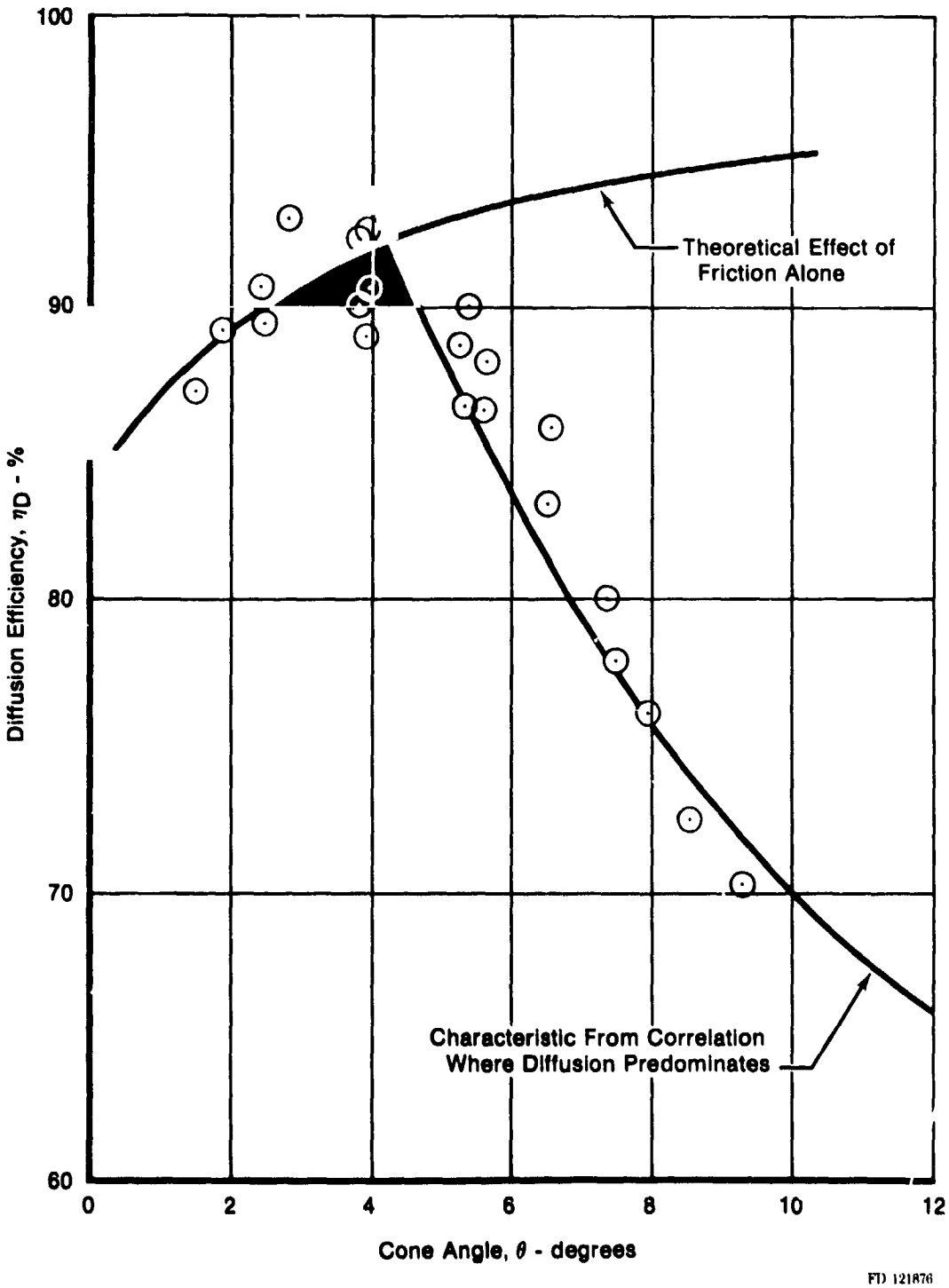

Figure 71. Typical 2-D Diffuser Performance

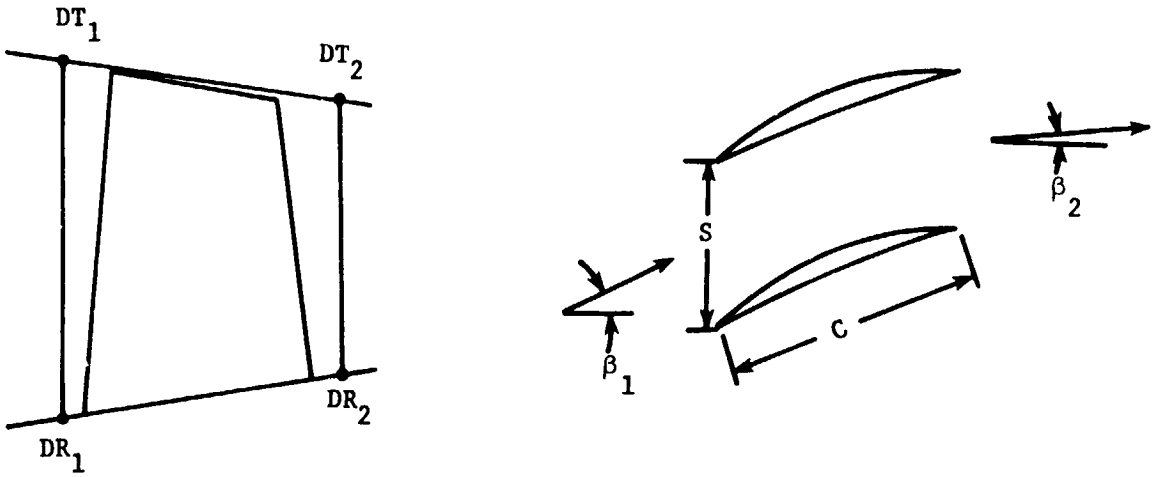

For a compressor bladerow, having converging (or diverging) walls,

$$\theta_{eq} = \tan^{-1}\left\{\frac{([D_{T_2}^2 - D_{R_2}^2]\cos\beta_2)^{1/2} - ([D_{T_1}^2 - D_{R_1}^2]\cos\beta_1)^{1/2}}{2c\sqrt{N}}\right\}$$

$$\eta D = \frac{(\Delta P_S/P_{T1} - P_{S1})_{TEST}}{1 - \left[\frac{(D_{T_1}^2 - D_{R_1}^2)\cos\beta_1}{(D_{T_2}^2 - D_{R_2}^2)\cos\beta_2}\right]^2}$$

where

D_T = Outer wall diameter
D_R = Inner wall diameter
β_1 = Inlet air angle
β_2 = Exit air angle
C = Chord length
N = Number of airfoils

Data from various cascade tests were used to ascertain the validity of the η_D vs. θeq diffuser characteristics as applied to compressor bladerows. These data were corrected to standard values of Reynolds number, relative roughness, inlet boundary layer thickness, and entrance length using techniques based on the work of Moody (reference 7), Ross (reference 8), Hanley (reference 9), and others. It was shown that the standardized cascade data agreed quite closely with the results of the pure pipe diffuser experiments.

Once the basic validity of the diffuser analogy had been verified, the technique was incorporated into a meanline computer program. The program requires the following input items: flowpath geometry, blade aspect ratio, solidity, and location of maximum camber; flowrate; stator exit air angle and desired pressure ratio. The calculation then iterates on β_2' until the desired pressure ratio is satisfied. The calculation proceeds axially rearward through the machine, one stage at a time, using values of boundary layer thickness (suitably transformed between absolute and relative reference frames) and blockage from the previous stage.

Extensive analysis of many compressor experiments has shown that the meanline calculation based on the diffuser analogy is quite accurate for prediction of compressor efficiency. The method also provides a valuable tool for study of the effects of aspect ratio, solidity, boundary layer thickness, and absolute scale.

APPENDIX B

AIRFOIL AND FLOWPATH GEOMETRY

This section contains the following information:

1. Flowpath geometry for:

   Base stage
   Scaled stage aerodynamic design
   Scaled stage as tested

2. Airfoil geometry for:

   Base stage IGV, rotor, and stator
   Scaled stage IGV, rotor, and stator

3. Airfoil section coordinates for scaled stage rotor and stator

Table X. Base Stage Flowpath Geometry

	XID		XOD		DID		DOD	
Station	cm	in	cm	in.	cm	in.	cm	in.
Station 1	-26 421	-10.402	-26.421	-10.402	41.910	16.500	61.341	24.150
IGV Inlet	-15.697	- 6.180	-15.697	- 6.180	41.910	16.500	58.052	22.855
IGV Exit	-11.913	- 4.690	-11.913	- 4.690	41.910	16.500	56.985	22.435
Station 2	- 7.577	- 2.983	- 7.577	- 2.983	41.910	16.500	55.753	21.950
Rotor Inlet	- 2.451	- 0.695	- 1.824	- 0.718	41.910	16.500	54.254	21.360
Rotor Exit	2.922	1.178	2.177	0.857	41.910	16.500	53.251	20.965
Station 3	3.340	1.315	3.340	1.315	41.910	16.500	52.941	20.843
Stator Inlet	3.785	1.490	3.734	1.470	41.910	16.500	52.832	20.800
Stator Exit	8.357	3.290	8.407	3.310	41.910	16.500	51.714	20.360
Station 4	10.709	4.216	10.709	4.216	41.910	16.500	51.247	20.176

X = Axial Spacing from Rotor Stacking Line
D = Diameter

Table XI. Scaled Stage Flowpath Geometry
(Aerodynamic Design)

	XID		XOD		DID		DOD	
Station	cm	in.	cm	in.	cm	in.	cm	in.
IGV Inlet	-4.778	-1.881	-4.778	-1.881	12.644	4.986	17.729	6.980
IGV Exit	-3.625	-1.427	-3.625	-1.427	12.672	4.989	17.402	6.851
Station 2	-2.304	-0.907	-2.304	-0.907	12.695	4.998	17.028	6.704
Rotor Inlet	-0.742	-0.292	-0.556	-0.219	12.720	5.008	16.548	6.515
Rotor Exit	0.912	0.359	0.665	0.262	12.598	4.960	16.307	6.420
Station 3	1.013	0.399	1.013	0.399	12.591	4.957	16.236	6.392
Stator Inlet	1.151	0.453	1.135	0.447	12.593	4.958	16.203	6.379
Stator Exit	2.543	1.001	2.558	1.007	12.621	4.969	15.822	6.229
Station 4	3.302	1.300	3.302	1.300	12.637	4.975	15.723	6.190

X = Axial Spacing from Rotor Stacking Line
D = Diameter

Table XII. Scaled Stage Flowpath Geometry
(Final Configuration as Tested)

	XID		XOD		DID		DOD	
Station	cm	in.	cm	in.	cm	in.	cm	in.
Station 1	-6.507	-2.562	-6.507	-2.562	12.746	5.018	18.214	7.171
IGV Inlet	-4.775	-1.880	-4.775	-1.880	12.746	5.018	17.727	6.979
IGV Exit	-3.602	-1.418	-3.609	-1.421	12.746	5.018	17 394	6.848
Station 2	-2.327	-0.916	-2.327	-0.916	12.746	5.018	17.028	6.704
Rotor Inlet	-0.737	-0.290	-0.556	-0.219	12.756	5.022	16.553	6.517
Rotor Exit	0.919	0.362	0.678	0.267	12.606	4.963	16.304	6.419
Station 3	1.057	0.416	1.057	0.416	12.591	4.957	16.210	6.382
Stator Inlet	1.168	0.460	1.133	0.446	12.588	4.956	16.187	6.373
Stator Exit	2.540	1.000	2.565	1.010	12.609	4.964	15.814	6.226
Station 4	3.305	1.301	3.305	1.301	12.621	4.969	15.723	6.190

X = Axial Spacing from Rotor Stacking Line
D = Diameter

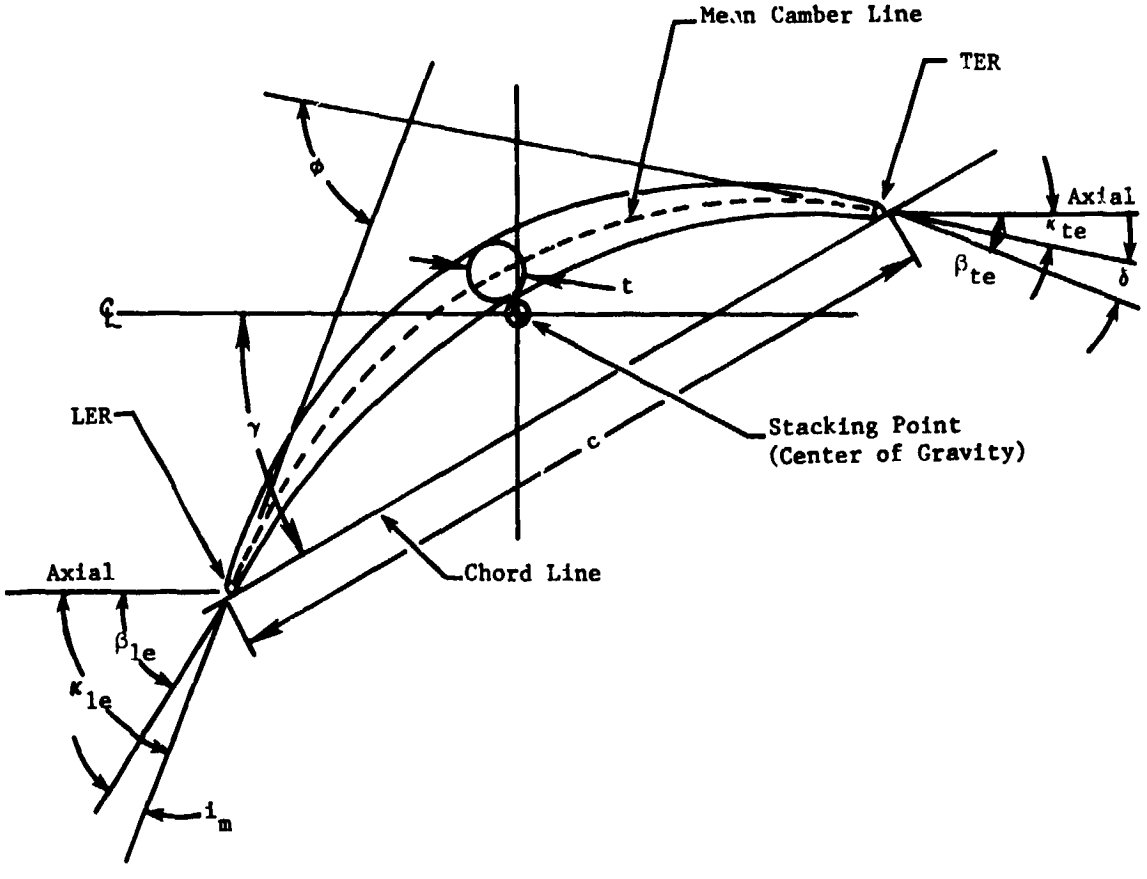

Geometry is defined along *constant diameter* cuts. The following nomenclature has been used:

DIA	- Diameter (cm./in.)
CL_o	- Lift coefficient
KAP1	- Vane leading edge metal angle (degrees)
KAP2	- Vane trailing edge metal angle (degrees)
KAP1′	- Blade leading edge metal angle (degrees)
KAP2′	- Blade trailing edge metal angle (degrees)
PHI	- Airfoil camber angle (degrees)
GAM	- Airfoil chord angle (degrees)
CHORD	- Chord length (cm./in.)
T/C	- Maximum thickness/chord length (ratio)
SOLIDITY	- Chord length/blade spacing (ratio)

Figure 72. Scaled Stage Flowpath Geometry

Table XIII. Base Stage Inlet Guide Vane Geometry

Dia (cm)	Dia (in.)	CL_o	KAP1	KAP2	PHI	GAM	Chord (cm)	Chord (in.)	T/C	Solidity
41.910	16.500	0.840	−22.13	12.96	−35.09	5.52	3.886	1.530	0.060	1.2397
43.950	17.303	0.883	−22.97	13.69	−36.66	5.87	3.886	1.530	0.060	1.1821
45.989	18.106	0.926	−23.79	14.41	−38.20	6.22	3.886	1.530	0.060	1.1297
48.029	18.909	0.969	−24.58	15.13	−39.72	6.56	3.886	1.530	0.060	1.0817
50.068	19.712	1.012	−25.35	15.86	−41.20	6.91	3.886	1.530	0.060	1.0377
52.108	20.515	1.055	−26.09	16.58	−42.66	7.26	3.886	1.530	0.060	0.9971
54.148	21.318	1.098	−26.80	17.30	−44.09	7.61	3.886	1.530	0.060	0.9595
56.187	22.121	1.141	−27.48	18.02	−45.50	7.96	3.886	1.530	0.060	0.9247
58.227	22.924	1.184	−28.14	18.74	−46.88	8.30	3.886	1.530	0.060	0.8923
60.272	23.729	1.227	−28.77	19.45	−48.23	8.65	3.886	1.530	0.060	0.8620
62.306	24.530	1.270	−29.39	20.17	−49.55	9.00	3.886	1.530	0.060	0.8339

Series NACA 63 — (CL_oA4K6) 06
No. Airfoils: 42

Table XIV. Base Stage Rotor Geometry

Dia (cm)	Dia (in.)	KAP1	KAP2	PHI	GAM	Chord (cm)	Chord (in.)	T/C	Solidity
41.910	16.500	57.61	−12.41	70.02	22.60	5.885	2.317	0.085	1.4306
42.672	16.800	56.62	−6.53	63.15	25.04	5.885	2.317	0.083	1.4045
43.688	17.200	55.89	0.22	55.67	28.06	5.885	2.317	0.080	1.3717
44.450	17.500	55.50	4.81	50.70	30.15	5.885	2.317	0.079	1.3477
45.212	17.800	55.33	8.15	47.17	31.74	5.885	2.317	0.077	1.3263
45.974	18.100	55.27	11.50	43.77	33.39	5.885	2.317	0.075	1.3038
46.990	18.500	55.29	15.66	39.63	35.47	5.885	2.317	0.072	1.2755
47.752	18.800	55.47	18.72	36.75	37.10	5.885	2.317	0.070	1.2547
48.514	19.100	55.65	21.25	34.40	38.45	5.885	2.317	0.068	1.2361
49.530	19.500	56.20	24.54	31.66	40.37	5.885	2.317	0.066	1.2107
50.292	19.800	56.63	26.76	29.87	41.70	5.885	2.317	0.064	1.1919
51.054	20.100	57.10	28.93	28.17	43.02	5.885	2.317	0.062	1.1737
52.070	20.500	57.73	31.48	26.25	44.61	5.885	2.317	0.059	1.1507
52.832	20.800	58.35	33.26	25.10	45.80	5.885	2.317	0.057	1.1351
53.696	21.140	59.17	35.45	23.71	47.31	5.885	2.317	0.055	1.1161

Series: Circular Arc
No. Airfoils: 32

Table XV. Base Stage Stator Geometry

Dia (cm)	Dia (in.)	KAP1	KAP2	PHI	GAM	Chord (cm)	Chord (in.)	T/C	Solidity
41.910	16.500	55.57	0.80	[illegible]	28.18	5.151	2.028	0.070	[illegible]085
42.672	16.800	53.11	1.33	[illegible]	27.22	5.151	2.028	0.071	1.3831
43.434	17.100	52.12	[illegible]	[illegible]	26.65	5.151	2.028	0.073	1.3587
44.196	17.400	51.33	[illegible]	49.31	26.17	5.151	2.028	0.074	1.3351
44.958	17.700	50.95	[illegible]	50.09	25.90	5.151	2.028	0.076	1.3123
45.466	17.900	50.75	[illegible]	49.99	25.76	5.151	2.028	0.077	1.2987
46.228	18.200	50.52	0.52	50.01	25.52	5.151	2.028	0.078	1.2771
46.990	18.500	50.52	0.26	50.26	25.39	5.151	2.028	0.080	1.2563
47.752	18.800	50.53	-0.12	50.66	25.21	5.151	2.028	0.081	1.2361
48.514	19.100	50.93	-0.53	51.46	25.20	5.151	2.028	0.083	1.2165
49.276	19.400	51.32	-1.02	52.34	25.15	5.151	2.028	0.084	1.1976
50.038	19.700	51.94	-1.55	53.49	25.19	5.151	2.028	0.086	1.1792
50.800	20.000	52.57	-2.14	54.72	25.21	5.151	2.028	0.087	1.1614
51.562	20.300	53.51	-2.98	56.49	25.26	5.151	2.028	0.089	1.1455
52.225	20.561	54.47	-3.89	58.37	25.29	5.151	2.028	0.090	1.1299

Series: 65 Series
No. Airfoils: 36

Table XVI. Scaled Stage Inlet Guide Vane Geometry

Dia (cm)	Dia (in.)	CL_o	KAP1	KAP2	PHI	GAM	Chord (cm)	Chord (in.)	T/C	Solidity
12.669	4.9877	0.840	-22.31	12.96	-35.09	5.52	1.183	0.4656	0.050	1.2481
13.158	5.1805	0.883	-22.97	13.69	-36.66	5.87	1.183	0.4656	0.056	1.2016
13.648	5.3732	0.926	-23.79	14.41	-38.20	6.22	1.183	0.4656	0.062	1.1585
14.138	5.5660	0.969	-24.58	15.13	-39.72	6.56	1.183	0.4656	0.068	1.1183
14.627	5.7587	1.012	-25.35	15.86	-41.20	6.91	1.183	0.4656	0.074	1.0809
15.117	5.9515	1.055	-26.09	16.58	-42.66	7.26	1.183	0.4656	0.080	1.0459
15.606	6.1442	1.098	-26.80	17.30	-44.09	7.61	1.183	0.4656	0.086	1.0131
16.096	6.3370	1.141	-27.48	18.02	-45.50	7.96	1.183	0.4656	0.092	0.9823
16.585	6.5297	1.184	-28.14	18.74	-46.88	8.30	1.183	0.4656	0.098	0.9533
17.075	6.7225	1.227	-28.77	19.45	-48.23	8.65	1.183	0.4656	0.104	0.9259
17.565	6.9152	1.270	-29.38	20.17	-49.55	9.00	1.183	0.4656	0.110	0.9001

Series: NACA 63 — (CL_oA4K6) 06
No. Airfoils: 42
Note: Vanes are titled 5° in direction of rotor rotation

Table XVII. Scaled Stage Rotor Geometry

Dia (cm)	Dia (in.)	KAP1	KAP2	PHI	GAM	Chord (cm)	Chord (in.)	T/C	Solidity
12.654	4.982	57.89	−10.86	68.75	23.51	1.778	0.700	0.085	1.4306
12.954	5.100	56.62	−4.17	60.78	26.22	1.778	0.700	0.083	1.3986
13.208	5.200	55.99	0.74	55.24	28.36	1.781	0.701	0.081	1.3736
13.462	5.300	55.57	5.16	50.41	30.36	1.783	0.702	0.079	1.3495
13.716	5.400	55.33	8.52	46.81	31.93	1.783	0.702	0.077	1.3245
13.970	5.500	55.27	11.88	43.39	33.58	1.786	0.703	0.074	1.3021
14.224	5.600	55.24	14.98	40.27	35.11	1.788	0.704	0.072	1.2804
14.732	5.800	55.64	20.71	34.93	38.17	1.791	0.705	0.068	1.2376
14.986	5.900	56.07	23.25	32.81	39.66	1.791	0.705	0.066	1.2180
15.240	6.000	56.54	25.56	30.98	41.05	1.793	0.706	0.064	1.1976
15.494	6.100	57.04	27.79	29.25	42.42	1.793	0.706	0.062	1.1792
15.748	6.200	57.56	29.85	27.71	43.70	1.796	0.707	0.060	1.1614
16.002	6.300	58.17	31.63	26.49	44.92	1.796	0.707	0.058	1.1442
16.256	6.400	58.89	33.51	25.38	46.20	1.798	0.708	0.056	1.1261
16.411	6.461	59.43	34.69	24.74	47.05	1.798	0.708	0.055	1.1161

Series: Circular Arc
No. Airfoils: 32

Table XVIII. Scaled Stage Stator Geometry

Dia (cm)	Dia (in.)	KAP1	KAP2	PHI	GAM	Chord (cm)	Chord (in.)	T/C	Solidity
12.606	4.963	55.39	0.77	54.63	28.08	1.549	0.610	0.070	1.4085
12.954	5.100	52.62	1.31	51.31	26.96	1.554	0.612	0.072	1.3736
13.208	5.200	51.77	1.13	50.64	26.45	1.557	0.613	0.074	1.3495
13.462	5.300	51.12	0.97	50.15	26.04	1.560	0.614	0.075	1.3263
13.716	5.400	50.82	0.81	50.01	25.82	1.562	0.615	0.076	1.3038
13.970	5.500	50.52	0.60	49.93	25.56	1.565	0.616	0.078	1.2821
14.224	5.600	50.52	0.34	50.19	25.43	1.567	0.617	0.079	1.2610
14.478	5.700	50.52	−0.01	50.52	25.26	1.570	0.618	0.081	1.2407
14.732	5.800	50.85	−0.40	51.25	25.22	1.570	0.618	0.082	1.2225
14.986	5.900	51.24	−0.88	52.12	25.18	1.572	0.619	0.084	1.2034
15.240	6.000	51.81	−1.38	53.19	25.21	1.575	0.620	0.085	1.1848
15.494	6.100	52.44	−1.98	54.43	25.23	1.577	0.621	0.087	1.1669
15.748	6.200	53.31	−2.71	56.02	25.30	1.580	0.622	0.088	1.1494
16.002	6.300	54.38	−3.75	58.13	25.32	1.580	0.622	0.090	1.1325
16.027	6.310	54.51	−3.86	58.37	25.32	1.580	0.622	0.090	1.1299

Series: 65 Series
No. Airfoils: 36
Note: Stators are tilted 5° in direction of rotor rotation

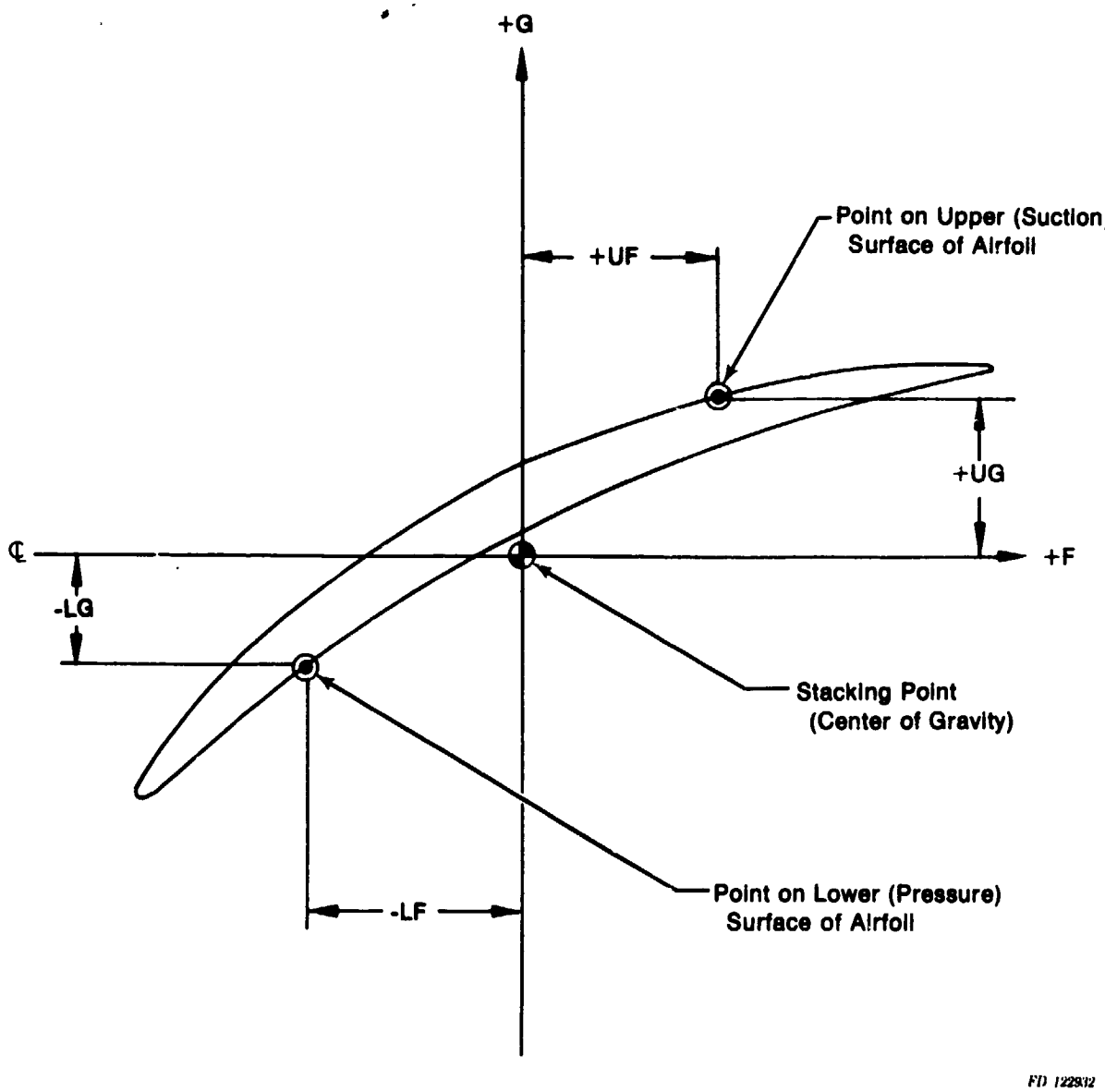

Figure 73. Section Coordinate Definitions

Table XIX. Airfoil Section Coordinates for Scaled Stage Rotor

SCALED STAGE ROTOR
SECTION NUMBER 1

DIAMETER = 12.5898 CM.(4.9566 IN.)
CHORD = 1.7765 CM.(0.6994 IN.)
CHORD ANGLE = 22.896 DEG.

UF(CM)	UF(IN)	UG(CM)	UG(IN)	LF(CM)	LF(IN)	LG(CM)	LG(IN)
-.7333	-.2887	-.5466	-.2152	-.7333	-.2887	-.5466	-.2152
-.7369	-.2901	-.5385	-.2120	-.7305	-.2876	-.5535	-.2179
-.6271	-.2469	-.3411	-.1343	-.5979	-.2354	-.4105	-.1616
-.5014	-.1974	-.1829	-.0720	-.4577	-.1802	-.2863	-.1127
-.3627	-.1428	-.0541	-.0213	-.3101	-.1221	-.1788	-.0704
-.2136	-.0841	0.0493	0.0194	-.1562	-.0615	-.0869	-.0342
-.0546	-.0215	0.1295	0.0510	0.0043	0.0017	-.0104	-.0041
0.1138	0.0448	0.1875	0.0738	0.1712	0.0674	0.0513	0.0202
0.2918	0.1149	0.2222	0.0875	0.3444	0.1356	0.0978	0.0385
0.4806	0.1892	0.2319	0.0913	0.5243	0.2064	0.1285	0.0506
0.6820	0.2685	0.2116	0.0833	0.7112	0.2800	0.1422	0.0560
0.8997	0.3542	0.1527	0.0601	0.9060	0.3567	0.1377	0.0542
0.9032	0.3556	0.1443	0.0568	0.9032	0.3556	0.1443	0.0568

SCALED STAGE ROTOR
SECTION NUMBER 2

DIAMETER = 13.6058 CM.(5.3566 IN.)
CHORD = 1.7833 CM.(0.7021 IN.)
CHORD ANGLE = 31.263 DEG.

UF(CM)	UF(IN)	UG(CM)	UG(IN)	LF(CM)	LF(IN)	LG(CM)	LG(IN)
-.6845	-.2695	-.5908	-.2326	-.6845	-.2695	-.5908	-.2326
-.6886	-.2711	-.5842	-.2300	-.6810	-.2681	-.5966	-.2349
-.5857	-.2306	-.4100	-.1614	-.5530	-.2177	-.4641	-.1827
-.4696	-.1849	-.2573	-.1013	-.4191	-.1650	-.3406	-.1341
-.3424	-.1348	-.1234	-.0486	-.2799	-.1102	-.2263	-.0891
-.2047	-.0806	-.0066	-.0026	-.1354	-.0533	-.1209	-.0476
-.0571	-.0225	0.0940	0.0370	0.0145	0.0057	-.0239	-.0094
0.1003	0.0395	0.1786	0.0703	0.1697	0.0668	0.0643	0.0253
0.2675	0.1053	0.2469	0.0972	0.3299	0.1299	0.1438	0.0566
0.4450	0.1752	0.2979	0.1173	0.4956	0.1951	0.2146	0.0845
0.6340	0.2496	0.3305	0.1301	0.6667	0.2625	0.2764	0.1088
0.8359	0.3291	0.3414	0.1344	0.8435	0.3321	0.3289	0.1295
0.8400	0.3307	0.3348	0.1318	0.8400	0.3307	0.3348	0.1318

Table XIX. Airfoil Section Coordinates for Scaled Stage Rotor (Continued)

SCALED STAGE ROTOR
SECTION NUMBER 3

DIAMETER = 13.9482 CM.(5.4914 IN.)
CHORD = 1.7856 CM.(0.7030 IN.)
CHORD ANGLE = 33.439 DEG.

UF(CM)	UF(IN)	UG(CM)	UG(IN)	LF(CM)	LF(IN)	LG(CM)	LG(IN)
-.6703	-.2639	-.6053	-.2383	-.6703	-.2639	-.6053	-.2383
-.6744	-.2655	-.5987	-.2357	-.6665	-.2624	-.6109	-.2405
-.5733	-.2257	-.4280	-.1685	-.5400	-.2126	-.4783	-.1883
-.4600	-.1811	-.2756	-.1085	-.4084	-.1608	-.3538	-.1393
-.3355	-.1321	-.1400	-.0551	-.2718	-.1070	-.2367	-.0932
-.2012	-.0792	0.0196	0.0077	-.1300	-.0512	-.1273	-.0501
-.0569	-.0224	0.0861	0.0339	0.0165	0.0065	-.0251	-.0099
0.0968	0.0381	0.1773	0.0698	0.1679	0.0661	0.0696	0.0274
0.2604	0.1025	0.2537	0.0999	0.3244	0.1277	0.1570	0.0618
0.4341	0.1709	0.3147	0.1239	0.4856	0.1912	0.2367	0.0932
0.6187	0.2436	0.3594	0.1415	0.6520	0.2567	0.3089	0.1216
0.8156	0.3211	0.3851	0.1516	0.8235	0.3242	0.3731	0.1469
0.8197	0.3227	0.3787	0.1491	0.8197	0.3227	0.3787	0.1491

SCALED STAGE ROTOR
SECTION NUMBER 4

DIAMETER = 14.0589 CM.(5.5350 IN.)
CHORD = 1.7864 CM.(0.7033 IN.)
CHORD ANGLE = 34.122 DEG.

UF(CM)	UF(IN)	UG(CM)	UG(IN)	LF(CM)	LF(IN)	LG(CM)	LG(IN)
-.6657	-.2621	-.6096	-.2400	-.6657	-.2621	-.6096	-.2400
-.6701	-.2638	-.6035	-.2376	-.6619	-.2606	-.6154	-.2423
-.5695	-.2242	-.4333	-.1706	-.5359	-.2110	-.4829	-.1901
-.4567	-.1798	-.2812	-.1107	-.4049	-.1594	-.3576	-.1408
-.3332	-.1312	-.1448	-.0570	-.2690	-.1059	-.2398	-.0944
-.1999	-.0787	-.0234	-.0092	-.1283	-.0505	-.1290	-.0508
-.0566	-.0223	0.0838	0.0330	0.0173	0.0068	-.0254	-.0100
0.0958	0.0377	0.1770	0.0697	0.1674	0.0659	0.0714	0.0281
0.2581	0.1016	0.2560	0.1008	0.3226	0.1270	0.1610	0.0634
0.4305	0.1695	0.3200	0.1260	0.4823	0.1899	0.2436	0.0959
0.6137	0.2416	0.3683	0.1450	0.6472	0.2548	0.3188	0.1255
0.8087	0.3184	0.3985	0.1569	0.8169	0.3216	0.3866	0.1522
0.8131	0.3201	0.3924	0.1545	0.8131	0.3201	0.3924	0.1545

Table XIX. Airfoil Section Coordinates for Scaled Stage Rotor (Continued)

SCALED STAGE ROTOR
SECTION NUMBER 5

DIAMETER = 14.1696 CM.(5.5786 IN.)
CHORD = 1.7869 CM.(0.7035 IN.)
CHORD ANGLE = 34.784 DEG.

UF(CM)	UF(IN)	UG(CM)	UG(IN)	LF(CM)	LF(IN)	LG(CM)	LG(IN)
-.6614	-.2604	-.6142	-.2418	-.6614	-.2604	-.6142	-.2418
-.6655	-.2620	-.6078	-.2393	-.6574	-.2588	-.6198	-.2440
-.5654	-.2226	-.4387	-.1727	-.5319	-.2094	-.4872	-.1918
-.4536	-.1786	-.2865	-.1128	-.4016	-.1581	-.3614	-.1423
-.3312	-.1304	-.1499	-.0590	-.2664	-.1049	-.2428	-.0956
-.1996	-.0782	-.0272	-.0107	-.1267	-.0499	-.1308	-.0515
-.0566	-.0223	0.0815	0.0321	0.0178	0.0070	-.0257	-.0101
0.0950	0.0374	0.1765	0.0695	0.1669	0.0657	0.0732	0.0288
0.2560	0.1008	0.2581	0.1016	0.3205	0.1262	0.1651	0.0650
0.4270	0.1681	0.3251	0.1280	0.4790	0.1886	0.2502	0.0985
0.6086	0.2396	0.3767	0.1483	0.6421	0.2528	0.3284	0.1293
0.8021	0.3158	0.4115	0.1620	0.8103	0.3190	0.3998	0.1574
0.8064	0.3175	0.4054	0.1596	0.8064	0.3175	0.4054	0.1596

SCALED STAGE ROTOR
SECTION NUMBER 6

DIAMETER = 14.2804 CM.(5.6222 IN.)
CHORD = 1.7877 CM.(0.7038 IN.)
CHORD ANGLE = 35.451 DEG.

UF(CM)	UF(IN)	UG(CM)	UG(IN)	LF(CM)	LF(IN)	LG(CM)	LG(IN)
-.6566	-.2585	-.6187	-.2436	-.6566	-.2585	-.6187	-.2436
-.6609	-.2602	-.6126	-.2412	-.6528	-.2570	-.6243	-.2458
-.5616	-.2211	-.4442	-.1749	-.5278	-.2078	-.4915	-.1935
-.4503	-.1773	-.2921	-.1150	-.3983	-.1568	-.3653	-.1438
-.3289	-.1295	-.1547	-.0609	-.2639	-.1039	-.2456	-.0967
-.1974	-.0777	-.0310	-.0122	-.1252	-.0493	-.1326	-.0522
-.0564	-.0222	0.0792	0.0312	0.0183	0.0072	-.0257	-.0101
0.0940	0.0370	0.1763	0.0694	0.1661	0.0654	0.0749	0.0295
0.2537	0.0999	0.2601	0.1024	0.3185	0.1254	0.1689	0.0665
0.4234	0.1667	0.3299	0.1299	0.4755	0.1872	0.2568	0.1011
0.6035	0.2376	0.3853	0.1517	0.6370	0.2508	0.3378	0.1330
0.7953	0.3131	0.4242	0.1670	0.8034	0.3163	0.4125	0.1624
0.7996	0.3148	0.4181	0.1646	0.7996	0.3148	0.4181	0.1646

Table XIX. Airfoil Section Coordinates for Scaled Stage Rotor (Continued)

SCALED STAGE ROTOR
SECTION NUMBER 7

DIAMETER = 14.3909 CM.(5.6657 IN.)
CHORD = 1.7882 CM.(0.7040 IN.)
CHORD ANGLE = 36.121 DEG.

UF(CM)	UF(IN)	UG(CM)	UG(IN)	LF(CM)	LF(IN)	LG(CM)	LG(IN)
-.6518	-.2566	-.6236	-.2455	-.6518	-.2566	-.6236	-.2455
-.6563	-.2584	-.6175	-.2431	-.6477	-.2550	-.6292	-.2477
-.5573	-.2194	-.4496	-.1770	-.5235	-.2061	-.4961	-.1953
-.4470	-.1760	-.2974	-.1171	-.3947	-.1554	-.3693	-.1454
-.3264	-.1285	-.1595	-.0628	-.2614	-.1029	-.2487	-.0979
-.1961	-.0772	-.0348	-.0137	-.1234	-.0486	-.1341	-.0528
-.0561	-.0221	0.0770	0.0303	0.0188	0.0074	-.0257	-.0101
0.0930	0.0366	0.1760	0.0693	0.1654	0.0651	0.0767	0.0302
0.2515	0.0990	0.2624	0.1033	0.3165	0.1246	0.1730	0.0681
0.4196	0.1652	0.3350	0.1319	0.4719	0.1858	0.2634	0.1037
0.5982	0.2355	0.3937	0.1550	0.6320	0.2488	0.3472	0.1367
0.7882	0.3103	0.4366	0.1719	0.7968	0.3137	0.4252	0.1674
0.7927	0.3121	0.4305	0.1695	0.7927	0.3121	0.4305	0.1695

SCALED STAGE ROTOR
SECTION NUMBER 8

DIAMETER = 14.5016 CM.(5.7093 IN.)
CHORD = 1.7889 CM.(0.7043 IN.)
CHORD ANGLE = 36.791 DEG.

UF(CM)	UF(IN)	UG(CM)	UG(IN)	LF(CM)	LF(IN)	LG(CM)	LG(IN)
-.6469	-.2547	-.6284	-.2474	-.6469	-.2547	-.6284	-.2474
-.6515	-.2565	-.6226	-.2451	-.6429	-.2531	-.6340	-.2496
-.5532	-.2178	-.4552	-.1792	-.5192	-.2044	-.5004	-.1970
-.4437	-.1747	-.3028	-.1192	-.3912	-.1540	-.3800	-.1496
-.3241	-.1276	-.1641	-.0646	-.2586	-.1018	-.2515	-.0990
-.1948	-.0767	-.0384	-.0151	-.1219	-.0480	-.1356	-.0534
-.0561	-.0221	0.0749	0.0295	0.0193	0.0076	-.0257	-.0101
0.0919	0.0362	0.1760	0.0693	0.1646	0.0648	0.0785	0.0309
0.2489	0.0980	0.2644	0.1041	0.3145	0.1238	0.1770	0.0697
0.4158	0.1637	0.3401	0.1339	0.4684	0.1844	0.2697	0.1062
0.5928	0.2334	0.4018	0.1582	0.6269	0.2468	0.3566	0.1404
0.7813	0.3076	0.4488	0.1767	0.7897	0.3109	0.4374	0.1722
0.7856	0.3093	0.4430	0.1744	0.7856	0.3093	0.4430	0.1744

Table XIX. Airfoil Section Coordinates for Scaled Stage Rotor (Continued)

SCALED STAGE ROTOR
SECTION NUMBER 9

DIAMETER = 14.6124 CM.(5.7529 IN.)
CHORD = 1.7894 CM.(0.7045 IN.)
CHORD ANGLE = 37.458 DEG.

UF(CM)	UF(IN)	UG(CM)	UG(IN)	LF(CM)	LF(IN)	LG(CM)	LG(IN)
-.6419	-.2527	-.6332	-.2493	-.6419	-.2527	-.6332	-.2493
-.6484	-.2545	-.6274	-.2470	-.6378	-.2511	-.6368	-.2515
-.5489	-.2161	-.4608	-.1814	-.5149	-.2027	-.5050	-.1988
-.4402	-.1733	-.3081	-.1213	-.3876	-.1526	-.3769	-.1484
-.3216	-.1266	-.1689	-.0665	-.2560	-.1008	-.2543	-.1001
-.1933	-.0761	-.0419	-.0165	-.1204	-.0474	-.1372	-.0540
-.0559	-.0220	0.0729	0.0287	0.0196	0.0077	-.0257	-.0101
0.0907	0.0357	0.1758	0.0692	0.1638	0.0645	0.0805	0.0317
0.2466	0.0971	0.2664	0.1049	0.3122	0.1229	0.1811	0.0713
0.4120	0.1622	0.3449	0.1358	0.4648	0.1830	0.2761	0.1087
0.5875	0.2313	0.4100	0.1614	0.6215	0.2447	0.3658	0.1440
0.7739	0.3047	0.4610	0.1815	0.7828	0.3082	0.4496	0.1770
0.7785	0.3065	0.4549	0.1791	0.7785	0.3065	0.4549	0.1791

SCALED STAGE ROTOR
SECTION NUMBER 10

DIAMETER = 14.7229 CM.(5.7964 IN.)
CHORD = 1.7902 CM.(0.7048 IN.)
CHORD ANGLE = 38.119 DEG.

UF(CM)	UF(IN)	UG(CM)	UG(IN)	LF(CM)	LF(IN)	LG(CM)	LG(IN)
-.6368	-.2507	-.6383	-.2513	-.6368	-.2507	-.6383	-.2513
-.6413	-.2525	-.6325	-.2490	-.6327	-.2491	-.6436	-.2534
-.5446	-.2144	-.4661	-.1835	-.5105	-.2010	-.5095	-.2006
-.4366	-.1719	-.3134	-.1234	-.3840	-.1512	-.3805	-.1498
-.3190	-.1256	-.1732	-.0682	-.2535	-.0998	-.2570	-.1012
-.1920	-.0756	-.0455	-.0179	-.1186	-.0467	-.1387	-.0546
-.0556	-.0219	0.0709	0.0279	0.0201	0.0079	-.0257	-.0101
0.0897	0.0353	0.1755	0.0691	0.1628	0.0641	0.0823	0.0324
0.2443	0.0962	0.2687	0.1058	0.3099	0.1220	0.1849	0.0728
0.4082	0.1607	0.3498	0.1377	0.4613	0.1815	0.2824	0.1112
0.5822	0.2292	0.4181	0.1646	0.6162	0.2426	0.3746	0.1475
0.7668	0.3019	0.4727	0.1861	0.7757	0.3054	0.4615	0.1817
0.7714	0.3037	0.4669	0.1838	0.7714	0.3037	0.4669	0.1838

Table XIX. Airfoil Section Coordinates for Scaled Stage Rotor (Continued)

SCALED STAGE ROTOR
SECTION NUMBER 11

DIAMETER = 14.8336 CM.(5.8400 IN.)
CHORD = 1.7907 CM.(0.7050 IN.)
CHORD ANGLE = 38.775 DEG.

UF(CM)	UF(IN)	UG(CM)	UG(IN)	LF(CM)	LF(IN)	LG(CM)	LG(IN)
-.6317	-.2487	-.6434	-.2533	-.6317	-.2487	-.6434	-.2533
-.6363	-.2505	-.6375	-.2510	-.6274	-.2470	-.6487	-.2554
-.5400	-.2126	-.4714	-.1856	-.5060	-.1992	-.5138	-.2023
-.4333	-.1706	-.3178	-.1251	-.3805	-.1498	-.3843	-.1513
-.3165	-.1246	-.1778	-.0700	-.2510	-.0988	-.2596	-.1022
-.1905	-.0750	-.0488	-.0192	-.1173	-.0462	-.1400	-.0551
-.0554	-.0218	0.0691	0.0272	0.0203	0.0080	-.0254	-.0100
0.0886	0.0349	0.1755	0.0691	0.1621	0.0638	0.0843	0.0332
0.2418	0.0952	0.2708	0.1066	0.3076	0.1211	0.1890	0.0744
0.4044	0.1592	0.3543	0.1395	0.4572	0.1800	0.2885	0.1136
0.5768	0.2271	0.4257	0.1676	0.6109	0.2405	0.3833	0.1509
0.7597	0.2991	0.4839	0.1905	0.7686	0.3026	0.4727	0.1861
0.7645	0.3010	0.4780	0.1882	0.7645	0.3010	0.4780	0.1882

SCALED STAGE ROTOR
SECTION NUMBER 12

DIAMETER = 14.9443 CM.(5.8836 IN.)
CHORD = 1.7915 CM.(0.7053 IN.)
CHORD ANGLE = 39.420 DEG.

UF(CM)	UF(IN)	UG(CM)	UG(IN)	LF(CM)	LF(IN)	LG(CM)	LG(IN)
-.6264	-.2466	-.6485	-.2553	-.6264	-.2466	-.6485	-.2553
-.6309	-.2484	-.6429	-.2531	-.6220	-.2449	-.6538	-.2574
-.5357	-.2109	-.4768	-.1877	-.5014	-.1974	-.5184	-.2041
-.4298	-.1692	-.3236	-.1274	-.3769	-.1484	-.3879	-.1527
-.3139	-.1236	-.1821	-.0717	-.2482	-.0977	-.2621	-.1032
-.1892	-.0745	-.0521	-.0205	-.1158	-.0456	-.1412	-.0556
-.0551	-.0217	0.0671	0.0264	0.0206	0.0081	-.0251	-.0099
0.0876	0.0345	0.1755	0.0691	0.1610	0.0634	0.0861	0.0339
0.2395	0.0943	0.2728	0.1074	0.3053	0.1202	0.1928	0.0759
0.4006	0.1577	0.3589	0.1413	0.4534	0.1785	0.2946	0.1160
0.5715	0.2250	0.4331	0.1705	0.6055	0.2384	0.3917	0.1542
0.7529	0.2964	0.4948	0.1948	0.7617	0.2999	0.4836	0.1904
0.7574	0.2982	0.4889	0.1925	0.7574	0.2982	0.4889	0.1925

Table XIX. Airfoil Section Coordinates for Scaled Stage Rotor (Continued)

SCALED STAGE ROTOR
SECTION NUMBER 13

DIAMETER = 15.9824 CM.(6.2923 IN.)
CHORD = 1.7965 CM.(0.7073 IN.)
CHORD ANGLE = 44.825 DEG.

UF(CM)	UF(IN)	UG(CM)	UG(IN)	LF(CM)	LF(IN)	LG(CM)	LG(IN)
-.5786	-.2278	-.6921	-.2725	-.5786	-.2278	-.6921	-.2725
-.5837	-.2298	-.6871	-.2705	-.5738	-.2259	-.6970	-.2744
-.4950	-.1949	-.5215	-.2053	-.4613	-.1816	-.5552	-.2186
-.3973	-.1564	-.3650	-.1437	-.3454	-.1360	-.4168	-.1641
-.2906	-.1144	-.2174	-.0856	-.2266	-.0892	-.2819	-.1110
-.1755	-.0691	-.0782	-.0308	-.1039	-.0409	-.1501	-.0591
-.0523	-.0206	0.0526	0.0207	0.0218	0.0086	-.0218	-.0086
0.0792	0.0312	0.1750	0.0689	0.1509	0.0594	0.1031	0.0406
0.2192	0.0863	0.2893	0.1139	0.2832	0.1115	0.2248	0.0885
0.3673	0.1446	0.3950	0.1555	0.4191	0.1650	0.3429	0.1350
0.5245	0.2065	0.4917	0.1936	0.5580	0.2197	0.4580	0.1803
0.6906	0.2719	0.5794	0.2281	0.7005	0.2758	0.5695	0.2242
0.6957	0.2739	0.5743	0.2261	0.6957	0.2739	0.5743	0.2261

SCALED STAGE ROTOR
SECTION NUMBER 14

DIAMETER = 16.4904 CM.(6.4923 IN.)
CHORD = 1.7988 CM.(0.7082 IN.)
CHORD ANGLE = 47.538 DEG.

UF(CM)	UF(IN)	UG(CM)	UG(IN)	LF(CM)	LF(IN)	LG(CM)	LG(IN)
-.5509	-.2169	-.7153	-.2816	-.5509	-.2169	-.7153	-.2816
-.5563	-.2190	-.7102	-.2796	-.5456	-.2148	-.7198	-.2834
-.4719	-.1858	-.5436	-.2140	-.4387	-.1727	-.5738	-.2259
-.3790	-.1492	-.3848	-.1515	-.3284	-.1293	-.4310	-.1697
-.2776	-.1093	-.2337	-.0920	-.2151	-.0847	-.2908	-.1145
-.1681	-.0662	-.0899	-.0354	-.0983	-.0387	-.1539	-.0606
-.0508	-.0200	0.0465	0.0183	0.0213	0.0084	-.0196	-.0077
0.0747	0.0294	0.1755	0.0691	0.1445	0.0569	0.1115	0.0439
0.2083	0.0820	0.2972	0.1170	0.2708	0.1066	0.2400	0.0945
0.3498	0.1377	0.4115	0.1620	0.4003	0.1576	0.3653	0.1438
0.4996	0.1967	0.5182	0.2040	0.5329	0.2098	0.4877	0.1920
0.6581	0.2591	0.6170	0.2429	0.6688	0.2633	0.6073	0.2391
0.6637	0.2613	0.6119	0.2409	0.6637	0.2613	0.6119	0.2409

Table XX. Airfoil Section Coordinates for Scaled Stage Stator

SCALED STAGE STATOR
SECTION NUMBER 1

DIAMETER = 12.3668 CM.(4.8688 IN.)
CHORD = 1.5469 CM.(0.6090 IN.)
CHORD ANGLE = 29.130 DEG.

UF(CM)	UF(IN)	UG(CM)	UG(IN)	LF(CM)	LF(IN)	LG(CM)	LG(IN)
-.5217	-.2054	-.4770	-.1878	-.5217	-.2054	-.4770	-.1878
-.5273	-.2076	-.4628	-.1822	-.5113	-.2013	-.4674	-.1840
-.5273	-.2076	-.4569	-.1799	-.5083	-.2001	-.4630	-.1823
-.5260	-.2071	-.4455	-.1754	-.5027	-.1979	-.4547	-.1790
-.5199	-.2047	-.4206	-.1656	-.4895	-.1927	-.4354	-.1714
-.5024	-.1978	-.3759	-.1480	-.4628	-.1822	-.4003	-.1576
-.4816	-.1896	-.3355	-.1321	-.4354	-.1714	-.3680	-.1449
-.4585	-.1805	-.2979	-.1173	-.4077	-.1605	-.3378	-.1330
-.4082	-.1607	-.2286	-.0900	-.3510	-.1382	-.2814	-.1108
-.3536	-.1392	-.1659	-.0653	-.2929	-.1153	-.2291	-.0902
-.2959	-.1165	-.1077	-.0424	-.2332	-.0918	-.1798	-.0708
-.2352	-.0926	-.0541	-.0213	-.1725	-.0679	-.1333	-.0525
-.1069	-.0421	0.0417	0.0164	-.0485	-.0191	-.0465	-.0183
0.0295	0.0116	0.1229	0.0484	0.0795	0.0313	0.0333	0.0131
0.1740	0.0685	0.1887	0.0743	0.2111	0.0831	0.1077	0.0424
0.3249	0.1279	0.2395	0.0943	0.3482	0.1371	0.1755	0.0691
0.4816	0.1896	0.2779	0.1094	0.4935	0.1943	0.2309	0.0909
0.5626	0.2215	0.2906	0.1144	0.5697	0.2243	0.2535	0.0998
0.6462	0.2544	0.2984	0.1175	0.6492	0.2556	0.2705	0.1065
0.7336	0.2888	0.2992	0.1178	0.7336	0.2888	0.2797	0.1101
0.8296	0.3266	0.2761	0.1087	0.8296	0.3266	0.2761	0.1087

SCALED STAGE STATOR
SECTION NUMBER 2

DIAMETER = 13.3828 CM.(5.2688 IN.)
CHORD = 1.5580 CM.(0.6134 IN.)
CHORD ANGLE = 26.149 DEG.

UF(CM)	UF(IN)	UG(CM)	UG(IN)	LF(CM)	LF(IN)	LG(CM)	LG(IN)
-.5603	-.2206	-.4315	-.1699	-.5603	-.2206	-.4315	-.1699
-.5652	-.2225	-.4173	-.1643	-.5486	-.2160	-.4244	-.1671
-.5646	-.2223	-.4117	-.1621	-.5448	-.2145	-.4211	-.1658
-.5624	-.2214	-.4011	-.1579	-.5382	-.2119	-.4143	-.1631
-.5540	-.2181	-.3777	-.1487	-.5230	-.2059	-.3983	-.1568
-.5324	-.2096	-.3365	-.1325	-.4925	-.1939	-.3683	-.1450
-.5080	-.2000	-.2995	-.1179	-.4620	-.1819	-.3406	-.1341
-.4818	-.1897	-.2649	-.1043	-.4310	-.1697	-.3145	-.1238
-.4257	-.1676	-.2017	-.0794	-.3691	-.1453	-.2652	-.1044
-.3660	-.1441	-.1443	-.0568	-.3058	-.1204	-.2192	-.0863
-.3038	-.1196	-.0909	-.0358	-.2421	-.0953	-.1755	-.0691
-.2393	-.0942	-.0422	-.0166	-.1775	-.0699	-.1341	-.0528
-.1041	-.0410	0.0447	0.0176	-.0465	-.0183	-.0559	-.0220
0.0376	0.0148	0.1181	0.0465	0.0871	0.0343	0.0173	0.0068
0.1859	0.0732	0.1768	0.0696	0.2230	0.0878	0.0869	0.0342
0.3393	0.1336	0.2217	0.0873	0.3627	0.1428	0.1511	0.0595
0.4971	0.1957	0.2558	0.1007	0.5093	0.2005	0.2050	0.0807
0.5779	0.2275	0.2672	0.1052	0.5855	0.2305	0.2273	0.0895
0.6607	0.2601	0.2743	0.1080	0.6642	0.2615	0.2449	0.0964
0.7460	0.2937	0.2756	0.1085	0.7465	0.2939	0.2555	0.1006
0.8382	0.3300	0.255_	0.1005	0.8382	0.3300	0.2553	0.1005

Table XX. Airfoil Section Coordinates for Scaled Stage Stator (Continued)

SCALED STAGE STATOR
SECTION NUMBER 3

DIAMETER = 13.9304 CM.(5.4844 IN.)
CHORD = 1.5634 CM.(0.6155 IN.)
CHORD ANGLE = 25.594 DEG.

UF(CM)	UF(IN)	UG(CM)	UG(IN)	LF(CM)	LF(IN)	LG(CM)	LG(IN)
-.5669	-.2232	-.4265	-.1679	-.5669	-.2232	-.4265	-.1679
-.5720	-.2252	-.4120	-.1622	-.5545	-.2183	-.4199	-.1653
-.5712	-.2249	-.4064	-.1600	-.5507	-.2168	-.4166	-.1640
-.5690	-.2240	-.3957	-.1558	-.5441	-.2142	-.4100	-.1614
-.5603	-.2206	-.3724	-.1466	-.5281	-.2079	-.3942	-.1552
-.5385	-.2120	-.3312	-.1304	-.4971	-.1957	-.3647	-.1436
-.5136	-.2022	-.2939	-.1157	-.4661	-.1835	-.3376	-.1329
-.4872	-.1918	-.2596	-.1022	-.4348	-.1712	-.3119	-.1228
-.4303	-.1694	-.1963	-.0773	-.3716	-.1463	-.2637	-.1038
-.3698	-.1456	-.1392	-.0548	-.3078	-.1212	-.2184	-.0860
-.3068	-.1208	-.0864	-.0340	-.2431	-.0957	-.1755	-.0691
-.2416	-.0951	-.0378	-.0149	-.1781	-.0701	-.1346	-.0530
-.1052	-.0414	0.0480	0.0189	-.0457	-.0180	-.0577	-.0227
0.0381	0.0150	0.1201	0.0473	0.0886	0.0349	0.0142	0.0056
0.1877	0.0739	0.1773	0.0698	0.2256	0.0888	0.0831	0.0327
0.3424	0.1348	0.2207	0.0869	0.3663	0.1442	0.1468	0.0578
0.5011	0.1973	0.2530	0.0996	0.5133	0.2021	0.1999	0.0787
0.5824	0.2293	0.2634	0.1037	0.5898	0.2322	0.2220	0.0874
0.6655	0.2620	0.2695	0.1061	0.6688	0.2633	0.2395	0.0943
0.7511	0.2957	0.2700	0.1063	0.7513	0.2958	0.2497	0.0983
0.8430	0.3319	0.2489	0.0980	0.8430	0.3319	0.2469	0.0980

SCALED STAGE STATOR
SECTION NUMBER 4

DIAMETER = 13.9962 CM.(5.5103 IN.)
CHORD = 1.5641 CM.(0.6158 IN.)
CHORD ANGLE = 25.545 DEG.

UF(CM)	UF(IN)	UG(CM)	UG(IN)	LF(CM)	LF(IN)	LG(CM)	LG(IN)
-.5674	-.2234	-.4262	-.1678	-.5674	-.2234	-.4262	-.1678
-.5725	-.2254	-.4117	-.1621	-.5550	-.2185	-.4196	-.1652
-.5718	-.2251	-.4061	-.1599	-.5512	-.2170	-.4163	-.1639
-.5697	-.2243	-.3955	-.1557	-.5443	-.2143	-.4097	-.1613
-.5608	-.2208	-.3721	-.1465	-.5286	-.2081	-.3940	-.1551
-.5390	-.2122	-.3307	-.1302	-.4976	-.1959	-.3647	-.1436
-.5141	-.2024	-.2936	-.1156	-.4663	-.1836	-.3376	-.1329
-.4877	-.1920	-.2591	-.1020	-.4351	-.1713	-.3119	-.1228
-.4308	-.1696	-.1958	-.0771	-.3719	-.1464	-.2637	-.1038
-.3701	-.1457	-.1387	-.0546	-.3078	-.1212	-.2184	-.0860
-.3071	-.1209	-.0861	-.0339	-.2431	-.0957	-.1758	-.0692
-.2418	-.0952	-.0376	-.0148	-.1781	-.0701	-.1349	-.0531
-.1052	-.0414	0.0485	0.0191	-.0457	-.0180	-.0579	-.0228
0.0381	0.0150	0.1204	0.0474	0.0889	0.0350	-.0140	-.0055
0.1877	0.0739	0.1775	0.0699	0.2258	0.0889	-.0828	-.0326
0.3426	0.1349	0.2207	0.0869	0.3665	0.1443	-.1463	-.0576
0.5014	0.1974	0.2527	0.0995	0.5138	0.2023	-.1994	-.0785
0.5829	0.2295	0.2631	0.1036	0.5903	0.2324	-.2215	-.0872
0.6660	0.2622	0.2692	0.1060	0.6693	0.2635	-.2388	-.0940
0.7518	0.2960	0.2695	0.1061	0.7518	0.2960	-.2489	-.0980
0.8438	0.3322	0.2482	0.0977	0.8438	0.3322	-.2482	-.0977

Table XX. Airfoil Section Coordinates for Scaled Stage Stator (Continued)

SCALED STAGE STATOR
SECTION NUMBER 5

DIAMETER = 14.0622 CM.(5.5363 IN.)
CHORD = 1.5646 CM.(0.6160 IN.)
CHORD ANGLE = 25.509 DEG.

UF(CM)	UF(IN)	UG(CM)	UG(IN)	LF(CM)	LF(IN)	LG(CM)	LG(IN)
-.5677	-.2235	-.4262	-.1678	-.5677	-.2235	-.4262	-.1678
-.5728	-.2255	-.4117	-.1621	-.5552	-.2186	-.4196	-.1652
-.5723	-.2253	-.4059	-.1598	-.5517	-.2172	-.4163	-.1639
-.5700	-.2244	-.3955	-.1557	-.5448	-.2145	-.4097	-.1613
-.5613	-.2210	-.3719	-.1464	-.5288	-.2082	-.3940	-.1551
-.5395	-.2124	-.3307	-.1302	-.4978	-.1960	-.3647	-.1436
-.5146	-.2026	-.2934	-.1155	-.4666	-.1837	-.3376	-.1329
-.4879	-.1921	-.2588	-.1019	-.4351	-.1713	-.3119	-.1228
-.4310	-.1697	-.1956	-.0770	-.3719	-.1464	-.2637	-.1038
-.3706	-.1459	-.1384	-.0545	-.3081	-.1213	-.2184	-.0860
-.3076	-.1211	-.0856	-.0337	-.2433	-.0958	-.1758	-.0692
-.2421	-.0953	-.0371	-.0146	-.1778	-.0700	-.1351	-.0532
-.1054	-.0415	0.0488	0.0192	-.0455	-.0179	-.0582	-.0229
0.0381	0.0150	0.1209	0.0476	0.0892	0.0351	0.0137	0.0054
0.1880	0.0740	0.1778	0.0700	0.2261	0.0890	0.0823	0.0324
0.3429	0.1350	0.2207	0.0869	0.3668	0.1444	0.1460	0.0575
0.5019	0.1976	0.2525	0.0994	0.5141	0.2024	0.1991	0.0784
0.5832	0.2296	0.2629	0.1035	0.5906	0.2325	0.2212	0.0871
0.6665	0.2624	0.2690	0.1059	0.6698	0.2637	0.2385	0.0939
0.7523	0.2962	0.2690	0.1059	0.7523	0.2962	0.2487	0.0979
0.8443	0.3324	0.2477	0.0975	0.8443	0.3324	0.2477	0.0975

SCALED STAGE STATOR
SECTION NUMBER 6

DIAMETER = 14.1282 CM.(5.5623 IN.)
CHORD = 1.5654 CM.(0.6163 IN.)
CHORD ANGLE = 25.479 DEG.

UF(CM)	UF(IN)	UG(CM)	UG(IN)	LF(CM)	LF(IN)	LG(CM)	LG(IN)
-.5682	-.2237	-.4262	-.1678	-.5682	-.2237	-.4262	-.1678
-.5733	-.2257	-.4117	-.1621	-.5558	-.2188	-.4196	-.1652
-.5728	-.2255	-.4059	-.1598	-.5519	-.2173	-.4163	-.1639
-.5705	-.2246	-.3952	-.1556	-.5451	-.2146	-.4097	-.1613
-.5616	-.2211	-.3719	-.1464	-.5291	-.2083	-.3940	-.1551
-.5397	-.2125	-.3305	-.1301	-.4981	-.1961	-.3647	-.1436
-.5151	-.2028	-.2931	-.1154	-.4669	-.1838	-.3376	-.1329
-.4884	-.1923	-.2586	-.1018	-.4354	-.1714	-.3119	-.1228
-.4315	-.1699	-.1953	-.0769	-.3721	-.1465	-.2637	-.1038
-.3708	-.1460	-.1382	-.0544	-.3081	-.1213	-.2187	-.0861
-.3078	-.1212	-.0853	-.0336	-.2431	-.0957	-.1760	-.0693
-.2423	-.0954	-.0368	-.0145	-.1778	-.0700	-.1351	-.0532
-.1057	-.0416	0.0493	0.0194	-.0455	-.0179	-.0584	-.0230
0.0381	0.0150	0.1212	0.0477	0.0894	0.0352	0.0135	0.0053
0.1880	0.0740	0.1781	0.0701	0.2263	0.0891	0.0820	0.0323
0.3432	0.1351	0.2210	0.0870	0.3673	0.1446	0.1458	0.0574
0.5022	0.1977	0.2525	0.0994	0.5146	0.2026	0.1989	0.0783
0.5837	0.2298	0.2629	0.1035	0.5911	0.2327	0.2210	0.0870
0.6670	0.2626	0.2685	0.1057	0.6703	0.2639	0.2380	0.0937
0.7529	0.2964	0.2687	0.1058	0.7529	0.2964	0.2482	0.0977
0.8448	0.3326	0.2471	0.0973	0.8448	0.3326	0.2471	0.0973

Table XX. Airfoil Section Coordinates for Scaled Stage Stator (Continued)

SCALED STAGE STATOR
SECTION NUMBER 7

DIAMETER = 14.1943 CM.(5.5883 IN.)
CHORD = 1.5659 CM.(0.6165 IN.)
CHORD ANGLE = 25.448 DEG.

UF(CM)	UF(IN)	UG(CM)	UG(IN)	LF(CM)	LF(IN)	LG(CM)	LG(IN)
-.5685	-.2238	-.4262	-.1678	-.5685	-.2238	-.4262	-.1678
-.5735	-.2258	-.4117	-.1621	-.5560	-.2189	-.4199	-.1653
-.5730	-.2256	-.4059	-.1598	-.5522	-.2174	-.4166	-.1640
-.5707	-.2247	-.3952	-.1556	-.5453	-.2147	-.4097	-.1613
-.5621	-.2213	-.3719	-.1464	-.5293	-.2084	-.3940	-.1551
-.5403	-.2127	-.3305	-.1301	-.4981	-.1961	-.3647	-.1436
-.5154	-.2029	-.2931	-.1154	-.4669	-.1838	-.3376	-.1329
-.4887	-.1924	-.2586	-.1018	-.4354	-.1714	-.3122	-.1229
-.4318	-.1700	-.1951	-.0768	-.3721	-.1465	-.2639	-.1039
-.3713	-.1462	-.1377	-.0542	-.3081	-.1213	-.2187	-.0861
-.3081	-.1213	-.0848	-.0334	-.2431	-.0957	-.1760	-.0693
-.2426	-.0955	-.0363	-.0143	-.1778	-.0700	-.1354	-.0533
-.1057	-.0416	0.0498	0.0196	-.0452	-.0178	-.0587	-.0231
0.0378	0.0149	0.1214	0.0478	0.0894	0.0352	0.0132	0.0052
0.1882	0.0741	0.1783	0.0702	0.2266	0.0892	0.0818	0.0322
0.3434	0.1352	0.2210	0.0870	0.3675	0.1447	0.1455	0.0573
0.5027	0.1979	0.2525	0.0994	0.5149	0.2027	0.1984	0.0781
0.5842	0.2300	0.2626	0.1034	0.5916	0.2329	0.2205	0.0868
0.6675	0.2628	0.2662	0.1056	0.6706	0.2640	0.2377	0.0936
0.7534	0.2966	0.2682	0.1056	0.7534	0.2966	0.2477	0.0975
0.8456	0.3329	0.2466	0.0971	0.8456	0.3329	0.2466	0.0971

SCALED STAGE STATOR
SECTION NUMBER 8

DIAMETER = 14.2603 CM.(5.6143 IN.)
CHORD = 1.5664 CM.(0.6167 IN.)
CHORD ANGLE = 25.407 DEG.

UF(CM)	UF(IN)	UG(CM)	UG(IN)	LF(CM)	LF(IN)	LG(CM)	LG(IN)
-.5690	-.2240	-.4262	-.1678	-.5690	-.2240	-.4262	-.1678
-.5740	-.2260	-.4117	-.1621	-.5563	-.2190	-.4196	-.1652
-.5735	-.2258	-.4059	-.1598	-.5524	-.2175	-.4163	-.1639
-.5712	-.2249	-.3952	-.1556	-.5456	-.2148	-.4097	-.1613
-.5626	-.2215	-.3716	-.1463	-.5296	-.2085	-.3940	-.1551
-.5408	-.2129	-.3302	-.1300	-.4983	-.1962	-.3647	-.1436
-.5159	-.2031	-.2929	-.1153	-.4671	-.1839	-.3376	-.1329
-.4892	-.1926	-.2581	-.1016	-.4356	-.1715	-.3122	-.1229
-.4323	-.1702	-.1946	-.0766	-.3724	-.1466	-.2639	-.1039
-.3716	-.1463	-.1374	-.0541	-.3081	-.1213	-.2187	-.0861
-.3084	-.1214	-.0846	-.0333	-.2433	-.0958	-.1763	-.0694
-.2428	-.0956	-.0361	-.0142	-.1778	-.0700	-.1354	-.0533
-.1059	-.0417	0.0500	0.0197	-.0452	-.0178	-.0589	-.0232
0.0378	0.0149	0.1219	0.0480	0.0897	0.0353	0.0130	0.0051
0.1882	0.0741	0.1786	0.0703	0.2268	0.0893	0.0815	0.0321
0.3437	0.1353	0.2210	0.0870	0.3678	0.1448	0.1450	0.0571
0.5029	0.1980	0.2522	0.0993	0.5154	0.2029	0.1981	0.0780
0.5845	0.2301	0.2624	0.1033	0.5918	0.2330	0.2200	0.0866
0.6680	0.2630	0.2680	0.1055	0.6711	0.2642	0.2372	0.0934
0.7539	0.2968	0.2677	0.1054	0.7539	0.2968	0.2471	0.0973
0.8461	0.3331	0.2459	0.0968	0.8461	0.3331	0.2459	0.0968

Table XX. Airfoil Section Coordinates for Scaled Stage Stator (Continued)

SCALED STAGE STATOR
SECTION NUMBER 9

DIAMETER = 14.3264 CM.(5.6403 IN.)
CHORD = 1.5872 CM.(0.6170 IN.)
CHORD ANGLE = 25.355 DEG.

UF(CM)	UF(IN)	UG(CM)	UG(IN)	LF(CM)	LF(IN)	LG(CM)	LG(IN)
-.5695	-.2242	-.4260	-.1677	-.5695	-.2242	-.4260	-.1677
-.5745	-.2262	-.4115	-.1620	-.5568	-.2192	-.4196	-.1652
-.5740	-.2260	-.4056	-.1597	-.5530	-.2177	-.4163	-.1639
-.5718	-.2251	-.3950	-.1555	-.5461	-.2150	-.4097	-.1613
-.5631	-.2217	-.3713	-.1462	-.5301	-.2087	-.3937	-.1550
-.5413	-.2131	-.3299	-.1299	-.4989	-.1964	-.3645	-.1435
-.5164	-.2033	-.2924	-.1151	-.4674	-.1840	-.3376	-.1329
-.4897	-.1928	-.2578	-.1015	-.4359	-.1716	-.3119	-.1228
-.4328	-.1704	-.1943	-.0765	-.3724	-.1466	-.2637	-.1038
-.3721	-.1465	-.1369	-.0539	-.3084	-.1214	-.2187	-.0861
-.3089	-.1216	-.0841	-.0331	-.2433	-.0958	-.1763	-.0694
-.2431	-.0957	-.0356	-.0140	-.1778	-.0700	-.1356	-.0534
-.1059	-.0417	0.0505	0.0199	-.0452	-.0178	-.0589	-.0232
0.0378	0.0149	0.1222	0.0481	0.0899	0.0354	-.0127	-.0050
0.1885	0.0742	0.1786	0.0703	0.2271	0.0894	-.0813	-.0320
0.3439	0.1354	0.2210	0.0870	0.3680	0.1449	-.1448	-.0570
0.5034	0.1982	0.2520	0.0992	0.5156	0.2030	-.1976	-.0778
0.5850	0.2303	0.2619	0.1031	0.5923	0.2332	-.2195	-.0864
0.6685	0.2632	0.2675	0.1053	0.6716	0.2644	-.2365	-.0931
0.7546	0.2971	0.2670	0.1051	0.7546	0.2971	-.2464	-.0970
0.8468	0.3334	0.2451	0.0965	0.8468	0.3334	-.2451	-.0965

SCALED STAGE STATOR
SECTION NUMBER 10

DIAMETER = 14.3924 CM.(5.6663 IN.)
CHORD = 1.5677 CM.(0.6172 IN.)
CHORD ANGLE = 25.303 DEG.

UF(CM)	UF(IN)	UG(CM)	UG(IN)	LF(CM)	LF(IN)	LG(CM)	LG(IN)
-.5697	-.2243	-.4260	-.1677	-.5697	-.2243	-.4260	-.1677
-.5751	-.2264	-.4112	-.1619	-.5570	-.2193	-.4194	-.1651
-.5745	-.2262	-.4054	-.1596	-.5532	-.2178	-.4161	-.1638
-.5723	-.2253	-.3947	-.1554	-.5464	-.2151	-.4094	-.1612
-.5636	-.2219	-.3711	-.1461	-.5304	-.2088	-.3937	-.1550
-.5418	-.2133	-.3294	-.1297	-.4991	-.1965	-.3645	-.1435
-.5169	-.2035	-.2921	-.1150	-.4676	-.1841	-.3373	-.1328
-.4902	-.1930	-.2573	-.1013	-.4361	-.1717	-.3119	-.1228
-.4333	-.1706	-.1938	-.0763	-.3726	-.1467	-.2637	-.1038
-.3724	-.1466	-.1364	-.0537	-.3084	-.1214	-.2187	-.0861
-.3091	-.1217	-.0836	-.0329	-.2433	-.0958	-.1763	-.0694
-.2433	-.0958	-.0351	-.0138	-.1778	-.0700	-.1356	-.0534
-.1062	-.0418	0.0511	0.0201	-.0450	-.0177	-.0592	-.0233
0.0378	0.0149	0.1224	0.0482	0.0899	0.0354	0.0124	0.0049
0.1885	0.0742	0.1788	0.0704	0.2273	0.0895	0.0810	0.0319
0.3442	0.1355	0.2210	0.0870	0.3686	0.1451	0.1443	0.0568
0.5039	0.1984	0.2517	0.0991	0.5161	0.2032	0.1971	0.0776
0.5855	0.2305	0.2616	0.1030	0.5928	0.2334	0.2189	0.0862
0.6690	0.2634	0.2670	0.1051	0.6723	0.2647	0.2360	0.0929
0.7551	0.2973	0.2664	0.1049	0.7551	0.2973	0.2456	0.0967
0.8476	0.3337	0.2441	0.0961	0.8476	0.3337	0.2441	0.0961

Table XX. Airfoil Section Coordinates for Scaled Stage Stato, (Continued)

SCALED STAGE STATOR
SECTION NUMBER 11

DIAMETER = 14.4584 CM.(5.6923 IN.)
CHORD = 1.5682 CM.(0.6174 IN.)
CHORD ANGLE = 25.263 DEG.

UF(CM)	UF(IN)	UG(CM)	UG(IN)	LF(CM)	LF(IN)	LG(CM)	LG(IN)
-.5702	-.2245	-.4260	-.1677	-.5702	-.2245	-.4260	-.1677
-.5756	-.2266	-.4112	-.1619	-.5575	-.2195	-.4194	-.1651
-.5751	-.2264	-.4054	-.1596	-.5537	-.2180	-.4161	-.1638
-.5728	-.2255	-.3947	-.1554	-.5466	-.2152	-.4094	-.1612
-.5641	-.2221	-.3711	-.1461	-.5306	-.2089	-.3937	-.1550
-.5420	-.2134	-.3294	-.1297	-.4994	-.1965	-.3645	-.1435
-.5174	-.2037	-.2918	-.1149	-.4679	-.1842	-.3376	-.1329
-.4907	-.1932	-.2570	-.1012	-.4361	-.1717	-.3119	-.1228
-.4336	-.1707	-.1935	-.0762	-.3726	-.1467	-.2637	-.1038
-.3729	-.1468	-.1361	-.0536	-.3084	-.1214	-.2169	-.0862
-.3094	-.1218	-.0831	-.0327	-.2433	-.0958	-.1763	-.0694
-.2436	-.0959	-.0345	-.0136	-.1778	-.0700	-.1359	-.0535
-.1064	-.0419	0.0513	0.0202	-.0450	-.0177	-.0594	-.0234
0.0378	0.0149	0.1229	0.0484	0.0902	0.0355	0.0122	0.0048
0.1887	0.0743	0.1791	0.0705	0.2276	0.0896	0.0805	0.0317
0.3444	0.1356	0.2210	0.0870	0.3688	0.1452	0.1440	0.0567
0.5042	0.1985	0.2517	0.0991	0.5166	0.2034	0.1966	0.0774
0.5860	0.2307	0.2614	0.1029	0.5933	0.2336	0.2186	0.0860
0.6695	0.2636	0.2664	0.1049	0.6728	0.2649	0.2355	0.0927
0.7559	0.2976	0.2657	0.1046	0.7556	0.2975	0.2451	0.0965
0.8481	0.3339	0.2433	0.0958	0.8481	0.3339	0.2433	0.0958

SCALED STAGE STATOR
SECTION NUMBER 12

DIAMETER = 14.5242 CM.(5.7182 IN.)
CHORD = 1.5690 CM.(0.6177 IN.)
CHORD ANGLE = 25.243 DEG.

UF(CM)	UF(IN)	UG(CM)	UG(IN)	LF(CM)	LF(IN)	LG(CM)	LG(IN)
-.5702	-.2245	-.4262	-.1678	-.5702	-.2245	-.4262	-.1678
-.5758	-.2267	-.4115	-.1620	-.5575	-.2195	-.4199	-.1653
-.5751	-.2264	-.4059	-.1598	-.5537	-.2180	-.4166	-.1640
-.5730	-.2256	-.3950	-.1555	-.5469	-.2153	-.4100	-.1614
-.5644	-.2222	-.3713	-.1462	-.5306	-.2089	-.3940	-.1551
-.5425	-.2136	-.3294	-.1297	-.4994	-.1966	-.3647	-.1436
-.5177	-.2038	-.2918	-.1149	-.4679	-.1842	-.3378	-.1330
-.4910	-.1933	-.2570	-.1012	-.4361	-.1717	-.3122	-.1229
-.4338	-.1708	-.1933	-.0761	-.3726	-.1467	-.2639	-.1039
-.3731	-.1469	-.1359	-.0535	-.3084	-.1214	-.2189	-.0862
-.3096	-.1219	-.0828	-.0326	-.2433	-.0958	-.1765	-.0695
-.2438	-.0960	-.0343	-.0135	-.1775	-.0699	-.1359	-.0535
-.1064	-.0419	0.0518	0.0204	-.0447	-.0176	-.0597	-.0235
0.0378	0.0149	0.1232	0.0485	0.0904	0.0356	0.0119	0.0047
0.1887	0.0743	0.1793	0.0706	0.2276	0.0896	0.0803	0.0316
0.3447	0.1357	0.2212	0.0871	0.3691	0.1453	0.1438	0.0566
0.5047	0.1987	0.2515	0.0990	0.5169	0.2035	0.1963	0.0773
0.5865	0.2309	0.2611	0.1028	0.5936	0.2337	0.2182	0.0859
0.670	0.2638	0.2662	0.1048	0.6731	0.2650	0.2349	0.0925
0.7564	0.2978	0.2654	0.1045	0.7562	0.2977	0.2446	0.0963
0.8489	0.3342	0.2428	0.0956	0.8489	0.3342	0.2428	0.0956

Table XX. Airfoil Section Coordinates for Scaled Stage Stator (Continued)

SCALED STAGE STATOR
SECTION NUMBER 13

DIAMETER = 15.3129 CM.(6.0737 IN.)
CHORD = 1.5756 CM.(0.6203 IN.)
CHORD ANGLE = 25.219 DEG.

UF(CM)	UF(IN)	UG(CM)	UG(IN)	LF(CM)	LF(IN)	LG(CM)	LG(IN)
-.5687	-.2239	-.4354	-.1714	-.5687	-.2239	-.4354	-.1714
-.5748	-.2263	-.4204	-.1655	-.5555	-.2187	-.4282	-.1686
-.5745	-.2262	-.4143	-.1631	-.5514	-.2171	-.4249	-.1673
-.5728	-.2255	-.4031	-.1587	-.5446	-.2144	-.4181	-.1646
-.5646	-.2223	-.3785	-.1490	-.5286	-.2081	-.4016	-.1581
-.5436	-.2140	-.3350	-.1319	-.4971	-.1957	-.3713	-.1462
-.5194	-.2045	-.2962	-.1166	-.4656	-.1833	-.3437	-.1353
-.4933	-.1942	-.2601	-.1024	-.4341	-.1709	-.3175	-.1250
-.4366	-.1719	-.1943	-.0765	-.3706	-.1459	-.2682	-.1056
-.3762	-.1481	-.1351	-.0532	-.3063	-.1206	-.2225	-.0876
-.3129	-.1232	-.0805	-.0317	-.2413	-.0950	-.1793	-.0706
-.2469	-.0972	-.0310	-.0122	-.1760	-.0693	-.1384	-.0545
-.1090	-.0429	0.0566	0.0223	-.0432	-.0170	-.0612	-.0241
0.0363	0.0143	0.1288	0.0507	0.0919	0.0362	0.0109	0.0043
0.1885	0.0742	0.1847	0.0727	0.2294	0.0903	0.0795	0.0313
0.3462	0.1363	0.2250	0.0886	0.3713	0.1462	0.1427	0.0562
0.5080	0.2000	0.2532	0.0997	0.5202	0.2048	0.1948	0.0767
0.5908	0.2326	0.2611	0.1028	0.5977	0.2353	0.2162	0.0851
0.6754	0.2659	0.2644	0.1041	0.6779	0.2669	0.2322	0.0914
0.7628	0.3003	0.2616	0.1030	0.7623	0.3001	0.2403	0.0946
0.8567	0.3373	0.2360	0.0929	0.8567	0.3373	0.2360	0.0929

SCALED STAGE STATOR
SECTION NUMBER 14

DIAMETER = 15.8206 CM.(6.2286 IN.)
CHORD = 1.5794 CM.(0.6218 IN.)
CHORD ANGLE = 25.306 DEG.

UF(CM)	UF(IN)	UG(CM)	UG(IN)	LF(CM)	LF(IN)	LG(CM)	LG(IN)
-.5654	-.2226	-.4450	-.1752	-.5654	-.2226	-.4450	-.1752
-.5725	-.2254	-.4298	-.1692	-.5519	-.2173	-.4374	-.1722
-.5723	-.2253	-.4234	-.1667	-.5481	-.2158	-.4338	-.1708
-.5707	-.2247	-.4120	-.1622	-.5410	-.2130	-.4265	-.1679
-.5631	-.2217	-.3863	-.1521	-.5250	-.2067	-.4092	-.1611
-.5431	-.2138	-.3416	-.1345	-.4938	-.1944	-.3780	-.1488
-.5194	-.2045	-.3012	-.1186	-.4628	-.1822	-.3492	-.1375
-.4938	-.1944	-.2642	-.1040	-.4313	-.1698	-.3223	-.1269
-.4381	-.1725	-.1963	-.0773	-.3683	-.1450	-.2718	-.1070
-.3782	-.1489	-.1354	-.0533	-.3043	-.1198	-.2250	-.0886
-.3152	-.1241	-.0795	-.0313	-.2398	-.0944	-.1811	-.0713
-.2494	-.0982	-.0287	-.0113	-.1748	-.0688	-.1394	-.0549
-.1115	-.0439	0.0607	0.0239	-.0424	-.0167	-.0612	-.0241
0.0345	0.0136	0.1336	0.0526	0.0922	0.0363	0.0112	0.0044
0.1877	0.0739	0.1892	0.0745	0.2296	0.0904	0.0803	0.0316
0.3465	0.1364	0.2289	0.0901	0.3719	0.1464	0.1435	0.0565
0.5095	0.2006	0.2550	0.1004	0.5215	0.2053	0.1948	0.0767
0.5931	0.2335	0.2619	0.1031	0.5994	0.2360	0.2154	0.0848
0.6787	0.2672	0.2634	0.1037	0.6807	0.2680	0.2304	0.0907
0.7671	0.3020	0.2586	0.1018	0.7661	0.3016	0.2372	0.0934
0.8623	0.3395	0.2301	0.0906	0.8623	0.3395	0.2301	0.0906

APPENDIX C

DEFINITION OF SYMBOLS

A	Area, m^2 ($in.^2$)
AR	Aspect ratio, H/C
C	Chord length, cm (in.); or clearance, mm (in.)
C/H	Clearance-to-height ratio
Cp	Specific heat at constant pressure
CPS	Cycles/Second
D	Diameter; cm, m (in.)
DF, D	Diffusion factor
E	Multiple of rotor frequency
g	Gravitational constant, 9.8066 kg-m/N-sec^2 (32.174 lbm-ft/lbf-sec^2)
H	Average blade height, cm (in.)
ID	Inner diameter, cm, m (in.)
IGV	Inlet guide vane
i_m	Incidence to mean camber line
J	Mechanical equivalent of heat, 0.1019 m-kg/J (778.161 ft-lbf/Btu)
$\bar{K}$	Blockage factor (effective area/actual area)
LER	Leading edge radius, cm (in.)
M	Mach number
N	Rotor speed, radians/sec (rpm)
OD	Outer diameter; cm, m (in.)
PR	Total pressure ratio
P_s	Static pressure, N/cm^2 (psia)
P_t	Total pressure, N/cm^2 (psia)
Q	Velocity head, $\frac{1}{2}pv^2$; N/cm^2 (psia)
R	Gas constant for air, 287.00 J/kg-°K (53.342) ft-lbf/lbm-°R)

DEFINITIONS OF SYMBOLS (Continued)

RN	Reynolds number
SF	Linear dimension scale factor
SL	Stacking line for airfoil
SM	Surge margin, %
T	Maximum blade thickness, cm (in.)
T/C	Maximum thickness-to-chord ratio
TDC	Top dead center
TER	Trailing edge radius
TR	Total temperature ratio
T_s	Static temperature, °K (°R)
T_t	Total temperature, °K (°R)
U	Rotor wheel velocity, m/sec (ft/sec)
V	Air velocity, m/sec (ft/sec)
W	Mass flowrate, kg/sec (lbm/sec)
β	Air angle, angle between velocity vector and axial direction, degrees
γ	Ratio of specific heats
$\gamma°$	Chord angle, angle between chordline and radial direction, degrees
Δ	Difference
δ	Ratio of total pressure to NASA standard sea level pressure of 10.1315 N/cm² (14.694 psia)
$\delta°$	Deviation angle, degrees
ϵ	Meridional flow angle, angle between axial velocity vector and centerline, degrees
η	Efficiency
θ	Ratio of total temperature to NASA standard sea level temperature of 288.17°K (518.7°R); Diffuser Cone Angle (degrees); Turning angle (degrees)

DEFINITION OF SYMBOLS (Continued)

κ	Blade metal angle from axial direction, degrees
μ	Dynamic viscosity
ρ	Fluid density, Kg/cm³ (lbm/in.³)
σ	Solidity, blade chord-to-spacing ratio
ϕ	Camber angle
$\bar{\omega}$	Loss coefficient
Subscripts	
ad	Adiabatic
C	Corrected to NASA standard sea level conditions
CA	Circular arc meanline
eq	Equivalent cone angle for a compressor stage
le	Leading edge
p	Polytropic
R	Rotor
ref	Reference
rel	Relative to the rotor
S	Stator
stg	Stage (IGV rotor and stator)
te	Trailing edge
tip	At the OD
Z	Axial direction
θ	Tangential direction
1	Referring to IGV inlet station
2	Referring to rotor inlet station
3	Referring to rotor exit station
4	Referring to stator exit station

DEFINITION OF SYMBOLS (Continued)

Superscripts

$'$	Relative to the rotor
$\tilde{M}$	Meridional component

APPENDIX D

DEFINITION OF VARIABLES

Absolute Mach number:

$$M = \sqrt{\frac{2}{\gamma-1}\left[\left(\frac{P_s}{P_t}\right)^{\frac{1-\gamma}{\gamma}} - 1\right]}$$

Static Temperature:

$$T_s = \frac{T_t}{1 + \frac{\gamma-1}{2} M^2}$$

Acoustic Velocity:

$$a = \sqrt{\gamma g R T_s}$$

Absolute Velocity:

$$V = Ma$$

Axial Component of Absolute Velocity:

$$V_z = \frac{V}{\sqrt{\sec^2\epsilon + \tan^2\beta}}$$

Meridional Component of Absolute Velocity:

$$V_m = V_z \sec\epsilon$$

Tangential Component of Absolute Velocity:

$$V_\theta = V_z \tan\beta$$

Radial Component of Absolute Velocity:

$$V_r = V_z \tan\epsilon$$

Absolute Air Angle (meridional plane):

$$\bar{\beta} = \tan^{-1}\left(\frac{V_\theta}{V_m}\right)$$

Wheel Speed:

$$U = \omega r = \frac{\Pi ND}{\text{constant}}$$

Tangential Component of Relative Velocity:

$$V_\theta' = U - V_\theta$$

Relative Air Angle:

$$\beta' = \tan^{-1} \frac{V_\theta'}{V_z} \qquad \text{(axial plane)}$$

$$\bar{\beta}' = \tan^{-1} \frac{V_\theta'}{V_m} \qquad \text{(meridional plane)}$$

Relative Velocity:

$$V' = V_m \sec\bar{\beta}'$$

Relative Mach Number:

$$M' = M \frac{\cos\bar{\beta}}{\cos\bar{\beta}'}$$

Relative Total Pressure:

$$P_t' = P_s \left[1 + \frac{\gamma-1}{2} (M')^2 \right] \frac{\gamma}{\gamma-1}$$

Relative Total Temperature:

$$T_t' = T_s \left[1 + \frac{\gamma-1}{2} (M')^2 \right]$$

Pressure Ratio:

$$PR = \frac{\text{exit } P_t}{\text{inlet } P_t}$$

Turning:

$$\theta' = \text{inlet } \bar{\beta}' - \text{exit } \bar{\beta}' \qquad \text{(rotor)}$$

$$\theta = \text{inlet } \bar{\beta} - \text{exit } \bar{\beta} \qquad \text{(stator)}$$

Loss Coefficient:

$$\bar{\omega}' = \frac{\text{exit ideal } P_t' - \text{exit } P_t'}{\text{inlet } P_t' - \text{inlet } P_s} \quad \text{(rotor)}$$

$$\bar{\omega} = \frac{\text{inlet } P_t - \text{exit } P_t}{\text{inlet } P_t - \text{inlet } P_s} \quad \text{(stator)}$$

where:

$$\text{ideal } P_t' = \text{inlet } P_t' \left\{ 1 + \frac{\gamma-1}{2} \frac{\text{exit } U^2}{\gamma g R \text{ inlet } T_t'} \left[1 - \left(\frac{\text{inlet radius}}{\text{exit radius}} \right)^2 \right] \right\}^{\frac{\gamma}{\gamma-1}}$$

Loss Parameter:

$$LP' = \frac{\bar{\omega}' \cos(\text{exit } \bar{\beta}')}{2\sigma} \quad \text{(rotor)}$$

$$LP = \frac{\bar{\omega} \cos(\text{exit } \bar{\beta})}{2\sigma} \quad \text{(stator)}$$

Diffusion Factor:

$$DF = 1 - \frac{\text{exit } V'}{\text{inlet } V'} + \frac{\text{exit } DV_\theta' - \text{inlet } DV_\theta'}{(\text{exit D} + \text{inlet D})\,\sigma \text{inlet } V'} \quad \text{(Rotor)}$$

$$DF = 1 - \frac{\text{exit } V}{\text{inlet } V} + \frac{\text{inlet } DV_\theta - \text{exit } DV_\theta}{(\text{exit D} + \text{inlet D})\,\sigma \text{inlet } V} \quad \text{(Stator)}$$

Adiabatic Efficiency:

$$\eta_{ad} = \frac{PR^{\frac{\gamma-1}{\gamma}} - 1}{TR - 1}$$

Polytropic Efficiency:

$$\eta_{pr} = \frac{\gamma-1}{\gamma} \left[\frac{\ln PR}{\ln TR} \right] \quad \text{(rotor)}$$

$$\eta_{ps} = \frac{\gamma-1}{\gamma} \left[\frac{\ln (\text{exit } P_s/\text{inlet } P_s)}{\ln (\text{exit } T_s/\text{inlet } T_s)} \right] \quad \text{(stator)}$$

Incidence Angle:

$$i_m = \text{inlet } \beta' - \text{inlet } K' \quad \text{(rotor)}$$

$$i_m = \text{inlet } \beta - \text{inlet } K \quad \text{(stator)}$$

Deviation Angle:

δ° = exit β' − exit K′ (rotor)

δ° = exit β − exit K (stator)

Surge margin:

$$\% \text{ SM} = \left\{ \left[\left(\frac{\text{PR}}{\text{W}\sqrt{\theta}/\delta} \right)_{\text{surge}} \left(\frac{\text{W}\sqrt{\theta}/\delta}{\text{PR}} \right)_{\text{given point}} \right] - 1 \right\} 100$$

REFERENCES

1. Rhoden, H. G.: Effects of Reynolds Number on the Flow of Air Through a Cascade of Compressor Blades. A.R.C. Technical Report, R. & M. No. 2919, London, 1952.

2. Lakshminarayana, B.: Methods of Predicting the Tip Clearance Effects in Axial Flow Turbomachinery. Transactions of the ASME, *Journal of Basic Engineering*, September 1970.

3. Holman, F. F.; Kidwell, J. R.; and Ware, T. C.: Small Axial Compressor Technology Program. NASA CR-134827, June 1976.

4. Wiggins, J. O.; and Waltz, G. L.: Some Experiences in the Scaling of the NACA 8-Stage Transonic Axial Flow Compressor. SAE Paper 720711, 1972.

5. Johnsen, I. A.; Bullock, R. O.; Editors: Aerodynamic Design of Axial-Flow Compressors/Revised. NASA SP-36, 1965.

6. Mechtly, E. A.; The International System of Units. NASA SP-7012, 1964.

7. Moody, L. F.: Friction Factors for Pipe Flow. Transactions of the ASME; November 1944.

8. Ross, R.: Turbulent Flow in the Entrance Region of a Pipe. ASME Report 54-A-89; July 1956.

9. Hanley, W. T.; A Correlation of Endwall Losses in Plane Compressor Cascades. Transactions of ASME Vol. 90 Series A No. 3; July 1968.